APPENDIX B

SEISMIC HAZARD ASSESSMENT

(Pages B-1 to B-196)

Seismic Hazard Assessment for the Yankee Doodle Tailings Impoundment Site, Butte, Montana

Final Report

Submitted to:

Knight Piesold Ltd.
750 West Pender, Suite 1400
Vancouver, BC V6C 2T8

Prepared by:

Linda Al Atik and Nick Gregor

February 19, 2016

Executive Summary

Site-specific probabilistic seismic hazard analysis (PSHA) and deterministic seismic hazard analysis (DSHA) have been performed for the Yankee Doodle Tailings Impoundment (YDTI) site in Butte, Montana. The site is located at latitude 46.034°N and longitude 112.504°W and lies within a region characterized by a number of late-Quaternary Basin and Range normal faults and historical seismicity. Two fault sources are located in close proximity to the site: the Continental fault, which intersects the site, has a maximum magnitude (Mmax) of 6.5 and the Rocker fault located within 10 km from the site with Mmax of 7.0. No information is available on the rates of activity of these faults and inferred slip rate values of 0.020, 0.005, and 0.012 mm/yr with weights of 0.6, 0.2, 0.2, respectively, were assigned to these faults based on the Wong et al. (2005) study.

The site-specific PSHA and DSHA were undertaken to develop 5%-damped horizontal acceleration response spectra for site class B/C (V_{S30} = 760 m/sec). The ground-motion characterization model consisted of the five equally-weighted NGA-West2 models and the stochastic-based model of Wong et al. (2005). PSHA uniform hazard spectra (UHS) were developed for return periods of 475, 1,000, 2,475, and 10,000 years. DSHA median and 84th percentile acceleration response spectra were developed for the maximum credible earthquake (MCE) scenarios on the Continental fault. Two scenarios with distance of 0.1 and 1.2 km were used in the DSHA representing two locations along the north-south and east-west embankments of the YDTI alignment, respectively. Vertical design spectra were developed by applying empirically-based vertical-to-horizontal ratios (V/H) to the horizontal spectra. Table 1 lists the peak ground acceleration (PGA) values obtained at the YDTI site for the different design levels.

Five sets of two-component (i.e., one horizontal and one vertical) spectrally-matched design time series were developed for each of the eight design levels: PSHA spectra with return periods of 475, 1,000, 2,475, and 10,000 years, and DSHA 50th and 84th percentile response spectra for the MCE scenarios on the Continental fault with rupture distances of 1.2 and 0.1 km.

Fault displacement hazard was evaluated for the MCE on the Continental fault using an informed deterministic approach (Pacific Gas and Electric 2015) which takes into consideration the epistemic uncertainty in defining the MCE and the aleatory and epistemic uncertainty in the fault displacement prediction equations (DPE). Median and 84th percentile values for the average displacement on the Continental fault were estimated as 0.51 and 1.44 m, respectively.

Table 1. Horizontal and vertical design PGA for 5% damping for the YDTI site for V_{S30} of 760 m/sec

	UHS PGA (g)				Deterministic PGA (g) Rrup = 1.2 km		Deterministic PGA (g) Rrup = 0.1 km	
Component	**475 yr**	**1,000 yr**	**2,475 yr**	**10,000 yr**	**Median**	**84th Percentile**	**Median**	**84th Percentile**
Horizontal	0.083	0.124	0.197	0.372	0.416	0.779	0.447	0.837
Vertical	0.052	0.078	0.139	0.263	0.332	0.633	0.357	0.680

Table of Contents

List of Tables

List of Figures

1. INTRODUCTION

This report describes the seismic hazard analysis conducted for the Yankee Doodle Tailings Impoundment site (YDTI, latitude 46.034°N and longitude 112.504°W) in Butte, Montana. This analysis is conducted as part of the engineering design work that Knight Piesold is performing to support a permit application for an impoundment raise to a design elevation of 6500 ft. Particularly, this study provides seismic parameters to be used as input to the downstream embankment stability analyses. A site location map is shown in Figure 1-1 and the project site layout is shown in Figure 1-2. The hazard results are provided for reference site class B/C (V_{S30} = 760 m/sec). The scope of work presented in this report includes the following tasks:

1. Perform a literature review to identify the relevant seismic sources and ground-motion models for the site.

2. Develop a seismic source characterization model based on the findings from the literature review in (1).

3. Develop a ground-motion characterization model to predict the median and aleatory variability of ground motions at the site from earthquakes defined in the seismic source model.

4. Conduct a probabilistic seismic hazard analysis (PSHA) for the site using the seismic source model and ground-motion models obtained in (2) and (3), respectively.

5. Conduct a deterministic seismic hazard analysis (DSHA) for the maximum credible earthquake (MCE) scenario on fault sources located in close proximity to the site.

6. Develop site-specific horizontal acceleration response spectra for earthquake ground motions covering the entire range of natural periods of vibration. Response spectra are provided for the following hazard levels:
   - DSHA 50th and 84th percentile horizontal response spectra for the MCE scenarios
   - PSHA uniform hazard spectra (UHS) for return periods of 475, 1,000, 2,475, and 10,000 years

7. Develop vertical response spectra for the horizontal spectra obtained in (6).

8. Perform a deterministic fault displacement analysis to evaluate the net and maximum surface displacement that may occur along the Continental fault.

9. Select and spectrally modify recorded ground-motion time series to be compatible with the design horizontal and vertical response spectra obtained from (6) and (7) (MCE, 475, 1,000, 2,475, and 10,000 years return period).

The next chapters of this report describe the inputs, methodology, and results obtained for the tasks listed above.

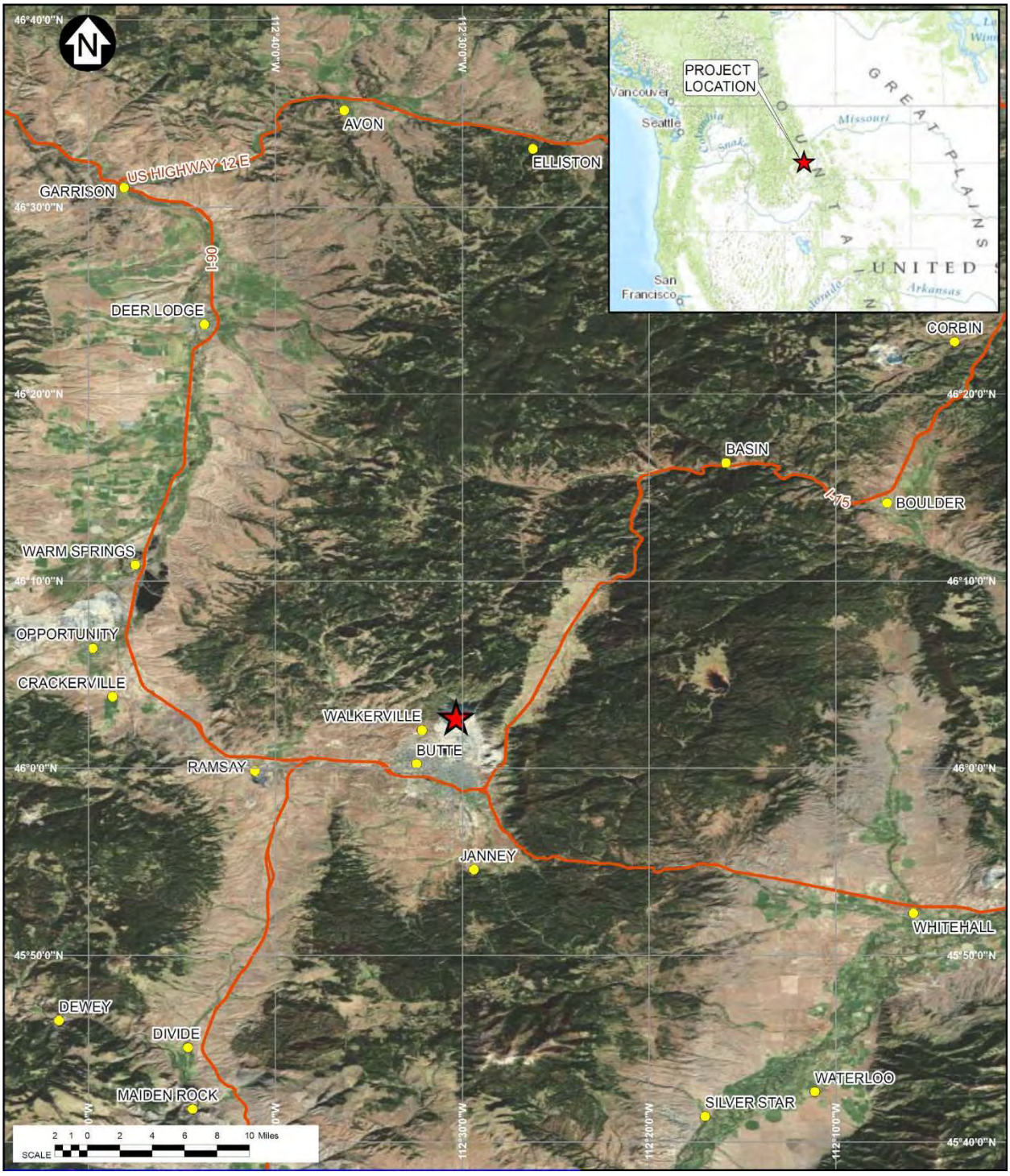

Figure 1-1. Site location map (source: Knight Piesold 2015)

Figure 1-2. Project site layout (source: Knight Piesold 2015)

2. LITERATURE REVIEW

A literature review of previous seismic hazard studies in western Montana was conducted to identify and assess the relevant seismic sources and ground-motion models previously developed for the seismicity in the region. Particularly, two studies were reviewed: probabilistic earthquake hazard maps for the state of Montana performed by Wong et al. (2005) and the 2014 United States Geological Survey (USGS) update to the national seismic hazard maps (NSHMs) documented in Petersen et al. (2014). A brief summary of these studies is given herein.

2.1 Probabilistic Earthquake Hazard Maps for the State of Montana

Wong et al. (2005) developed a set of probabilistic earthquake hazard maps for the Montana Department of Natural Resources and Conservation (DNRC) Dam safety program. Their seismic source characterization model included 92 faults, mostly located in western Montana, and background sources. Plate 1 of electronic Appendix I shows the historical (1809-2001) seismicity, Quaternary faults and regional seismic source zones in the state of Montana used in Wong et al. (2005). The quaternary faults in the proximity of Butte are shown in Plate 2a of electronic Appendix I. The faults located within 100 km from the YDTI site are listed in Table 2-1. Wong et al. (2005) characterized the faults in terms of probability of activity, geometry, rupture behavior, maximum magnitude (Mmax), recurrence model, and rates of activity. They noted that most of the quaternary faults in Montana have not been studied in any detail and relatively few data are available to constrain rates of activity. They relied on Quaternary fault compilations done by others and estimated maximum magnitudes based on fault lengths using the Wells and Coppersmith (1994) empirical relationships. For the background seismicity, Wong et al. (2005) used a catalog of historical earthquakes (1850 to 1999) to calculate recurrence rates for each of their nine regional seismic zones. For the background sources in western Montana, they adopted an Mmax of 6.5 ± 0.3.

For western Montana, Wong et al. (2005) used the following empirical ground-motion prediction equations (GMPEs): Abrahamson and Silva (1997), Spudich et al. (1997), Sadigh et al. (1997), and Campbell (1997). None of these models were specific to Montana due to the lack of recorded ground motions in the region. These models were subjectively weighted 0.4, 0.4, 0.1, and 0.1, respectively. To compensate for the lack of region-specific GMPEs, a stochastic single-corner source model with variable stress drop was used to develop a ground-motion model for western Montana and the details are presented in Wong et al. (2005). Both empirical and stochastic models were weighted 0.4 and 0.6, respectively, and used in the hazard analysis.

Wong et al. (2005) developed mean probabilistic hazard maps for peak ground acceleration (PGA) and spectral periods of 0.2 and 1.0 sec for return periods of 500, 2500, and 5000 years for soft rock site condition (NEHRP B/C site category) and at the ground surface. Their calculated PGA values on soft rock in Butte are 0.07, 0.12, and 0.17 g for the 500, 2500, and 5000 year return periods, respectively. Based on the published maps of Wong et al. (2005), the spectral accelerations on soft rock in the vicinity of the YDTI

site in Butte are listed in Table 2-2. In addition to these ground-motion values, their modal magnitude and distance deaggregation values for PGA on rock are listed in Table 2-3.

Table 2-1. Quaternary faults within 100 km from the YDTI site in the Wong et al. (2005) study

Fault Number	Fault Name
677	Beaver Creek fault
644	Blacktail fault
676	Boulder River Valley western border fault
690	Bull Mountain western border fault
671	Canyon Ferry fault
695	Carmichael fault
670	Central Park fault
688	Continental fault
694	Elk Creek fault
685	Fort Harrison fault
684	Franklin Mine Road fault
667	Georgia Gulch fault
678	Helena valley fault
674	Hilger fault
673	Indian Creek faults
672	Lower Duck Creek fault
655	Madison fault
680	Regulating Reservoir faults
669	Rocker fault
666	Ruby range northern border fault
665	Ruby Range western border fault
675	Soup Creek fault
681	Spokane Bench fault
679	Spokane Hills fault
645	Sweetwater fault
649	Tobacco Root fault
668	Vendome fault
689	Whitetail Creek fault

Table 2-2. Spectral accelerations on soft rock in the vicinity of the YDTI site in Butte based on the probabilistic earthquake hazard maps for the state of Montana (Wong et al. 2005) at PGA and spectral periods of 0.2 and 1.0 sec

	500 years	2500 years	5000 years
PGA	0.07 g	0.12 g	0.17 g
Sa (0.20 sec)	0 to 0.3 g	0.3 to 0.6 g	0.3 to 0.6 g
Sa (1.0 sec)	0 to 0.2 g	0 to 0.2 g	0 to 0.2 g

Table 2-3. Modal magnitude and distance deaggregation of the hazard on soft rock in the vicinity of the YDTI site in Butte based on the probabilistic earthquake hazard maps for the state of Montana (Wong et al. 2005) at PGA

	500 years	2500 years	5000 years
Magnitude	5.5 – 5.9	6.0 – 6.4	6.0 – 6.4
Distance (km)	31 – 40	11 – 20	3 – 10

2.2 The 2014 Update to the United States National Seismic Hazard Maps

In 2014, the USGS released a set of national seismic hazard maps (NSHMs) for the conterminous United States to update the 2008 set of maps accounting for new methods, models, and data available since the previous set of maps (Petersen et al. 2014). This update includes the development of an updated moment magnitude-based earthquake catalog through 2012, updated smoothing algorithms for background seismicity, the use of new ground-motion models, and numerous other updates. The maps are provided for a soft rock site condition with V_{S30} of 760 m/sec at PGA and spectral periods of 0.2 and 1.0 sec.

For western U.S. (WUS), the seismic source model in Petersen et al. (2014) includes seismicity-based background models and fault models. Historical seismicity (gridded and smoothed spatially) is used to estimate the hazard from earthquakes on unidentified fault sources. These models use the rates and distances from nearby historical earthquakes above a certain size to estimate the rate of future events. Geologic and geodetic data are used to estimate slip rates on faults. For the Intermountain West, the 2014 update of the maps includes new recommendations on fault modeling from the Basin and Range Province Earthquake Working Group incorporating a new earthquake catalog and background seismicity model as well as new geologic and geodetic inversion of slip rate models.

For WUS, the 2014 update to the NSHMs uses the newly-developed GMPEs from the Enhancement of Next Generation Attenuation Relationships for Western US (NGA-West2) project. These models and their assigned weights are listed in Table 2-4. Additional epistemic uncertainty to the median predictions was incorporated with these models based on the number of earthquakes used in the development of these GMPEs. Figures 2-1 and 2-2 show the logic trees for the background seismicity in WUS and the fault sources in the Intermountain West and the Pacific Northwest used in the 2014 update to the NSHMs. For a location in close proximity to the YDTI site (i.e., gridded USGS location is within 3 km of the YDTI site

location), the PGA and spectral acceleration values at 0.2 and 1.0 sec obtained from the 2014 NSHMs are given in Table 2-5 for return periods of 475, 1,000, 2,475, and 10,000 years.

Table 2-4. Ground-motion prediction equations used in the 2014 update to the NSHMs for crustal sources in WUS (source: Petersen et al. 2014)

GMPEs	Abbreviation	Source	Weight
Abrahamson et al. (2014)	ASK13	NGA-West2	0.22
Boore et al. (2014)	BSSA13	NGA-West2	0.22
Campbell and Bozorgnia (2014)	CB13	NGA-West2	0.22
Chiou and Youngs (2014)	CY13	NGA-West2	0.22
Idriss (2014)	I13	NGA-West2	0.12

Table 2-5. Spectral accelerations on soft rock with V_{S30} of 760 m/sec in the vicinity of the YDTI site at PGA and spectral periods of 0.2 and 1.0 sec based on the 2014 update to the NSHMs

	475 years	1,000 years	2,475 years	10,000 years
PGA	0.084 g	0.124 g	0.192 g	0.349 g
Sa (0.20 sec)	0.188 g	0.280 g	0.437 g	0.802 g
Sa (1.0 sec)	0.057 g	0.080 g	0.121 g	0.218 g

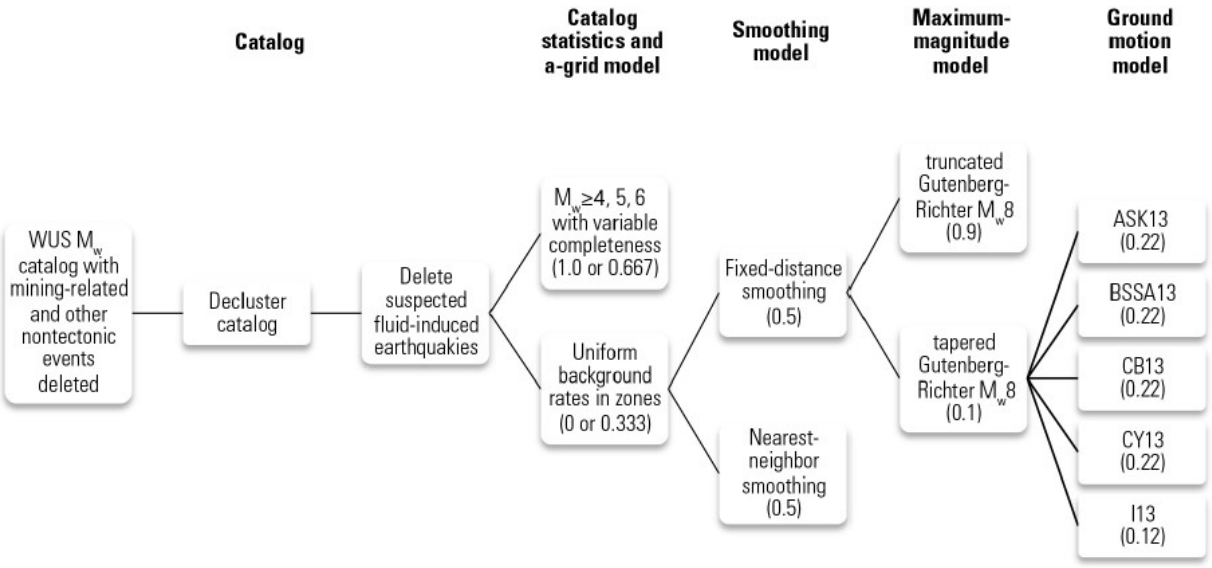

Figure 2-1. Logic tree for seismicity-based background sources in the WUS used in the development of the 2014 NSHMs. Assigned branch weights are shown in parentheses. (Source: Petersen et al. 2014)

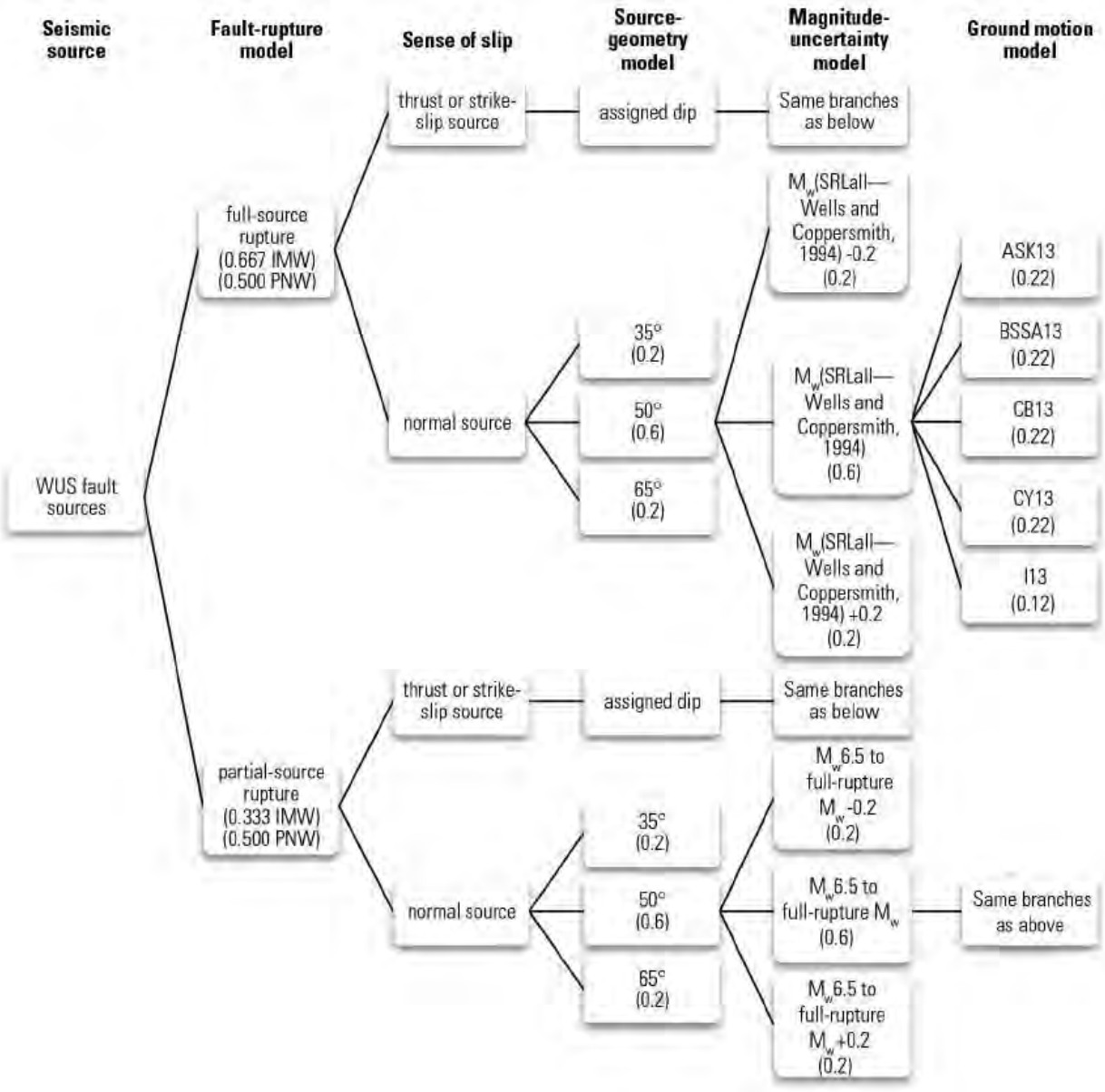

Figure 2-2. Logic tree for crustal sources in the Intermountain West and Pacific Northwest used in the development of the 2014 NSHMs. Assigned branch weights are shown in parentheses. (Source: Petersen et al. 2014)

3. SOURCE CHARACTERIZATION

The area of western Montana, located in the northern Intermountain region of the U.S., is characterized by a number of late-Quaternary Basin and Range normal faults and historical seismicity. The two largest historical events in the region are the 1959 Hebgen Lake earthquake with moment magnitude **M** 7.3 and the 1925 Clarkson earthquake with **M** 6.6 whose fault source remains unknown (Wong et al. 2005). The seismic source model used to compute the probabilistic hazard at the YDTI site is primarily based on the source model developed for the 2014 update to the National Seismic Hazard Maps (NSHMs). Updates to the NSHMs source model were made to incorporate fault sources from Wong et al. (2005) located in close proximity to the site but not included in the NSHMs source model. The seismic source model consists of a seismicity-based background source model and a fault-based source model as described below.

3.1 Seismicity-Based Background Model

The seismicity-based background model used for this study is based on the model developed by Petersen et al. (2014) as part of the 2014 update to the NSHMs with the logic tree shown in Figure 2-1. The parameters of the background model used in this study are listed in Table 3-1. The closest distance from source to site is also included in the table. The b-value, activity rate, and maximum earthquake magnitude describe the modeled magnitude recurrence within each individual source zone. On a log scale, the b-value is the slope of the Gutenberg-Richter distribution, relating the number of earthquakes in a given area over a fixed period of time to the magnitude of those earthquakes. Higher b-values, for example, lead to models that generate more small magnitude earthquakes with respect to larger magnitude earthquakes. The activity rate for the background sources is defined as the annual rate of earthquakes greater than or equal to a minimum magnitude of 5.0 [N(**M**>5)]. The maximum magnitude (Mmax) defines the upper truncation point for the magnitude recurrence models. The lower truncation point is defined by the minimum **M** of 5.0 for the background model used in the PSHA. The rates of different sized-earthquakes are based on a truncated exponential magnitude-frequency distribution.

Petersen et al. (2014) developed a composite, uniform seismicity catalog with moment magnitude for western North America through 2012. A b-value of 0.8 was used for the background sources based on the statistical analysis of the declustered catalog. The epicenters were spatially smoothed using a fixed-length and adaptive smoothing methods. These smoothing methods were given weights of 0.6 and 0.4, respectively.

Two alternative Mmax values were selected for the background model: **M** 7.45 and 7.95 with weights of 0.9 and 0.1, respectively. These Mmax values used in the 2014 update of the NSHMs are larger than those used in previous studies. This is due to several factors discussed in Petersen et al. (2014); particularly the incomplete inventory of potential sources and the fact that possible linkage of short faults into a long rupture is not considered in the current NSHMs source model. Moreover, the NSHMs source model does not include all known fault sources because most of the known Quaternary faults have insufficient

information to characterize recurrence rates of moderate to large magnitude earthquakes (Petersen et al. 2014).

Figures 3-1 and 3-2 show contour plots of the seismicity rate (a-value) for the extensional and compressional regime background sources, respectively, with respect to the YDTI site location. Each figure shows the a-value contours for the fixed and the adaptive smoothing methods. For the extensional regime source zone, Figure 3-1 shows that the fixed smoothing method results in a large area of higher seismicity towards the southeast of the YDTI site. The adaptive smoothing method results in more concentrated clusters of higher seismicity. Figure 3-2 shows that the seismicity associated with the compressional regime source zone is relatively low with the site located in an area of zero a-value for the fixed smoothing case.

Table 3-1. Source parameters of the seismicity-based background sources based on Petersen et al. (2014). Weights are given in parentheses. Magnitude recurrence model is the truncated exponential model and top of rupture is at 2 km.

Source	Source Name	Smoothing	Closest Distance to Site (km)	b-value	Mmin	Activity Rate - N(M>Mmin)	Mmax	Dip (degrees)	Sense of Slip
WUSExt	Extensional Regime	Fixed (0.6)	0.3	0.8	5.00	0.5567	7.45 (0.9)	45	Strike-Slip (0.33)
							7.95 (0.1)		Normal (0.67)
		Adaptive (0.4)	0.3	0.8	5.00	0.6674	7.45 (0.9)	45	Strike-Slip (0.33)
							7.95 (0.1)		Normal (0.67)
WUSCmp	Compressional Regime	Fixed (0.6)	103.4	0.8	5.00	0.0103	7.45 (0.9)	45	Strike-Slip (0.33)
							7.95 (0.1)		Reverse (0.67)
		Adaptive (0.4)	0.3	0.8	5.00	0.0161	7.45 (0.9)	45	Strike-Slip (0.33)
							7.95 (0.1)		Reverse (0.67)

3.2 Fault Sources

The fault sources used in this PSHA study are primarily based on the faults included in the USGS 2014 update to the NSHMs (Petersen et al. 2014) located within 200 km from the YDTI site. These fault sources are shown in Figure 3-3 and their parameters are summarized in Tables 3-2 to 3-4. A more detailed discussion on the fault parameters can be found in Petersen et al. (2014). The closest source-to-site distance is also listed in Tables 3-2 to 3-4. The Georgia Gulch fault is the closest fault from the USGS dataset to the YDTI site located at a distance of 49 km.

Petersen et al. (2014) modeled fault rupture as full-source rupture and floating partial-source ruptures that generate earthquakes with **M** 6.5 to the magnitude of the full-source rupture. These two models of rupture are given weights of 0.667 and 0.333, respectively. The magnitude recurrence for the full-source

ruptures is modeled with the maximum magnitude model (characteristic model) as a truncated normal distribution with a standard deviation σ of 0.12 and truncated on the lower end at 2σ. The truncated exponential model with a minimum **M** of 6.5 is used to model the magnitude recurrence on the partial-source ruptures. A b-value of 0.8 was used for all sources. The Well and Coppersmith (1994) relations were used to assign maximum magnitudes for the full-source ruptures of the faults. All the faults included in this analysis have normal sense of slip. Each fault source extends from the earth's surface to a depth of 15 km and is assigned a nominal dip angle of 50 $\pm$ 15 degrees.

Slip rate is used to characterize the activity on faults. Slip rate is a measure of the displacement on a fault resolved to the three-dimensional fault plane divided by the appropriate time period. The dimensions of the fault source constrain its maximum magnitude, which along with the slip rate determine the annual frequency of future earthquakes. Slip rates on fault sources were estimated using a geologic-based model with weight of 0.8 and two equally-weighted geodetic-based models (Bird 2013 and Zeng and Shen 2013) with a total weight of 0.2.

3.2.1 Continental and Rocker Faults

The NSHMs model includes a fault as a source of future earthquakes only if the paleoseismic history of this fault has been sufficiently studied and there is evidence of the size, extent of surface rupture, and timing of earthquakes (Petersen et al. 2014). Nearly 75 percent of the Quaternary faults in WUS are poorly understood and only characterized by location. These faults are not included in the NSHMs model and Petersen et al. (2014) acknowledges that these uncharacterized faults could generate significant earthquakes. Figure 3-3 shows fault sources located within 50 km from the YDTI site that were included in the Wong et al. (2015) study but not included in the NSHMs model. Of particular importance to this study are the Continental fault which intersects the YDTI site and the Rocker fault located at less than 10 km from the site. The source parameters for the Continental and Rocker faults are listed in Table 3-5.

A review of a compilation of Quaternary faults in western Montana by Haller et al. (2000) indicates that the Continental fault is a poorly studied fault (i.e., most studies associated with this fault are 40 or more years old). The presence of this fault is suggested on the basis of abrupt range-front topography and the reliability of its location is characterized as poor. No information is available on the rates of activity of this fault and associated scarps are not known. Wong et al. (2005) assigned inferred slip rates to the Continental fault based on lack of scarps.

The Rocker fault located to the southwest of the site was also included in Wong et al. (2005). Preliminary reconnaissance including a trench investigation has been conducted along some of the fault but little is known about its rate of activity (Haller et al. 2000). The reliability of the location of this fault is poor. Wong et al. (2005) inferred slip rates for the Rocker fault based on the absence of scarps on late Quaternary deposits and the presence of steep facets along the linear range front.

Given the proximity of the Continental and the Rocker faults to the YDTI site and because they were included as active sources in past studies (e.g., Wong et al. 2005 and the 2012 seismic study for the YDTI site), we include them in the seismic source model for this study with probability of activity of 1.0.

However, there is no conclusive evidence that these faults are active; particularly for the Continental fault (Stickney, personal communication). Because of the impact of the Continental fault on the results of the hazard analysis for the YDTI site, particularly on the deterministic results and the fault displacements, we recommend that a fault study be carried out to determine whether the Continental fault is indeed active.

The source parameters of the Continental and the Rocker faults used in this study are primarily based on Wong et al. (2005). Magnitude recurrence is modeled with the Youngs and Coppersmith (1985) composite model. Maximum magnitudes were estimated based on the Wells and Coppersmith (1994) relationships. A minimum **M** of 5.0 was used for these faults. Wong et al. (2005) assigned dip angles of 55, 30, and 70 degrees for the Continental fault with weights of 0.6, 0.2, and 0.2, respectively. Based on a review of later publications on the fault (Houston et al. 2013), we assign a dip of 70 degrees for the Continental fault. We note that using a dip angle of 70 degrees for the Continental fault versus the dip angles based on Wong et al. (2005) leads to almost identical results in the PSHA.

A sensitivity analysis was conducted to evaluate the impact of including additional faults from Wong et al. (2005) not included in the NSHMs model and located within 50 km from the site. This analysis showed that including these additional faults had only a minimal impact on the PSHA results. We, therefore, did not include them in the final source model.

Table 3-2. Source parameters of the faults based on Petersen et al. (2014). Weights are given in parentheses. All faults have a normal style-of-faulting and top of rupture is at 0 km.

Fault Number	Fault Name	Closest Distance to Site (km)	b-value	Mmin	Recurrence Model	Slip Rate (mm/yr)	Recurrence Interval (yr) (1)	Activity Rate - N(M>Mmin) (2)	Slip Rate / Recurrence Interval / Activity Rate Weight	Mmax	Dip (degrees)	Fault Width (km)	Fault Length (km)
667	Georgia Gulch fault	49.2	0.8	5.00	Max Mag (1)	0.040	14006	n/a	(0.8)	6.42 (0.6)	50 W (0.6)	15	14
						0.360	1575	n/a	(0.1)	6.22 (0.2)	35 W (0.2)		
						0.050	11338	n/a	(0.1)	6.62 (0.2)	65 W (0.2)		
678	Helena Valley fault	82.1	0.8	6.50	Max Mag (0.667) Trunc Exp (0.333)	0.013	57143	0.000023	(0.8)	6.60 (0.6)	50 S (0.6)	15	20
						0.050	14925	0.000087	(0.1)	6.40 (0.2)	35 S (0.2)		
						0.010	74627	0.000017	(0.1)	6.80 (0.2)	65 S (0.2)		
655	Madison fault	94.1	0.8	6.50	Max Mag (0.667) Trunc Exp (0.333)	0.522	4951	0.000285	(0.8)	7.45 (0.6)	50 W (0.6)	15	111
						0.510	5051	0.000278	(0.1)	7.25 (0.2)	35 W (0.2)		
						0.480	5376	0.000262	(0.1)	7.65 (0.2)	65 W (0.2)		
671	Canyon Ferry fault	87.7	0.8	6.50	Max Mag (0.667) Trunc Exp (0.333)	0.170	6993	0.000107	(0.8)	6.92 (0.6)	50 SW (0.6)	15	39
						0.070	16920	0.000044	(0.1)	6.72 (0.2)	35 SW (0.2)		
						0.220	5376	0.000139	(0.1)	7.12 (0.2)	65 SW (0.2)		
644	Blacktail fault	97.1	0.8	6.50	Max Mag (0.667) Trunc Exp (0.333)	0.039	31546	0.000025	(0.8)	6.94 (0.6)	50 NE (0.6)	15	40
						0.030	41153	0.000019	(0.1)	6.74 (0.2)	35 NE (0.2)		
						0.050	24691	0.000032	(0.1)	7.14 (0.2)	65 NE (0.2)		
645	Sweetwater fault	99.3	0.8	5.00	Max Mag (1)	0.052	10373	n/a	(0.8)	6.38 (0.6)	50 NE (0.6)	15	13
						0.100	5405	n/a	(0.1)	6.18 (0.2)	35 NE (0.2)		
						0.060	9009	n/a	(0.1)	6.58 (0.2)	65 NE (0.2)		
648	Red Rock Hills fault	123.3	0.8	5.00	Max Mag (1)	0.222	2041	n/a	(0.8)	6.27 (0.6)	50 W (0.6)	15	11
						0.180	2519	n/a	(0.1)	6.07 (0.2)	35 W (0.2)		
						0.220	2058	n/a	(0.1)	6.47 (0.2)	65 W (0.2)		

(1) Recurrence interval was used for the characteristic model

(2) Activity rate was used for the truncated exponential model

Table 3-3. Source parameters of the faults based on Petersen et al. (2014). Weights are given in parentheses. All faults have a normal style-of-faulting and top of rupture is at 0 km (cont'd).

Fault Number	Fault Name	Closest Distance to Site (km)	b-value	Mmin	Recurrence Model	Slip Rate (mm/yr)	Recurrence Interval (yr) (1)	Activity Rate - N(M>Mmin) (2)	Slip Rate / Recurrence Interval / Activity Rate Weight	Mmax	Dip (degrees)	Fault Width (km)	Fault Length (km)
641	Red Rock fault	137	0.8	6.50	Max Mag (0.667) Trunc Exp (0.333)	0.653	1372	0.000667	(0.8)	6.73 (0.6)	50 E (0.6)	15	27
						0.100	8929	0.000102	(0.1)	6.53 (0.2)	35 E (0.2)		
						0.820	1092	0.000839	(0.1)	6.93 (0.2)	65 E (0.2)		
603	Beaverhead fault	150.2	0.8	6.50	Trunc Exp (1)	0.157	n/a	0.000319	(0.8)	7.00 (0.6)	50 SW (0.6)	15	134
						0.310	n/a	0.000631	(0.1)	6.80 (0.2)	35 SW (0.2)		
						0.210	n/a	0.000428	(0.1)	7.20 (0.2)	65 SW (0.2)		
642	Emigrant fault	151.2	0.8	6.50	Max Mag (0.667) Trunc Exp (0.333)	0.326	4926	0.000168	(0.8)	7.12 (0.6)	50 NW (0.6)	15	57
						0.170	9259	0.000087	(0.1)	6.92 (0.2)	35 NW (0.2)		
						0.420	3759	0.000215	(0.1)	7.32 (0.2)	65 NW (0.2)		
656	Hebgen-Red Canyon fault	157.6	0.8	6.50	Max Mag (0.667) Trunc Exp (0.333)	0.653	10299	0.000094	(0.8)	7.30 (0.6)	50 SW (0.6)	15	25
						1.250	5376	0.000181	(0.1)	7.10 (0.2)	35 SW (0.2)		
						0.730	9174	0.000106	(0.1)	7.50 (0.2)	65 SW (0.2)		
643	Centennial fault	155.5	0.8	6.50	Max Mag (0.667) Trunc Exp (0.333)	0.914	1862	0.000504	(0.8)	7.17 (0.6)	50 N (0.6)	15	64
						0.910	1869	0.000501	(0.1)	6.97 (0.2)	35 N (0.2)		
						1.390	1224	0.000766	(0.1)	7.37 (0.2)	65 N (0.2)		
698	Jocko fault	160.8	0.8	5.00	Max Mag (1)	0.104	5814	n/a	(0.8)	6.47 (0.6)	50 NW (0.6)	15	16
						0.220	2770	n/a	(0.1)	6.27 (0.2)	35 NW (0.2)		
						0.100	6098	n/a	(0.1)	6.67 (0.2)	65 NW (0.2)		

(1) Recurrence interval was used for the characteristic model

(2) Activity rate was used for the truncated exponential model

Table 3-4. Source parameters of the faults based on Petersen et al. (2014). Weights are given in parentheses. All faults have a normal style-of-faulting and top of rupture is at 0 km (cont'd).

Fault Number	Fault Name	Closest Distance to Site (km)	b-value	Mmin	Recurrence Model	Slip Rate (mm/yr)	Recurrence Interval (yr) (1)	Activity Rate - N(M>Mmin) (2)	Slip Rate / Recurrence Interval / Activity Rate Weight	Mmax	Dip (degrees)	Fault Width (km)	Fault Length (km)
699	Mission fault	173.4	0.8	6.50	Max Mag (0.667) Trunc Exp (0.333)	0.418	5435	0.000208	(0.8)	7.36 (0.6)	50 W (0.6)	15	92
						0.280	8065	0.000139	(0.1)	7.16 (0.2)	35 W (0.2)		
						0.430	5263	0.000214	(0.1)	7.56 (0.2)	65 W (0.2)		
602	Lemhi fault	189.9	0.8	6.50	Trunc Exp (1)	0.287	n/a	0.000642	(0.8)	7.00 (0.6)	50 SW (0.6)	15	147
						0.310	n/a	0.000693	(0.1)	6.80 (0.2)	35 SW (0.2)		
						0.380	n/a	0.000849	(0.1)	7.20 (0.2)	65 SW (0.2)		

(1) Recurrence interval was used for the characteristic model

(2) Activity rate was used for the truncated exponential model

Table 3-5. Source parameters of the Continental and Rocker faults based on Wong et al. (2005). Weights are given in parentheses.

Fault Number	Fault Name	Closest Distance to Site (km)	b-value	Mmin	Recurrence Model	Slip Rate (mm/yr)	Mmax	Slip Sense	Dip (degrees)	Rupture Top (km)	Fault Width (km)	Fault Length (km)
688	Continental fault	1.2	0.8	5.00	Y & C	0.020 (0.6)	6.5 (0.6)	Normal	70 W	0	15 (0.6)	18.2
						0.005 (0.2)	6.2 (0.2)				12 (0.2)	
						0.120 (0.2)	6.8 (0.2)				18 (0.2)	
669	Rocker fault	8.5	0.8	5.00	Y & C	0.020 (0.6)	7.0 (0.6)	Normal	55 W (0.6)	0	15 (0.6)	43.5
						0.005 (0.2)	6.7 (0.2)		30 W (0.2)		12 (0.2)	
						0.120 (0.2)	7.3 (0.2)		70 W (0.2)		18 (0.2)	

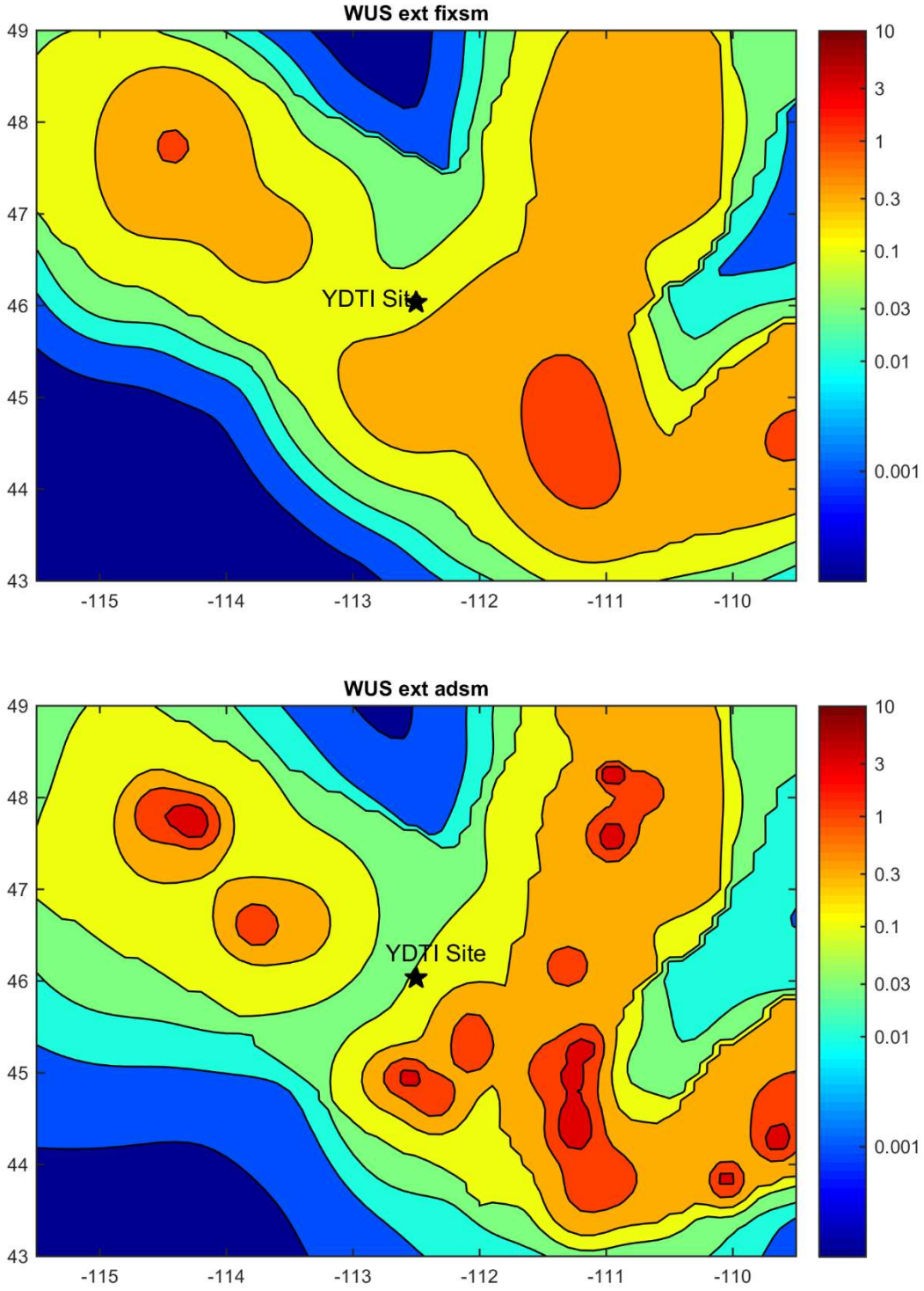

Figure 3-1. Seismicity rate (a-value) contour plots for the extensional regime background source for the fixed smoothing method (top) and adaptive smoothing method (bottom)

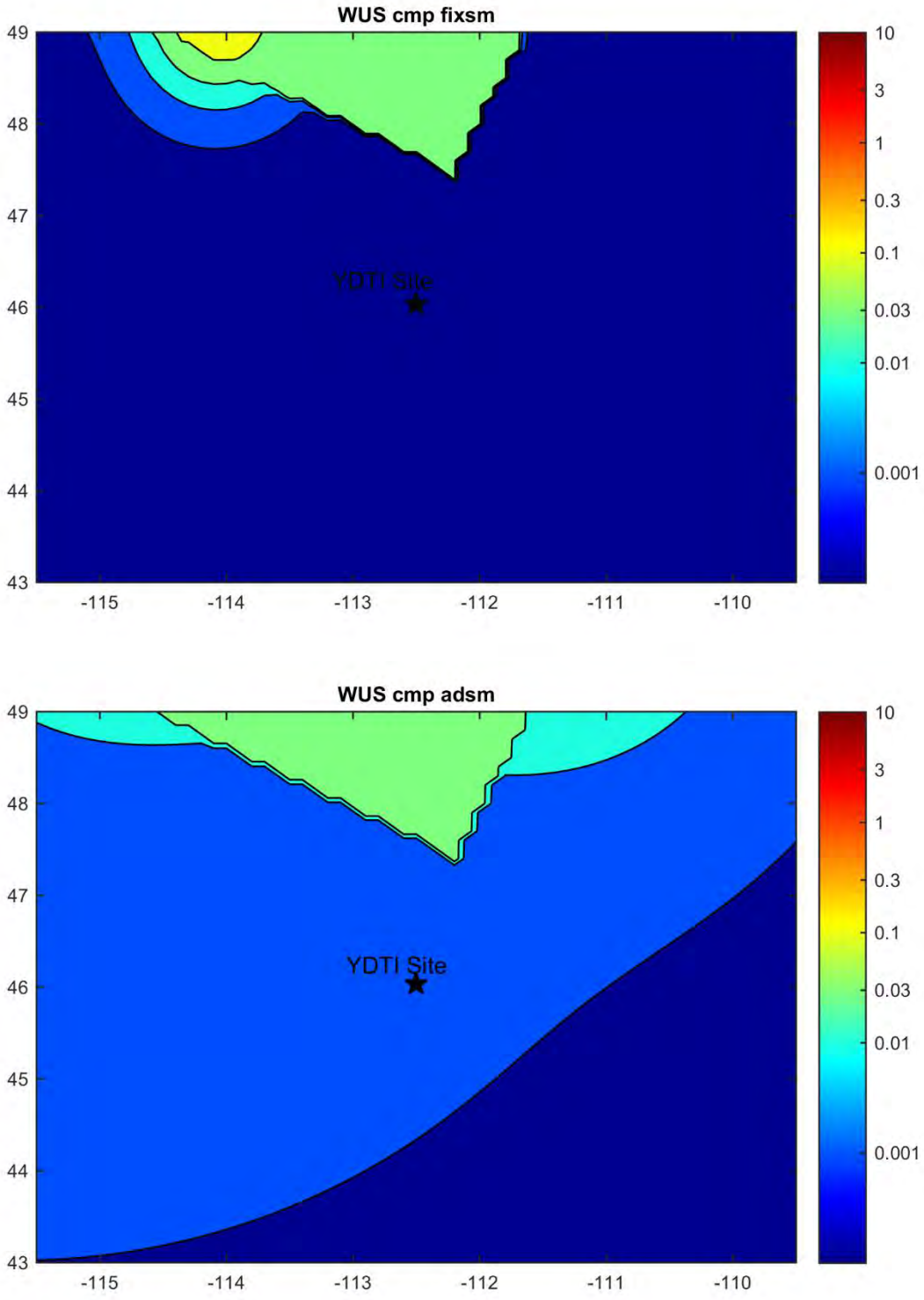

Figure 3-2. Seismicity rate (a-value) contour plots for the compressional regime background source for the fixed smoothing method (top) and adaptive smoothing method (bottom)

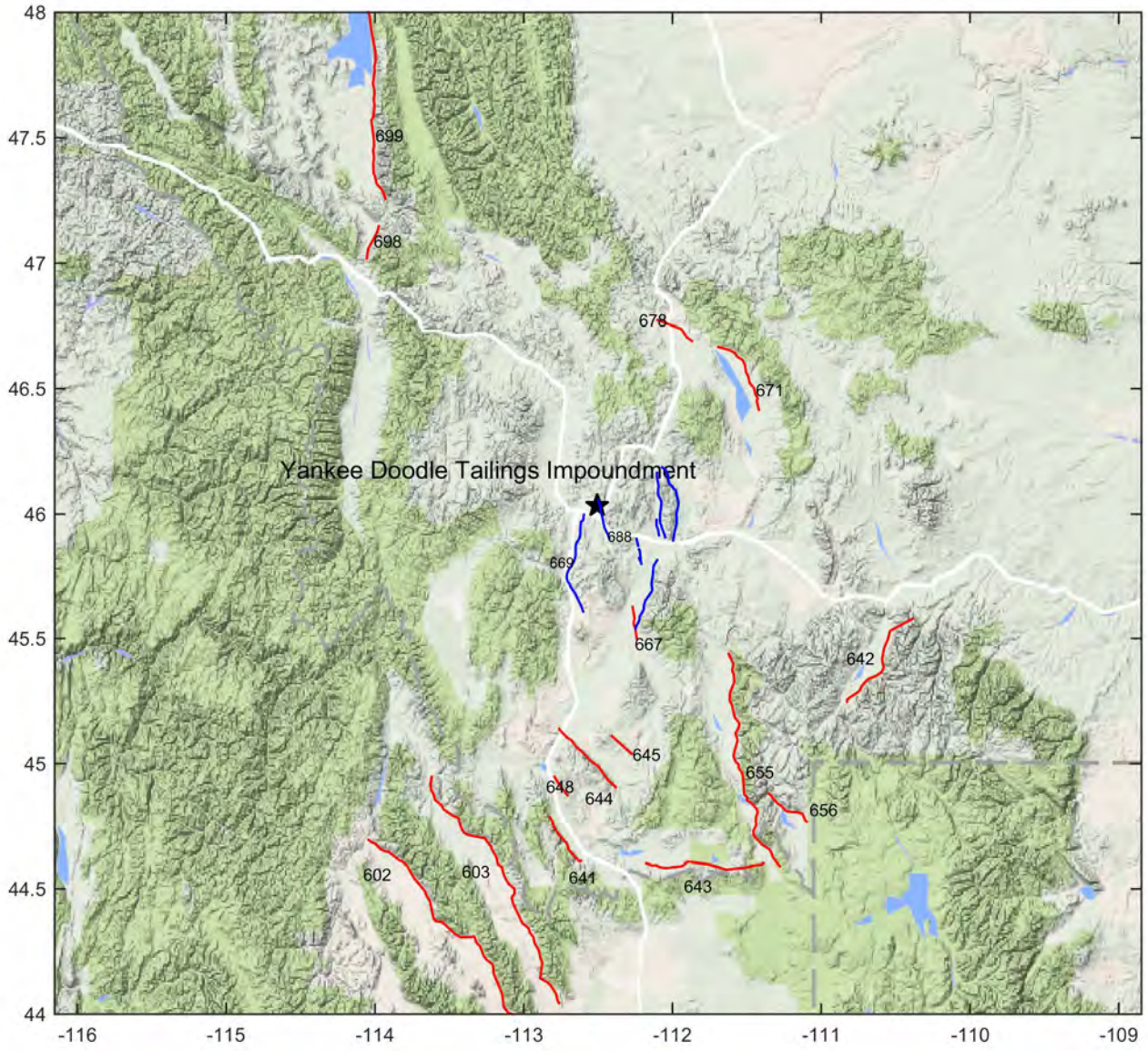

Figure 3-3. Fault sources in the vicinity of the YDTI site. Faults in red are based on the NSHMs model (Petersen et al. 2014). Faults in blue are additional faults based on Wong et al. (2005) within 50 km of the site.

4. GROUND MOTION PREDICTION EQUATIONS

In the 2014 update to the NSHMs, the USGS used five NGA-West2 models to predict the ground motion in WUS with weights shown in Table 2-4. Additional epistemic uncertainty was assigned to the median predictions of these GMPEs based on the number of earthquakes used in developing the models. For this PSHA study, we evaluated the use of the five NGA-West2 GMPEs as well as the stochastic-based GMPE of Wong et al. (2005) specifically developed for western Montana.

The NGA-West2 GMPEs were selected over their predecessor NGA-West1 (NGA-West 2008) models because of improvements in these more recent models such as expanded earthquake database particularly in the large distance and small magnitude range, improvements in the small-magnitude scaling and large-distance scaling of the GMPEs, and in the quality of the site data and shear-wave velocity classification. Moreover, the NGA-West2 GMPEs have a larger magnitude and distance applicability range compared to the NGA-West1 models and are therefore more suited for this study.

Wong et al. (2005) developed a stochastic-based GMPE for eastern and western Montana to compensate for the lack of region-specific ground-motion models. The point-source stochastic model was used to model earthquakes with **M** 5.5, 6.5, and 7.5 in the distance range of 1 to 400 km. A single-corner source model with variable stress drop was used for western Montana. The final model, which is a function of magnitude and rupture distance, was developed for soft-rock site condition with V_{S30} of 760 m/sec.

We used recorded ground-motion data from the Helena MT (mainshock and aftershock) and the Dillon MT earthquakes to evaluate the applicability of the NGA-West2 GMPEs and the stochastic GMPE of Wong et al. (2005) (median models) to western Montana. The parameters of the ground-motion recordings used in this evaluation are listed in Table 4-1. For the Dillon earthquake, recordings located at distance less than 200 km are used for the comparisons and V_{S30} of 550 m/sec was assumed for the stations that are not part of the NGA-West2 database. The Helena and the Dillon earthquakes have **M** of 6.0 and 5.6, respectively. Only one recording at short source-to-site distance is available from each of the two Helena earthquakes. Seven recordings from the Dillon earthquake are available with source-to-site distances of 23 to 198 km.

Figures 4-1 to 4-9 show comparisons of the response spectra for the recorded ground motion (two horizontal components and their geometric mean) to the median ground-motion predictions from the NGA-West2 and the stochastic GMPEs. The average response spectra of the five equally-weighted NGA-West2 GMPEs are also shown in the figures. Figure 4-1 indicates that the median stochastic-based GMPE of Wong et al. (2005) fits better the Helena mainshock recording than the median of the NGA-West2 GMPEs, while all of the GMPEs predict spectra that are significantly larger than the recorded Helena aftershock shown in Figure 4-2. For the Dillon earthquake recordings, Figures 4-3 to 4-9 indicate that the median predictions of the NGA-West2 and the stochastic-based GMPEs generally fit the recorded data reasonably well, particularly for the short-distance recordings. In general, the stochastic-based GMPE of Wong et al. (2005) predicts lower median ground motions than the NGA-West2 GMPEs.

Based on these comparisons, we assign to the median NGA-West2 GMPEs and the stochastic-based median GMPE weights of 0.667 and 0.333, respectively. A higher weight is given to the NGA-West2 GMPEs because these models are based on a large empirical dataset and have features that represent significant advances in ground-motion modeling. All five NGA-West2 GMPEs are given equal weight because Figures 4-1 to 4-9 showed similar behavior of the median spectra from all five GMPEs. Because the NGA-West2 GMPEs were developed in a collaborative effort with interactions and exchange of ideas among the developers, the NGA-West2 developers indicated that additional epistemic uncertainty needs to be incorporated into the median ground-motion estimation from their GMPEs. The proposed additional epistemic uncertainty model of Al Atik and Youngs (2014) was used in this study. The additional epistemic uncertainty is distance-independent but depends on magnitude, style-of-faulting, and spectral period with the largest uncertainty assigned to normal style-of-faulting. We note that using the equally-weighted NGA-West2 GMPEs with additional epistemic uncertainty on the median predictions based on Al Atik and Youngs (2014) results in very similar results to those obtained with the NGA-West2 implementation of the NSHMs. The median ground motion logic tree used in this study is shown in Figure 4-10.

The aleatory variability model of the stochastic-based GMPE of Wong et al. (2005) was compared to the NGA-West2 aleatory models. The standard deviation model of Wong et al. (2005) is homoscedastic and period-dependent while the NGA-West2 standard deviation models are magnitude- and period-dependent. Figure 4-11 presents a comparison of the Wong et al. (2005) and NGA-West2 (computed for **M** 6.5) standard deviation models. Figure 4-11 shows that the Wong et al. (2005) standard deviation model is significantly larger than the corresponding NGA-West2 models and is larger than 1.0 at periods greater than 2.0 sec. This large aleatory variability of Wong et al. (2005) is not only the result of ground-motion variations but also reflects the limitations in the stochastic modeling process. Therefore, we use the median ground-motion model of Wong et al. (2005) along with the standard deviation model of Abrahamson et al. (2014) in this PSHA study. Uncoupling the median and the variability models is considered standard practice in PSHA studies (e.g., Renault et al. 2010, Coppersmith et al. 2014, GeoPentech 2015) and it allows the use of reliable variability models that are based on empirical data. The aleatory variability models published with each of the five NGA-West2 GMPEs were used along with the GMPE-specific median predictions. A sigma truncation value of 6.0 was used for the PSHA.

Table 4-1. Parameters of the ground-motion recordings from earthquakes in western Montana

Earthquake	Station	Magnitude	Style of Faulting	Dip	Top of Rupture (km)	R_{rup} (km)	R_{jb} (km)	V_{S30} (m/sec)
Helena, MT	Carrol College	6.0	Strike-slip	90	0	2.86	2.07	593.35
Helena Aftershock, MT	Helena Fed Bldg	6.0	Strike-slip	90	0	2.92	2.09	551.82
Dillon, MT	University of Montana Western	5.6	Normal(1)	60	0	22.8	22.2	550(2)
Dillon, MT	Montana Tech	5.6	Normal(1)	60	0	68.2	68.0	550(2)
Dillon, MT	Hebgen Lake Ranger Station	5.6	Normal(1)	60	0	115.2	115.1	550(2)
Dillon, MT	Montana State Univ.	5.6	Normal(1)	60	0	117.3	117.2	550(2)
Dillon, MT	Carroll College	5.6	Normal(1)	60	0	139.4	139.3	593.35
Dillon, MT	Ft. Harrison VA Hospital	5.6	Normal(1)	60	0	140	139.9	550(2)
Dillon, MT	Missoula Fire Station #1	5.6	Normal(1)	60	0	198.2	198.1	550(2)

(1) Station located on the footwall
(2) Assumed V_{S30} values

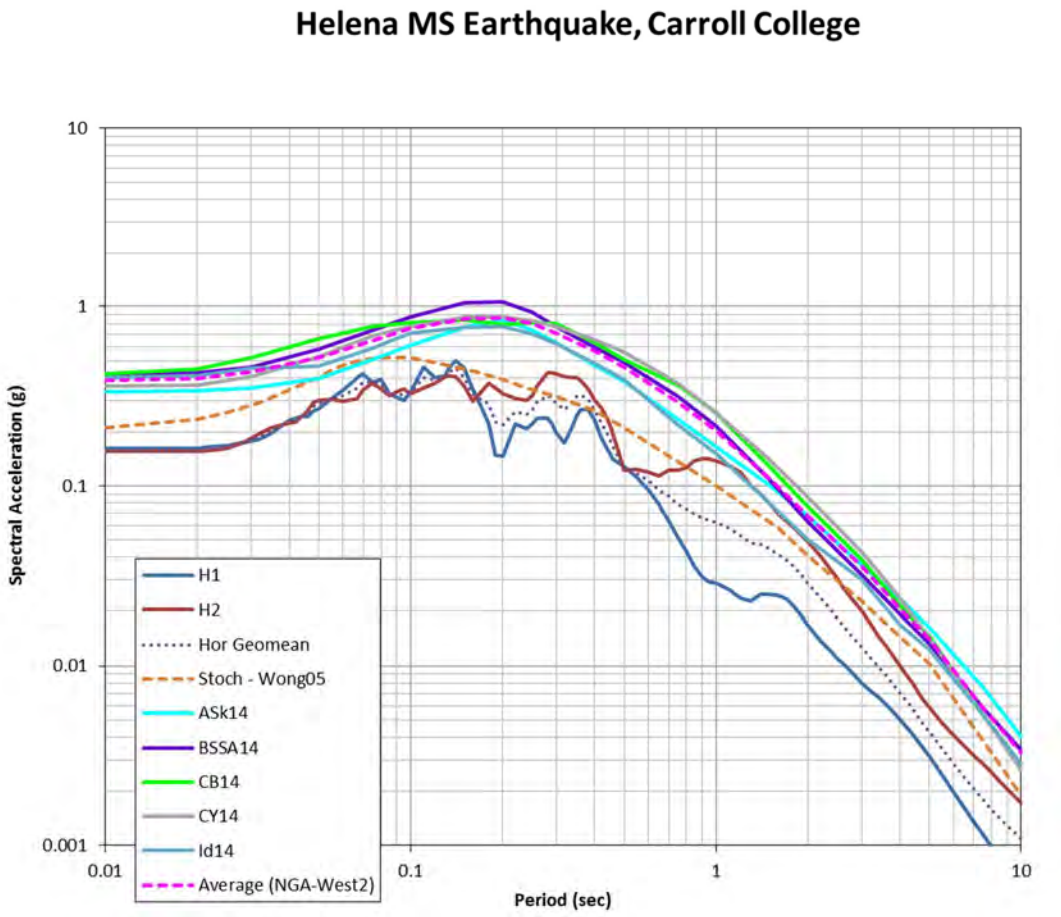

Figure 4-1. Comparison of recorded horizontal response spectra from the Helena mainshock earthquake at Carroll College to median response spectra predicted by the NGA-West2 GMPEs and the stochastic-based GMPE of Wong et al. (2005)

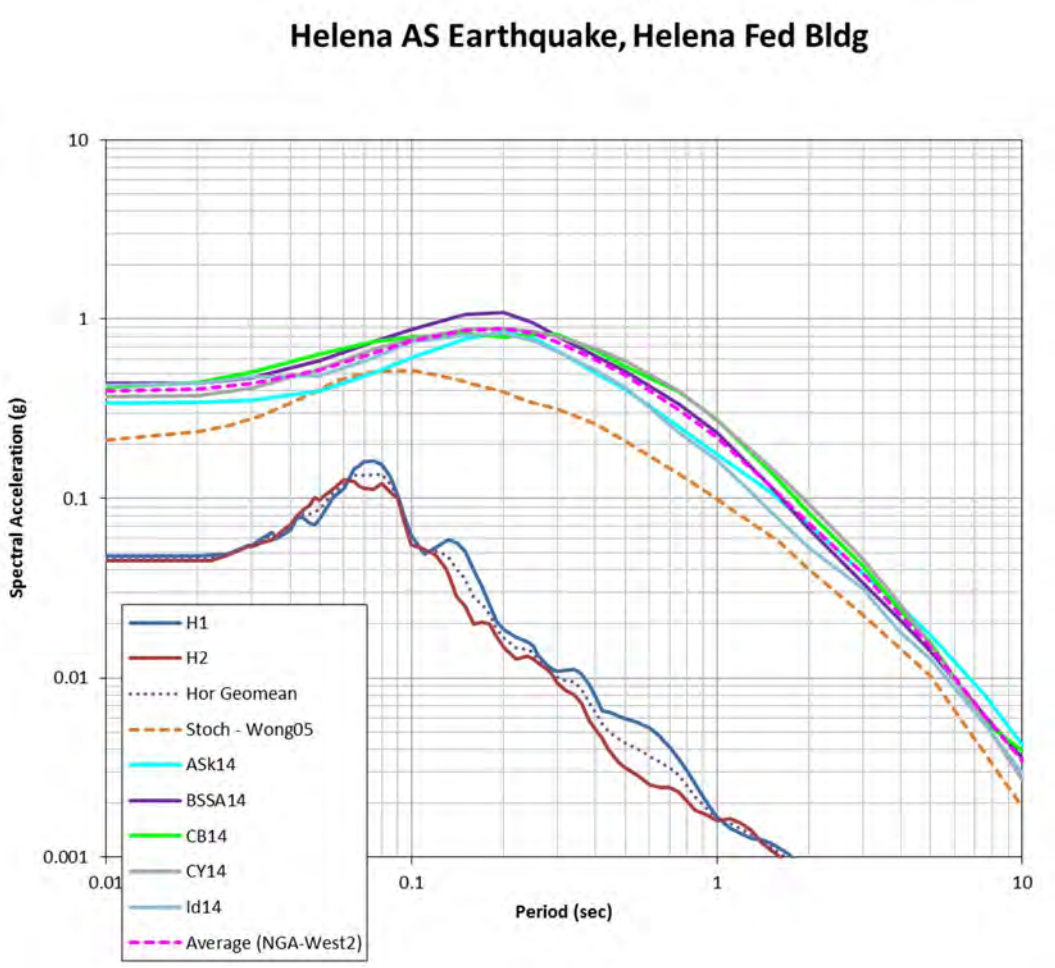

Figure 4-2. Comparison of recorded horizontal response spectra from the Helena aftershock earthquake at Helena Fed. Bldg. to median response spectra predicted by the NGA-West2 GMPEs and the stochastic-based GMPE of Wong et al. (2005)

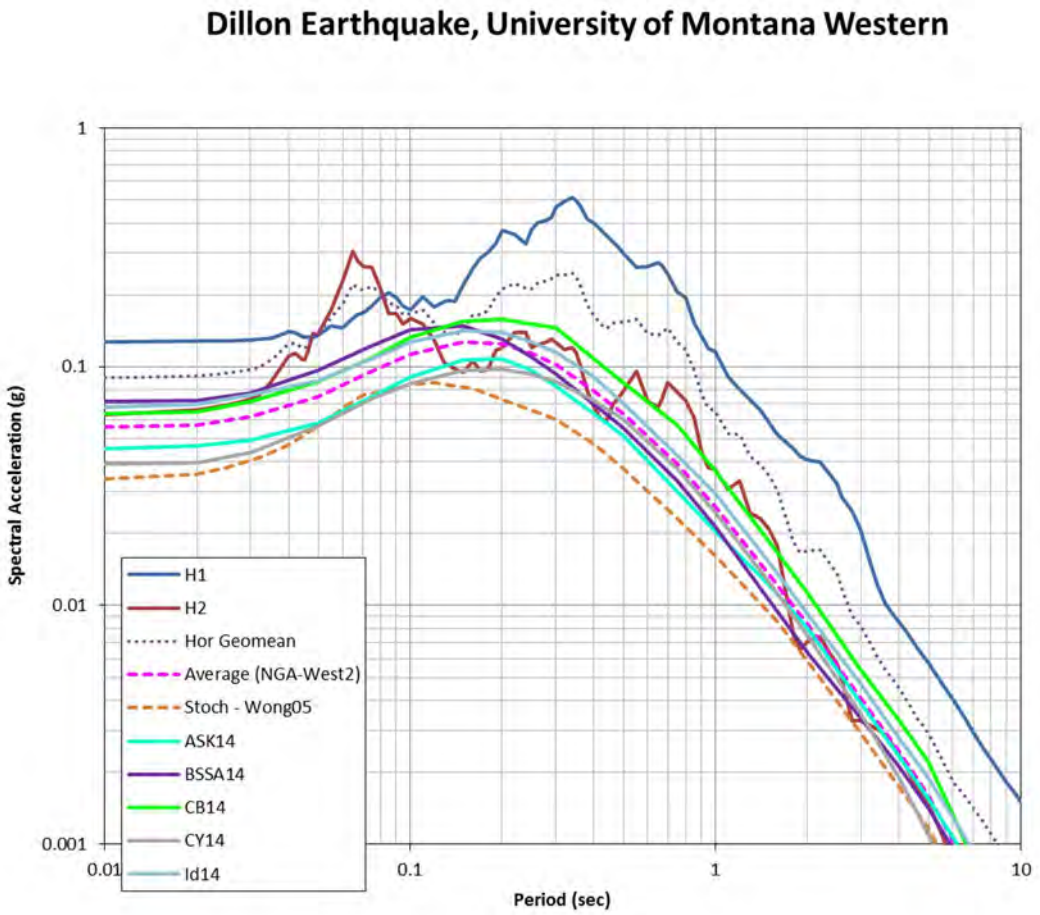

Figure 4-3. Comparison of recorded horizontal response spectra from the Dillon earthquake at the University of Montana Western to median response spectra predicted by the NGA-West2 GMPEs and the stochastic-based GMPE of Wong et al. (2005)

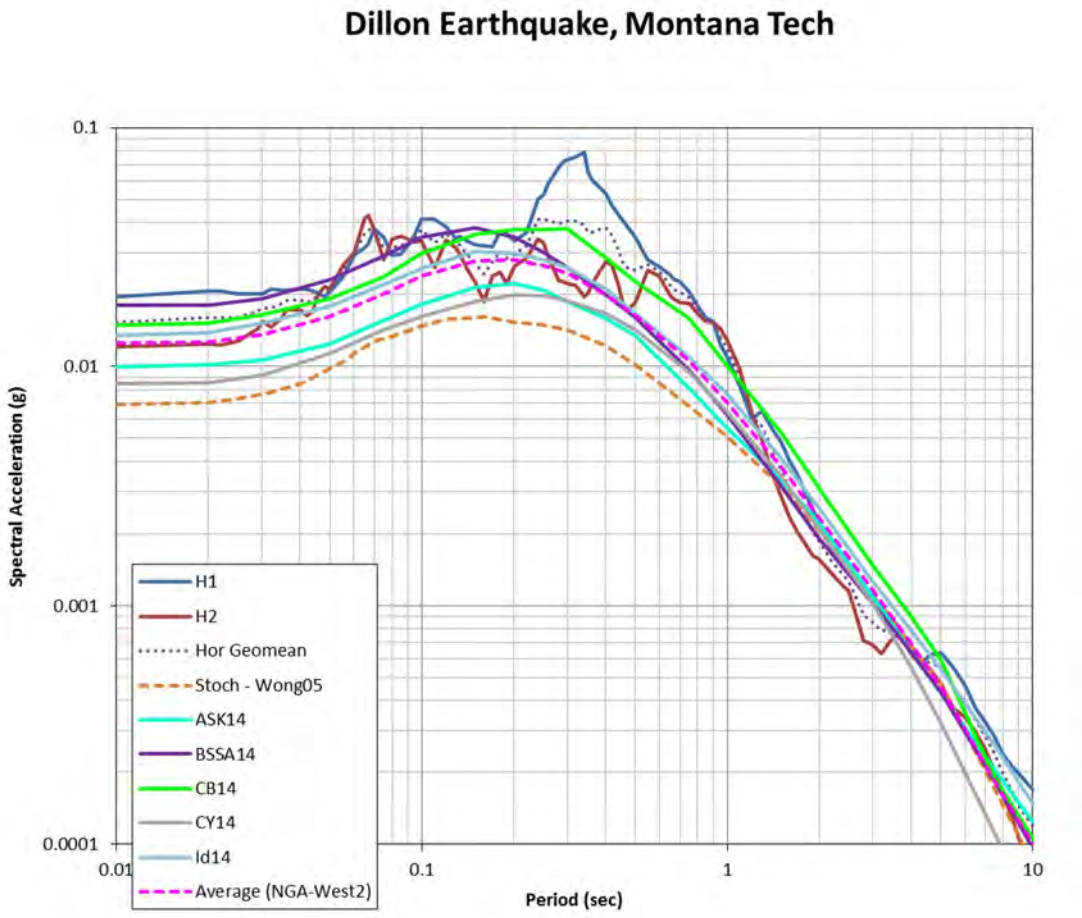

Figure 4-4. Comparison of recorded horizontal response spectra from the Dillon earthquake at Montana Tech to median response spectra predicted by the NGA-West2 GMPEs and the stochastic-based GMPE of Wong et al. (2005)

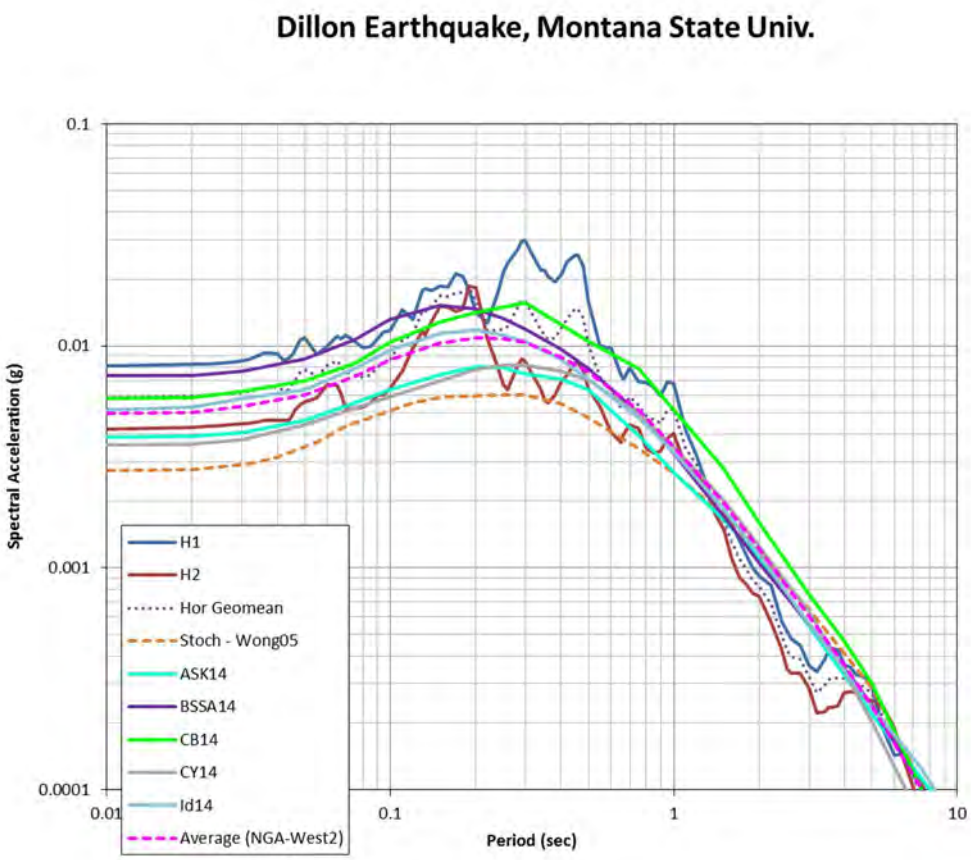

Figure 4-5. Comparison of recorded horizontal response spectra from the Dillon earthquake at Montana State University to median response spectra predicted by the NGA-West2 GMPEs and the stochastic-based GMPE of Wong et al. (2005)

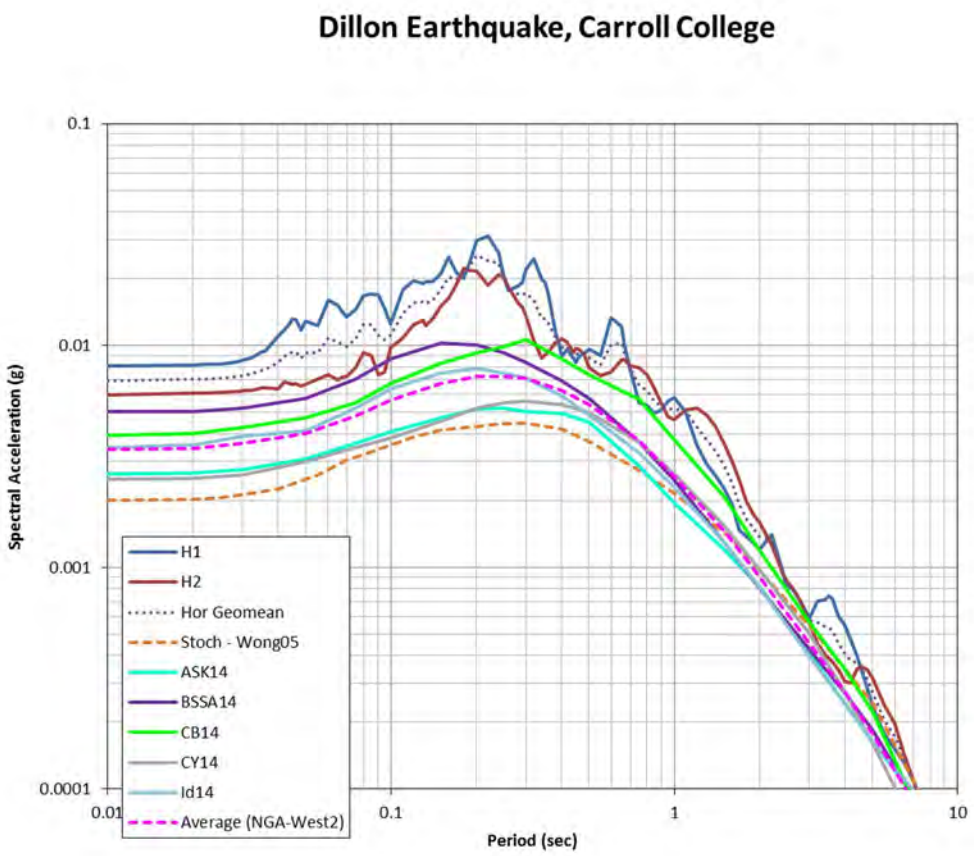

Figure 4-6. Comparison of recorded horizontal response spectra from the Dillon earthquake at Carroll College to median response spectra predicted by the NGA-West2 GMPEs and the stochastic-based GMPE of Wong et al. (2005)

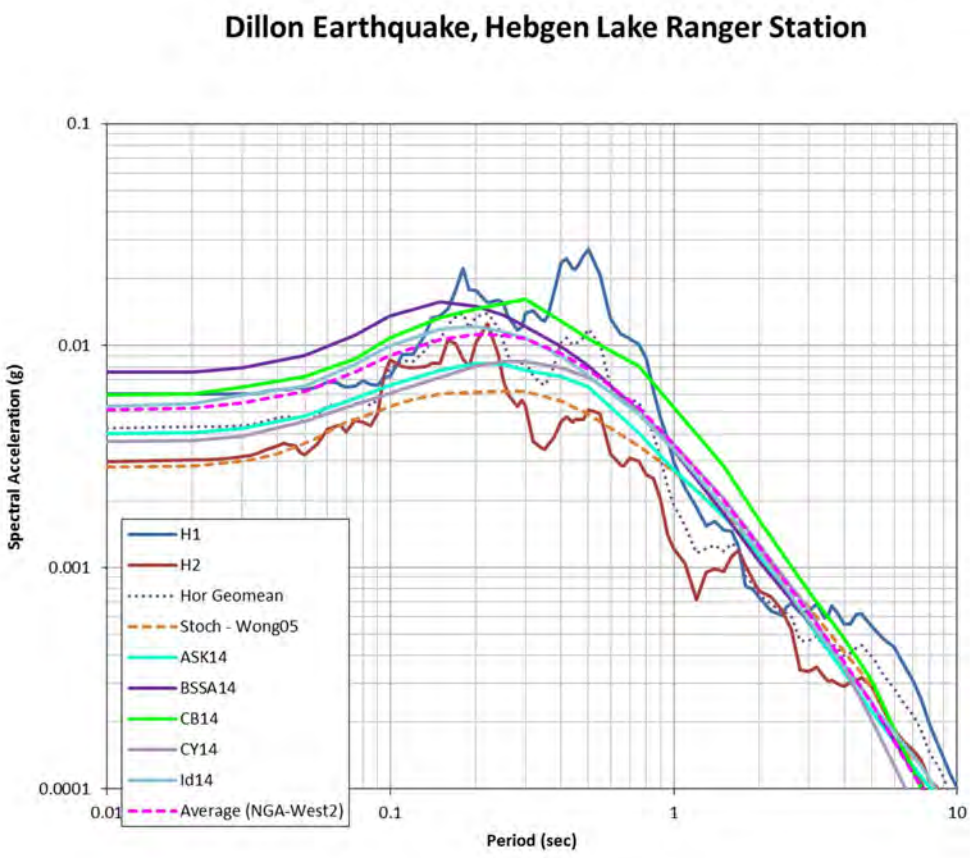

Figure 4-7. Comparison of recorded horizontal response spectra from the Dillon earthquake at Hebgen Lake Ranger Station to median response spectra predicted by the NGA-West2 GMPEs and the stochastic-based GMPE of Wong et al. (2005)

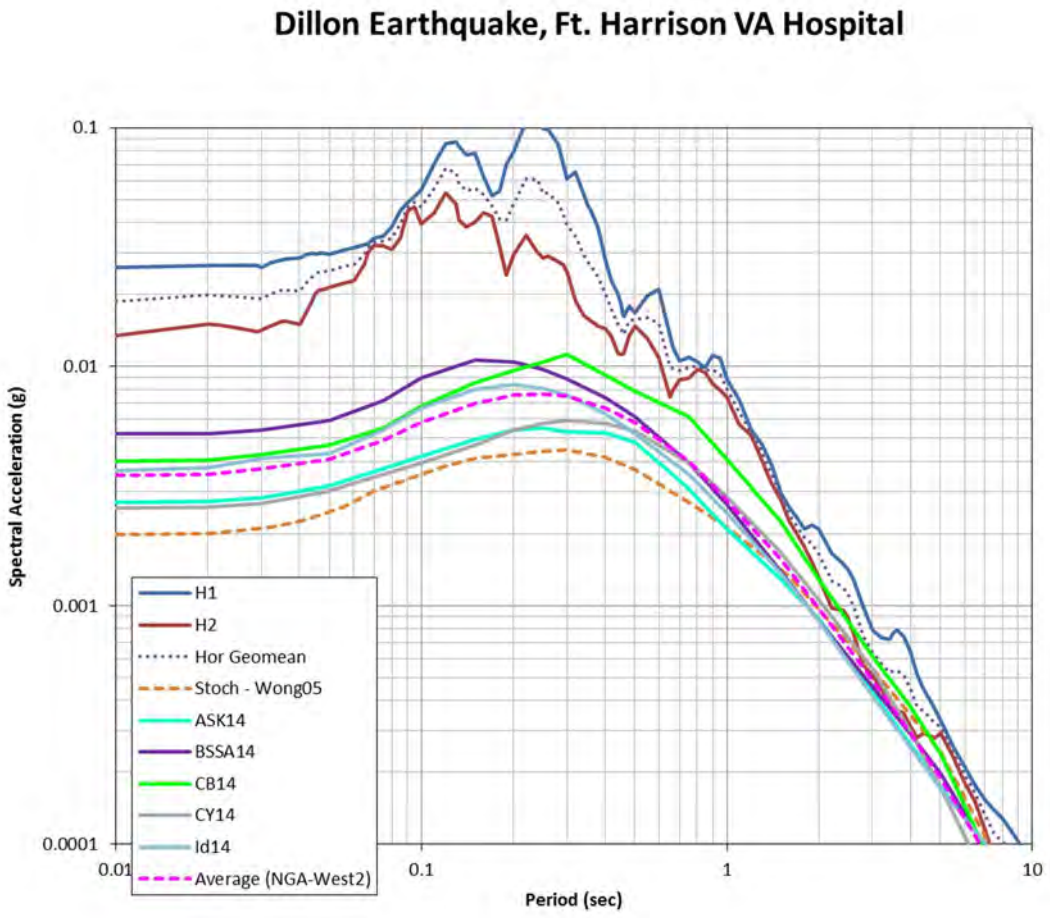

Figure 4-8. Comparison of recorded horizontal response spectra from the Dillon earthquake at Ft. Harrison VA Hospital to median response spectra predicted by the NGA-West2 GMPEs and the stochastic-based GMPE of Wong et al. (2005)

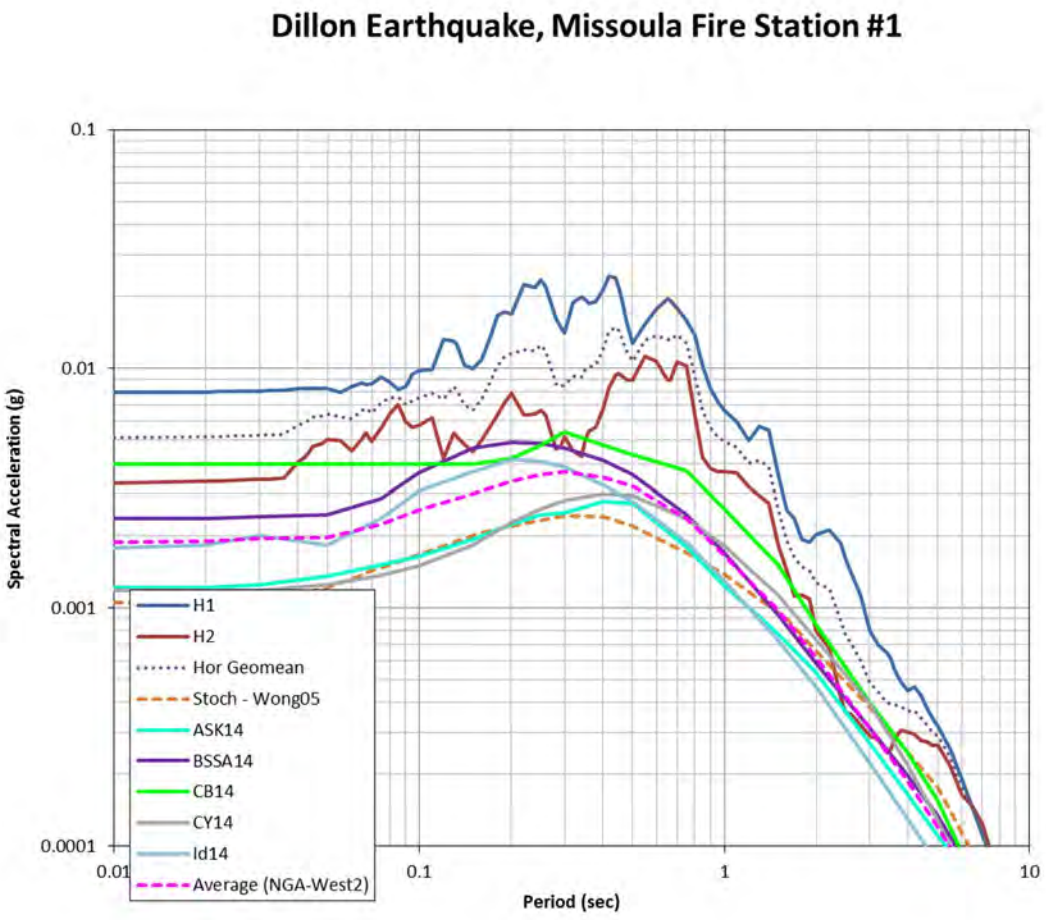

Figure 4-9. Comparison of recorded horizontal response spectra from the Dillon earthquake at Missoula Fire Station #1 to median response spectra predicted by the NGA-West2 GMPEs and the stochastic-based GMPE of Wong et al. (2005)

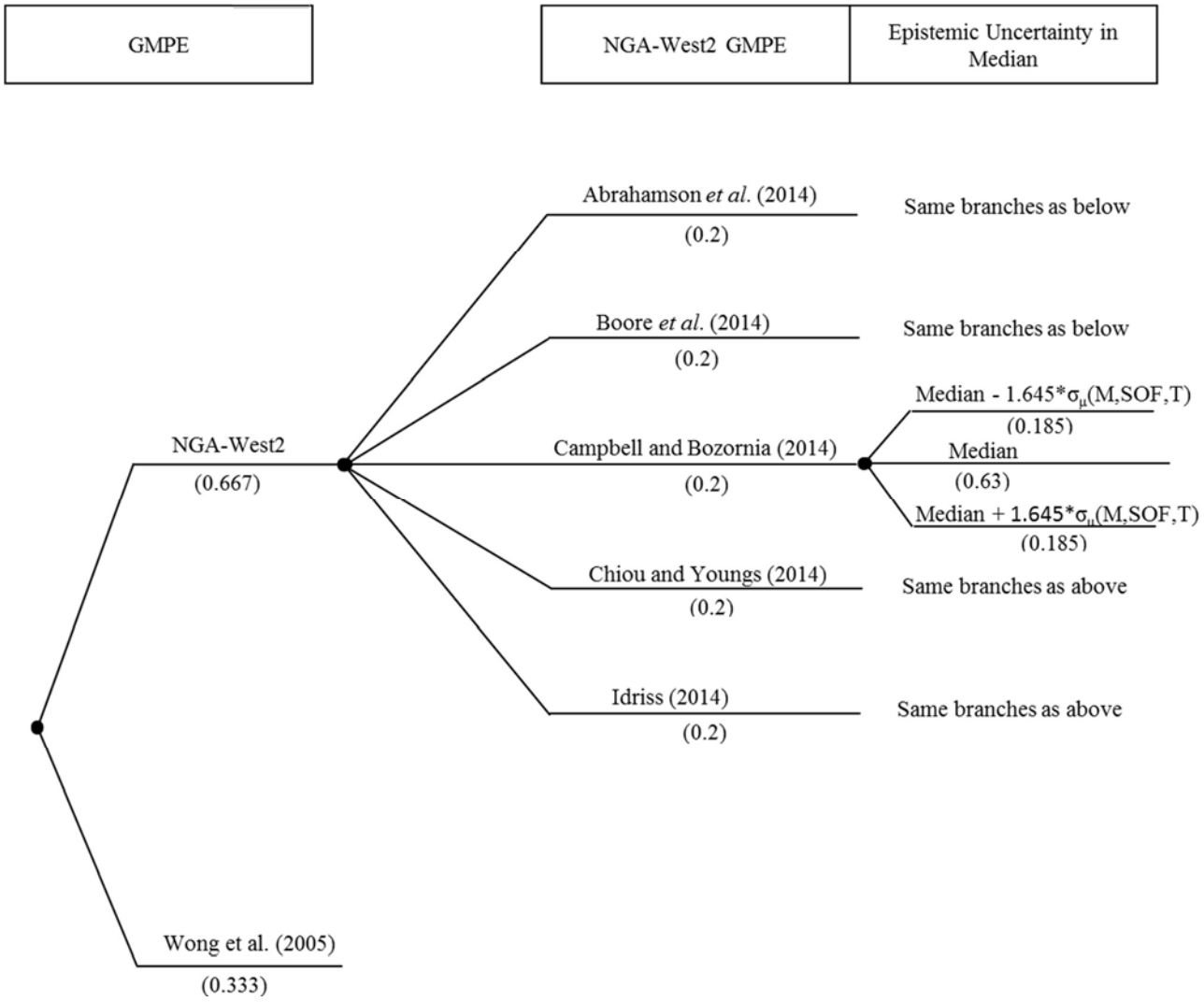

Figure 4-10. Logic tree for the median ground-motion model used in this study. σ refers to the additional epistemic uncertainty in LN units based on Al Atik and Youngs (2014). M refers to magnitude, SOF to style-of-faulting, and T to spectral period.

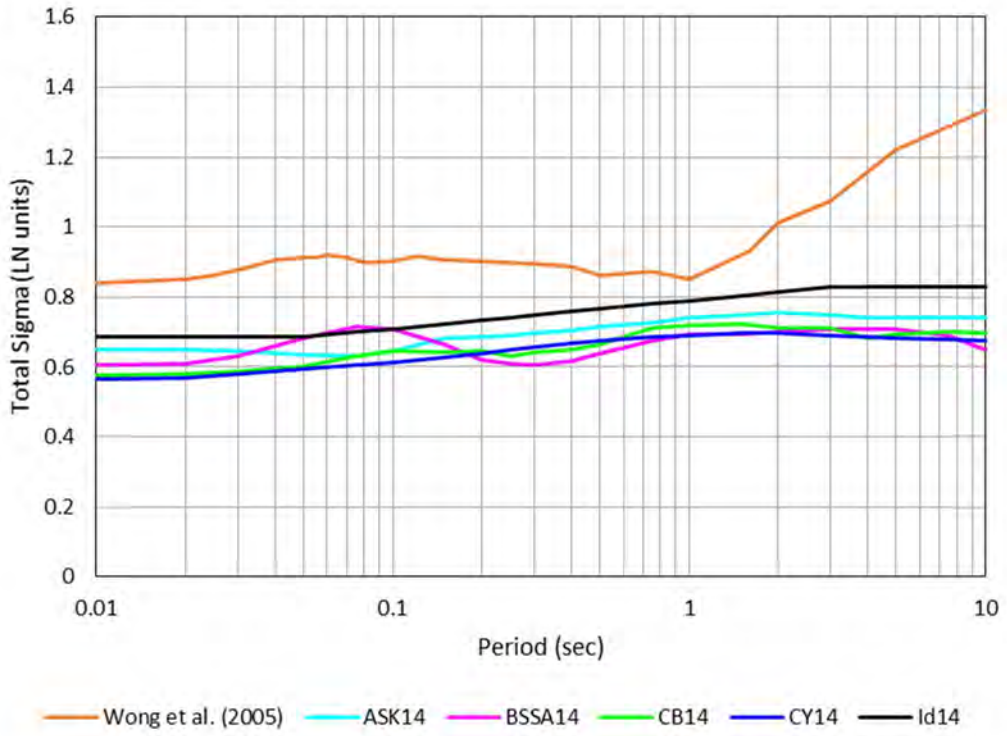

Figure 4-11. Comparison of the aleatory variability models of Wong et al. (2005) and the NGA-West2 models for M 6.5

5. HAZARD RESULTS

5.1 PSHA Results

Probabilistic seismic hazard calculations were carried out using the computer program Haz45 (Abrahamson and Gregor 2015). Probabilistic mean hazard curves are shown in Figures 5-1 to 5-3 for PGA and periods of 0.2, and 1 sec, respectively, for the YDTI site. The hazard curves are shown by source for the important sources controlling the hazard at the site. The hazard curves obtained from the 2014 NSHMs at a nearby location to the YDTI site at PGA and periods of 0.2 and 1 sec are also included in the plots for comparison. Figures 5-1 to 5-3 show that at all three spectral periods, the seismicity-based background sources control the hazard at return periods less than about 10,000 years. At the 10,000 year return period, the Continental fault has a significant contribution to the hazard at all three spectral periods with the background sources still having larger contribution. The fault sources based on the NSHMs model and located at distance of 49 to 200 km from the YDTI site have small contribution to the hazard. The Rocker fault is a contributor to the hazard at the site but to a less extend than the Continental fault.

Figures 5-1 to 5-3 show that the total calculated hazard curves at the site are slightly larger than those obtained from the 2014 NSHMs. This is mainly due to the inclusion of the Continental and Rocker faults in this study as well as the use of a different ground-motion characterization model. The difference is on the order of 0.01 to 0.04 g at the 10,000-year return period at PGA and spectral periods of 0.2 and 1 sec. Table 5-1 compares the 500 and 2,475 year return period PGA and spectral acceleration at 0.2 and 1 sec obtained from this study to those from the probabilistic hazard maps for the state of Montana (Wong et al. 2005) in the vicinity of the YDTI site. Table 5-1 shows that the PGA values obtained from this study are larger than the maps values for Butte but the spectral accelerations at periods of 0.2 and 1.0 sec are within the range of the maps predictions for Butte.

Table 5-1. Comparison of the 475 and 2,475 year spectral accelerations obtained from this study to values based on the probabilistic earthquake hazard maps for the State of Montana in the vicinity of the site for V_{S30} of 760 m/sec

	475 years		2,475 years	
	Wong et al. 2005 Maps	**This Study**	**Wong et al. 2005 Maps**	**This Study**
PGA	0.07 g	0.083 g	0.12 g	0.197 g
Sa (0.20 sec)	0 to 0.3 g	0.183 g	0.3 to 0.6 g	0.439 g
Sa (1.0 sec)	0 to 0.2 g	0.057 g	0 to 0.2 g	0.125 g

The deaggregations of the 475, 1,000, 2,475, and 10,000 years mean hazard are shown in Figures 5-4 to 5-9 for the YDTI site at PGA and spectral periods of 0.2, and 1.0 sec. Looking at the deaggregation plots alone can be somewhat misleading in attributing the short-distance contribution to be primarily coming from the Continental fault. As shown in the hazard curves (Figures 5-1 to 5-3), all contributions at the 475, 1,000, and 2,475 year return periods are primarily attributed to the background zones at all three spectral periods which are also located at close distances to the site. For the longer 10,000 year return period case,

the contribution for the close distances shown in the deaggregation plots is approximately equal between the gridded background zones and the Continental fault.

At PGA and period of 0.2 sec, the 475 and 1,000 year deaggregation plots show that the background sources in the range of 10 – 50 km and magnitudes in the range of 5.0 – 6.5 are the controlling sources of the hazard at the site. At period of 1.0 sec, the 475 and 1,000 year deaggregation plots show a more diffuse distribution of significant contribution from the background sources over the distance range of 10 – 150 km and magnitudes 6.0 to 7.5. For the longer 2,475 year and 10,000 year return period, the 1.0 sec deaggregation results show the significant contribution coming from similar magnitude ranges but with closer distances. For PGA and 0.2 sec, the controlling distance range is less than 30 km for the 2,475 year and 10,000 year return periods. For the 1 sec case, the distance range is reduced to less than about 100 km and 50 km for the 2,475 year and 10,000 year deaggregation results, respectively.

The dominant scenarios characterized in terms of the mean magnitude and distance are listed in Table 5-2 for PGA and periods of 0.2 and 1 sec for return periods of 475, 1,000, 2,475, and 10,000 years. The uniform hazard spectra (UHS) are computed using the mean hazard curves for the 475, 1,000, 2,475, and 10,000 years return period for the site. The UHS curves are shown in Figure 5-10 and their corresponding values are listed in Table 5-3.

Table 5-2. Mean magnitude and distance deaggregation of the hazard at PGA and spectral periods of 0.2 and 1.0 sec for the 475, 1,000, 2,475, and 10,000 year return period

	PGA		T 0.2 sec		T 1.0 sec	
	M	**R (km)**	**M**	**R (km)**	**M**	**R (km)**
475 yr	6.13	40.5	6.14	40.5	6.61	73.3
1,000 yr	6.14	31.2	6.16	32.6	6.63	60.3
2,475 yr	6.16	21.0	6.19	23.1	6.63	45.3
10,000 yr	6.19	13.0	6.23	14.2	6.59	26.4

Table 5-3. Horizontal mean UHS for 5% damping for the YDTI site for V_{S30} of 760 m/sec

	UHS PSA (g)			
Period (sec)	**475 yr**	**1,000 yr**	**2,475 yr**	**10,000 yr**
0.01/PGA	0.083	0.124	0.197	0.372
0.02	0.085	0.128	0.204	0.388
0.03	0.095	0.142	0.227	0.434
0.05	0.122	0.185	0.295	0.562
0.075	0.156	0.238	0.386	0.739
0.1	0.177	0.269	0.434	0.834
0.15	0.191	0.287	0.461	0.884
0.2	0.183	0.274	0.439	0.843
0.3	0.154	0.228	0.360	0.678
0.4	0.128	0.187	0.290	0.543
0.5	0.109	0.158	0.244	0.455
0.75	0.076	0.110	0.168	0.311
1	0.057	0.082	0.125	0.231
1.5	0.037	0.055	0.083	0.150
2	0.027	0.040	0.061	0.110
3	0.017	0.025	0.039	0.072
4	0.013	0.019	0.028	0.053
5	0.011	0.015	0.023	0.042
7.5	0.006	0.009	0.013	0.022
10	0.003	0.005	0.008	0.014

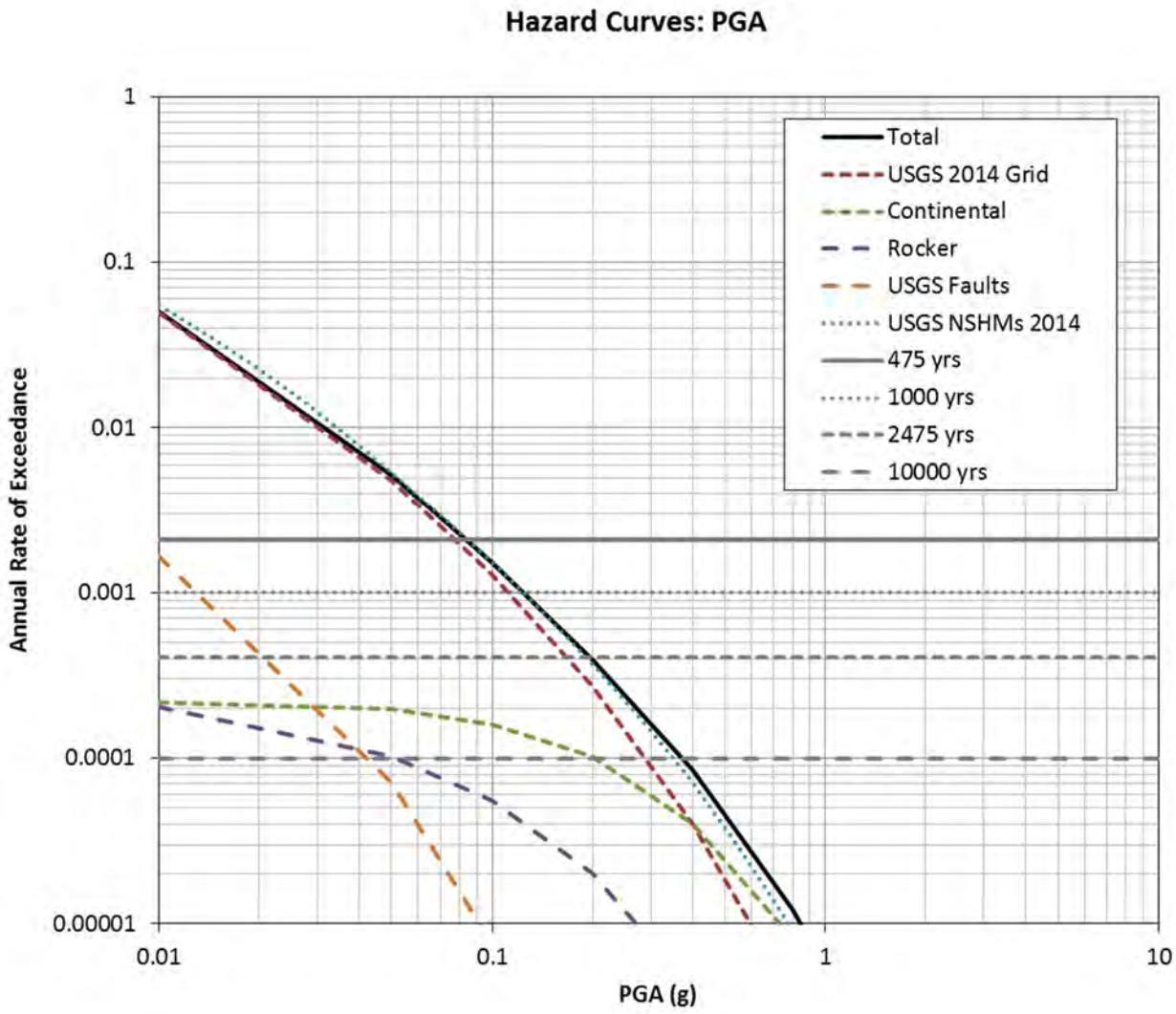

Figure 5-1. Hazard curves for the YDTI site at PGA

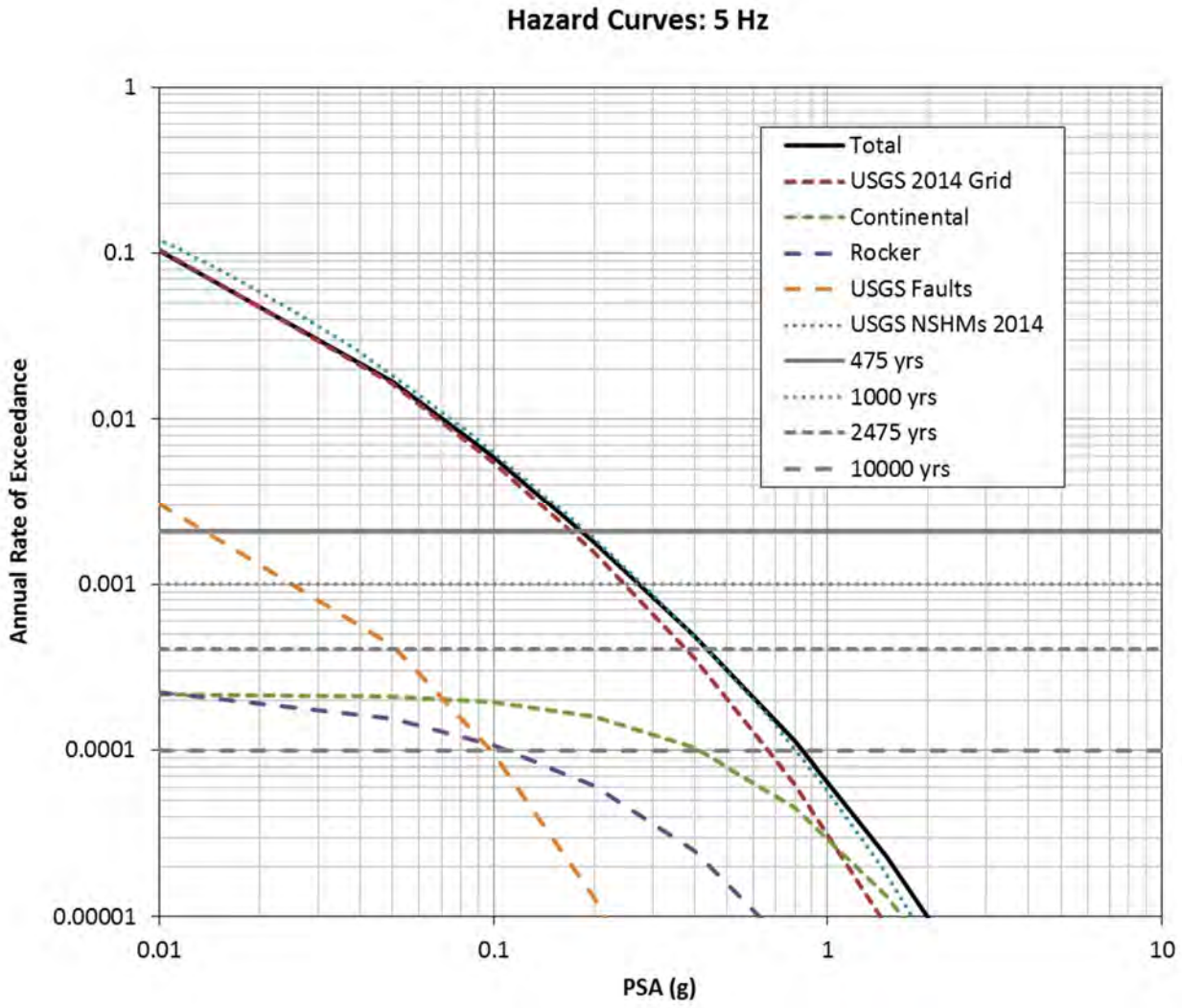

Figure 5-2. Hazard curves for the YDTI site at a period of 0.2 sec

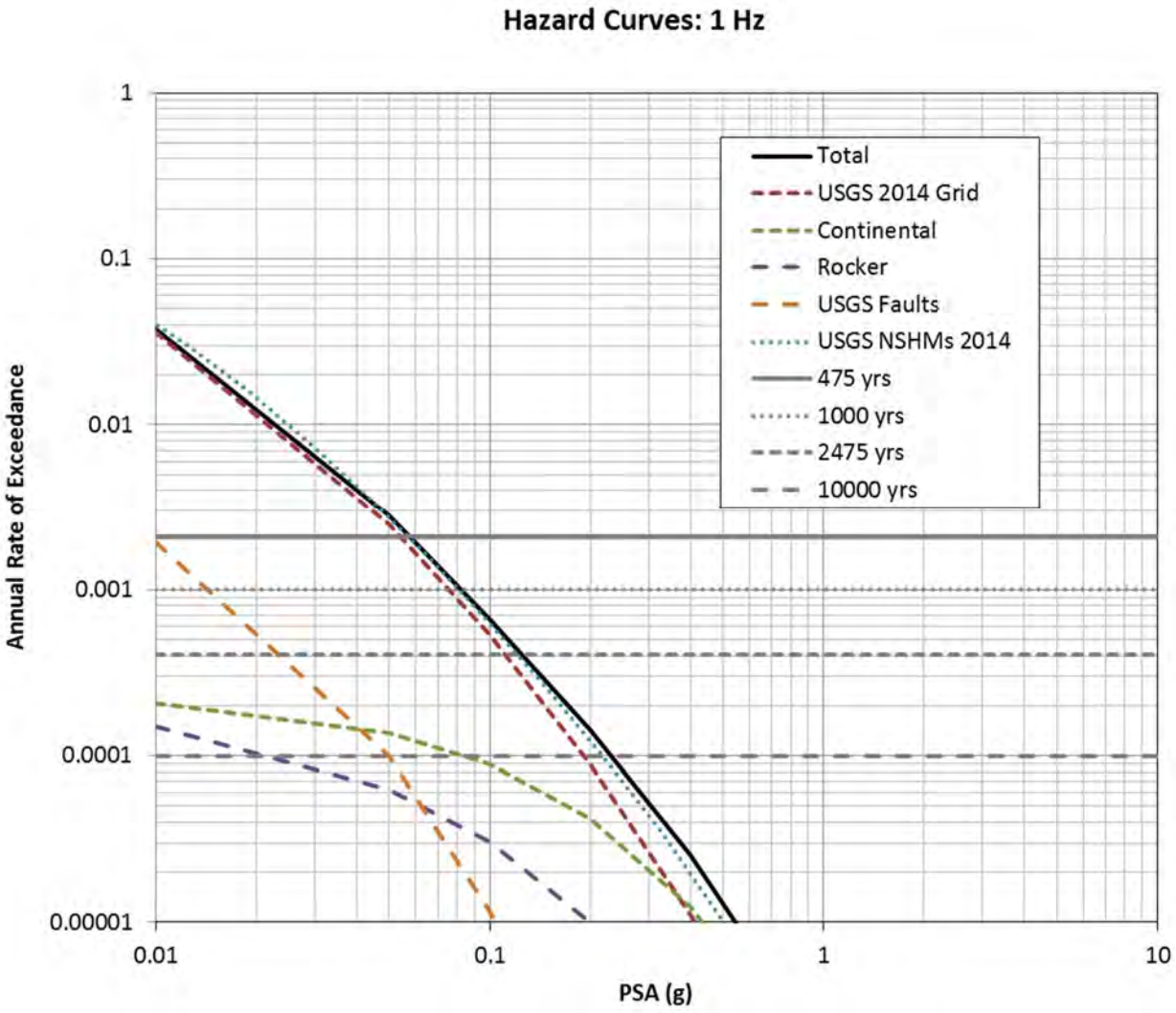

Figure 5-3. Hazard curves for the YDTI site at a period of 1.0 sec

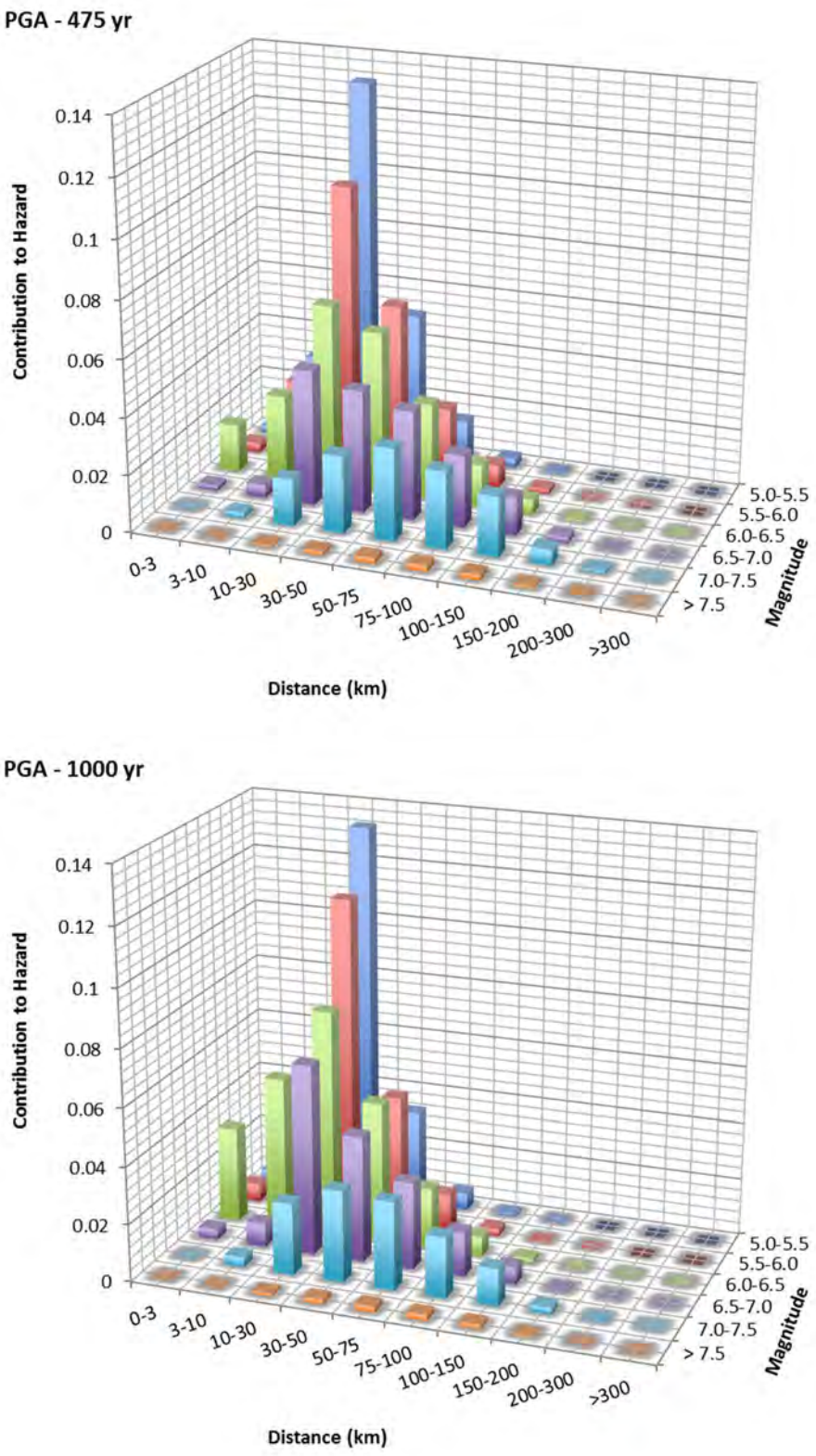

Figure 5-4. Deaggregation of the mean hazard at the YDTI site for PGA at return periods of 475 years (top) and 1,000 year (bottom)

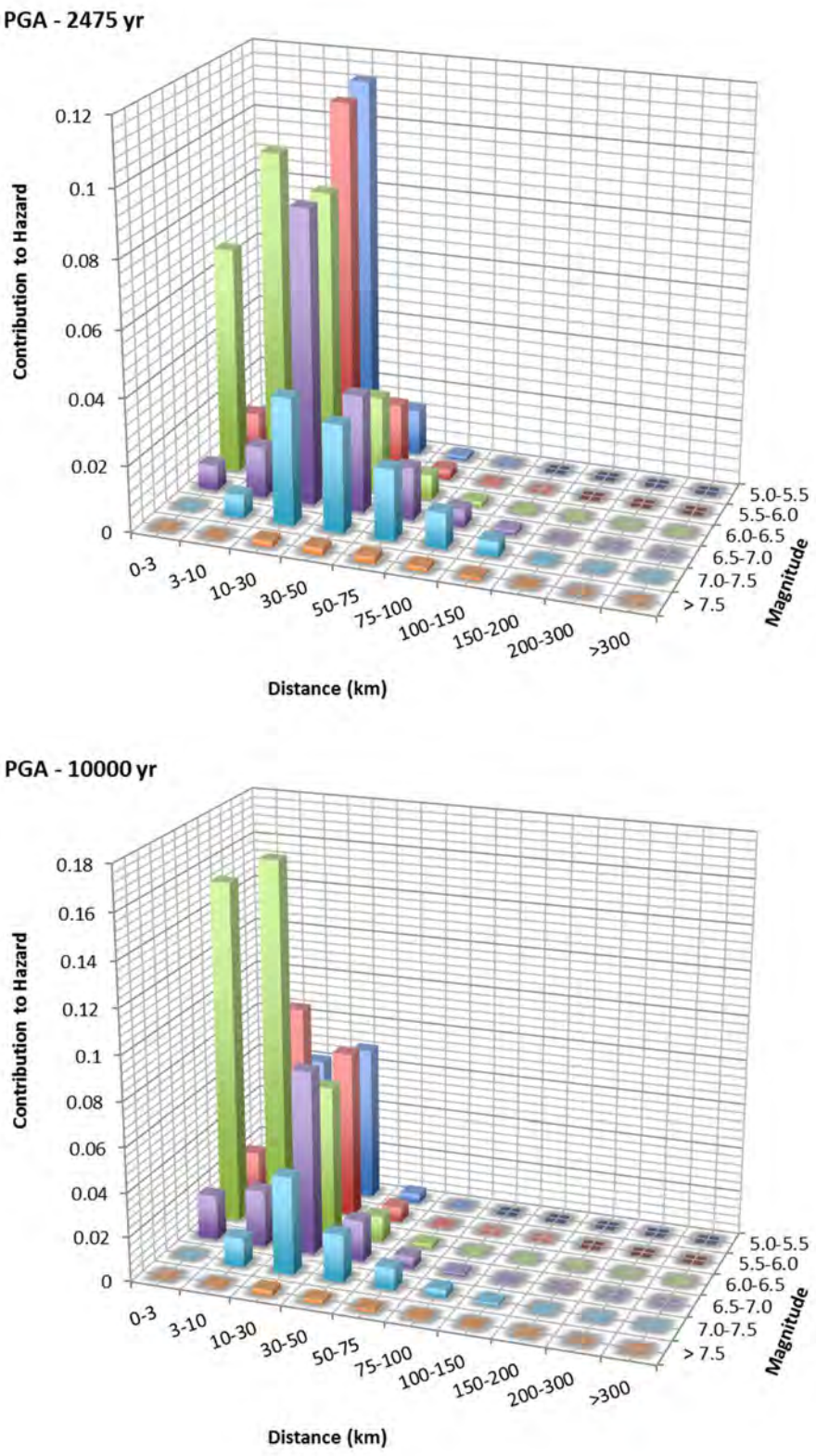

Figure 5-5. Deaggregation of the mean hazard at the YDTI site for PGA at return periods of 2,475 years (top) and 10,000 year (bottom)

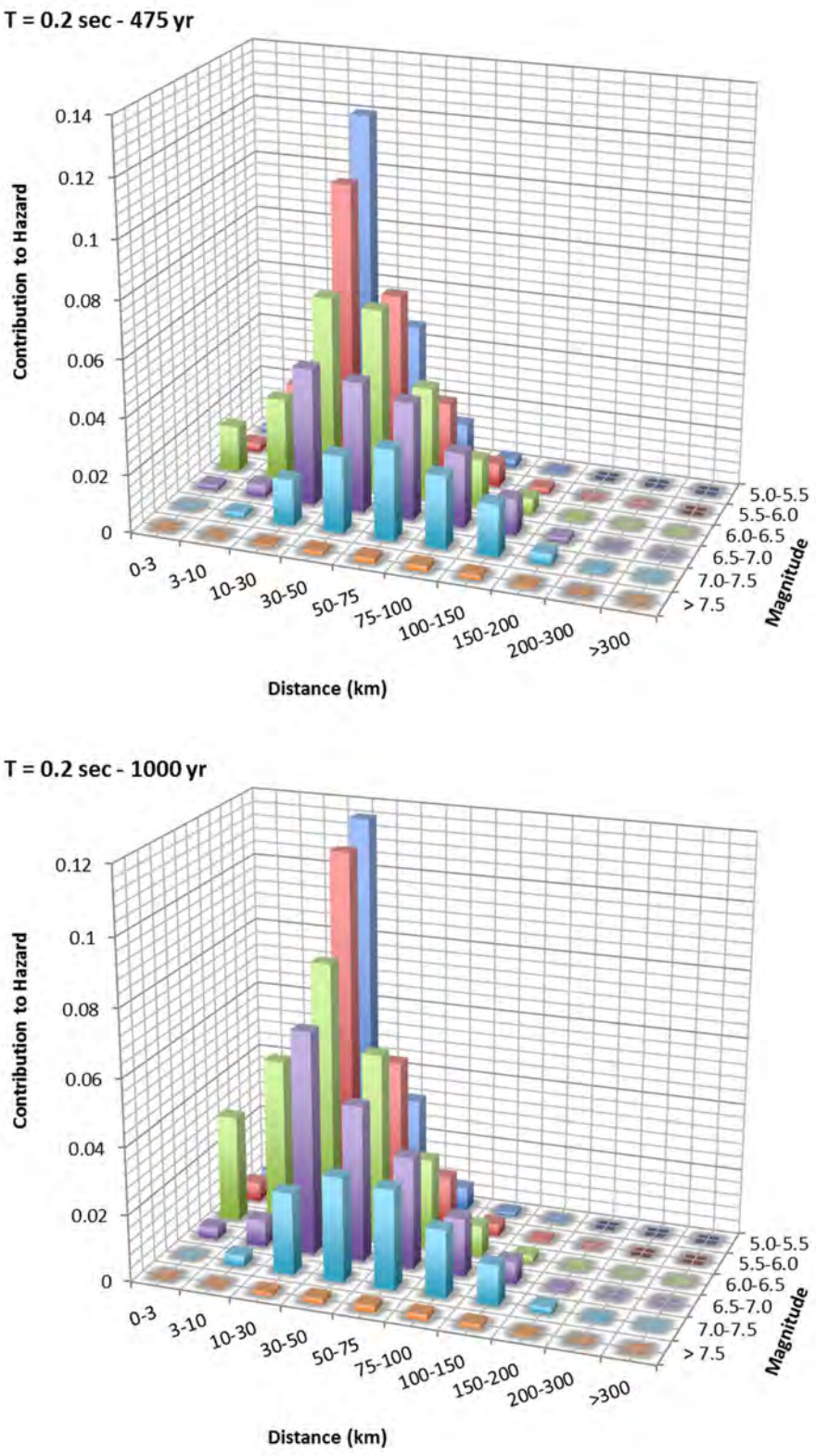

Figure 5-6. Deaggregation of the mean hazard at the YDTI site for T = 0.2 sec at return periods of 475 years (top) and 1,000 year (bottom)

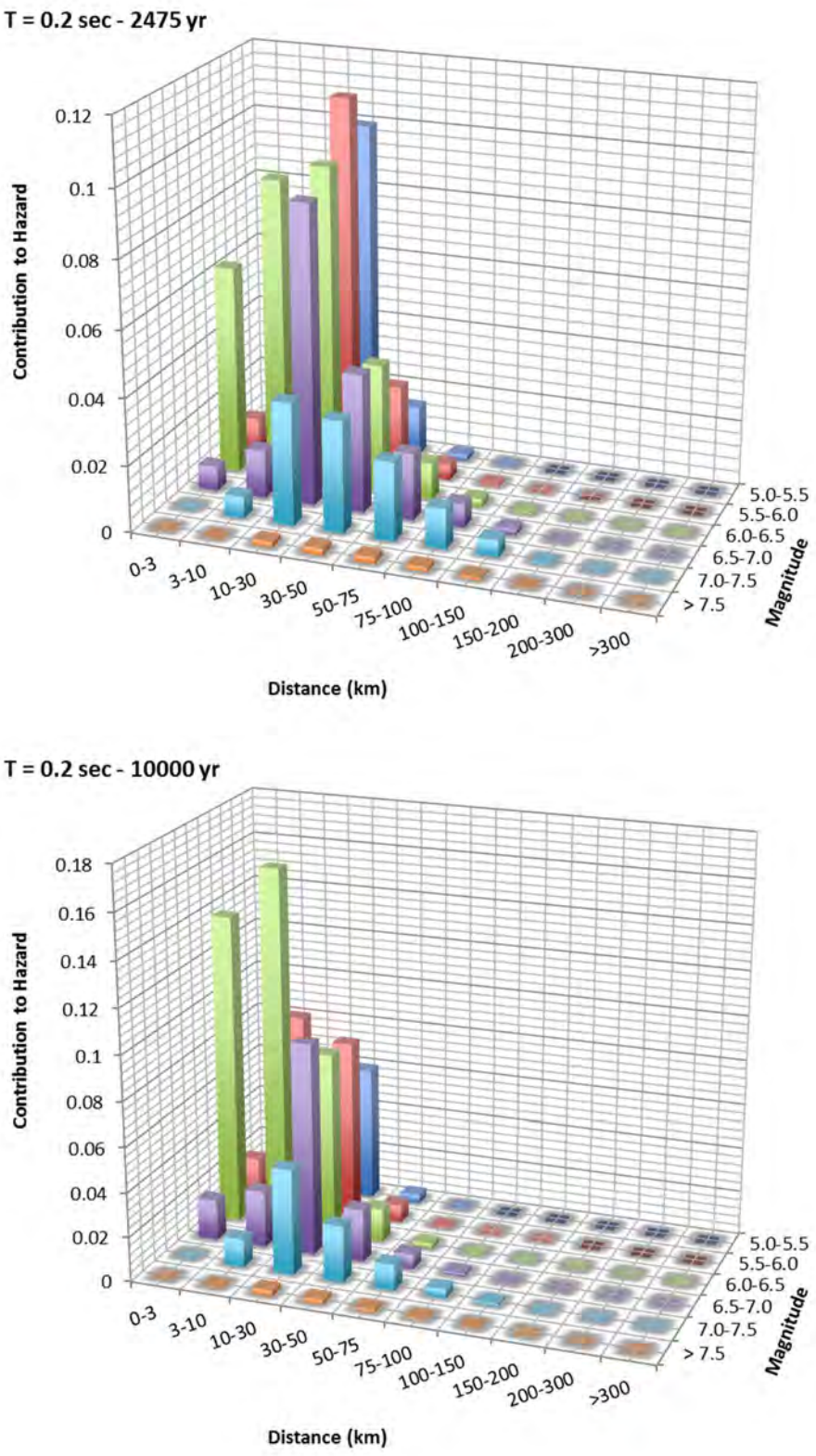

Figure 5-7. Deaggregation of the mean hazard at the YDTI site for T = 0.2 sec at return periods of 2,475 years (top) and 10,000 year (bottom)

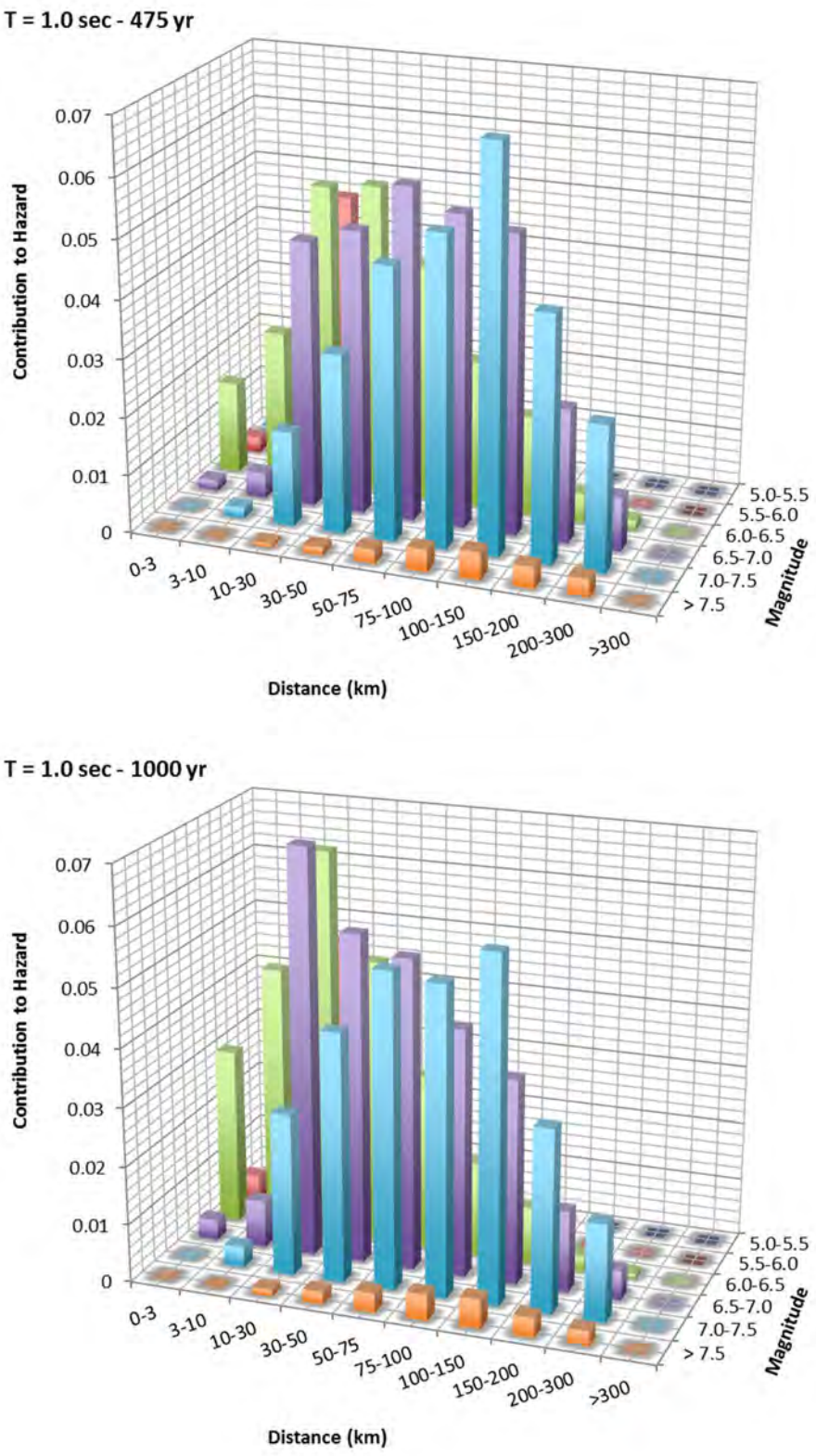

Figure 5-8. Deaggregation of the mean hazard at the YDTI site for T = 1.0 sec at return periods of 475 years (top) and 1,000 year (bottom)

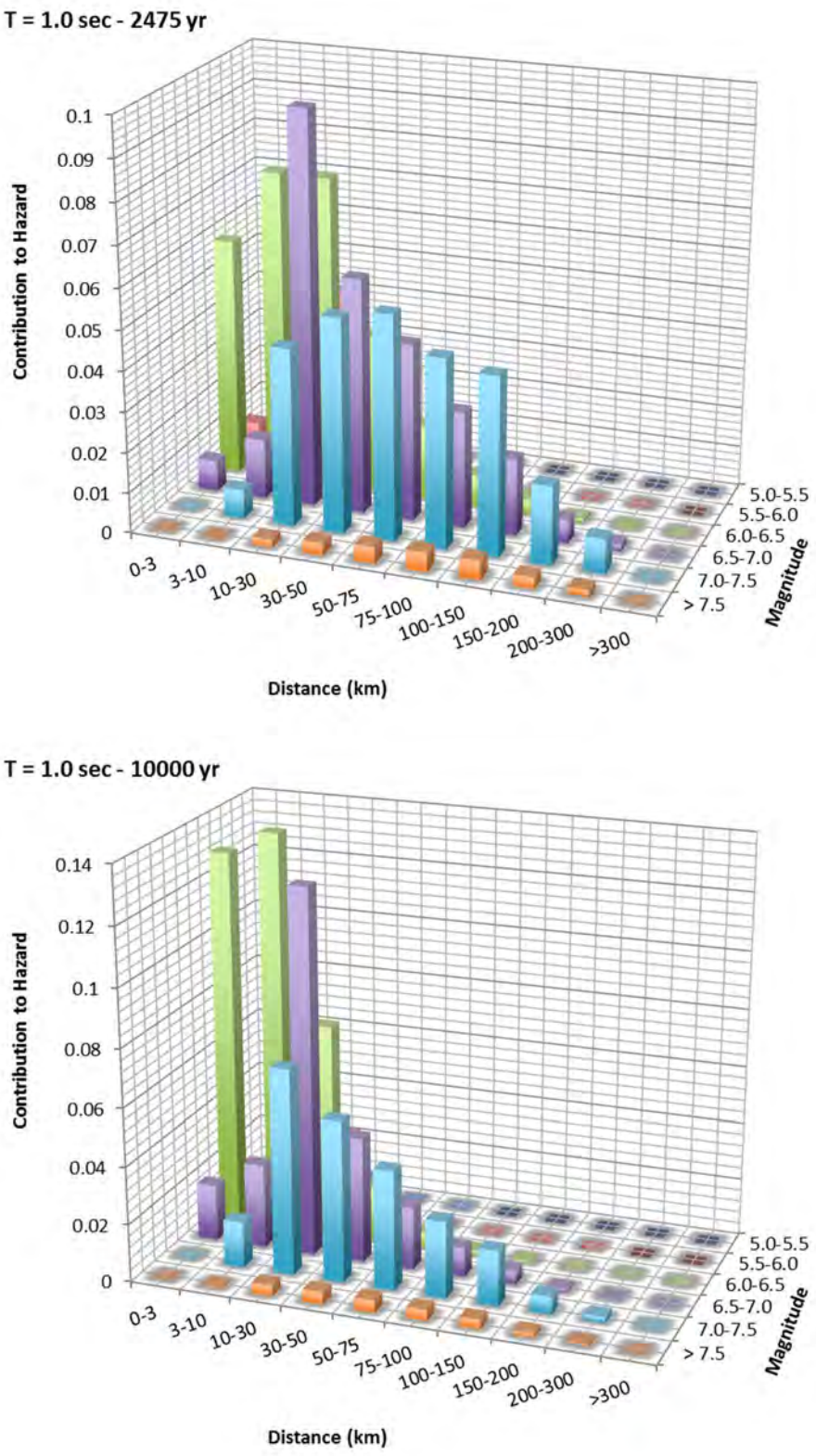

Figure 5-9. Deaggregation of the mean hazard at the YDTI site for T = 1.0 sec at return periods of 2,475 years (top) and 10,000 year (bottom).

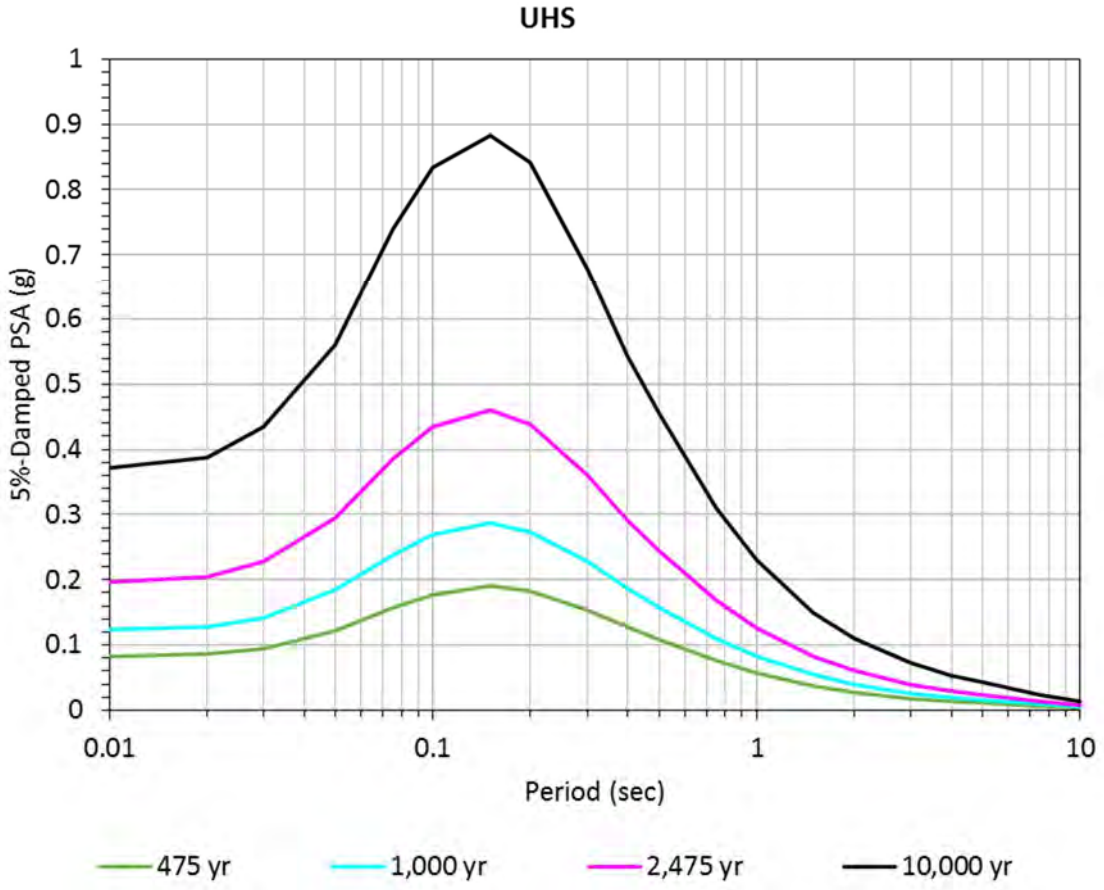

Figure 5-10. Uniform hazard spectra for the 475, 1,000, 2,475, and 10,000 years return period for the YDTI site for V_{S30} of 760 m/sec.

5.2 DSHA Results

Median and 84th percentile deterministic response spectra were calculated for the maximum credible earthquake (MCE) on the Continental and the Rocker faults using the ground-motion characterization model discussed in Chapter 4. The five equally-weighted NGA-West2 GMPEs were given a total weight of 0.667 and the Wong et al. (2005) stochastic-based model was given a weight of 0.333. The standard deviation model of Abrahamson et al. (2014) is used along with the median prediction from Wong et al. (2005).

For the Continental fault, an earthquake scenario with **M** 6.5 and rupture distance of 1.2 km was used to calculate the response spectra for V_{S30} of 760 m/sec. The YDTI site is located on the hanging wall of the normal Continental fault (i.e., Rjb=0 km). The top of the fault is modeled as coming to the surface (i.e., Ztor = 0 km) and the dip angle is 70 degrees. Figure 5-11 shows the median and 84th percentile deterministic response spectra for the MCE on the Continental fault. The spectra are shown for each of the six GMPEs used along with the weighted average according to the weights discussed above.

For the Rocker fault, an earthquake scenario with **M** 7.0 and rupture distance of 8.5 km was used to compute the deterministic response spectra at the YDTI site located on the footwall of the normal fault with a dip angle of 55 degrees. Figure 5-12 shows the median and the 84th percentile response spectra for each of the six GMPEs used as well as their weighted average. Figure 5-13 compares the median and the 84th percentile response spectra for the MCE scenarios on both the Continental and Rocker faults. Figure 5-13 shows that the median and 84th percentile response spectra for the Continental fault are significantly larger than the corresponding ones for the Rocker fault due to the very close proximity of Continental fault to the site. Therefore, deterministic spectra from the MCE on the Continental fault will be used for design purposes for this study.

Median and 84th percentile deterministic response spectra were also computed for an MCE scenario on the Continental fault for another location at the YDTI site closer to the fault with a rupture distance of 0.1 km. Figure 5-14 show the median and 84th percentile deterministic response spectra for the MCE scenarios on the Continental fault with rupture distance of 0.1 and 1.2 km. The maximum observed difference in the response spectra for the rupture distance scenarios of 0.1 and 1.2 km is on the order of 10%.

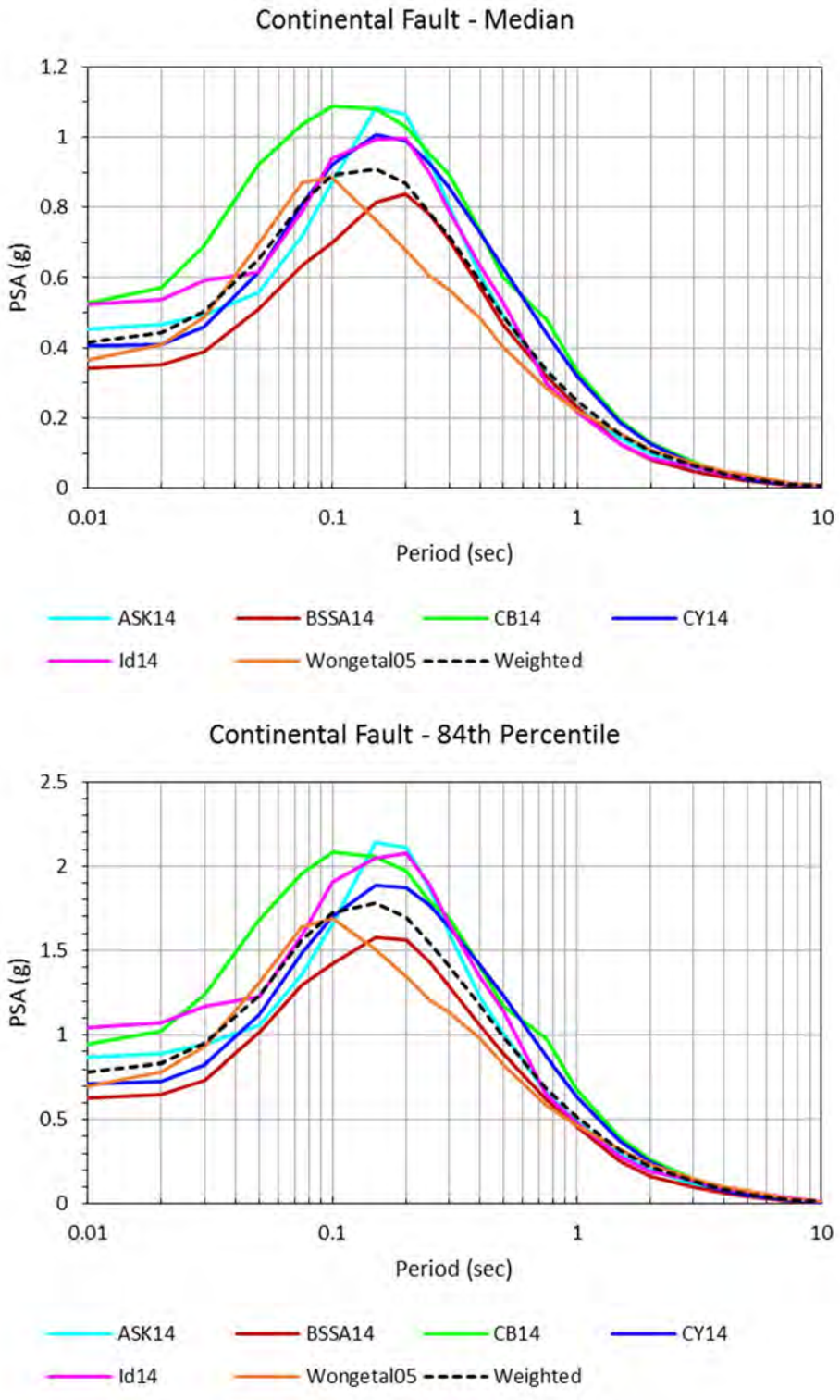

Figure 5-11. Median and 84th percentile deterministic response spectra for an M 6.5 and rupture distance of 1.2 km scenario on the Continental fault for V_{S30} of 760 m/sec

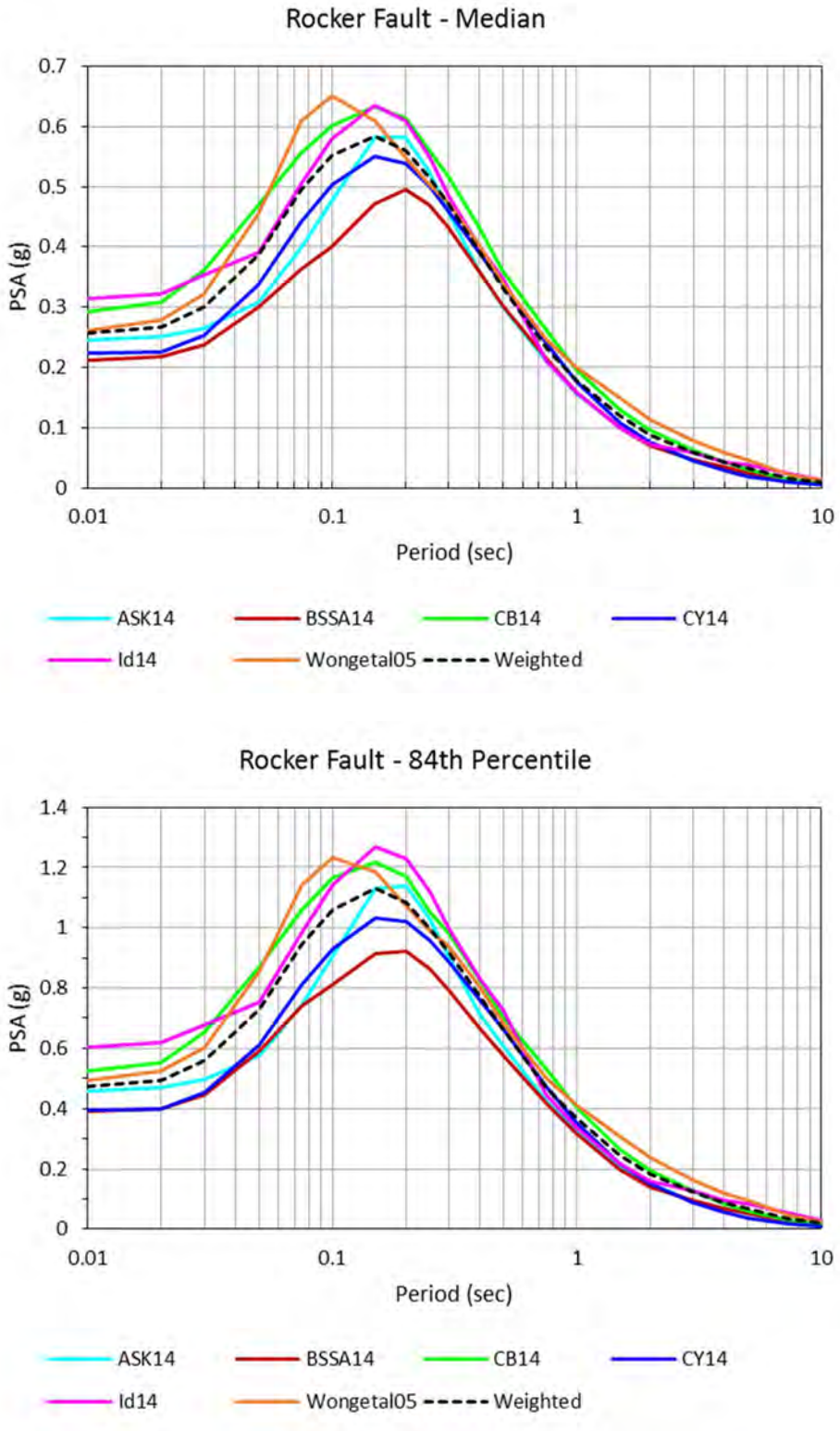

Figure 5-12. Median and 84th percentile deterministic response spectra for an M 7.0 and rupture distance of 8.5 km scenario on the Rocker fault for V_{S30} of 760 m/sec

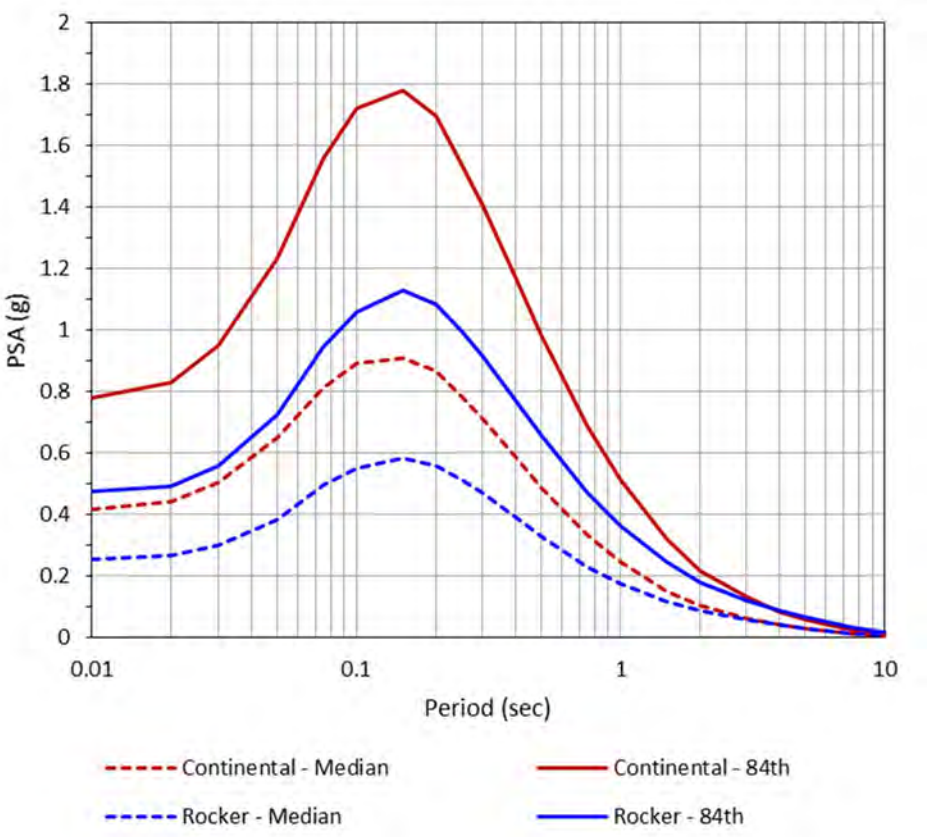

Figure 5-13. Comparison of the median and 84th percentile deterministic response spectra for the MCE scenarios on the Continental and the Rocker faults at the YDTI site with V_{S30} of 760 m/sec

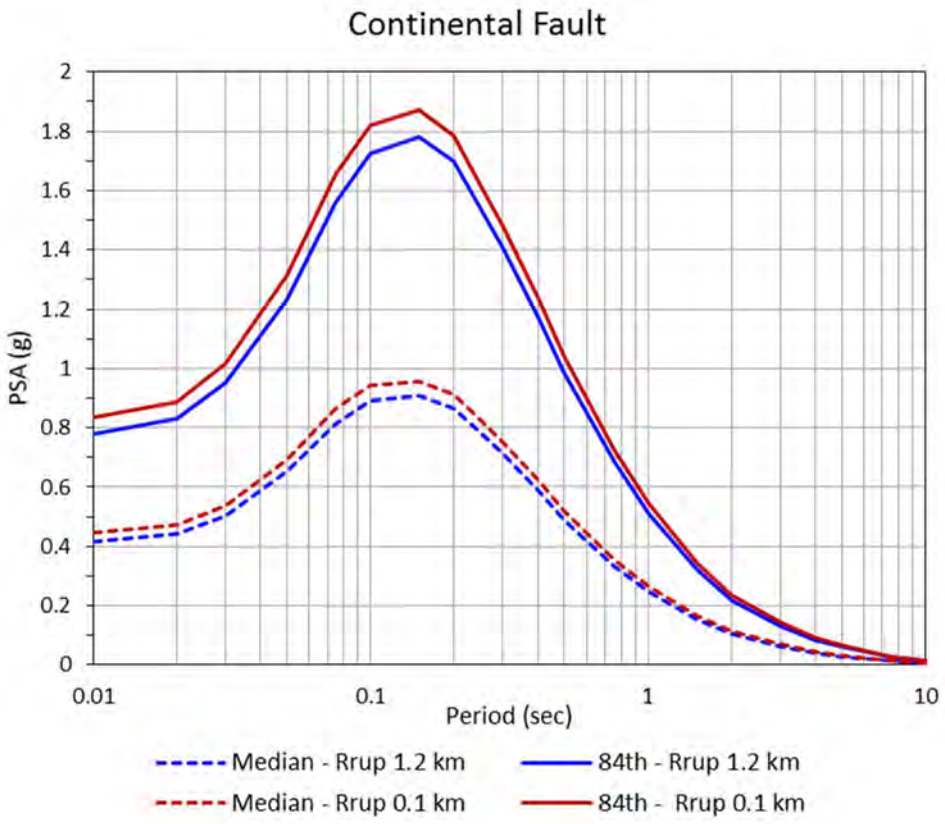

Figure 5-14. Median and 84th percentile deterministic response spectra for the MCE scenarios on the Continental fault at two locations at the YDTI site with rupture distances of 0.1 and 1.2 km for V_{S30} of 760 m/sec

6. DESIGN SPECTRA

6.1 Horizontal Design Spectra

Figure 6-1 presents a comparison of the UHS at the YDTI site for return periods of 475, 1,000, 2,475, and 10,000 years to the deterministic median and 84th percentile spectra for the MCE scenarios on the Continental fault. For comparison purposes, the UHS for a return period of 100,000 years is also included in the plot. Figure 6-1 indicates that the median deterministic spectra for the Continental fault correspond to a PSHA return period greater than 10,000 years. The 84th percentile deterministic spectra correspond to a return period close to 100,000 years.

For the deterministic case, the choice of using the median versus the 84th percentile response spectra needs to be carefully evaluated. As noted above, the 84th percentile response spectra for the MCE scenarios on the Continental fault correspond to a very rare probabilistic case with a return period close to 100,000 years. Moreover, we note the presence of a precedence for using median deterministic spectra for dam design. Specifically, the California Division of Safety of Dams (DSOD) published guidelines for selecting the deterministic PGA level based on the fault's slip rate and the damage potential at the site Dams (DSOD, 2000). The DSOD consequence-hazard matrix is shown in Table 6-1. For faults with low slip rates such as the Continental fault, the hazard matrix requires the use of 50th to 84th percentile ground motion parameters for dams with high and extreme consequences of failure. For moderate and low consequence of failure, the hazard matrix requires the use of the median ground-motion parameters for faults with low slip rates.

Figure 6-2 presents the UHS and the deterministic median and 84th percentile spectra at the YDTI site for V_{S30} of 760 m/sec with the values listed in Table 6-2. The decision to use the median versus the 84th percentile deterministic design spectrum depends on the regulatory body governing the YDTI site and needs to be made based on feedback reviews from the client or the independent reviewers.

Table 6-1. DSOD Hazard matrix (DSOD 2000)

Slip Rate

Consequence	Very High 9 or greater mm/yr	High 8.9 to 1.1 mm/yr	Moderate 1.0 to 0.1 mm/yr	Low less than 0.1 mm/yr
Extreme Total Class Weight 31-36	84^{th}	84^{th}	84^{th}	50^{th} to 84^{th}
High Total Class Weight 19-30	84^{th}	84^{th}	50^{th} to 84^{th}	50^{th} to 84^{th}
Moderate Total Class Weight 7-18	84^{th}	50^{th} to 84^{th}	50^{th} to 84^{th}	50^{th}
Low Total Class Weight 0-6	50^{th}	50^{th}	50^{th}	50^{th}

Table 6-2. Horizontal design spectra for 5% damping for the YDTI site for V_{S30} of 760 m/sec

	UHS PSA (g)				Deterministic PSA (g) Rrup = 1.2 km		Deterministic PSA (g) Rrup = 0.1 km	
Period (sec)	475 yr	1,000 yr	2,475 yr	10,000 yr	Median	84^{th} Percentile	Median	84^{th} Percentile
0.01/PGA	0.083	0.124	0.197	0.372	0.416	0.779	0.447	0.837
0.02	0.085	0.128	0.204	0.388	0.443	0.830	0.472	0.885
0.03	0.095	0.142	0.227	0.434	0.505	0.951	0.539	1.015
0.05	0.122	0.185	0.295	0.562	0.652	1.234	0.694	1.314
0.075	0.156	0.238	0.386	0.739	0.815	1.561	0.864	1.654
0.1	0.177	0.269	0.434	0.834	0.892	1.723	0.942	1.820
0.15	0.191	0.287	0.461	0.884	0.908	1.779	0.955	1.870
0.2	0.183	0.274	0.439	0.843	0.867	1.698	0.912	1.786
0.3	0.154	0.228	0.360	0.678	0.715	1.411	0.752	1.484
0.4	0.128	0.187	0.290	0.543	0.589	1.173	0.622	1.238
0.5	0.109	0.158	0.244	0.455	0.490	0.986	0.518	1.043
0.75	0.076	0.110	0.168	0.311	0.335	0.687	0.355	0.729
1	0.057	0.082	0.125	0.231	0.247	0.513	0.264	0.548
1.5	0.037	0.055	0.083	0.150	0.153	0.321	0.165	0.344
2	0.027	0.040	0.061	0.110	0.104	0.219	0.112	0.236
3	0.017	0.025	0.039	0.072	0.064	0.133	0.069	0.145
4	0.013	0.019	0.028	0.053	0.041	0.086	0.045	0.094
5	0.011	0.015	0.023	0.042	0.030	0.061	0.033	0.068
7.5	0.006	0.009	0.013	0.022	0.013	0.026	0.014	0.029
10	0.003	0.005	0.008	0.014	0.007	0.015	0.008	0.016

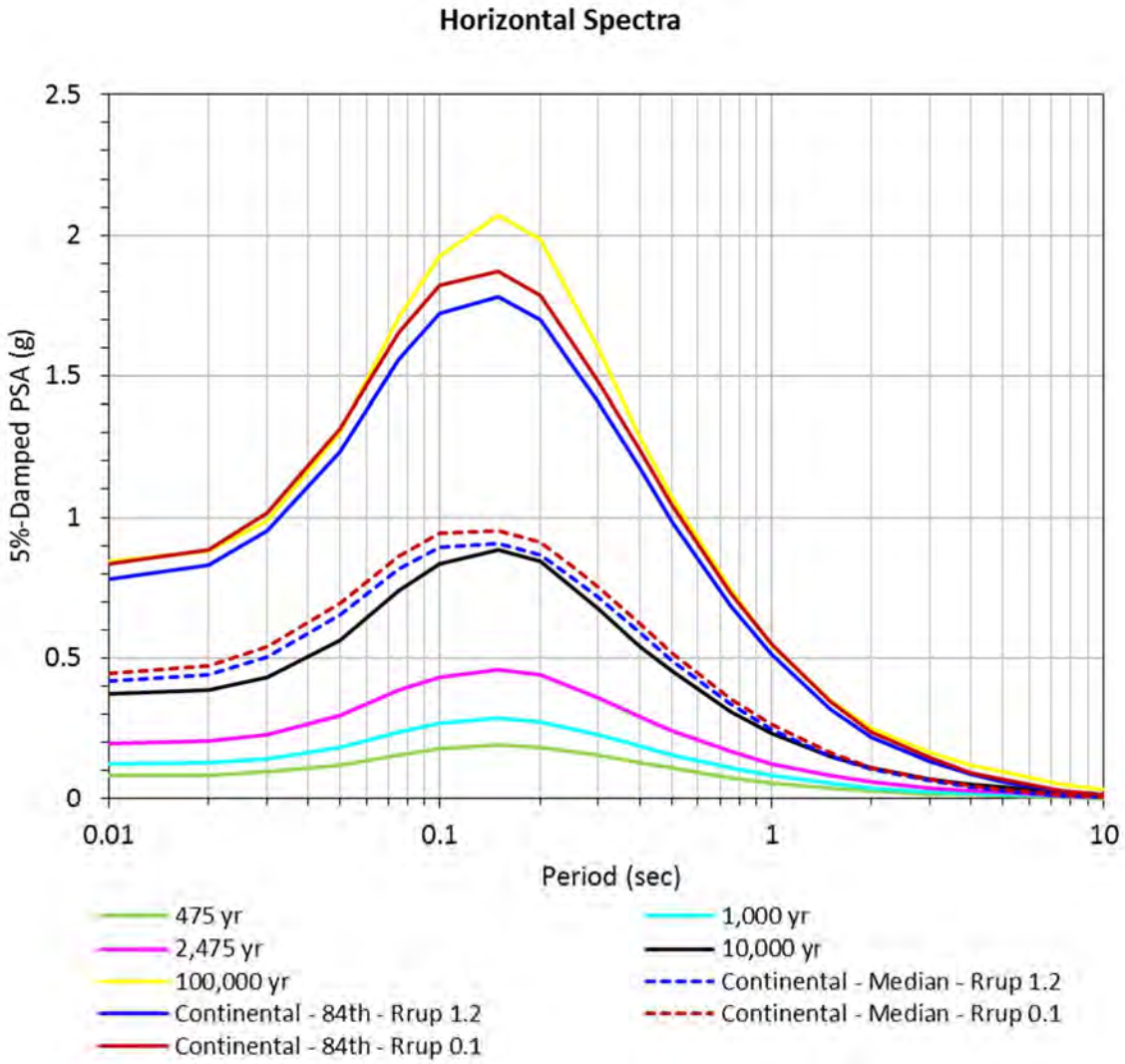

Figure 6-1. Comparison of the UHS (475, 1,000, 2,475, 10,000, and 100,000 years return period) to the median and 84th percentile deterministic response spectra for the MCE scenarios on the Continental fault at the YDTI site with V_{S30} of 760 m/sec

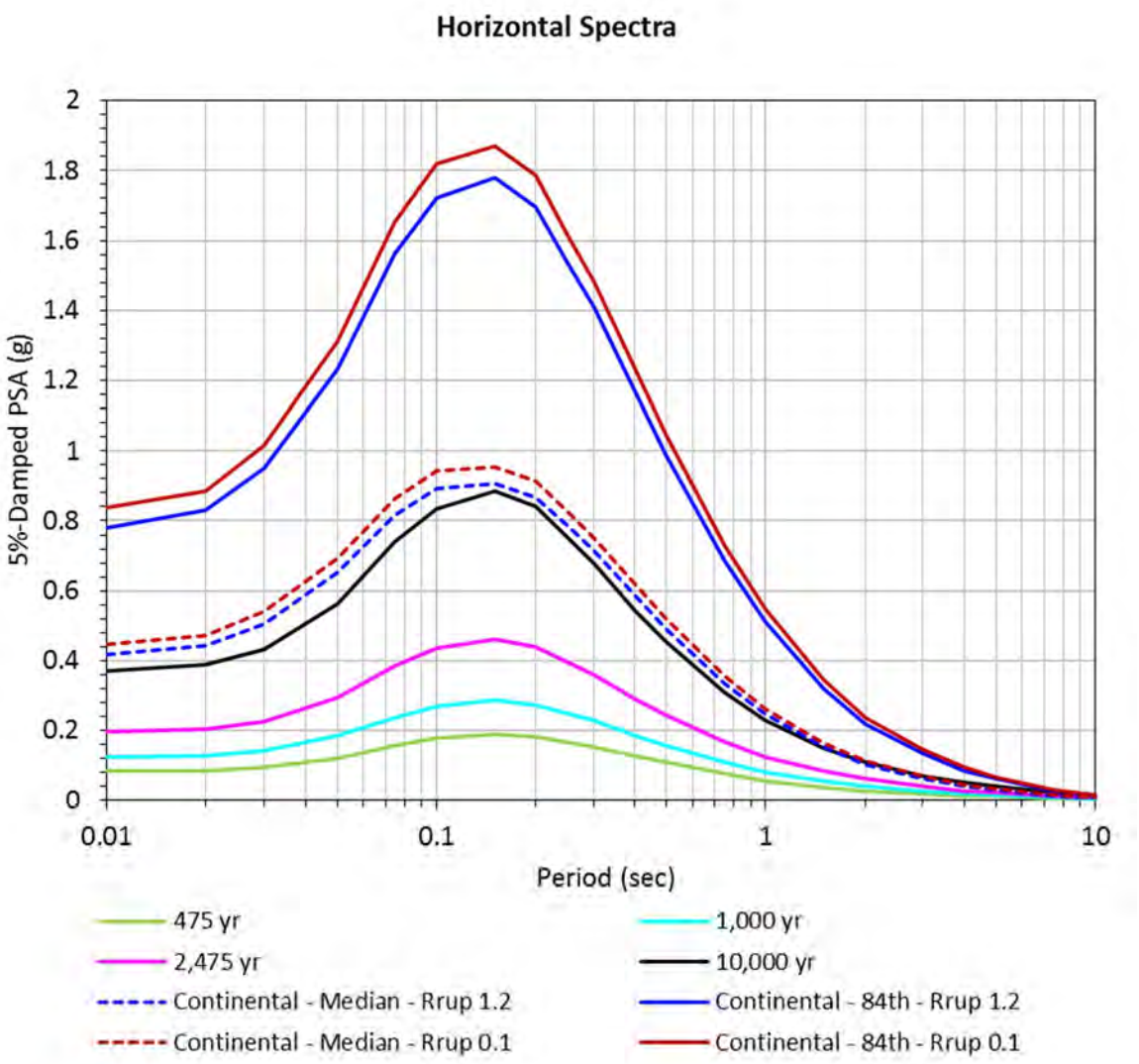

Figure 6-2. Horizontal design spectra at the YDTI site for V_{S30} of 760 m/sec

6.2 Vertical Design Spectra

Two primary methodologies can be used for the development of vertical design motions: perform a PSHA or DSHA using vertical-component GMPE models or apply an appropriate vertical-to-horizontal ratio (V/H) to the horizontal ground motions. The first approach is limited based on the availability of vertical-component GMPEs, which until recently had been rather limited. As part of the NGA-West2 project, vertical-component GMPEs are being developed based on the same dataset and developer teams that developed the horizontal models. Three of these models are currently being published and are expected to be used more frequently in the future. One noted limitation in using a vertical GMPE in a PSHA is that the resulting horizontal and vertical spectra could be a result of different scenario earthquakes within the PSHA methodology. For these reasons, the standard state of practice is to develop appropriate V/H ratios

from the controlling scenario events for the horizontal spectra and apply these ratio factors to develop the vertical spectra. This approach is used for this project.

For the estimation of the V/H ratios, the empirically-based V/H model from Gulerce and Abrahamson (2011) is used. This model is based on the empirical database associated with the NGA-West project, which consists of strong ground-motion recordings from active tectonic regions. Note that this model was developed prior to the development of the more expansive NGA-West2 database. Based on the deaggregation results presented earlier in this report, scenario events are selected for the controlling earthquakes. As expected, these controlling events are dependent on the spectral period of interest and the hazard level. For the deterministic analysis, the same earthquake parameters used for the horizontal motions are applied for the V/H model. Table 6-3 summarizes the scenario events used for the V/H estimates.

Table 6-3. Scenario events used for the estimation of the V/H ratios

Hazard Level	PGA, 0.2 sec	1.0 sec
475 yr and 1,000 yr	Magnitude 6.15 Distance 30 km	Magnitude 6.6 Distance 60 km
2,475 yr and 10,000 yr	Magnitude 6.15 Distance 15 km	Magnitude 6.6 Distance 30 km
Continental Fault	Magnitude 6.5 - Distance 1.2 km Magnitude 6.5 - Distance 0.1 km	

For each of the probabilistic scenario events, the faulting mechanism was assigned to be normal with a dip angle of 45 degrees and the top of rupture at the ground surface to be consistent with the source models used in the analysis. For the Continental fault scenario events, the faulting mechanism was assumed to be normal with a dip angle of 70 degrees and a top of rupture at the ground surface. The Gulerce and Abrahamson (2011) V/H model accounts for the expected non-linear site response of the V/H ratio by assuming a linear response of vertical ground motions (i.e., based on the analysis of the strong ground-motion data) and the horizontal site response model of Walling et al. (2008). This model is dependent on the PGA value for a reference condition with a V_{S30} = 1,100 m/sec.

Based on the scenario events listed in Table 6-3, the V/H functions for the 475 and 1,000 year hazard levels are plotted in Figure 6-3. Minor numerical differences are noted for the scenario events at the different hazard levels based on the site response aspect of the V/H model. For the low period (i.e., high frequency) range, the V/H function from the scenario event associated with the PGA and 0.2 sec cases exceed the V/H function for the 1 sec case. For the longer spectral periods, the opposite is observed. Based on this observation, the recommended V/H ratio is taken as the envelope of these V/H functions.

The results for the 2,475 and 10,000 year cases are plotted in Figure 6-4 and the same observations and recommendation of the V/H being the envelope of the V/H functions is concluded. The recommended V/H ratio functions including the results for the Continental fault (enveloping the V/H ratios for the two

distance scenarios for each of the median and 84th percentile cases) are shown in Figure 6-5. The V/H values are listed in Table 6-4.

For the vertical spectra, the recommended V/H ratios are used to scale the corresponding horizontal spectra (see Table 6-2). The resulting vertical spectra are listed in Table 6-5 and comparisons of the horizontal and vertical spectra are presented in Figures 6-6 through 6-11.

Table 6-4. Recommended V/H ratios

Period (sec)	475 and 1,000 yr	2,475 and 10,000 yr	Continental (Median)	Continental (84th)
0.01/PGA	0.6324	0.7075	0.7975	0.8130
0.02	0.6325	0.7079	0.7981	0.8140
0.03	0.7079	0.8089	0.9262	0.9515
0.05	0.7625	0.9444	1.1515	1.2209
0.075	0.7140	0.8770	1.0592	1.1365
0.1	0.6390	0.7505	0.8731	0.9325
0.15	0.5750	0.6217	0.6710	0.6948
0.2	0.5734	0.5734	0.5691	0.5691
0.3	0.5843	0.5722	0.5494	0.5494
0.4	0.6139	0.5923	0.5558	0.5558
0.5	0.6347	0.6052	0.5578	0.5578
0.75	0.7175	0.6775	0.6139	0.6139
1	0.7987	0.7541	0.6833	0.6833
1.5	0.8552	0.8074	0.7316	0.7316
2	0.8281	0.7819	0.7085	0.7085
3	0.8094	0.7642	0.6924	0.6924
4	0.8424	0.7954	0.7207	0.7207
5	0.8543	0.8066	0.7309	0.7309
7.5	0.8543	0.8066	0.7309	0.7309
10	0.8543	0.8066	0.7309	0.7309

Table 6-5. Vertical design spectra for 5% damping for the YDTI site for V_{S30} of 760 m/sec

	UHS PSA (g)				Deterministic PSA (g) Rrup = 1.2 km		Deterministic PSA (g) Rrup = 0.1 km	
Period (sec)	475 yr	1,000 yr	2,475 yr	10,000 yr	Median	84th Percentile	Median	84th Percentile
0.01/PGA	0.052	0.078	0.139	0.263	0.332	0.633	0.357	0.680
0.02	0.054	0.081	0.144	0.275	0.354	0.676	0.377	0.720
0.03	0.067	0.101	0.184	0.351	0.468	0.905	0.499	0.966
0.05	0.093	0.141	0.279	0.531	0.751	1.507	0.799	1.604
0.075	0.111	0.170	0.339	0.648	0.863	1.774	0.915	1.880
0.1	0.113	0.172	0.326	0.626	0.779	1.607	0.822	1.697
0.15	0.110	0.165	0.287	0.550	0.609	1.236	0.641	1.299
0.2	0.105	0.157	0.252	0.483	0.493	0.966	0.519	1.016
0.3	0.090	0.133	0.206	0.388	0.393	0.775	0.413	0.815
0.4	0.079	0.115	0.172	0.322	0.327	0.652	0.346	0.688
0.5	0.069	0.100	0.148	0.275	0.273	0.550	0.289	0.582
0.75	0.055	0.079	0.114	0.211	0.206	0.422	0.218	0.448
1	0.046	0.065	0.094	0.174	0.169	0.351	0.180	0.374
1.5	0.032	0.047	0.067	0.121	0.112	0.235	0.121	0.252
2	0.022	0.033	0.048	0.086	0.074	0.155	0.079	0.167
3	0.014	0.020	0.030	0.055	0.044	0.092	0.048	0.100
4	0.011	0.016	0.022	0.042	0.030	0.062	0.032	0.068
5	0.009	0.013	0.019	0.034	0.022	0.045	0.024	0.050
7.5	0.005	0.008	0.010	0.018	0.010	0.019	0.010	0.021
10	0.003	0.004	0.006	0.011	0.005	0.011	0.006	0.012

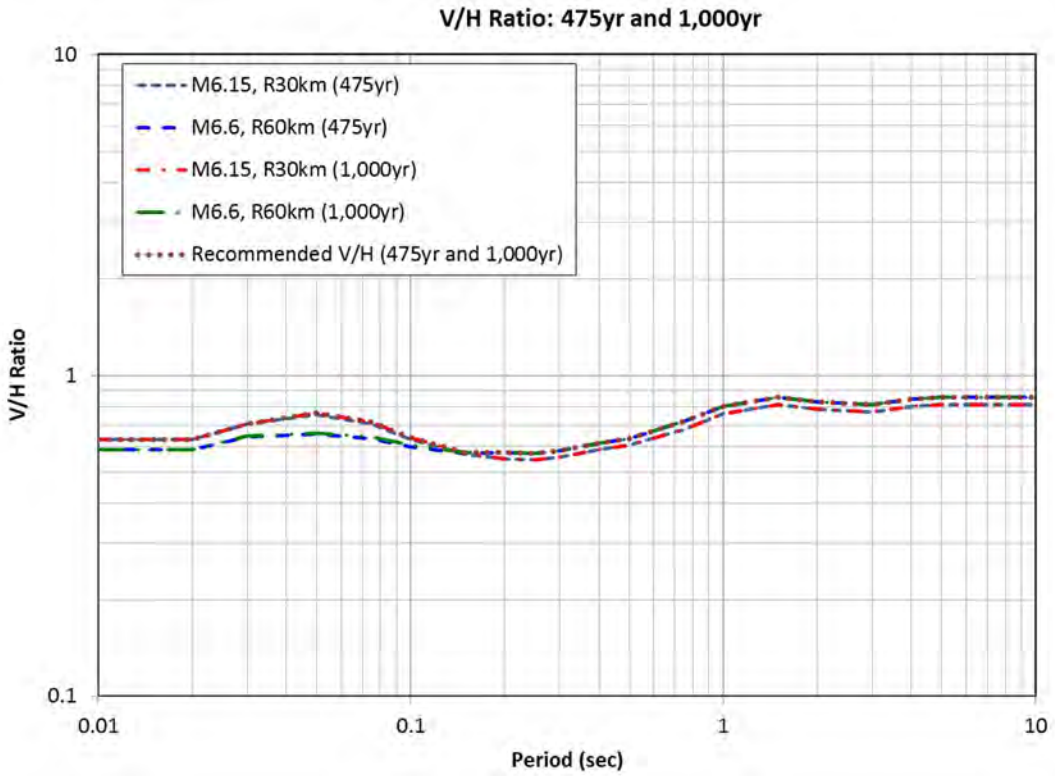

Figure 6-3. V/H ratios for the 475 year and 1,000 year hazard level

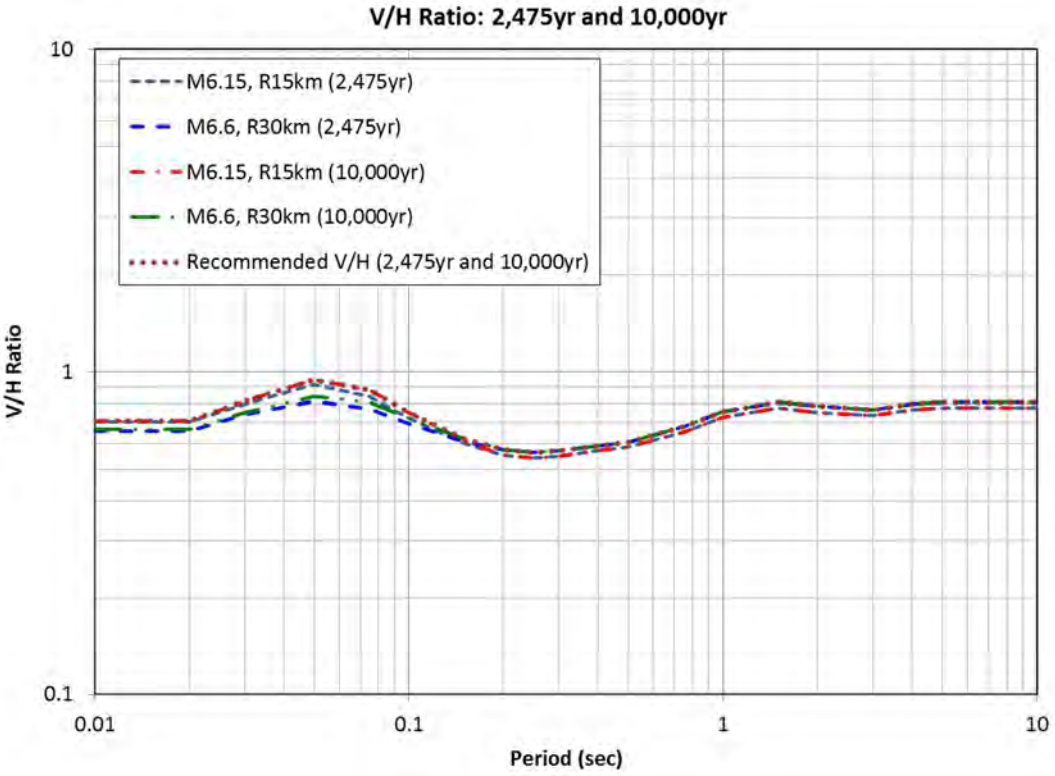

Figure 6-4. V/H ratios for the 2,475 year and 10,000 year hazard level

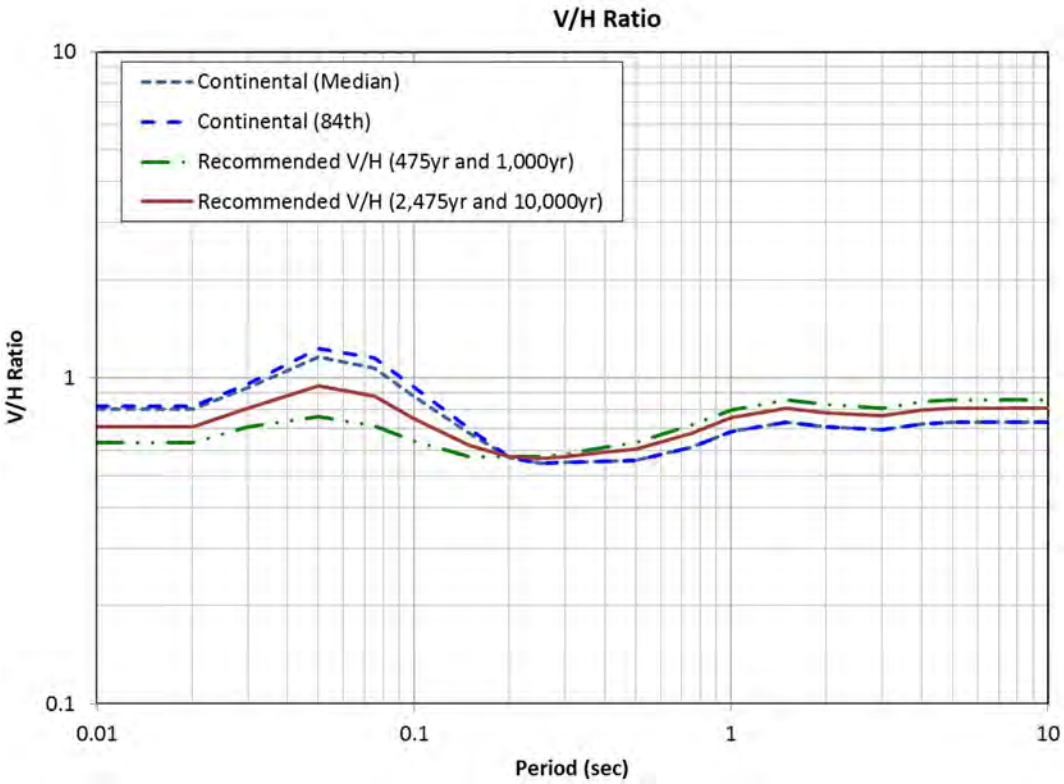

Figure 6-5. Recommended V/H ratios

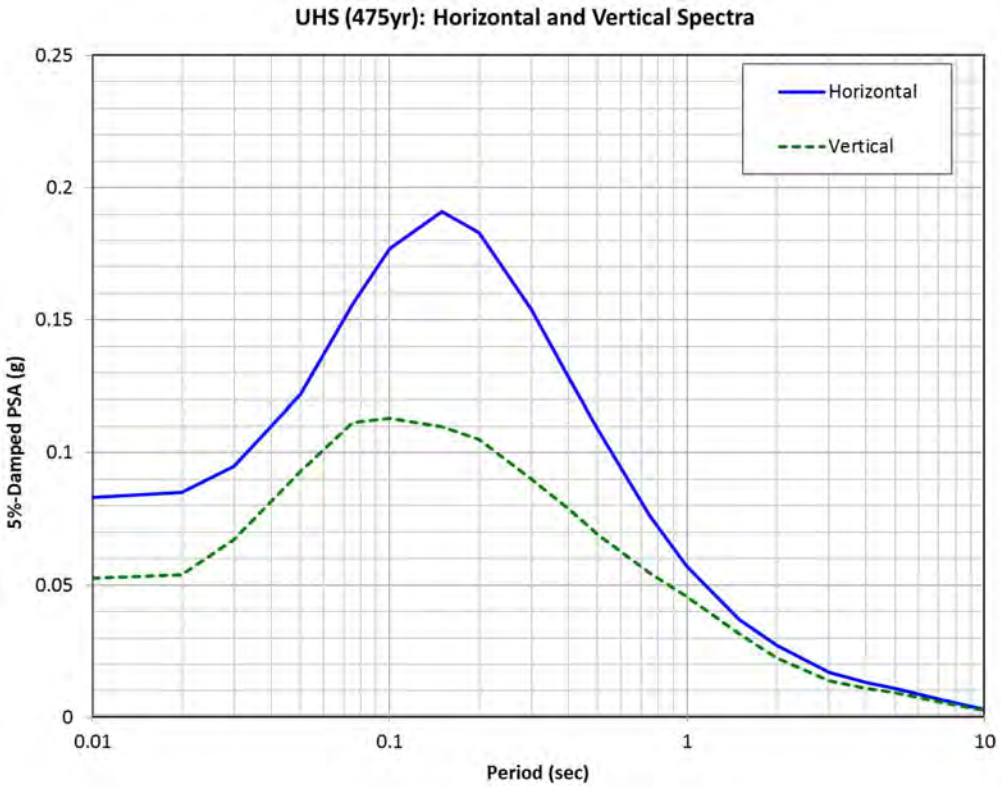

Figure 6-6. Horizontal and vertical design spectra for the 475 year hazard level

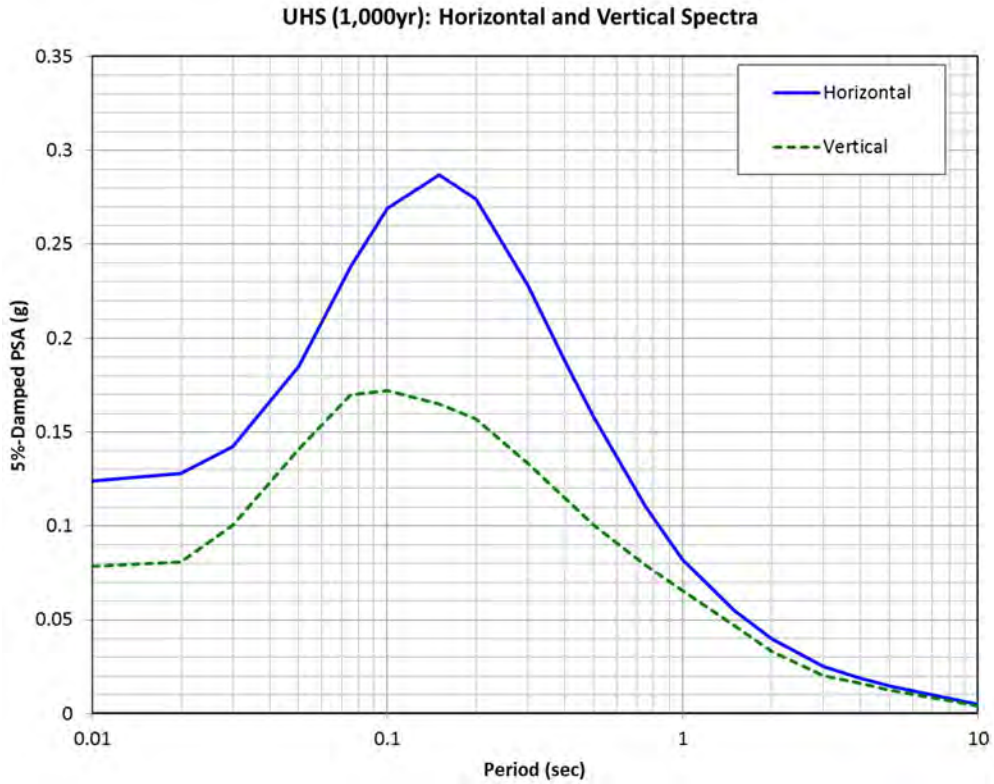

Figure 6-7. Horizontal and vertical design spectra for the 1,000 year hazard level

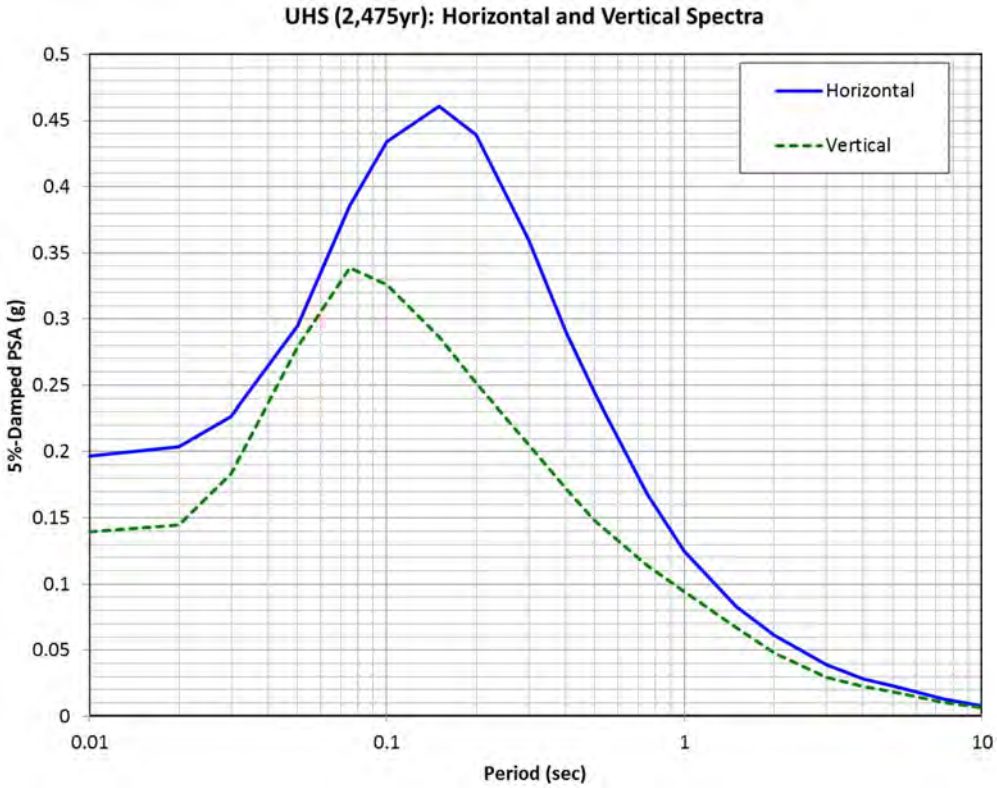

Figure 6-8. Horizontal and vertical design spectra for the 2,475 year hazard level

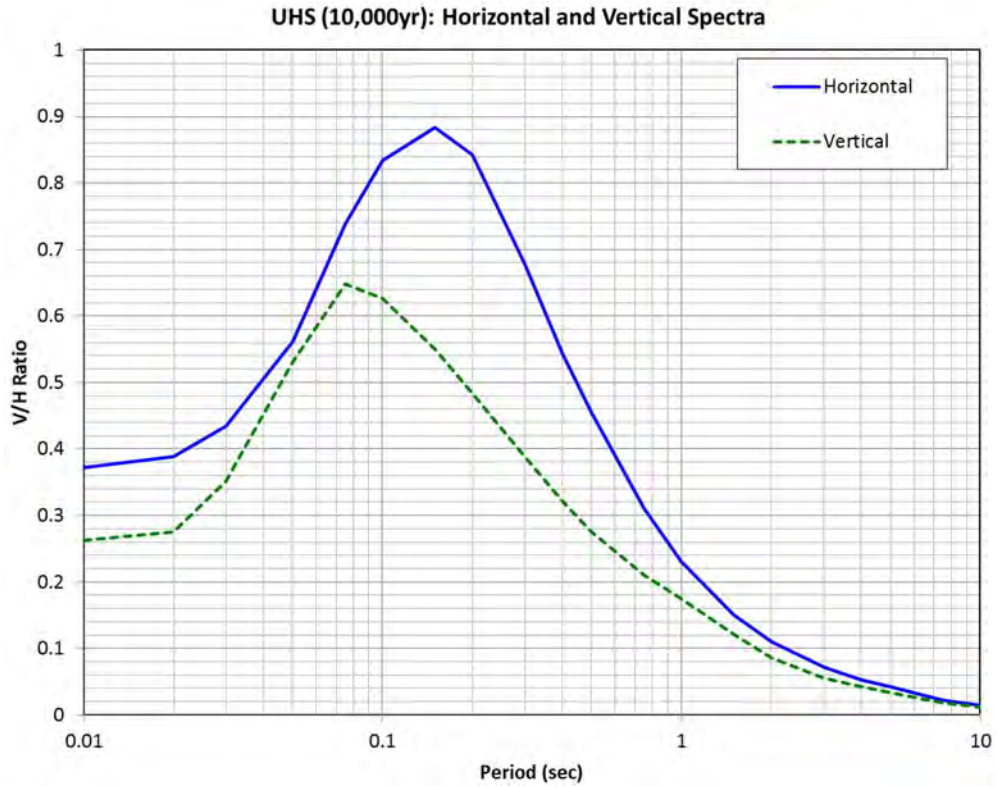

Figure 6-9. Horizontal and vertical design spectra for the 10,000 year hazard level

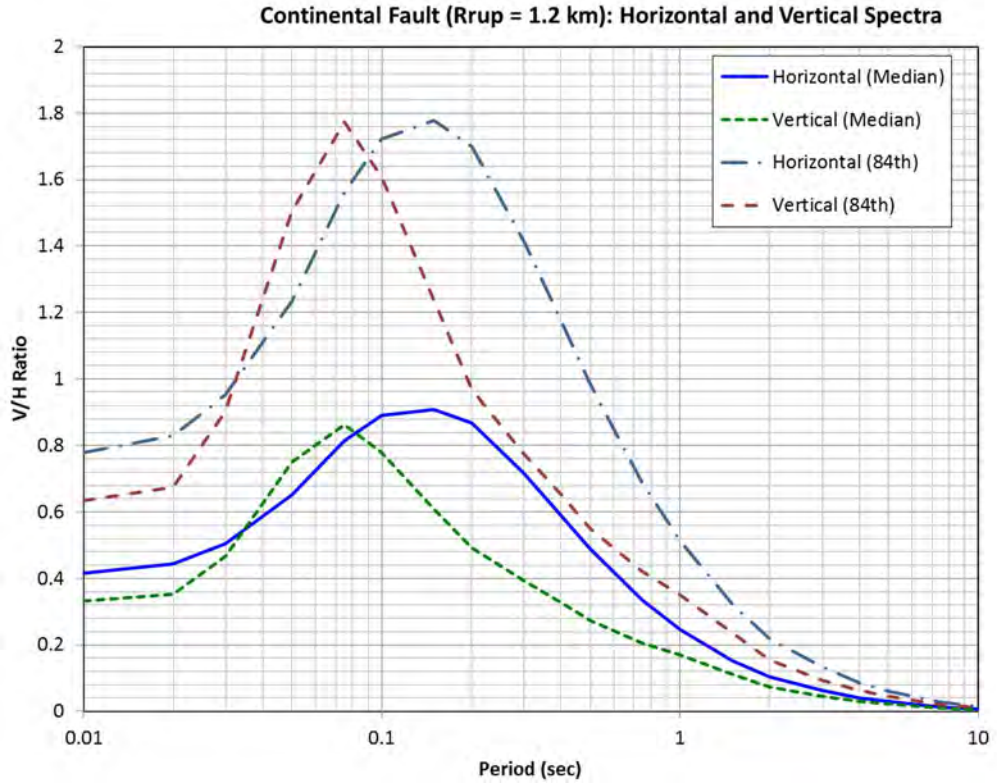

Figure 6-10. Horizontal and vertical design spectra for the deterministic case with Rrup = 1.2 km

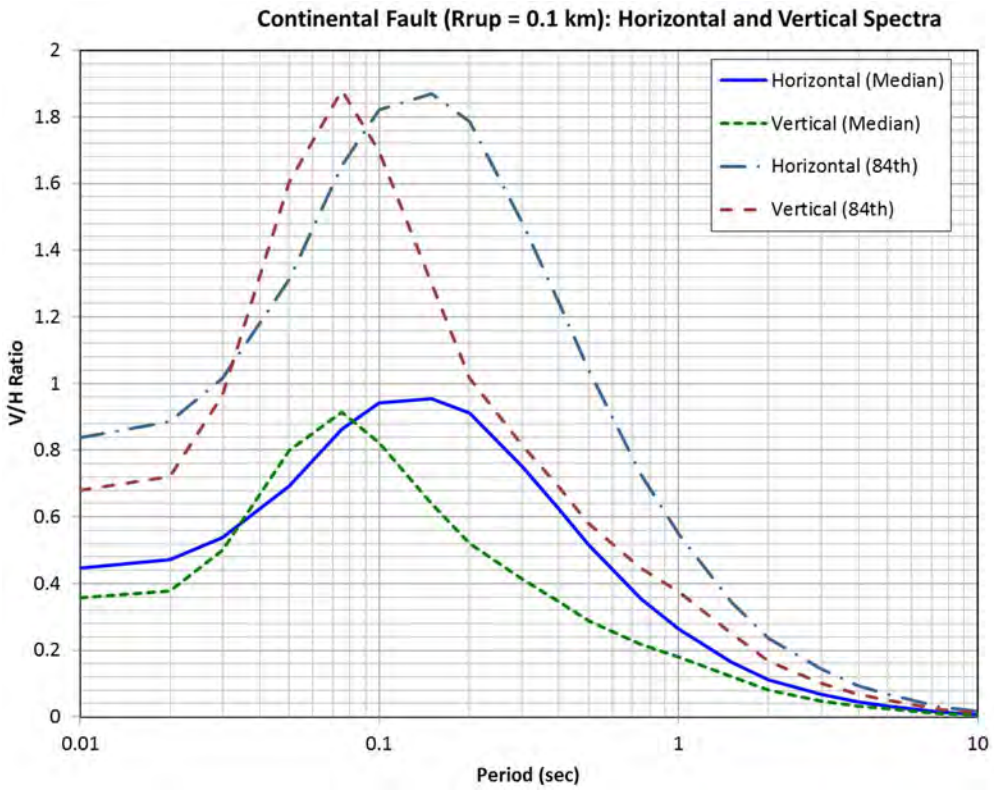

Figure 6-11. Horizontal and vertical design spectra for the deterministic case with Rrup = 0.1 km

7. CONTINENTAL FAULT DISPLACEMENT HAZARD

Deterministic hazard analysis is typically used to evaluate surface fault displacements whereby a single maximum credible earthquake (MCE) and a single fault displacement prediction equation (DPE) are used to calculate average or maximum displacement (median or 84th percentile) on a fault. In contrast, probabilistic methods have not been employed to a great extent in the evaluation of fault rupture hazard. Youngs et al. (2003) developed a methodology for probabilistic fault displacement hazard analysis whereby the likelihood of exceeding various levels of surface displacement from earthquakes is assessed. They applied this approach to a normal faulting environment at Yucca Mountain, Nevada.

Herein, we evaluate the net displacement hazard on the Continental fault using an "informed deterministic" approach following the methodology described in Pacific Gas and Electric (2015). This approach was used for PG&E's pipeline fault crossing evaluation program and represents the future state of practice for fault displacement analysis. Net displacement is typically calculated from the vector sum of horizontal and vertical slip components measured at a single location along the rupture. The informed deterministic approach is deterministic in principle (i.e., does not consider earthquake rates as a parameter) but unlike traditional deterministic approach where a single MCE scenario is used to calculate fault displacement, this approach considers the epistemic uncertainty in defining the MCE. Epistemic uncertainty and aleatory variability in the fault DPEs are also included. The informed deterministic approach results in hazard curves with exceedance probability ranging from 0 to 1 (as opposed to annual rate of exceedance in the probabilistic approach) plotted versus displacement. As a result of accounting for the uncertainties in the MCE and the DPE, the informed deterministic approach acknowledges the considerable uncertainty involved in estimating the net fault displacement at a project site.

In addition to the assessment of the net displacement hazard at the Continental fault crossing the YDTI site, the maximum displacement hazard on the fault is also evaluated. The maximum displacement represents the largest expected surface slip at a point along the fault rupture. Given that it is unknown prior to a rupture event whether the intersection of the YDTI site with the Continental fault lies where the maximum displacement will occur, the maximum displacement hazard represents a conservative upper estimate of fault displacement at the crossing location. Comparisons and discussions of the net versus maximum fault displacement estimates are provided below. We note that our analysis provides estimates of primary displacement on the Continental fault and does not consider off-fault distributed deformation or secondary or triggered deformation that may occur on adjacent faults.

7.1 Approach

Fault displacement calculations require estimates of the MCE magnitude and selection of fault DPEs. The informed deterministic approach accounts for the epistemic uncertainty in the MCE and DPE through the use of logic trees whereby each path on the tree represents a viable set of parameters and equations for estimating fault displacement. The confidence in each path is reflected by the combined path weight. Logic trees can be constructed to capture the epistemic uncertainty in the MCE magnitude estimates (or MCE rupture dimensions and magnitude-area or magnitude-length scaling relationships) and alternative

DPEs. The aleatory variability in the displacement along each logic tree path is captured though the use of a probability density function. This variability is typically represented by the standard deviation of the prediction equations.

Fault displacement is calculated for each path of the logic tree. Results can be expressed as a weighted mean displacement hazard curve in the form of a complementary cumulative distribution function (CCDF); whereby the probability from 0 to 1 of a displacement value being exceeded is plotted against displacement. In addition to the mean hazard curve, CCDFs can be plotted for the individual logic tree paths as well as hazard fractiles (i.e., 50th, 10th, and 90th fractiles). The mean and the median hazard curves represent the central tendency of the hazard results while the separation among the fractile curves represents the epistemic uncertainty in the models and parameters used on the results and provides a measure of confidence in the mean hazard estimate.

7.2 Source and Displacement Characterization

We use the logic tree presented in Figure 7-1 to capture the epistemic uncertainty in the source characterization (magnitude estimates) and displacement characterization (candidate DPEs). Predicting fault displacement is usually based on either magnitude or paleoseismic slip or a combination of both. For the Continental fault, there are no historic or paleoseismic measurements of prior surface-fault displacements at or near the fault crossing site. As a result, estimates of maximum magnitude used in the PSHA for the Continental fault are used in this analysis (**M** 6.2, 6.5, and 6.8 with weights of 0.2, 0.6, and 0.2, respectively).

The displacement characterization consists of alternative methods to calculate fault displacement; typically based on published empirical magnitude-displacement relations and consideration of the variability in displacement at a point along the fault. The use of multiple DPEs captures the epistemic uncertainty in the DPE. The aleatory variability for each DPE represents variability in the event-to-event displacement as well as measurement errors in the dataset used to derive a DPE. Three alternative DPEs are used to estimate the average displacement on the Continental fault: Wells and Coppersmith (1994) for all slip types, Wells and Coppersmith (1994) for normal faults, and Hecker et al. (2013). These relationships have the following form:

$$\log_{10} AD = a\boldsymbol{M} + b \pm \sigma_{AD} \qquad (1)$$

where AD is the average surface displacement (i.e., mean displacement along the rupture length) and $\sigma_{AD}$is the regression standard deviation in log10 units. Average displacement (median estimate) versus magnitude predicted by these 3 empirical relationships is shown in Figure 7-2. Figure 7-2 indicates that the Wells and Coppersmith (1994) relationships for all slip types and for normal faults predict similar average fault displacement as a function of magnitude. Because the relationship for all fault types is based on a larger dataset and provides more reliable results, we give the Wells and Coppersmith relationships for all fault types and for normal faults weights of 0.5 and 0.3, respectively. The Hecker et al. (2013) relationship is based on a least-squares fit to data from Wesnousky (2008). As shown in Figure 7-2, this

relationship has a smaller slope than the Wells and Coppersmith relationships. We give the Hecker et al. (2013) relationship a weight of 0.2 since the dataset used to derive it is smaller than that of Wells and Coppersmith (1994) (a total of 37 versus 56 events). Table 7-1 lists the a- and b-coefficients of the three DPEs along with their published standard deviations (σ_{AD}). The σ_{AD} values represent the variability in predicting the average surface-fault displacement from magnitude. Since our goal is to estimate the primary surface displacement at the intersection of the Continental fault with the YDTI site and not the average surface displacement over the entire surface rupture, the variability in displacement along the surface rupture about the average displacement must be included to estimate the total standard deviation of the net surface displacement at a site (rather than average displacement) given an earthquake of magnitude **M** (Abrahamson 2008). Equation (1) is modified as follows:

$$\log_{10} AD = a\boldsymbol{M} + b \pm \sigma_T \qquad (2)$$

where σ_T is the square root of the sum of squares of regression standard deviation (σ_{AD}) and the along-strike standard deviation (σ_{AS}). Estimates of σ_{AS} are obtained from the analysis of along-strike displacements in Hecker et al. (2013) that suggested a coefficient of variation of 0.6 for strike-slip fault ruptures with comparable estimate for other slip types. This coefficient of variation results in σ_{AS} of 0.24 applied to all three DPEs used in this analysis.

Total standard deviations for each DPE are listed in Table 7-1. The σ_T estimates represent a combination of epistemic uncertainty resulting from imperfect empirical datasets and true aleatory variability in displacement at a particular location along the rupture estimated based on magnitude. Hecker et al. (2013) analyzed available paleoseismic data and observed that the aleatory variability in displacement at a site is lower than the values presented in Table 7-1. They estimated the aleatory standard deviation to be about 0.22 compared to the σ_T values of about 0.4 listed in Table 7-1. The epistemic uncertainty standard deviation part of σ_T, denoted as $\sigma_{\mu e}$, can be estimated using the true aleatory variability of 0.22 and the σ_T estimates in Table 7-1. This additional epistemic uncertainty belongs in the logic tree and can be represented by a 5-point approximation based on Miller and Rice (1983) to discretely sample the values of $\sigma_{\mu e}$. Using the three alternative DPEs and the 5-point approximation to discretize the epistemic uncertainty component of σ_T results in 15 branches describing the median displacement at a site given the MCE magnitude. All 15 DPE branches have an aleatory variability of 0.22 (value based on Hecker et al. (2013) and assumed to apply to the other DPEs).

Table 7-1. Parameters of the DPEs used in the net fault displacement hazard analysis for the YDTI site crossing of the Continental fault

DPE	Weight	a	b	σ_{AD}	σ_{AS}	σ_T
Wells and Coppersmith (1994) – All slip types	0.5	0.69	-4.80	0.36	0.24	0.43
Wells and Coppersmith (1994) – Normal Faults	0.3	0.63	-4.45	0.33	0.24	0.41
Hecker et al. (2013) – All slip types	0.2	0.41	-2.79	0.33	0.24	0.41

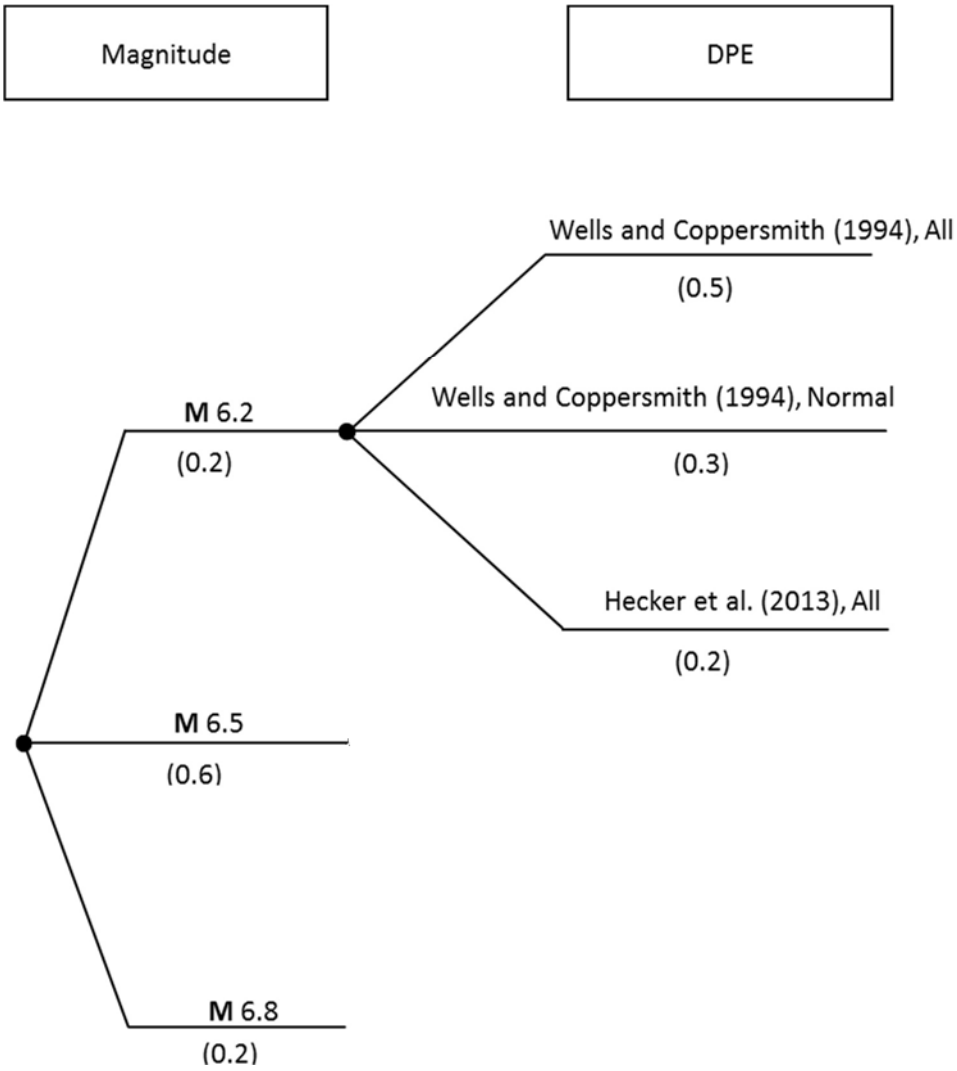

Figure 7-1. Logic tree for fault displacement hazard. Weights are given between parentheses.

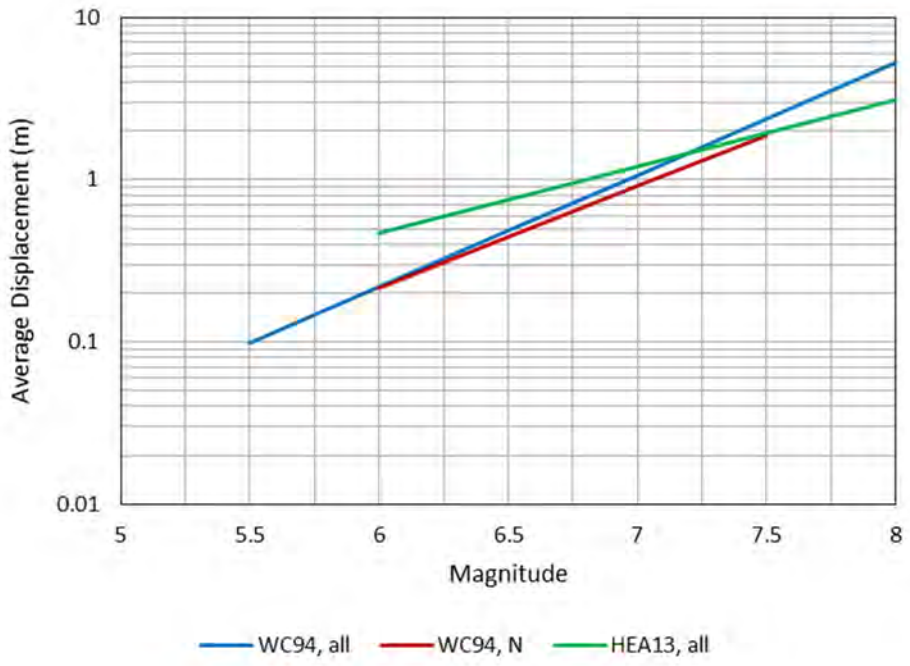

Figure 7-2. Empirical relationships of average displacement (median estimates) versus magnitude

7.3 Results

The three MCE magnitude branches and the 15 DPE branches yield a total of 45 logic tree paths. The exceedance probabilities for each of the 45 logic tree paths as well as for their weighted mean are calculated as a function of displacement. Figure 7-3 shows the displacement exceedance curves for the weighted mean as well as the 10th, 25th, 50th, 75th, 84th, and 90th fractiles. These fractiles are selected logic tree combinations that may represent the correct model, with the steeper slope of the exceedance curve representing only the aleatory variability. For example, the 50th fractile represents the median logic tree combination (i.e., half of the branch combinations produce lower displacement values) while the 84th fractile represents a model for which approximately 84% of the weighted logic tree combinations yield lower displacement values.

The informed deterministic approach was also applied to compute the maximum surface displacement hazard on the Continental fault. MCE magnitudes of 6.5, 6.2, and 6.8 with weights of 0.6, 0.2, and 0.2, respectively, were used along with the Wells and Coppersmith (1994) relationship for all slip types to estimate the maximum displacement. This relationship is defined with the same functional form as Equation (1) and has a slope, intercept and regression standard deviation (aleatory variability) of 0.82, -5.46, and 0.42, respectively. This results in three logic tree paths for calculating maximum displacement. The exceedance curves for the weighted mean and the 50th fractile of the maximum surface displacement on the Continental fault are shown in Figure 7-3 for comparison. Table 7-2 summarizes the average displacement hazard results and lists the median and 84th percentile predictions of the net displacement on a point on the Continental fault. Also listed in Table 7-2 are the median and 84th percentile maximum

displacement predictions from the hazard results on the Continental fault. Table 7-2 indicates that the mean and 84th percentile net displacement values are 0.51 and 1.44 m, respectively. Moreover, the maximum predicted displacement on the Continental fault is close to 1.5 times the predicted net displacement at a point on the fault.

We note that the use of the net displacement at a point rather than the maximum displacement result is more appropriate for design considerations at the YDTI site. The maximum displacement values represent a conservative upper bound of the predicted displacement on the Continental fault. Moreover, the intersection of the YDTI site with the Continental fault occurs towards the northern end of the fault. Youngs et al. (2003) studied the variation in the amount of surface displacement along the principal rupture for historical Basin and Range normal faulting events compiled by Wheeler (1989). Figure 7-4 presents their distribution of D/MD (fault displacement normalized by maximum displacement) as a function of X/L, where X/L expresses the location of a point along the rupture (X is the distance from one end of the rupture to the point in question and L is the rupture length). As shown in Figure 7-4, fault surface displacement tends to die out towards the end of the fault rupture and displacement peaks at a limited interval along the rupture primarily towards the midpoint. As a result, we consider the use of the net average displacement values for the YDTI site to be more appropriate than the maximum displacement values. Similar to the discussion regarding the use of the median versus 84th percentile deterministic response spectra presented in Section 6.1, the decision to use the median versus 84th percentile values of the net displacement should be carefully evaluated. Given the low slip rate on the Continental fault, a hazard matrix similar to the one presented in Table 6-1 can be developed. For high or extreme consequences of failure, the 50th or the 84th percentile average displacement can be used. For low to moderate consequences, the use of the 50th percentile net displacement is recommended.

Finally, Youngs et al. (2003) evaluated the conditional probability that a rupture on the fault causing the earthquake reaches or nears the surface. Their analysis was based on an empirical approach fitting datasets that define the rates at which earthquakes of various magnitudes rupture the surface. Figure 7-5 shows their resulting probability of surface fault rupture versus magnitude. For the MCE magnitude of 6.5 on the Continental fault, the probability of a surface rupture ranges from about 0.5 to 0.8 as indicated in Figure 7-4. This reinforces our recommendation for using the net displacement as opposed to maximum fault displacement values.

Table 7-2. Surface fault displacement hazard results on the Continental fault

Exceedance	Percentile	Average Displacement (m)	Maximum Displacement (m)
0.50	50	0.51	0.74
0.16	84	1.44	2.07

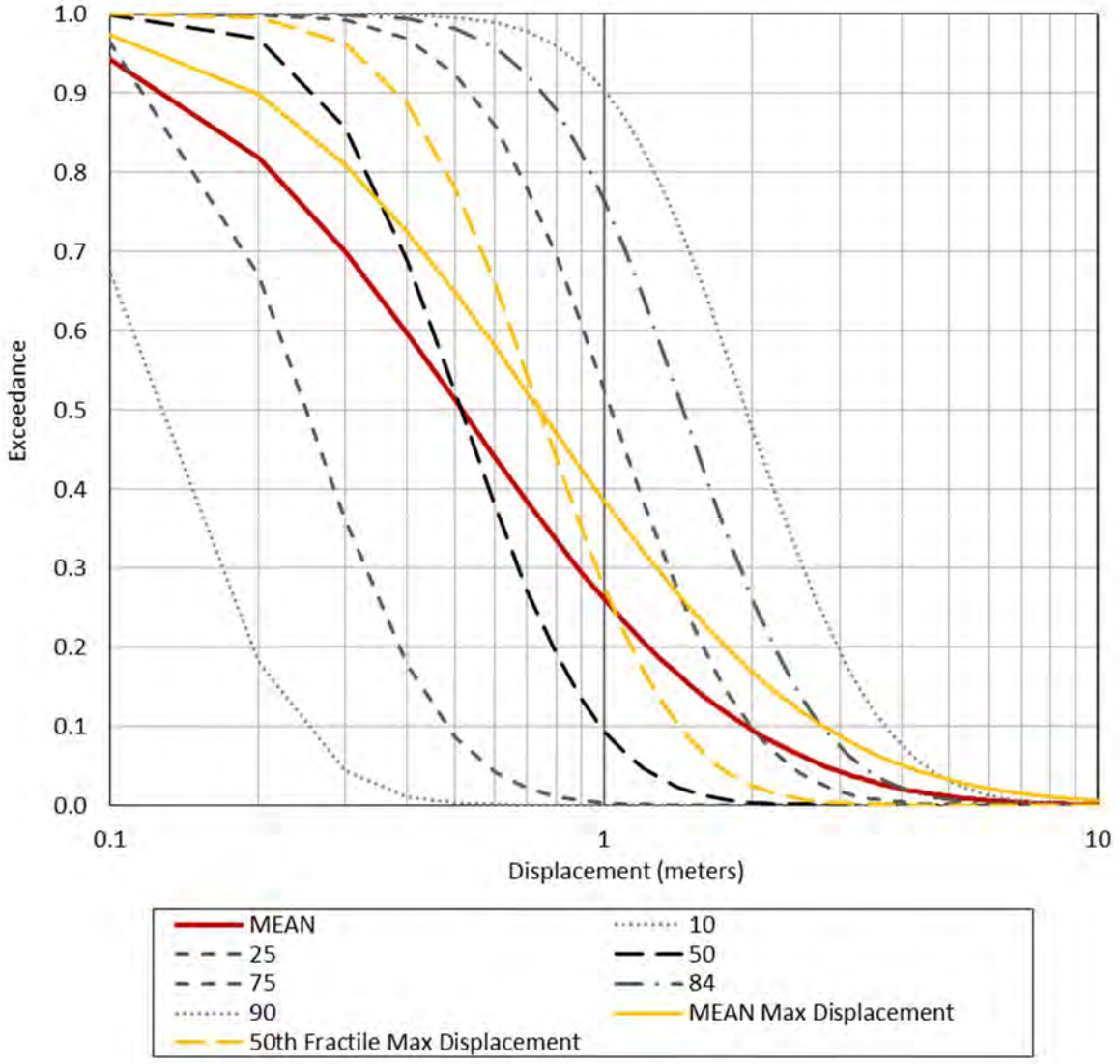

Figure 7-3. Displacement exceedance curves for the net displacement at a point on the Continental fault compared to the maximum displacement exceedance curves (in yellow) on the Continental fault

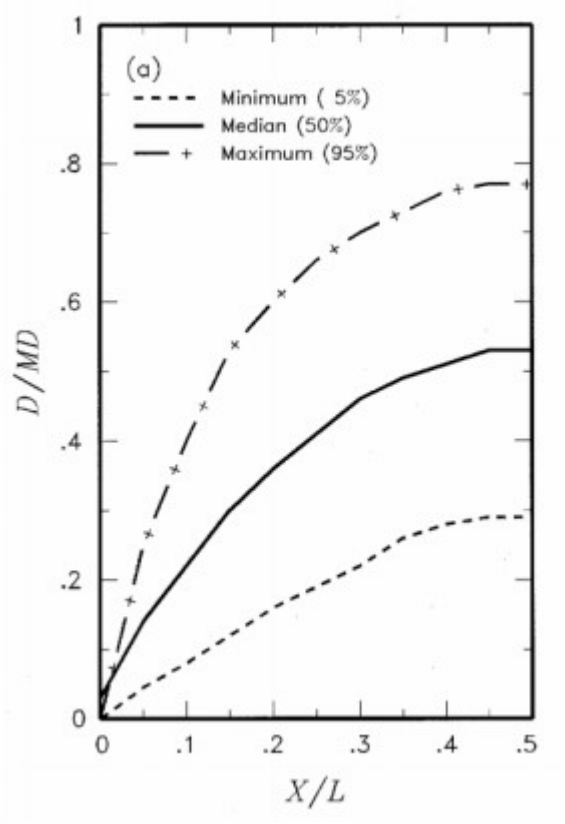

Figure 7-4. Distribution of the ratio of D/MD based on the data in Wheeler (1989) (source: Youngs et al. 2003)

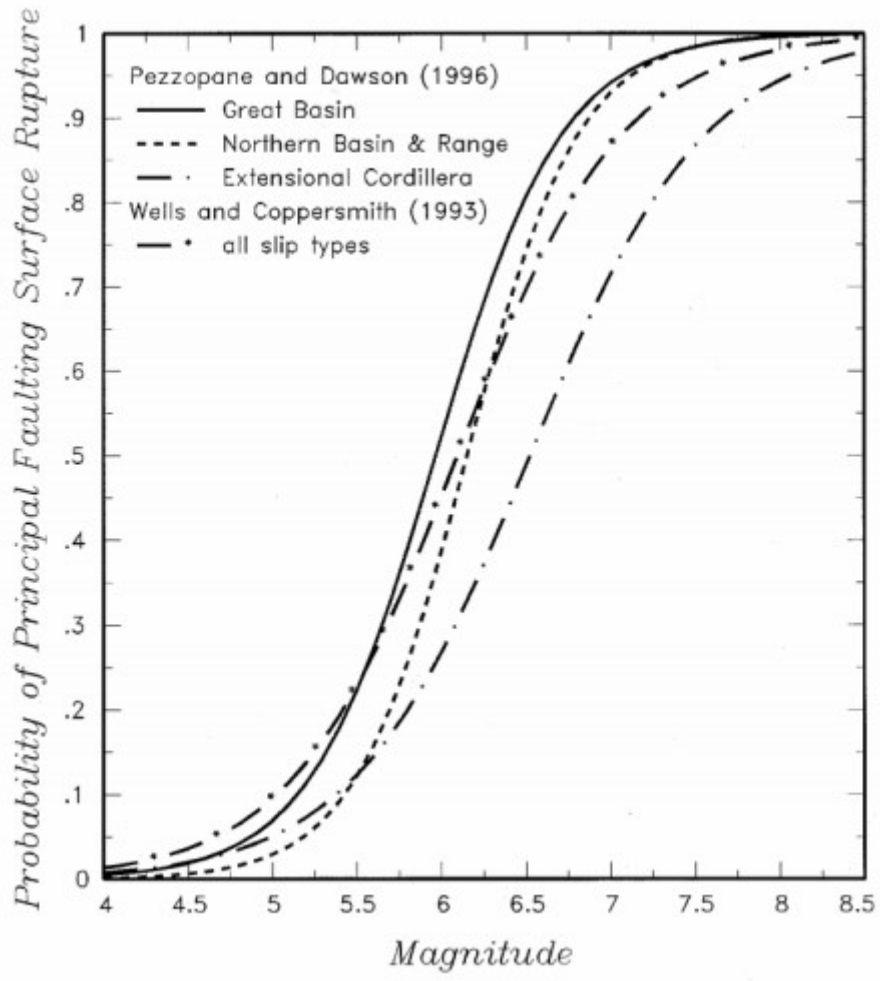

Figure 7-5. Empirical models for conditional probability of surface rupture for principal faulting (source: Youngs et al. 2003)

8. DESIGN TIME SERIES

8.1 Ground Motion Selection

A total of five sets of two-component (i.e., one horizontal and one vertical) design time series were developed for the each of following design levels:

- Probabilistic spectra with return periods of 475, 1,000, 2,475, and 10,000 years
- DSHA 50th and 84th percentile response spectra for the MCE scenarios on the Continental fault with rupture distances of 1.2 and 0.1 km.

The selection of seed input time series was based on project-specific parameters such magnitude, source-to-site distance and tectonic setting as determined from the hazard deaggregation and MCE scenarios as well as the overall agreement in spectral shape between the time series response spectra for the horizontal and vertical components and the design spectra. Fault rupture mechanism and site conditions were not restricted in the selection process because these criteria are considered less important in the selection of representative time series (Al Atik and Abrahamson 2010). Moreover, the spectral matching process corrects for differences in the frequency content resulting from different site conditions.

Figure 8-1 presents the spectral shapes (PSA/PGA) for all eight horizontal and vertical design spectra for the YDTI site. Based on the similarities in spectral shapes of the probabilistic spectra for both horizontal and vertical components, we use the same set of five input time series for all the PSHA-based design spectra. Similarly, the deterministic spectra (median and 84th percentile; rupture distances of 1.2 and 0.1 km) show similar spectral shapes for both horizontal and vertical components. As a result, the same set of input time series was used for all the deterministic design levels.

The deaggregation results of the PSHA presented in Section 5.1 and the summary of scenario events controlling the hazard at the different return periods presented in Table 6-3 were used to guide the selection of input time series for the PSHA-based design spectra. Two input time series were selected with **M** 6 to 6.5 and distance up to 15 km to represent the short-distance and moderate-magnitude scenarios from the background source controlling the short-period UHS with 2,475 and 10,000 year return period. One input time series was selected with moderate-magnitude range (**M** 6 to 6.5) and distance of 20 to 40 km to represent the controlling scenarios at short period for the 475 and 1,000 year spectra. The last two input time series were selected to represent the long-period controlling scenarios with **M** 6.5 to 7 and distance of 30 to 60 km. A recording from the Helena, Montana-01 earthquake recorded at Carroll College station with **M** 6 and distance of 2.86 km was used as part of the set of input time series. In addition to satisfying the magnitude and distance selection criteria and having overall agreement in spectral shape with the design spectra, this recording was selected for being local and likely representative of the general ground-motion character in Montana.

For the DSHA-based design spectra, a set of five two-component time series were selected with **M** 6.2 to 6.8 and distance up to 10 km to represent the MCE scenarios on the Continental fault. The selected set of

time series also includes the recording from the Helena, Montana-01 earthquake recorded at Carroll College for the reasons discussed above. All ground motions were obtained from the Pacific Earthquake Engineering Research Center (PEER) NGA-West2 ground motion database (http://ngawest2.berkeley.edu). Tables 8-1 and 8-2 summarize the parameters of the selected seed input time series for the PSHA-based and deterministic design spectra.

Table 8-1. Parameters of the selected input time series for the PSHA-based design spectra. Comp stands for component, Mech for mechanism, SS for strike-slip, and RV for reverse.

Set #	Earthquake	Station Name	Comp	NGA #	M	Mech	Rrup (km)
1	Helena, Montana-01	Carroll College	H2, Up	1	6	SS	2.86
2	Parkfield	Cholame - Shandon Array #8	H1, Up	31	6.19	SS	12.9
3	Chi-Chi, Taiwan-03	TCU067	H1, Up	2619	6.2	RV	28.46
4	Chuetsu-oki, Japan	Kawaguchi	H2, Up	4869	6.8	RV	29.25
5	Niigata, Japan	NIGH18	H2, Up	4234	6.63	RV	55.84

Table 8-2. Parameters of the selected input time series for the DSHA-based design spectra. Comp stands for component, Mech for mechanism, SS for strike-slip, RV for reverse, and NM for normal.

Set #	Earthquake	Station Name	Comp	NGA #	M	Mech	Rrup (km)
1	Helena, Montana-01	Carroll College	H2, Up	1	6	SS	2.86
2	San Fernando	Pacoima Dam	H1, Up	77	6.61	RV	1.81
3	Imperial Valley-06	El Centro Array #5	H1, Up	180	6.53	SS	3.95
4	Niigata, Japan	NIG020	H1, Up	4210	6.63	RV	8.47
5	L’Aquila, Italy	L'Aquila - Parking	H2, Up	4483	6.3	NM	5.38

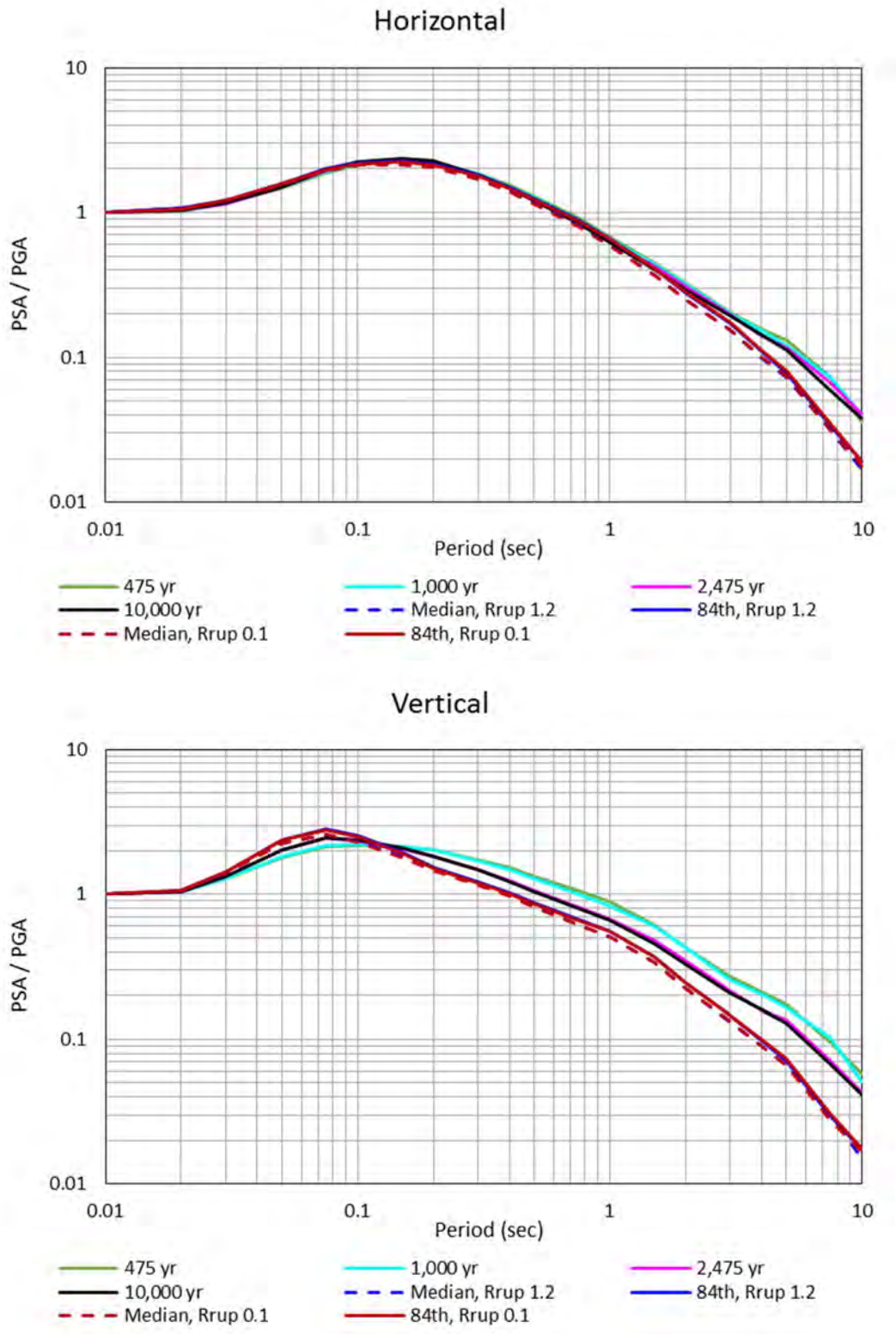

Figure 8-1. Spectral shapes for the horizontal (top) and vertical (bottom) design spectra

8.2 Ground Motion Modification

Each component of the selected seed acceleration time series was modified such that its response spectrum matches the corresponding target design spectrum. Time-domain spectral matching as implemented in the computer program RSPMatch (Abrahamson 2003) was used for the ground-motion modification. This procedure involves adding finite wavelets in the time domain to decrease the spectral differences between the seed motion and the target spectra. The objective of spectral matching is to reduce the individual spectral peaks and troughs of the seed input motion while preserving the non-stationary characteristics of the seed motion (Al Atik and Abrahamson 2010).

Spectral matching was performed in incremental period ranges from 0.01 to 5 sec and baseline correction was applied to the spectrally-matched time series to remove the resulting drift in the displacement time series. Acceleration response spectra of the modified motion were compared to the target response spectra to ensure a close match between the two. In addition, comparisons were performed to ensure that the non-stationary characteristics of the seed input time series and modified time series (i.e., acceleration, velocity, and displacement) and the associated peak ground motion parameters and durations were reasonable and acceptable.

Comparisons of the spectrally-matched motion to the original seed motion for the five sets of time series (summarized in Table 8-1) matched to the four target PSHA-based design spectra (horizontal and vertical) are shown in Appendices II to V for return periods of 475, 1,000, 2,475, and 10,000 years. Similarly, Appendices VI to IX present comparisons of the spectrally-matched motions of the original input time series (Table 8-2) matched to the four target DSHA-based design spectra (median and 84^{th} percentile, distance of 1.2 and 0.1 km). The initial acceleration response spectra were scaled to the design PGA values. Comparisons between the matched and scaled seed motions are provided for the acceleration, velocity and displacements as well as the response spectra, Fourier amplitude spectra, and normalized Arias intensity. Comparisons of the normalized displacement for the matched and seed time series are also provided to better evaluate the differences resulting from the spectral matching.

Figure 8-2 compares the target PSHA-based spectra with 475 year return period to the average response spectra of the five matched time series for the horizontal and vertical components. For both components, a spectral mismatch of less than 4% was achieved between the average matched and the target design spectra in the period range of 0.01 to 5 sec. For spectral periods of 5 to 10 sec, the spectral mismatch between the average matched and the target spectra was allowed to be larger in order to avoid significantly altering the waveform of the seed motions. Similarly, Figures 8-3 to 8-9 present the comparisons of the seven remaining target probabilistic and deterministic design spectra to the average response spectra of the five matched time series for the horizontal and vertical components.

Some regulations require that the average response spectrum of the matched time series should be equal to or higher than the target design spectra in the period range of interest. If this requirement is applicable to this project, we recommend that each of the matched motions be scaled by a scaling factor in the range of 1.02 to 1.05 required to ensure than the average matched response spectra are always equal to or

higher than the target response spectra in the period range of 0.01 to 5 seconds. The recommended scaling factors are presented in Table 8-3 for the probabilistic and deterministic design spectra.

The digital values of the five sets of matched acceleration time series to the design spectra are given in the accompanying folder "MatchedTH". A description of the acceleration file format is given in the file "Format.txt".

Table 8-3. Recommended scaling factors for the matched time series

Target Design Level	Scaling Factor	
	Horizontal Component	**Vertical Component**
475 year	1.0442	1.0375
1,000 year	1.0332	1.0308
2,475 year	1.0331	1.0267
10,000 year	1.0332	1.0201
MCE 1.2 km - Median	1.0248	1.0261
MCE 1.2 km – 84th percentile	1.0461	1.0309
MCE 0.1 km - Median	1.0442	1.0329
MCE 0.1 km – 84th percentile	1.0465	1.0447

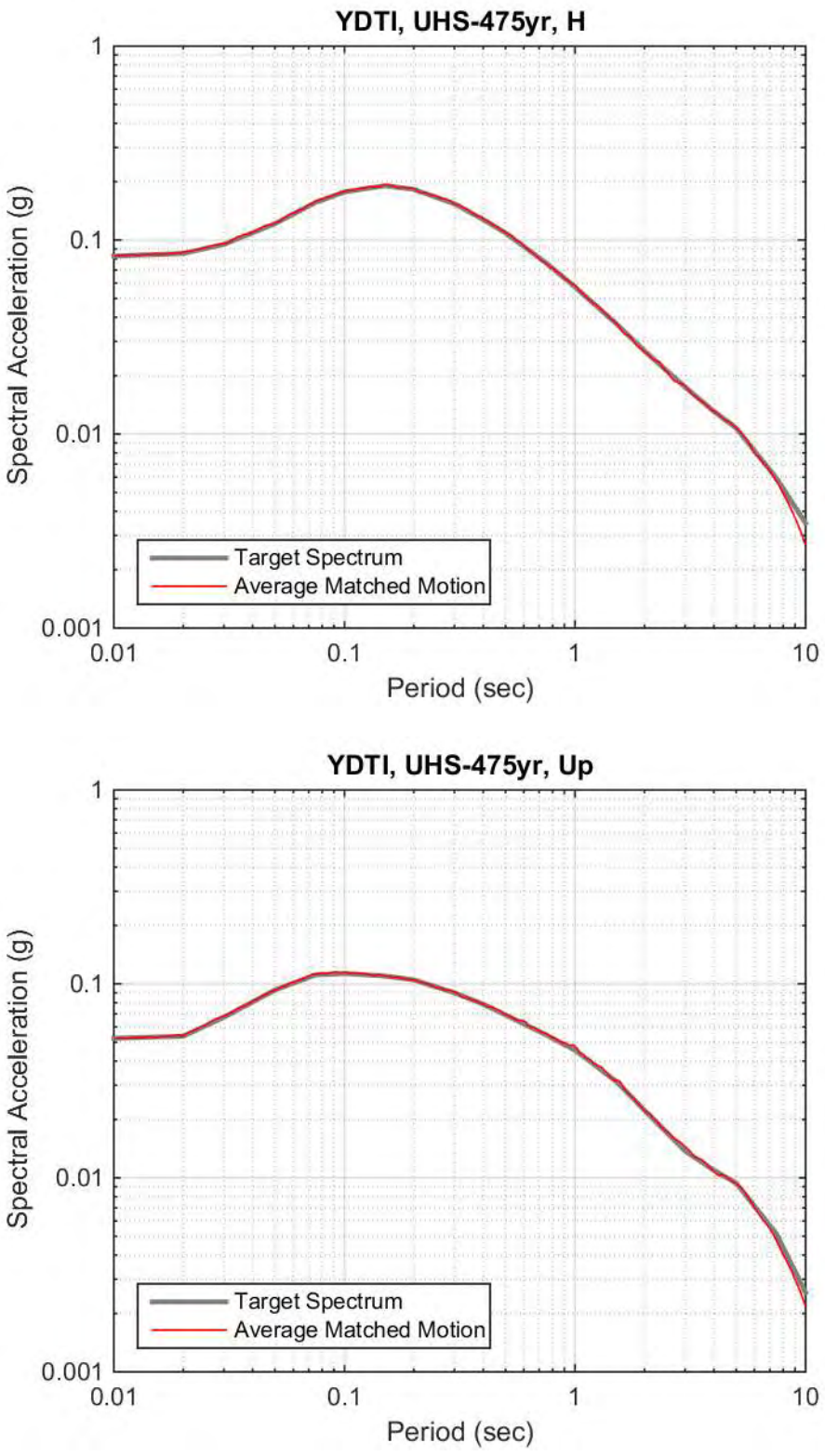

Figure 8-2. Comparison of the average response spectra of the five matched motions (horizontal and vertical) to the target 475 year design spectra

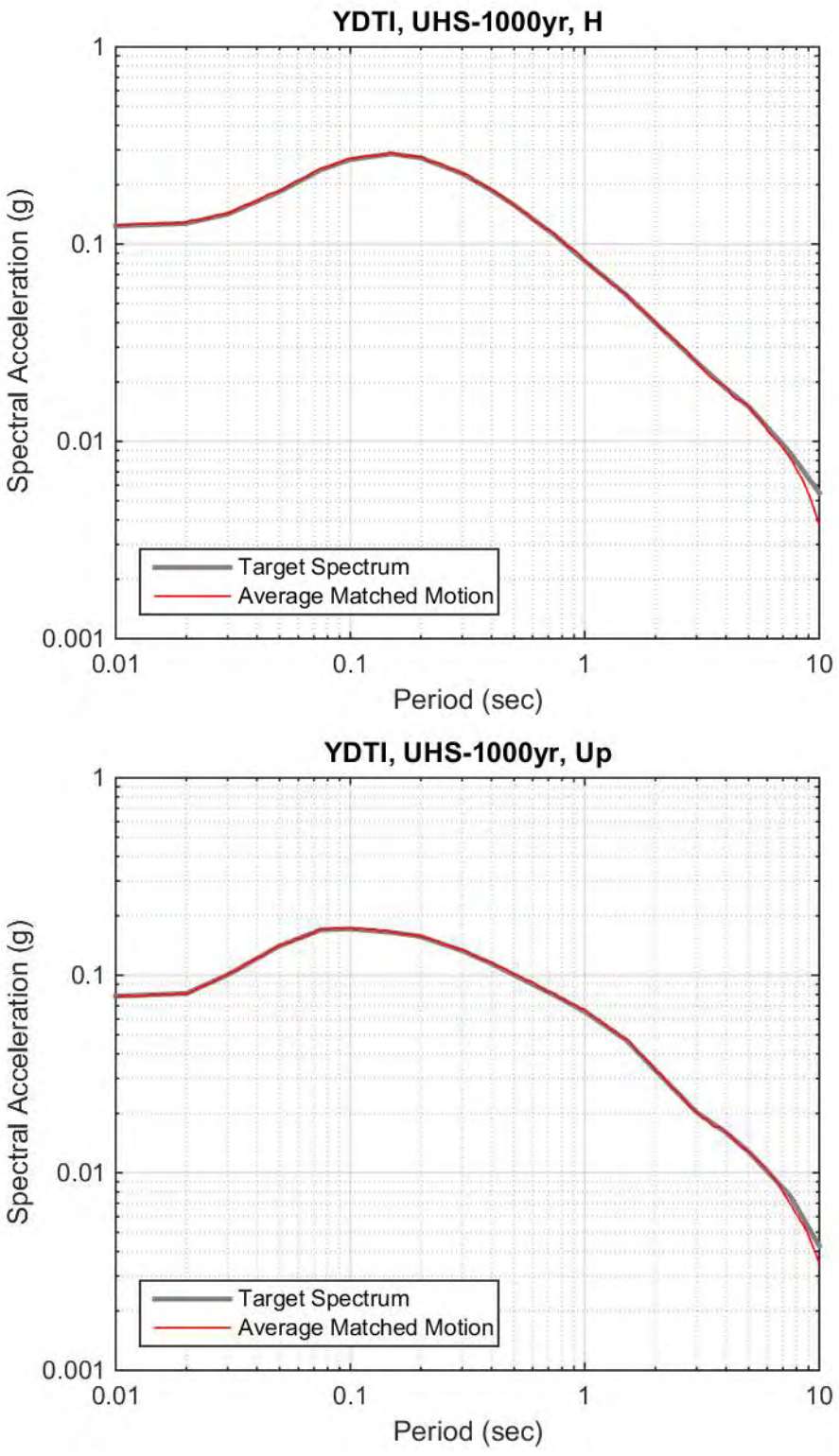

Figure 8-3. Comparison of the average response spectra of the five matched motions (horizontal and vertical) to the target 1,000 year design spectra

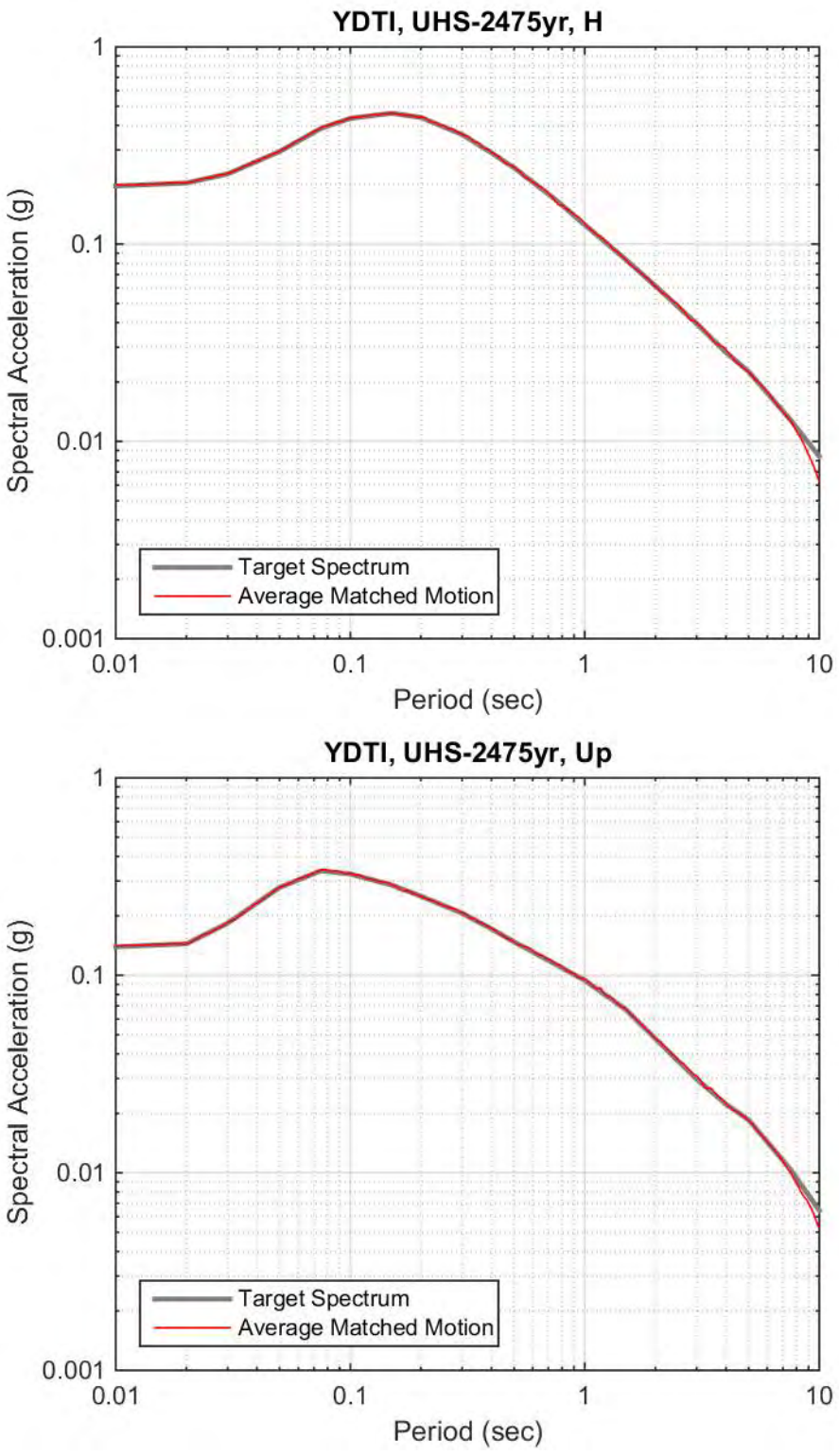

Figure 8-4. Comparison of the average response spectra of the five matched motions (horizontal and vertical) to the target 2,475 year design spectra

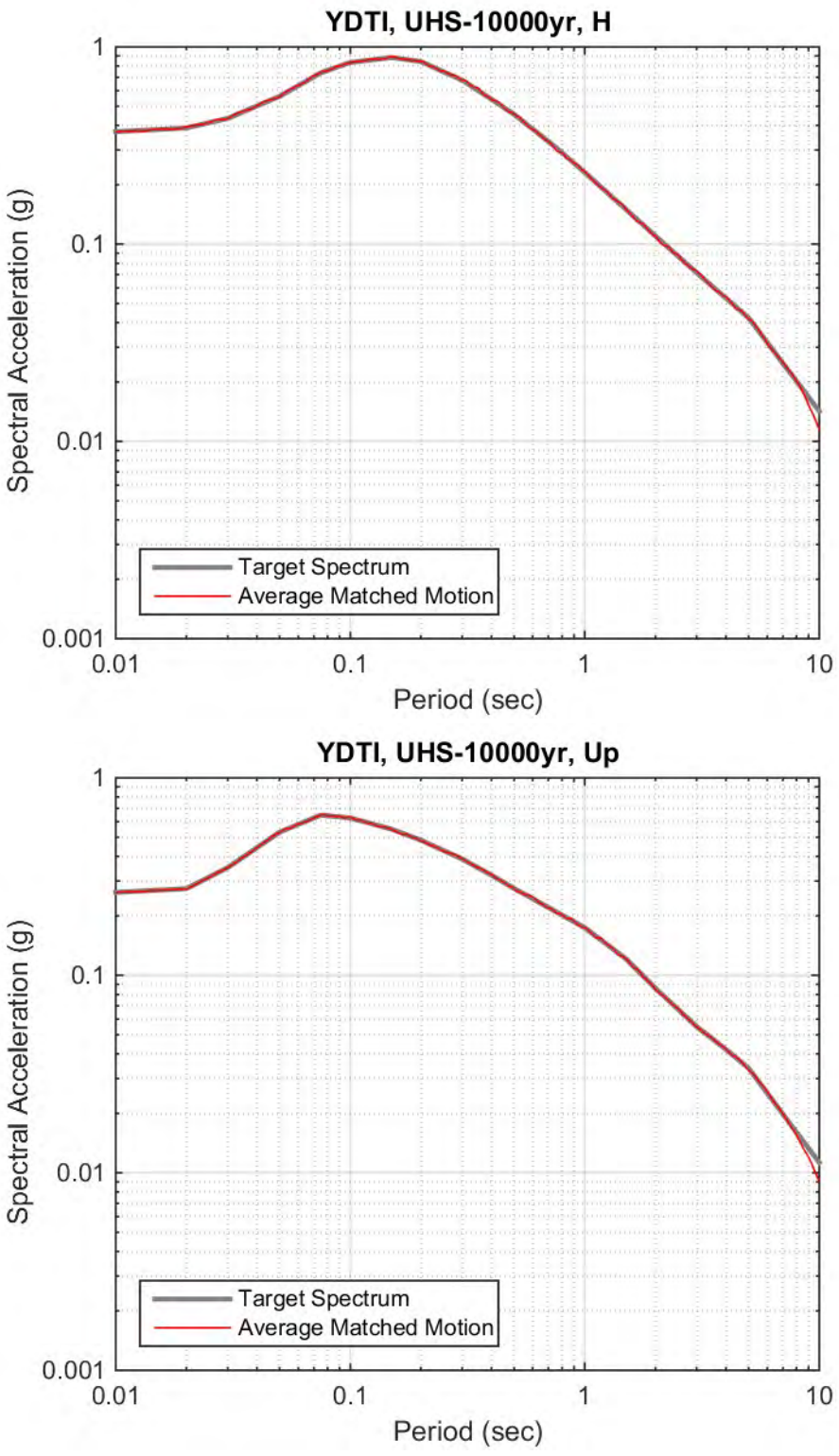

Figure 8-5. Comparison of the average response spectra of the five matched motions (horizontal and vertical) to the target 10,000 year design spectra

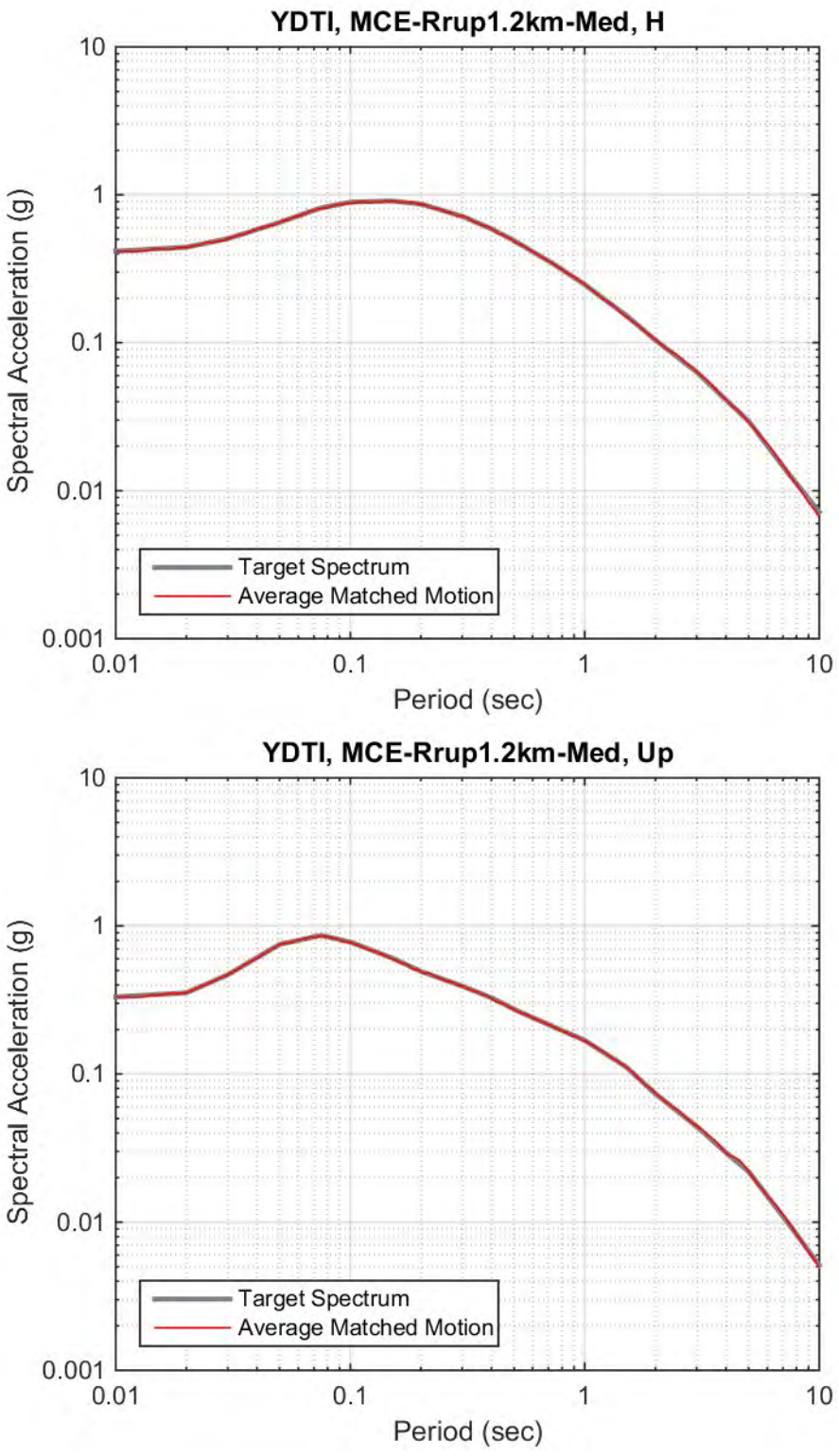

Figure 8-6. Comparison of the average response spectra of the five matched motions (horizontal and vertical) to the target MCE median design spectra with Rrup = 1.2 km

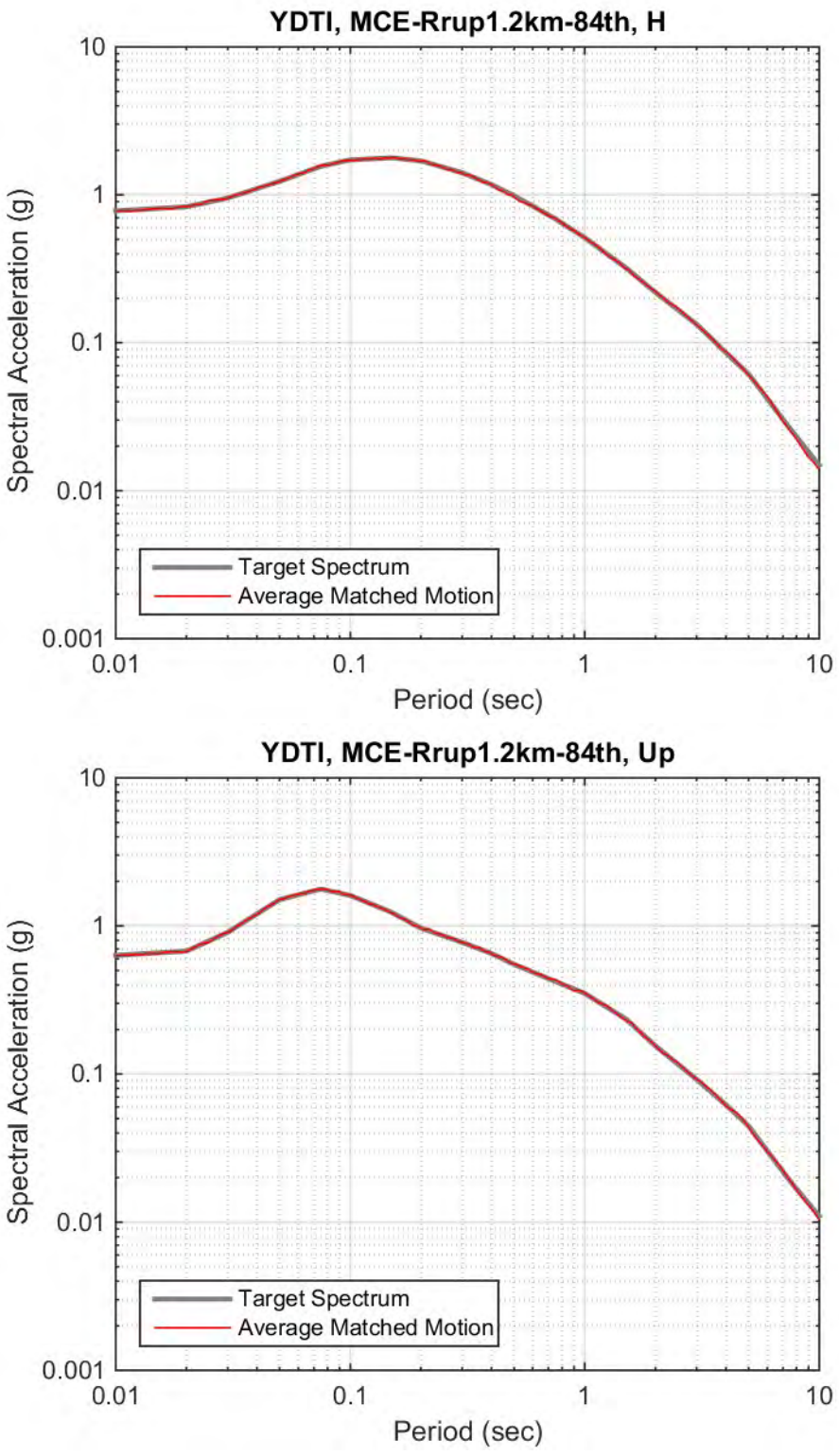

Figure 8-7. Comparison of the average response spectra of the five matched motions (horizontal and vertical) to the target MCE 84th percentile design spectra with Rrup = 1.2 km

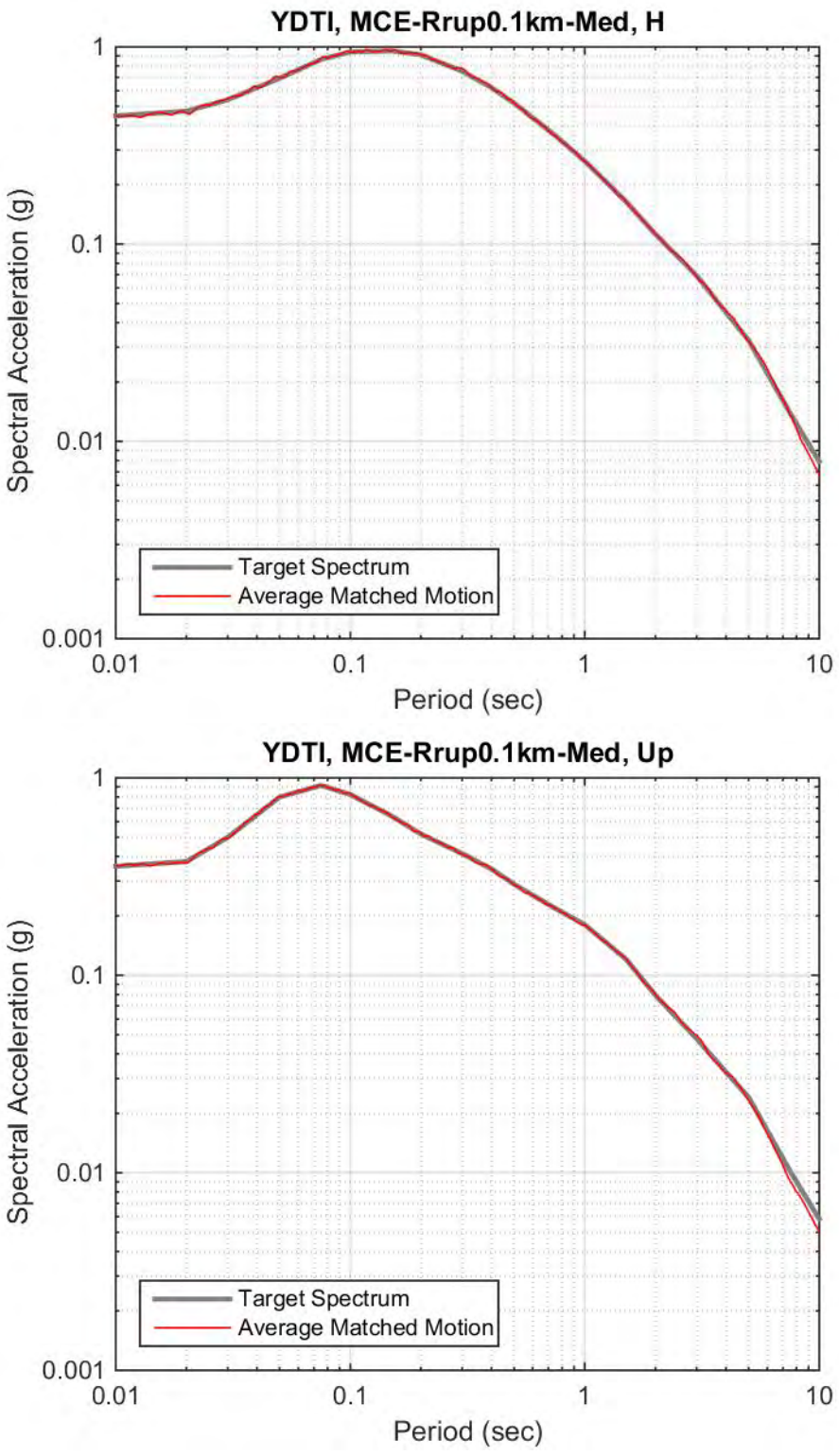

Figure 8-8. Comparison of the average response spectra of the five matched motions (horizontal and vertical) to the target MCE median design spectra with Rrup = 0.1 km

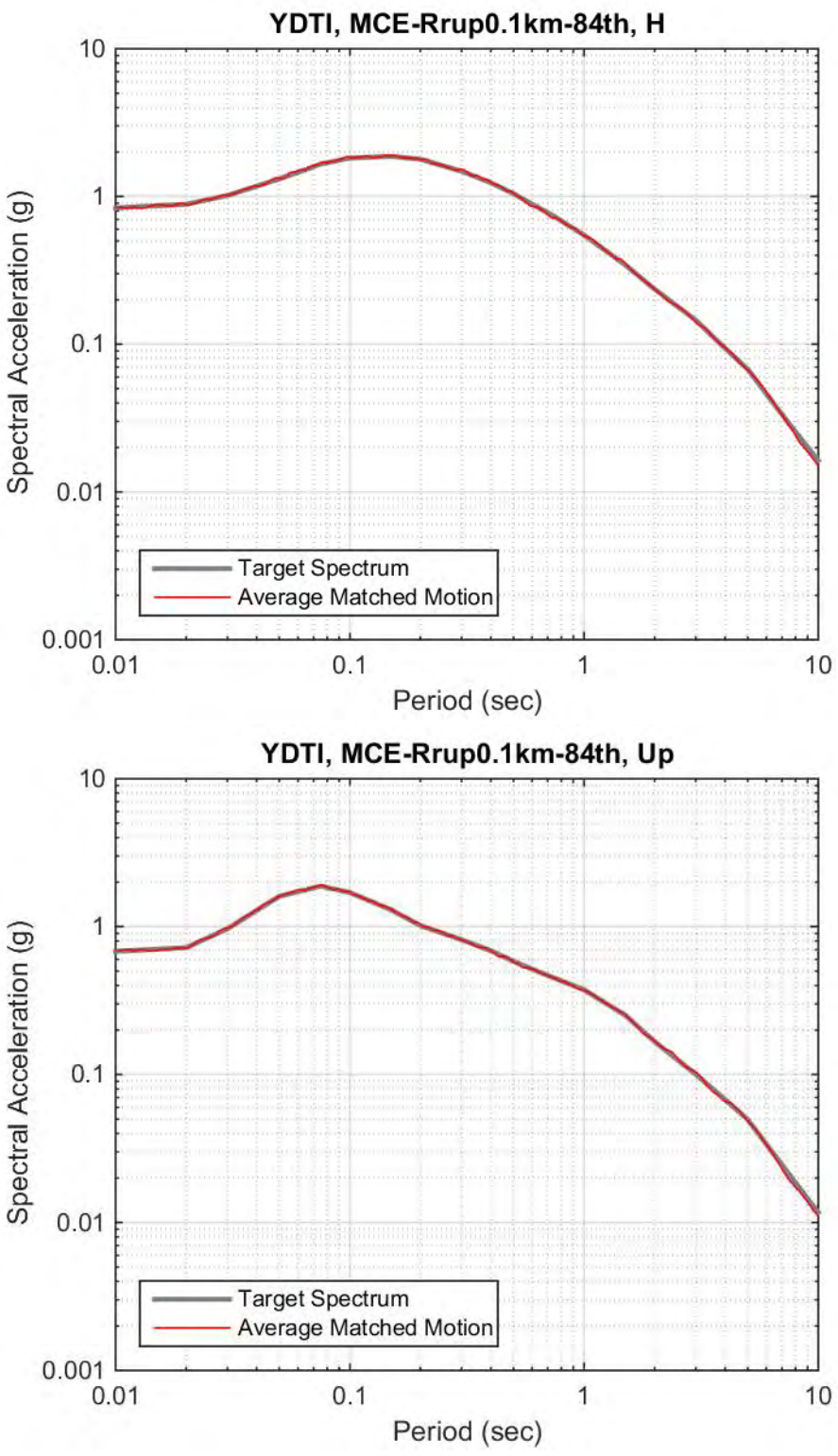

Figure 8-9. Comparison of the average response spectra of the five matched motions (horizontal and vertical) to the target MCE 84th percentile design spectra with Rrup = 0.1 km

9. POTENTIAL FOR FAULT INTERACTION

The maximum magnitude on a fault is related to the maximum possible rupture length on the fault. The potential for nearby faults to interact and generate larger magnitude earthquakes (through larger rupture areas) has been investigated in the literature. These interactions usually happen across disconnected stepovers between parallel faults or parallel faults with another fault linking them. We discuss here the potential for fault interaction between the Continental and the Rocker faults and its effects on the ground motion at the YDTI site.

Previous studies of stepovers in strike-slip faults in the absence of linking faults showed that the ability of rupture to jump across a stepover is a function of the width of the stepover and the degree of overlap between the faults. Closer stepovers and positive overlaps allow the rupture to jump across more easily. Harris and Day (1993) studied stepovers on parallel strike-slip faults and found that ruptures are not likely to propagate over stepovers with a separation wider than about 5 km. While rupture propagation across both the Continental and the Rocker faults is not impossible, it is unlikely given that the closest distance between the Continental and the Rocker faults on the surface is on the order of 9 km. Moreover, there are no mapped faults between the Continental and Rocker faults that could link the rupture between the two faults.

The study of the potential for rupture propagation across stepovers requires complex seismic source modeling that is usually based on simulations and state-wide inversions of geologic, geodetic, and seismicity data. Such complex ruptures have been incorporated in the seismic source model for California where the linking of faults is considered on closely-located fault segments with similar strikes and geometries. In light of the limited amount of available data on the Continental and the Rocker faults, such complex fault rupture studies are difficult to perform.

Finally, we note that the occurrence of large magnitude events resulting from rupture propagation across both the Continental and the Rocker faults would have a very low probability. At the short distance of the YDTI site to a rupture on the Continental fault (Rrup of 0.1 km), ground motions have been observed to show saturation or oversaturation with large magnitudes at PGA and at short spectral periods ($T \leq 0.2$ sec). The concept of magnitude oversaturation refers to decreasing ground motion with increasing magnitude at large magnitudes. While oversaturation is typically not allowed to occur in ground-motion models, saturation is incorporated in some GMPEs (e.g. Campbell and Bozorgnia 2014), by constraining the magnitude scaling to remain constant at large magnitudes (**M** greater than about 6.5) and Rrup of 0 km. Figure 9.1 shows the magnitude scaling of four NGA-West2 GMPEs for a scenario on the Continental fault with Rrup = 0.1 km at a period of 0.01 sec. Figure 9.1 shows that most of the models exhibit magnitude saturation where the ground motion approaches a constant for **M** greater than about 6.5. Therefore, at the close distance of the YDTI site to the Continental fault, rupture propagation across both the Continental and the Rocker fault would generate larger magnitudes but ground motions that are not expected to be much larger at short periods.

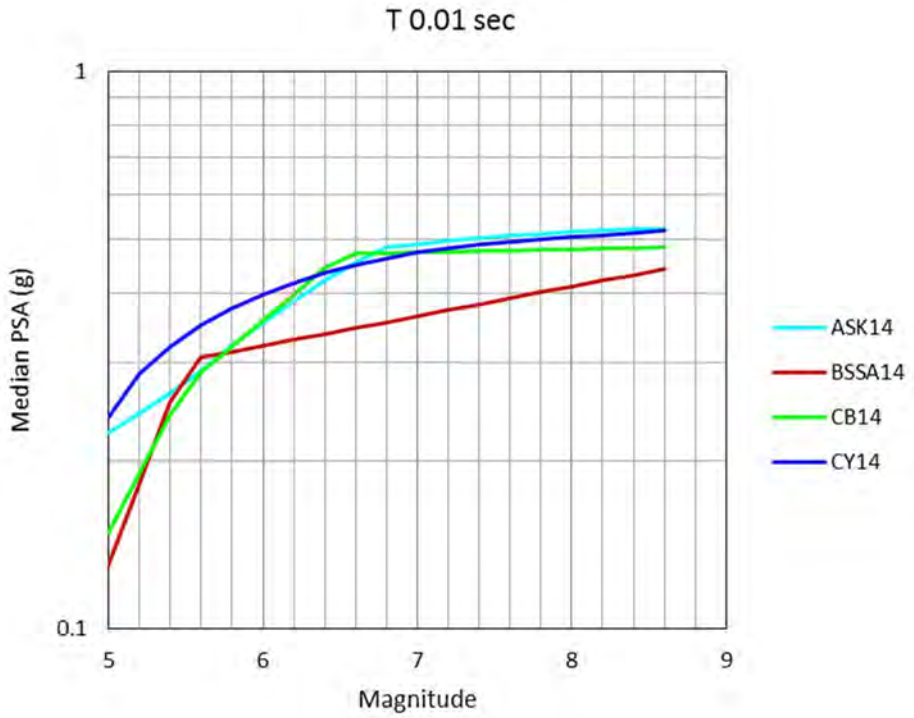

Figure 9-1. Magnitude scaling of the NGA-West2 GMPEs at a period of 0.01 sec for Rrup = 0.1 km

10. OTHER GEOLOGIC FAULTS

The seismic source model used in the hazard analysis for the YDTI site is based on the source model developed for the 2014 update to the National Seismic Hazard Maps (NSHMs) and the Wong et al. (2005) source characterization for western Montana. Following Wong et al. (2005), the seismic source model discussed in Chapter 3 of this report includes faults as seismic sources when these faults are longer than 5 km and have evidence of repeated Quaternary movement. Moreover, fault sources need to be characterized and have published parameters such as fault location, dimensions, slip rate or activity rate, maximum magnitude, dip angle, and sense of slip to be included in the source model. As a result, faults that have been identified but do not meet the criteria discussed here were not included in the source model for the YDTI project. Houston and Dilles (2013a) identifies three faults near the YTDI site that have not been included in this study: Rampart, Klepper, and East Ridge faults. Figure 10-1 shows these faults in relation to the Yankee Doodle dam contour. The map legend along with the original Houston and Dilles (2013a) map is included in electronic Appendix X. Because of their proximity to the YDTI site, this section discusses the Rampart, Klepper, and East Ridge faults and their potential impact on the hazard results at the YDTI site.

The Rampart, Klepper, and East Ridge faults have not been included in the source model for the 2014 update to the NSHMs. Moreover, they have also not been included in Wong et al. (2005) which characterized 92 known fault sources most of which are located in western Montana and are associated with Quaternary Basin and Range style extension. These faults are also not part of the Quaternary fault compilations by Haller et al. (2000) and Stickney et al. (2000). Houston and Dilles (2013b) discusses the Klepper and East Ridge faults and indicates that they are Miocene with dip angles of around 85°E and 60°W, respectively. The previous seismic studies for the YDTI site (HLA 1993 and IECO 1981) both mention the presence of the Klepper fault but don't explicitly use it in their seismic studies. As a result of our literature review, we conclude that while these three faults (Rampart, Klepper, and East Ridge) likely exist, there is no published evidence for slip on them and the age of potential activity is not likely to be within the Quaternary period (Stickney, personal communication). The uncertainty regarding the location and activity of these faults coupled with the lack of characterization (only approximate location, sense of slip and dip angles are published in Houston and Dilles 2013b) justifies not including them in the source model for this study.

We performed a sensitivity analysis to evaluate the potential impact of including these three faults on the hazard results for the YDTI site. Table 10-1 shows the parameters for the Rampart, Klepper, and East Ridge faults used in the sensitivity analysis. Table 10-1 lists the closest distance of the faults to the YDTI site (latitude 46.034°N and longitude 112.504°W). These distances as well as fault length measurements are a rough estimate based on the location of the faults as digitized from the Houston and Dilles (2013a) map. We note that these faults are mostly shown as dashed lines on the map, which indicates that they are approximately located. The Rampart fault has a length of about 4 km and intersects the Continental and the Klepper faults. The Klepper fault extends to the north end of the map and it is unclear if it continues further north. Guided by the estimated lengths, we assign maximum magnitude (Mmax) values for the Rampart, Klepper, and East Ridge faults to be 6.0, 6.6, and 6.3, respectively. We note that based on the 4 km length of the Rampart fault, its estimated Mmax based the Wells and Coppersmith (1994) relations

would be 5.8. Therefore, our assigned Mmax values represent conservative estimates given the apparent faults length.

The dip angles for the Klepper and East Ridge faults are based on Houston and Dilles (2013b). The dip angle for the Rampart fault was assumed to be 55° based on typical dips for range-bounding normal faults. For all three faults, the depth to top of rupture, fault width, magnitude recurrence model, and slip rate were assumed to be the same as those for the Continental fault. We note that the slip rates used in this sensitivity analysis represent a conservative upper bound given that the Rampart, Klepper, and East Ridge faults are likely less active than the Continental fault. A probability of activity of 1.0 was used for all three faults, which also represents a conservative upper bound case. The probability of activity typically reflects the likelihood that a fault is structurally capable of independently generating earthquakes and the likelihood that it is still active within the modern stress field. Wong et al. (2005) assigned probability of activity of 1.0 to faults with definitive evidence for repeated Quaternary activity. Faults that do not show definitive evidence for repeated Quaternary activity were assigned probability of activity of less than 1.0.

Figure 10-2 shows a comparison of the deterministic spectra for MCE scenarios on the Continental fault to those on the Rampart, Klepper and East Ridge faults. The best estimate Mmax values and the closest distances to site listed in Table 10-1 were used in calculating the deterministic spectra for the scenarios on the Rampart, Klepper, and East Ridge faults. Figure 10-2 indicates that the deterministic spectra for the scenarios on the Continental fault are larger than those for the other three faults for both the median and 84th percentile cases. Therefore, assuming that the Rampart, Klepper, and East Ridge faults are active and using the conservative magnitude estimates listed in Table 10-1 does not impact the deterministic design spectra used for this study.

Figure 10-3 shows a comparison of the horizontal design spectra developed for this study to the 475, 1,000, 2,475, and 10,000 year UHS values obtained from the inclusion of the Rampart, Klepper, and East Ridge faults in the PSHA for PGA and spectral periods of 0.2 and 1.0 sec. Figure 10-3 indicates that the inclusion of the three faults with the conservative parameters listed in Table 10-1 causes an increase in the UHS values at PGA and periods of 0.2 and 1.0 sec at all return periods. This increase is the largest for the 10,000 years return period (on the order of 27 to 28% at PGA and T = 0.2 sec). Compared to the deterministic spectra, the 10,000 year UHS obtained from the inclusion of the Rampart, Klepper, and East Ridge faults exceed the median spectra by 10 to 23% for the Rrup 1.2 km scenario and 4 to 17% for the Rrup 0.1 km scenario. Given that the deterministic spectra are expected to be used for design at the YDTI site and given the uncertainty in the activity of the three faults and the conservative parameters used in the sensitivity analysis, we conclude that further characterization of the Rampart, Klepper, and East Ridge faults and their inclusion in this seismic study is not crucial for ground motion shaking.

Figure 10-1 shows that the Rampart fault crosses the YDTI dam contour. We performed a sensitivity analysis to evaluate surface fault displacement from an MCE scenario on the Rampart fault. Following the methodology discussed in Chapter 7, Mmax values of 6.0, 5.7, and 6.3 with weights of 0.6, 0.2, and 0.2, respectively, were used for the MCE scenario on the Rampart fault. Table 10-2 shows the median and 84th percentile average surface displacement on the Rampart fault compared to the values obtained for the Continental fault. Given the larger magnitude for the MCE on the Continental fault compared to the Rampart fault, the average surface fault displacement on the Continental fault is expected to be larger. Given that the Rampart and Continental faults intersect, we add the length of both faults to estimate the

maximum magnitude in case of a joint rupture on both faults. Based on their total length, we estimate an Mmax of 6.6 for an MCE on both faults. The resulting median and 84th percentile average surface displacements would be on the order of 0.59 and 1.66 m.

Finally, we note that the sensitivity analysis performed to evaluate the impact of assuming that the Rampart, Klepper, and East Ridge faults are active and including them in the hazard analysis is of preliminary nature. In addition to the uncertainty on the level of activity of these faults, there is a significant uncertainty in their assigned parameters used in this analysis. While fault studies are needed to confirm whether or not these three faults are active and characterize their parameters, we believe, based on this sensitivity analysis, that their exclusion from the seismic source model for this study is justified.

Table 10-1. Assumed source parameters for the Rampart, Klepper, and East Ridge faults. Weights are given in parentheses. Mmin is 5.0 and b-value is 0.8.

Fault Name	Closest Distance to Site (km)	Recurrence Model(1)	Slip Rate (mm/yr) (1)	Mmax	Slip Sense	Dip (degrees)	Rupture Top (km) (1)	Fault Width (km) (1)
Rampart fault	0.9	Y & C	0.020 (0.6)	6.0 (0.6)	Normal	55 S (0.6)	0	15 (0.6)
			0.005 (0.2)	5.7 (0.2)		30 S (0.2)		12 (0.2)
			0.120 (0.2)	6.3 (0.2)		70 S (0.2)		18 (0.2)
Klepper fault	2.9	Y & C	0.020 (0.6)	6.6 (0.6)	Normal	85 E	0	15 (0.6)
			0.005 (0.2)	6.3 (0.2)				12 (0.2)
			0.120 (0.2)	6.9 (0.2)				18 (0.2)
East Ridge fault	3.1	Y & C	0.020 (0.6)	6.3 (0.6)	Normal	60 W	0	15 (0.6)
			0.005 (0.2)	6.0 (0.2)				12 (0.2)
			0.120 (0.2)	6.6 (0.2)				18 (0.2)

(1) Parameters are assumed to be the same as those for the Continental fault

Table 10-2. Surface fault displacement hazard results on the Continental and the Rampart faults

		Average Displacement (m)		
Exceedance	Percentile	Continental Fault	Rampart Fault	Continental + Rampart fault
0.50	50	0.51	0.25	0.59
0.16	84	1.44	0.73	1.66

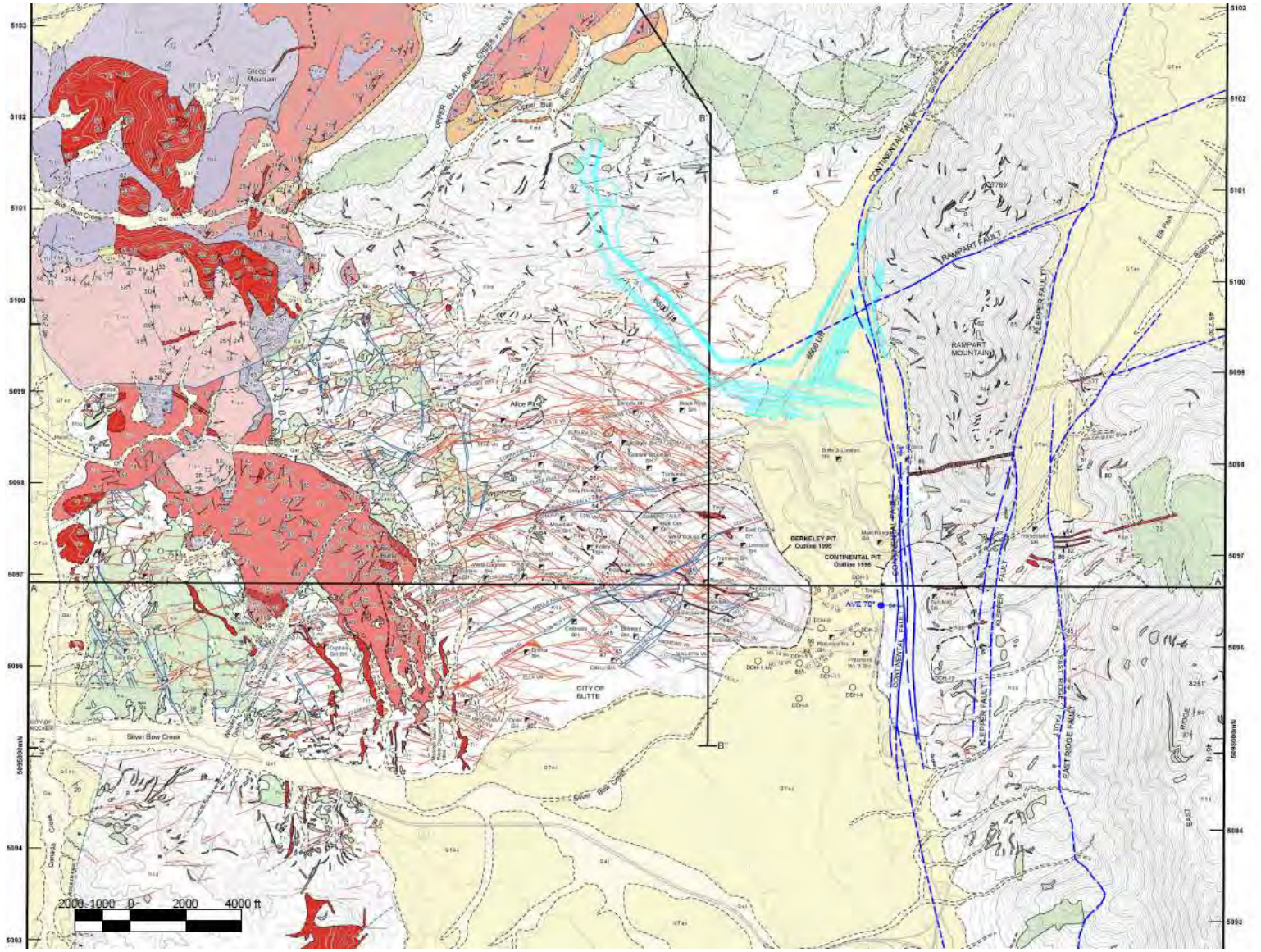

Figure 10-1. Location of the Rampart, Klepper, and East Ridge faults in relation to the Yankee Doodle dam contour shown in cyan (source: Montana Resources 2016; map based on Houston and Dilles 2013a along with Montana Resources interpretation of the Continental fault)

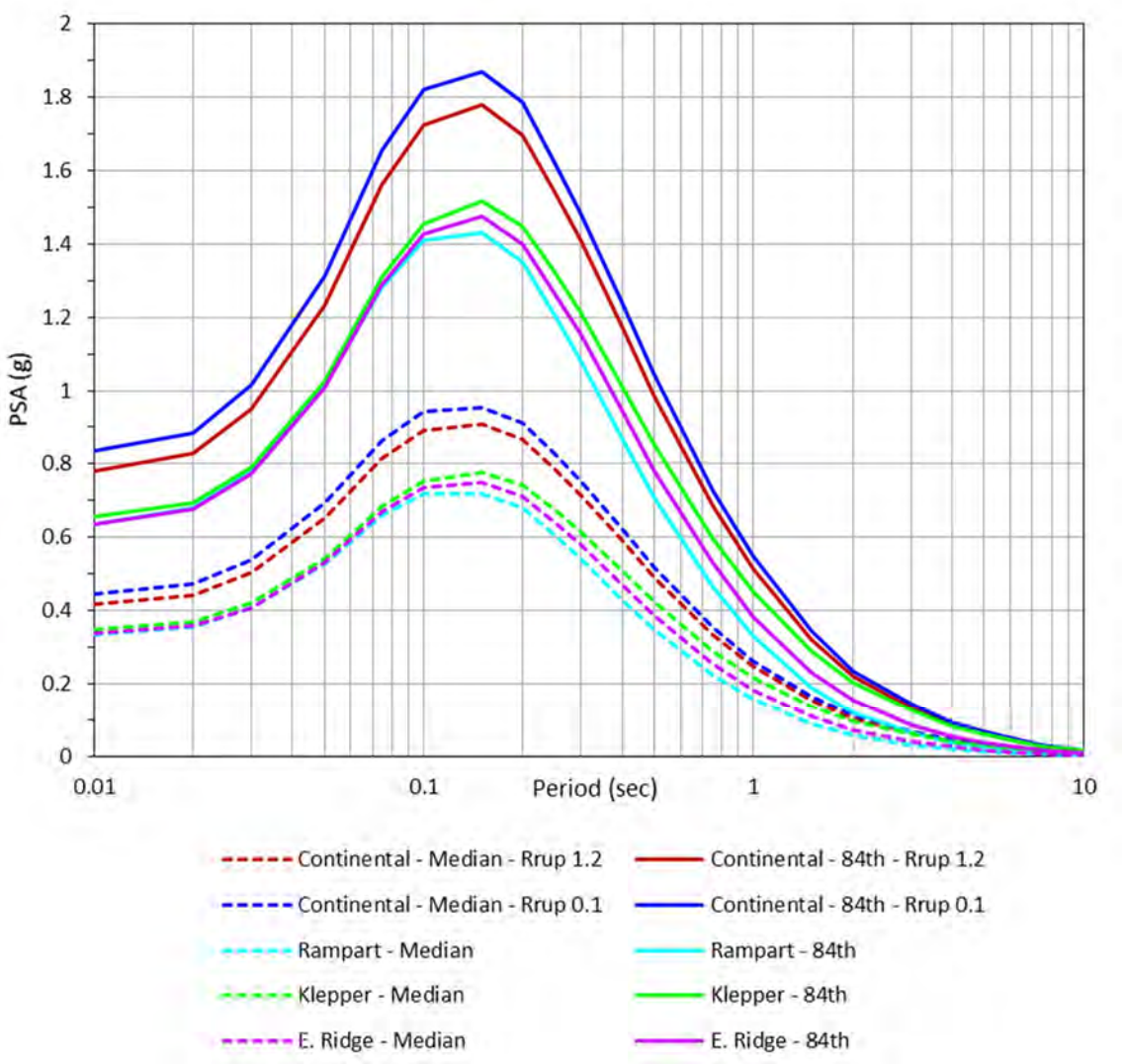

Figure 10-2. Comparison of median and 84th percentile deterministic response spectra for MCE scenarios on the Continental, Rampart, Klepper, and East Ridge faults for V_{S30} of 760 m/sec

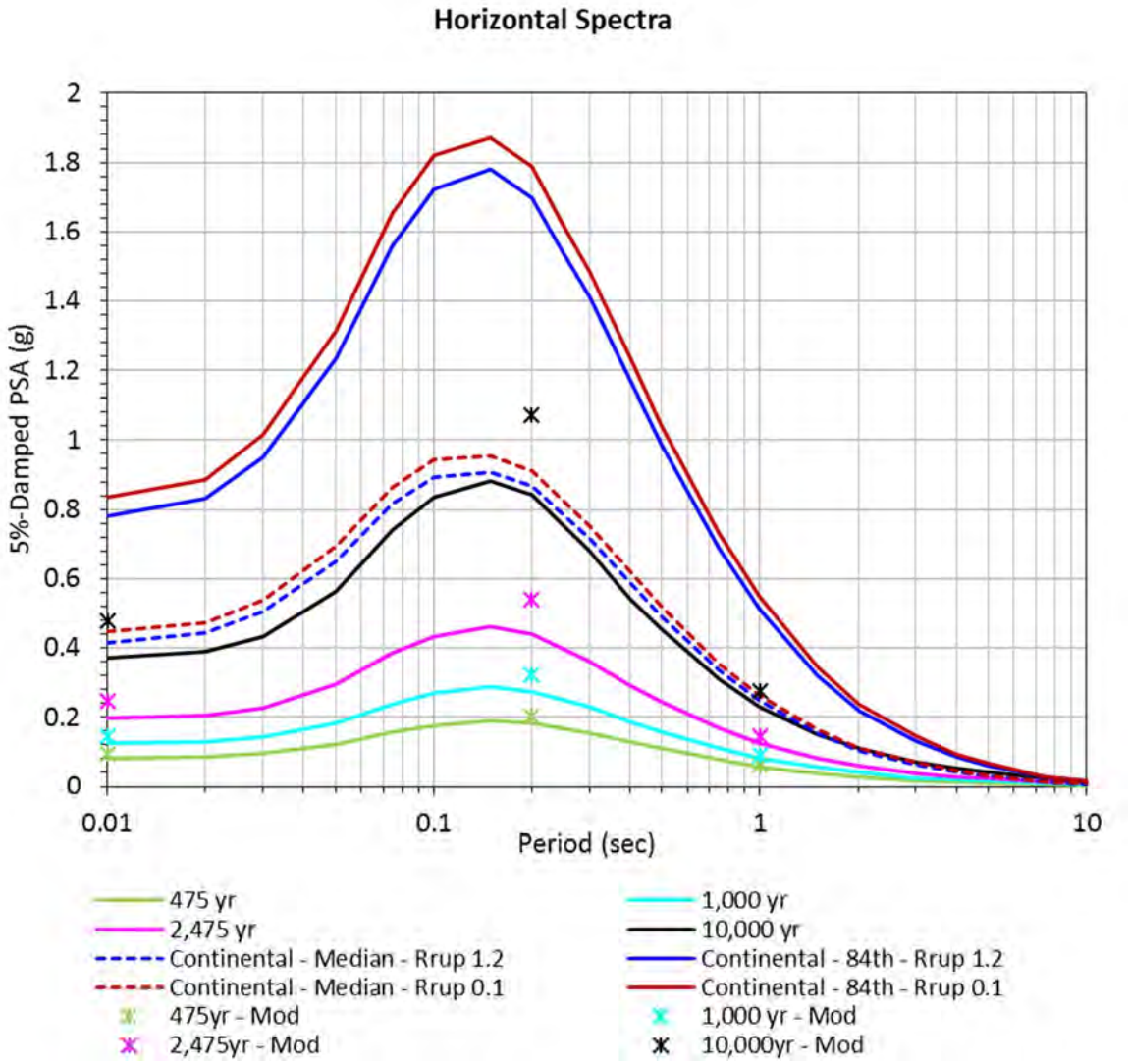

Figure 10-3. Comparison of the horizontal design spectra for this study to the UHS obtained from the inclusion of the Rampart, Klepper, and East Ridge faults in the PSHA for V_{S30} of 760 m/sec

11. REFERENCES

Abrahamson, N. A. 2003. RSPMATCH, Personal Communication.

Abrahamson, N. A. and N. Gregor. 2015. Haz45, Seismic Hazard Analysis Software.

Abrahamson, N. A. and W. J. Silva. 1997. Empirical response spectral attenuation relations for shallow crustal earthquakes. Seismological Research Letters, Vol. 68, pp. 94-127.

Abrahamson, N. A., Silva, W. J., and R. Kamai. 2014. Summary of the ASK14 ground motion relation for active crustal regions. Earthquake Spectra, Vol. 30, No. 3, pp. 1025-1055.

Abrahamson, N. 2008. Appendix C—Probabilistic fault rupture hazard analysis, in San Francisco Public Utilities Commission (SFPUC), Seismic Design Criteria, revised 2008, 7 pages.

Al Atik, L. and N. Abrahamson. 2010. An improved method for nonstationary spectral matching. Earthquake Spectra, Vol. 26, No. 3, pp. 601-617.

Al Atik, L. and R. R. Youngs. 2014. Epistemic uncertainty for NGA-West2 Models. Earthquake Spectra, Vol. 30, No. 3, pp. 1301-1318.

Bird, P. 2013. Estimation of fault slip rates in the conterminous Western United States with statistical and kinematic finite-element programs, Appendix C, in Petersen, M.D., Zeng, Yuehua, Haller, K.M., McCaffrey, Robert, Hammond, W.C., Bird, Peter, Moschetti, Morgan, and Thatcher, Wayne, Geodesy- and geology-based slip-rate models for the Western United States (excluding California) national seismic hazard maps: U.S. Geological Survey Open-File Report 2013-1293, p. 48–57.

Boore, D. M, Stewart, J. P., Seyhan, E. and G. M. Atkinson. 2014. NGA-West2 equations for predicting PGA, PGV, and 5% damped PSA for shallow crustal earthquakes. Earthquake Spectra, Vol. 30, No. 3, pp. 1057-1085.

Campbell, K. W. 1997. Empirical near-source attenuation relationships for horizontal and vertical components of peak ground acceleration, velocity, and pseudo-absolute acceleration response spectra. Seismological Research Letters, Vol. 68, pp. 154-179.

Campbell, K. W. and Y. Bozorgnia. 2014. NGA-West2 ground motion model for the average horizontal components of PGA, PGV, and 5% damped linear acceleration response spectra. Earthquake Spectra, Vol. 30, No. 3, pp. 1087-1115.

Chiou, B. S.-J., and R. R. Youngs. 2014. Update of the Chiou and Youngs NGA model for the average horizontal component of peak ground motion and response spectra. Earthquake Spectra, Vol. 30, No. 3, pp. 1117-1153.

Coppersmith K. J., Bommer J., Hanson K., Coppersmith R., Unruh J. R., Wolf L., Youngs R., Al Atik L., Rodriguez-Marek A., Toro G., and V. Montaldo-Falero. 2014. Hanford sitewide probabilistic seismic hazard analysis, PNNL-23361, Pacific Northwest National Laboratory, Richland, WA.

Division of Safety of Dams. 2000. Guidelines for use of the consequence-hazard matrix and selection of ground motion parameters. October 4, 2002.

GeoPentech. 2015. Southwestern United States ground motion characterization SSHAC Level 3. Technical Report Rev.2, March 2015.

Gulerce, Z. and N. A. Abrahamson. 2011. Site-specific design spectra for vertical ground motion, Earthquake Spectra, Vol. 27, pp. 1023-1047.

Haller, K. M., Dart, R. L., Machette, M. N., and M. C. Stickney. 2000. Data for Quaternary faults in western Montana: Montana Bureau of Mines and Geology Open-File Report 411, 241 p.

Harris, R. A., and S. M. Day. 1993. Dynamics of fault interaction: Parallel strike-slip faults, Journal of Geophysical Research, Vol. 98, pp. 4461-4472.

Hecker, S., Abrahamson, N. A., and K. E. Wooddell. 2013. Variability of displacement at a point: Implications for earthquake-size distribution and rupture hazard on faults, Bulletin of the Seismological Society of America, Vol. 103, pp. 651-674.

Harding Lawson Associates (HLA). 1993. Seismic stability evaluation Yankee Doodle tailings Dam Butte, Montana, Appendix D, Report prepared for Montana Resources, April 9, 1993.

Houston, R. A., and J. H. Dilles. 2013a. Geology of the Butte mining district, Montana: Montana Bureau of Mines and Geology Open-File Report 627, 1 sheet, scale 1:24,000.

Houston, R. A., and J. H. Dilles. 2013b. Structural geologic evolution of the Butte District, Montana, Economic Geology, Vol. 108, pp. 1397-1424.

Idriss, I. M. 2014. An NGA-West2 empirical model for estimating the horizontal spectral values generated by shallow crustal earthquakes. Earthquake Spectra, Vol. 30, No. 3, pp. 1155-1177.

IECO. 1981. Geotechnical and hydrologic studies Yankee Doodle Tailings dam Butte, Montana, Report August, 1981.

Knight Piesold. 2015. Montana Resources – Yankee Doodle Tailings Impoundment request for proposal for seismic hazard assessment services, VA15-03097.

Miller, A. C., and T. R., Rice. 1983. Discrete approximation of probability distributions, Management Science, Vol. 29, pp. 352-362.

Pacific Gas and Electric. 2015. Deterministic fault displacement hazard analysis procedure for PG&E gas pipelines, Rev 1, September 16, 2015.

Petersen, M. D., Moschetti, M. P., Powers, P. M., Mueller, C. S., Haller, K. M., Frankel, A. D., Zeng, Y., Rezaeian, S., Harmsen, S. C., Boyd, O. S., Field, N., Chen, R., Rukstales, K. S., Luco, N., Wheeler, R. L., Williams, R. A., and H. O. Olsen. 2014. Documentation for the 2014 update of the United States national seismic hazard maps, Open-File Report 2014-1091, U.S. Geological Survey.

Renault P., Heuberger S., and N. A., Abrahamson. 2010. PEGASOS Refinement Project: An improved PSHA for Swiss nuclear power plants, Proceedings, 14th European Conference of Earthquake Engineering, Ohrid, Republic of Macedonia, Paper ID 991.

Sadigh, K. Chang, C.-Y., Egan, J. A., Makdisi, F., and R. R. Youngs. 1997. Attenuation relationships for shallow crustal earthquakes based on California strong motion data. Seismological Research Letters, Vol. 68, pp. 180-189.

Spudich, P., Fletcher, J. B., Hellweg, M., Boatwright, J., Sullivan, C., Joyner, W. B., Hanks, T. C., Boore, D. M., MvGarr, A., Baker, L. M., and A. G. Lindh. 1997. SEA96 – A new predictive relation for earthquake ground motions in extensional tectonic regimes. Seismological Research Letters, Vol. 68, pp. 190-198.

Stickney, M. C., Haller, K. M., and M. N. Machette. 2000. Quaternary faults and seismicity in western Montana: Montana Bureau of Mines and Geology Special Publication 114.

Walling, M., W. Silva, and N. A. Abrahamson. 2008. Nonlinear site amplification factors for constraining the NGA models, Earthquake Spectra, Vol. 24, pp. 243-255.

Wells, D. L. and K. J., Coppersmith. 1994. New empirical relationships among magnitude, rupture length, rupture width, rupture area, and surface displacement. *Bull. Seismol. Soc. Am.* 84, 974–1002.

Wesnousky, S. G. 2008. Displacement and geometrical characteristics of earthquake surface ruptures: Issues and implications for seismic hazard analysis and the earthquake rupture process, Bulletin of the Seismological Society of America, 98 (4): 1609-1632.

Wheeler, R. L. 1989. Persistent segment boundaries on basin-range normal faults, in Proceedings, Conference XLV-Fault Segmentation and Controls on Rupture Initiation and Termination, eds. D. P. Schwartz and R. H. Sibson, U.S. Geological Survey Open-File Report 89-315, 432-444.

Wong, I., Olig, S., Dober, M., Wright, D., Nemser, E., Lageson, D., Silva, W., Stickney, M., Lemieux, M., and L. Anderson. 2005. Probabilistic earthquake hazard maps for the state of Montana, Special Publication 117, Montana Bureau of Mines and Geology.

Youngs, R. R. and K. J. Coppersmith. 1985. Implications of fault slip rates and earthquake recurrence models to probabilistic seismic hazard estimates. Bulletin of the Seismological Society of America, Vol. 75, No. 4, pp. 939-964.

Youngs, R. R., Arabasz, W. J., Anderson, R. E., Ramelli, A. R., Ake, J. P., Slemmons, D. B., McCalpin, J. P., Doser, D. I., Fridrich, C. J. , Swan III, F. H., Rogers, A. M., Yount, J. C., Anderson, L. W., Smith, K. D., Bruhn, R. L., Knuepfer, P. L. K., Smith, R. B., dePolo, C. M., O'Leary, D. W., Coppersmith, K. J.,

Pezzopane, S. K., Schwartz, D. P., Whitney, , J. W., Olig, S. S. and Toro, G. R. 2003. A methodology for probabilistic fault displacement hazard analysis (PFDHA), Earthquake Spectra 19 (1): 191-219.

Zeng, Y. and Z., Shen. 2013. A fault-based model for crustal deformation in the Western United States, Appendix D, in Petersen, M.D., Zeng, Yuehua, Haller, K.M., McCaffrey, Robert, Hammond, W.C., Bird, Peter, Moschetti, Morgan, and Thatcher, Wayne, Geodesy- and geology-based slip-rate models for the Western United States (excluding California) national seismic hazard maps: U.S. Geological Survey Open-File Report 2013-1293, p. 58–68. (Also available at http://pubs.er.usgs.gov/publication/ofr20131293.)

Plate 1
Historical Seismicity (1809 to 2001), Quaternary Faults, and Regional Seismic Source Zones

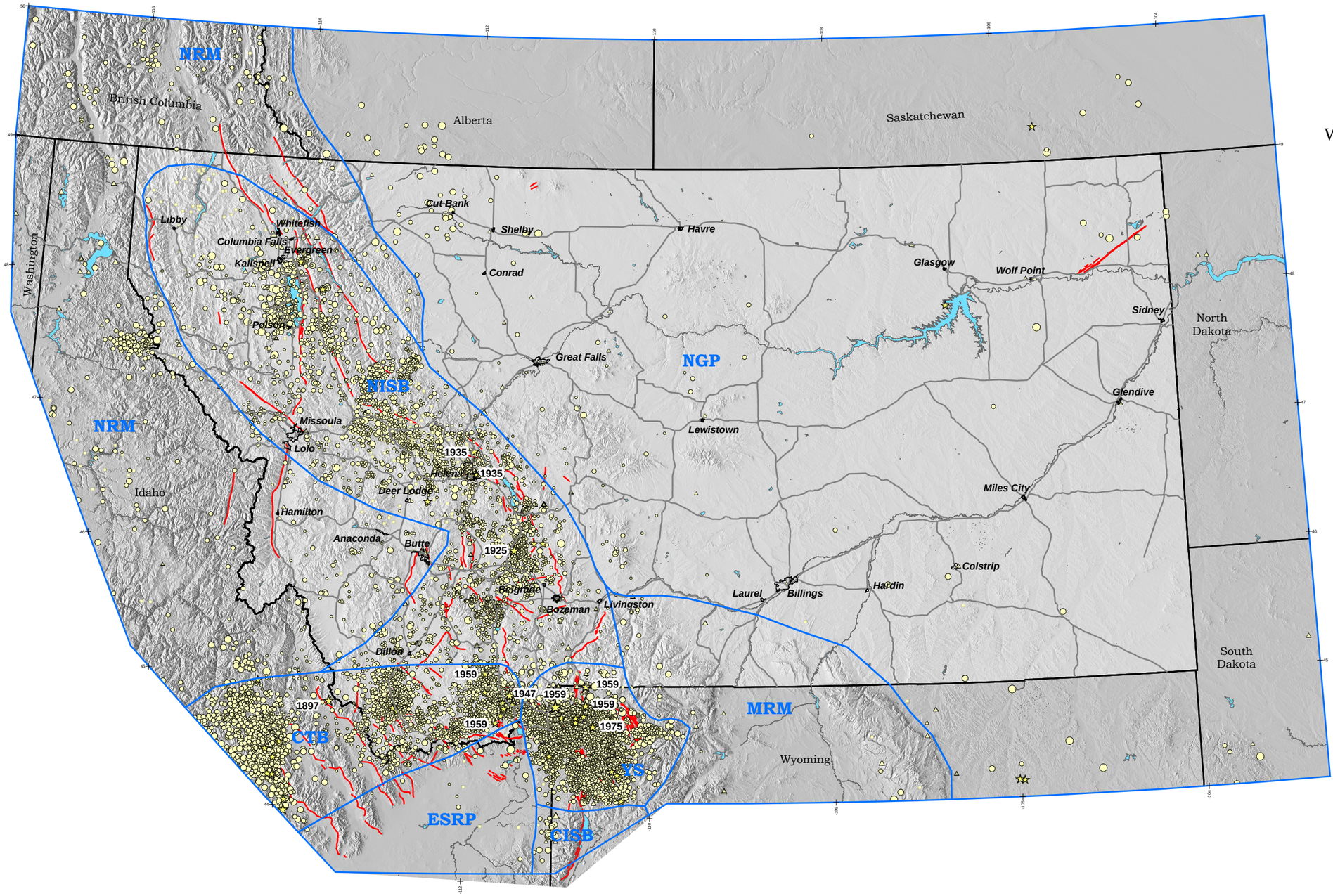

Project suported by the Montana Department of Natural Resources and Conservation and the Federal Emergency Management Agency. Basemap data from Montana State Library, Natural Resource Information System, GIS and layout by URS Corporation. Published by Montana Bureau of Mines and Geology.

MBMG Publication XXX

Probabilistic Earthquake Ground Shaking Maps for the State of Montana

by
Ivan Wong, Susan Olig, Mark Dober, Douglas Wright, Eliza Nemser, David Lageson, Walter Silva, Michael Stickney, Michele Lemieux and Larry Anderson

2005

Legend

Magnitude > 5

- 5 - 6
- 6.1 - 7
- 7.1 - 8

Magnitude

- 1.5 - 2
- 2.1 - 3
- 3.1 - 4
- 4.1 - 5

MMI Intensity

- II
- III
- IV
- V
- VI
- No Measure

Quaternary Faults

Seismic Source Zones

CISB	Central Intermountain Seismic Belt
CTB	Centennial Tectonic Belt
ESRP	Eastern Snake River Plain
MRM	Middle Rocky Mountains
NGP	Northern Great Plain
NISB	Northern Intermountain Seismic Belt
NRM	Northern Rocky Mountains
YS	Yellowstone

Zone boundaries shown by blue lines

Fault Database modified from Stickney and others, 2000
(See Appendix for other fault map sources)

N W E S

20 0 20 40 60 80 100 Kilometers

20 0 20 40 60 80 100 Miles

Plate 2a
Quaternary Faults in Western Montana

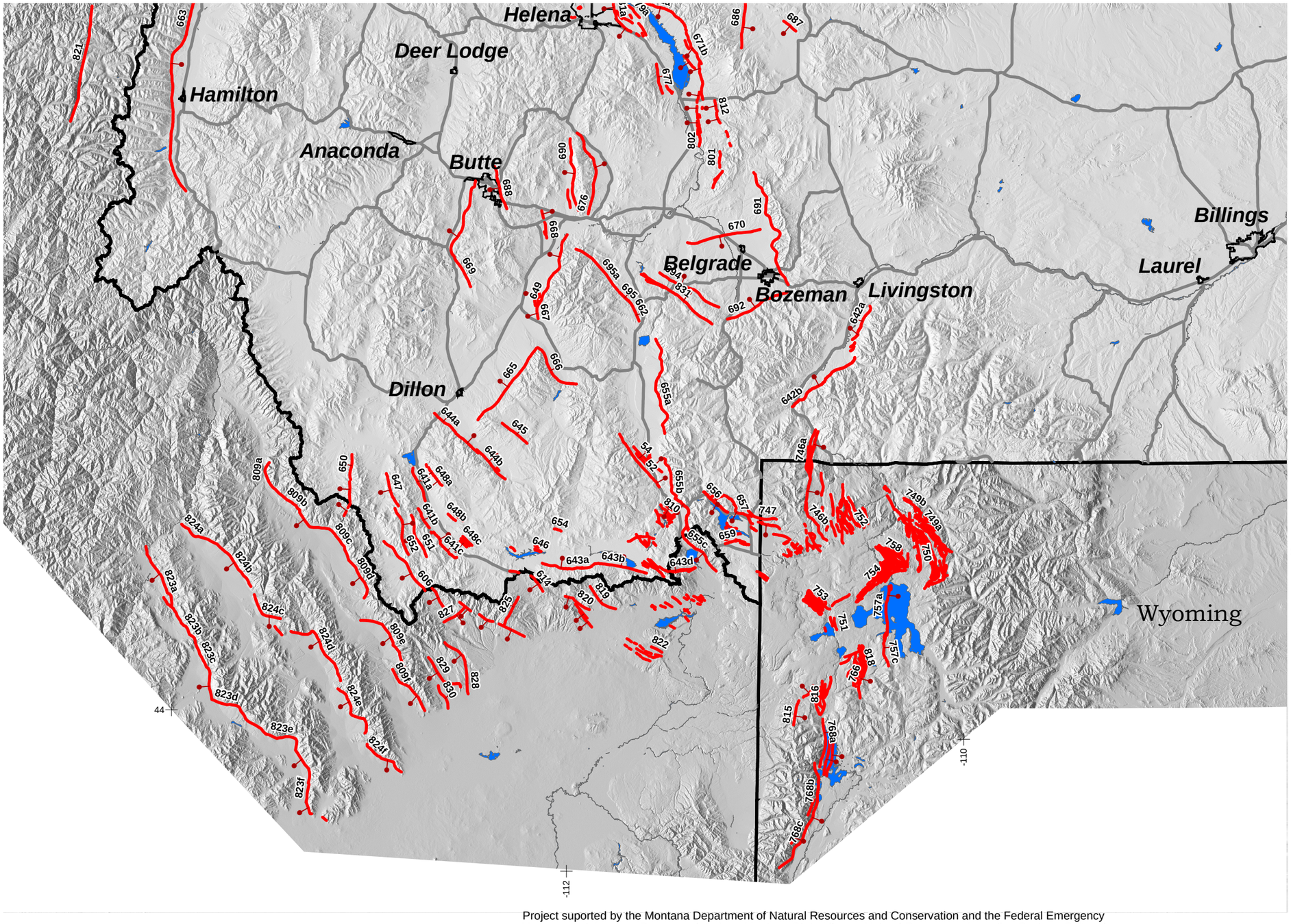

MBMG Publication XXX

Probabilistic Earthquake Ground Shaking Maps for the State of Montana

by
Ivan Wong, Susan Olig, Mark Dober,
Douglas Wright, Eliza Nemser, David Lageson,
Walter Silva, Michael Stickney, Michele Lemieux
and Larry Anderson

2005

Quaternary Faults
Fault Database modified from Stickney and others, 2000
(See Appendix for other fault map sources)

N
W E
S

0 10 20 40 60 80 Kilometers
0 10 20 40 60 80 Miles

Map Index

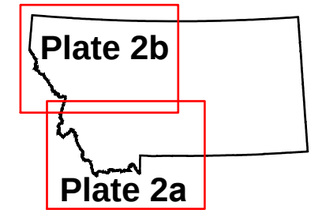

Project suported by the Montana Department of Natural Resources and Conservation and the Federal Emergency Management Agency. Basemap data from Montana State Library, Natural Resource Information System, GIS and layout by URS Corporation. Published by Montana Bureau of Mines and Geology.

APPENDIX II: SPECTRAL MATCHING PLOTS
475 YEAR DESIGN SPECTRA

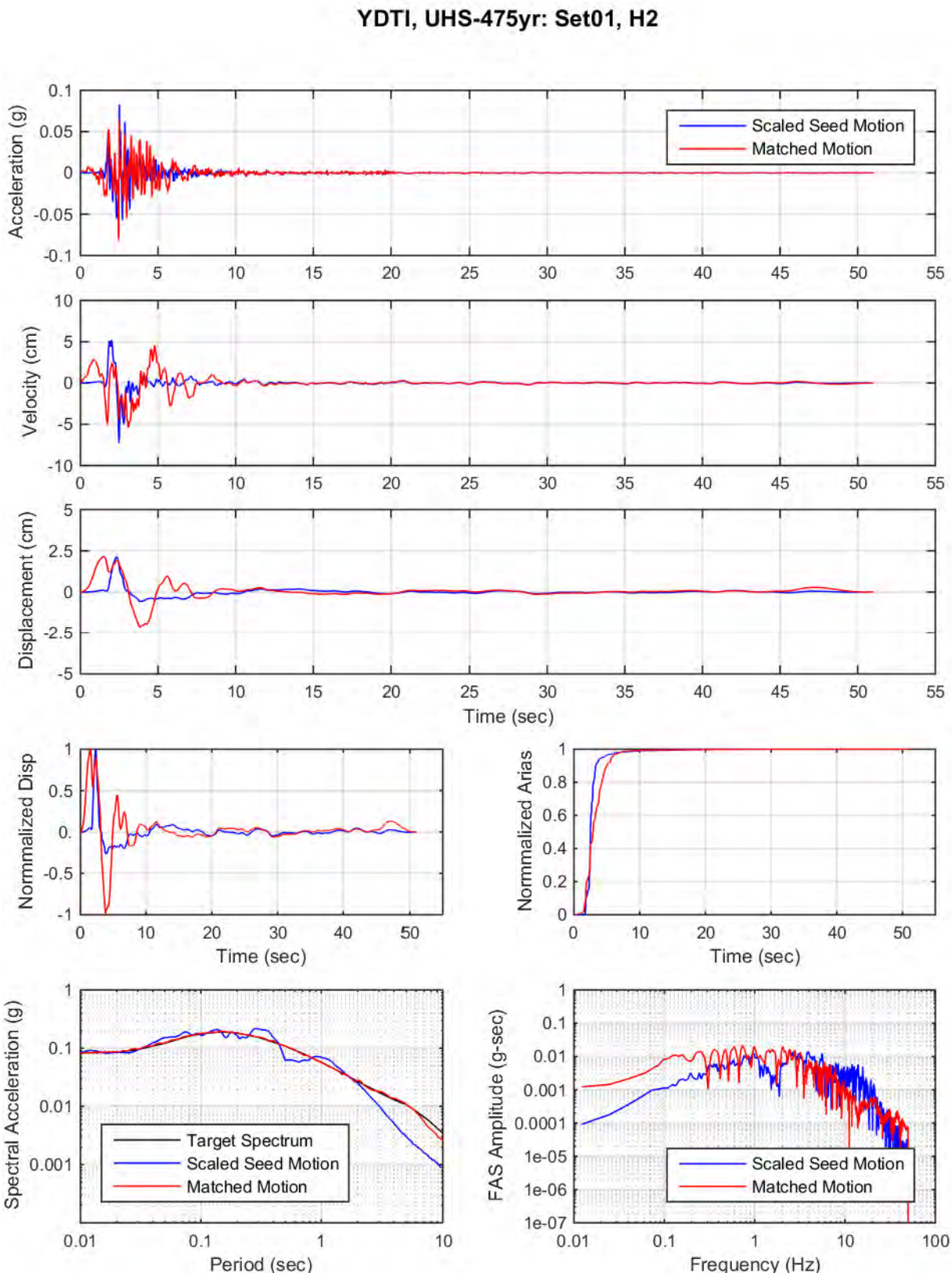
YDTI, UHS-475yr: Set01, H2
Acceleration (g)
Scaled Seed Motion
Matched Motion
Velocity (cm)
Displacement (cm)
Time (sec)
Normmalized Disp
Time (sec)
Normmalized Arias
Time (sec)
Spectral Acceleration (g)
Target Spectrum
Scaled Seed Motion
Matched Motion
Period (sec)
FAS Amplitude (g-sec)
Scaled Seed Motion
Matched Motion
Frequency (Hz)

YDTI, UHS-475yr: Set01, UP

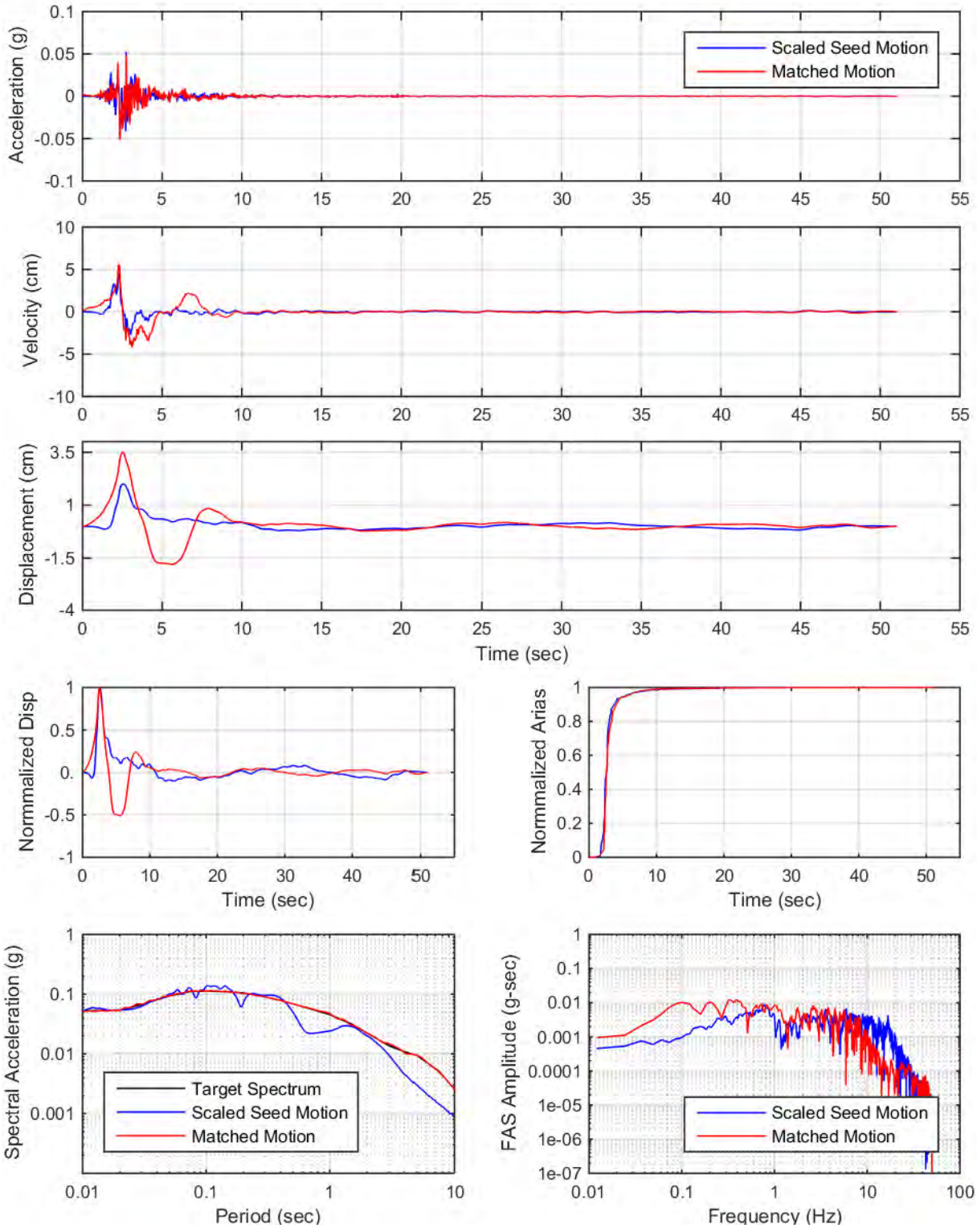

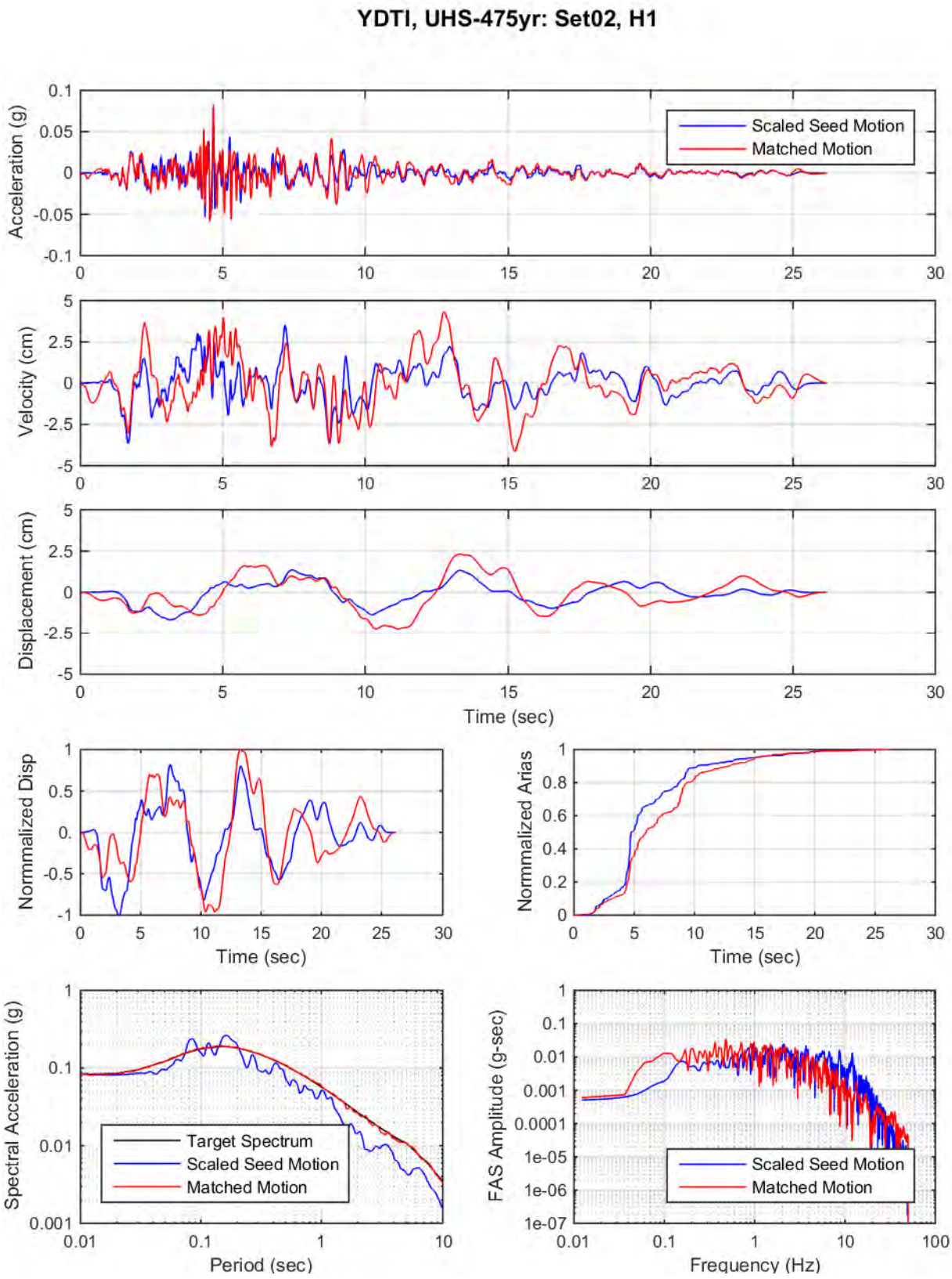
YDTI, UHS-475yr: Set02, H1
Acceleration (g)
Scaled Seed Motion
Matched Motion
Velocity (cm)
Displacement (cm)
Time (sec)
Normmalized Disp
Time (sec)
Normmalized Arias
Time (sec)
Spectral Acceleration (g)
Target Spectrum
Scaled Seed Motion
Matched Motion
Period (sec)
FAS Amplitude (g-sec)
Scaled Seed Motion
Matched Motion
Frequency (Hz)

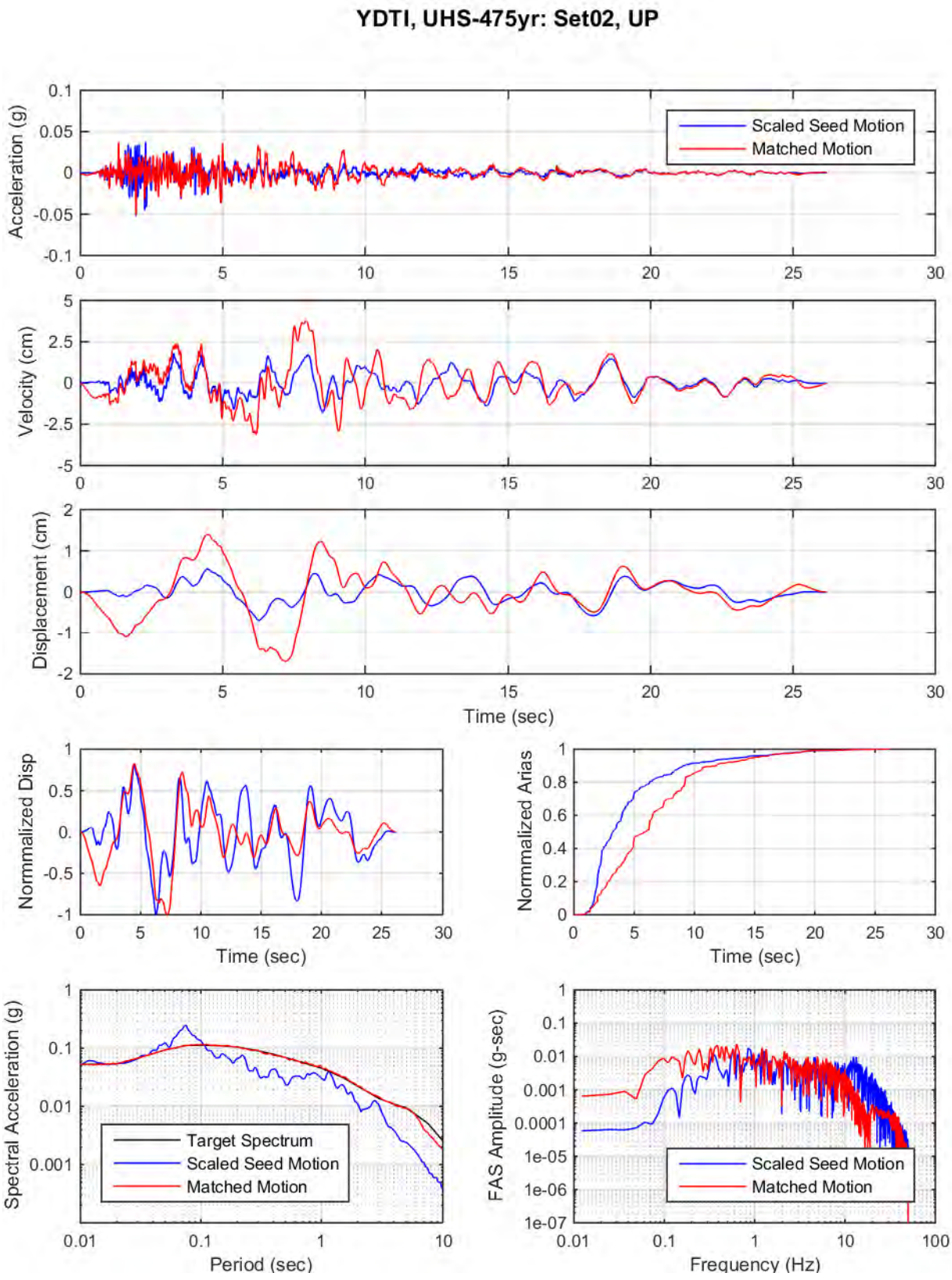
YDTI, UHS-475yr: Set02, UP
Acceleration (g)
Scaled Seed Motion
Matched Motion
Velocity (cm)
Displacement (cm)
Time (sec)
Normmalized Disp
Time (sec)
Normmalized Arias
Time (sec)
Spectral Acceleration (g)
Target Spectrum
Scaled Seed Motion
Matched Motion
Period (sec)
FAS Amplitude (g-sec)
Scaled Seed Motion
Matched Motion
Frequency (Hz)

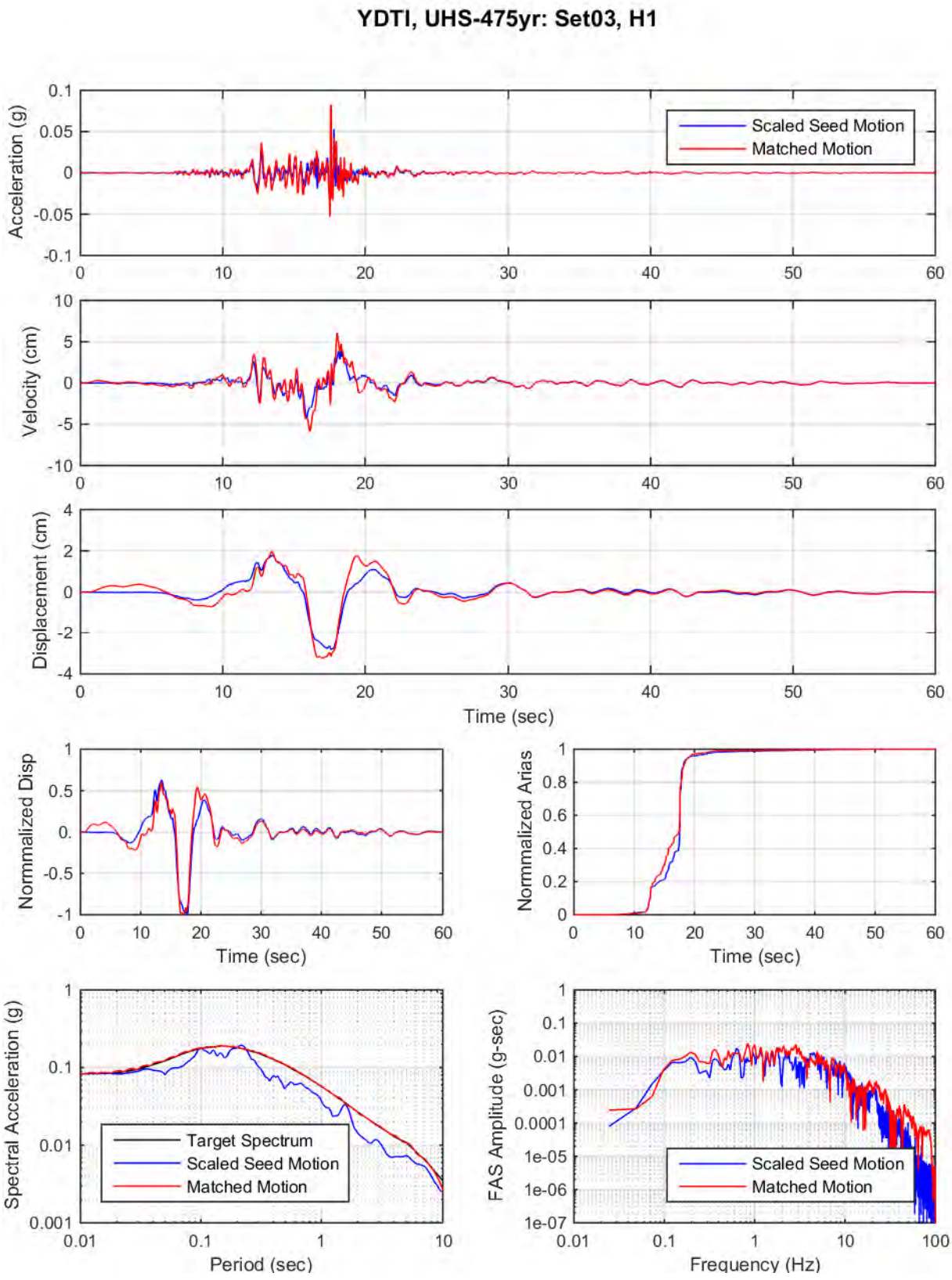
YDTI, UHS-475yr: Set03, H1
Acceleration (g)
Scaled Seed Motion
Matched Motion
Velocity (cm)
Displacement (cm)
Time (sec)
Normmalized Disp
Time (sec)
Normmalized Arias
Time (sec)
Spectral Acceleration (g)
Target Spectrum
Scaled Seed Motion
Matched Motion
Period (sec)
FAS Amplitude (g-sec)
Scaled Seed Motion
Matched Motion
Frequency (Hz)

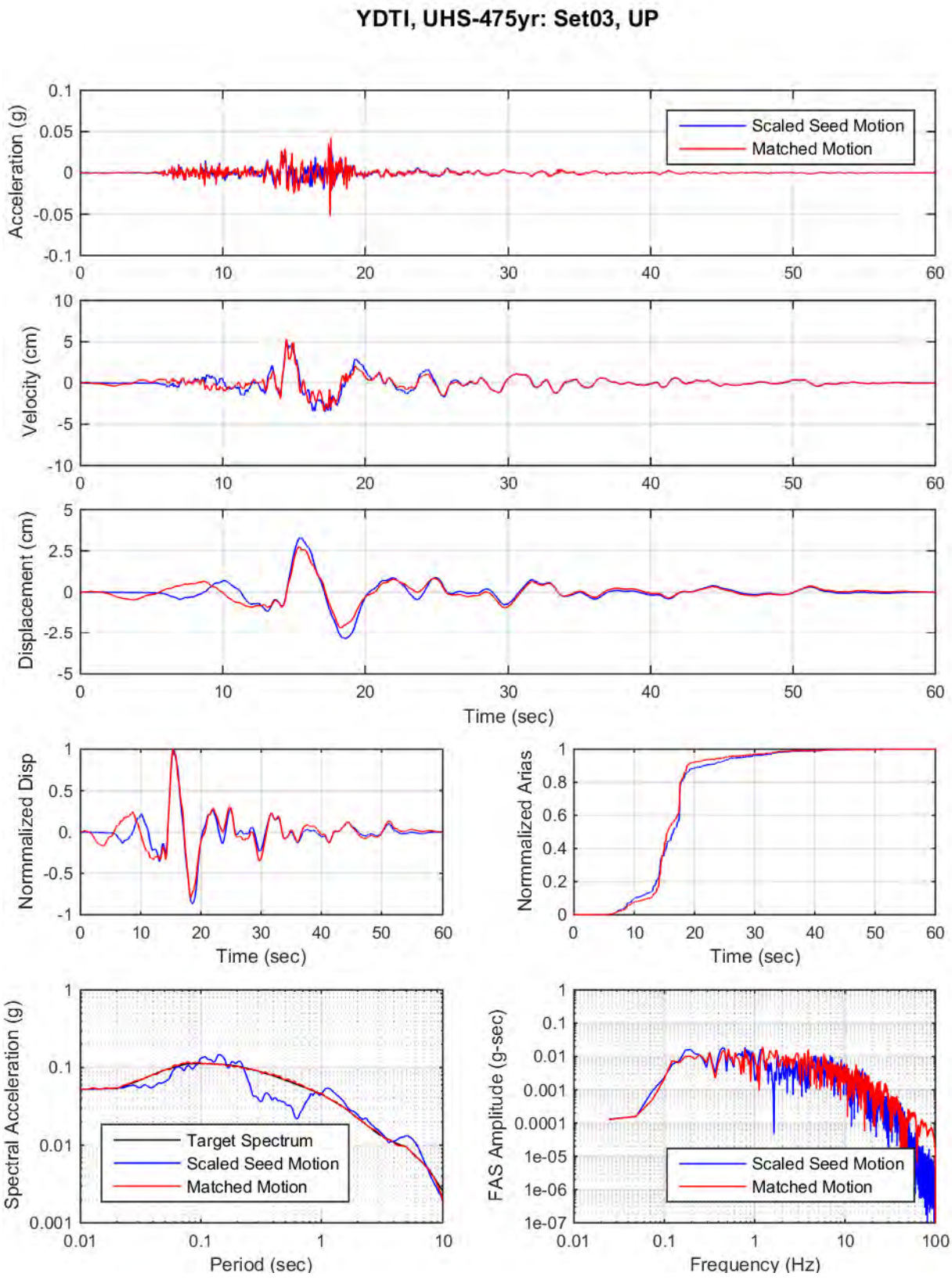
YDTI, UHS-475yr: Set03, UP
Acceleration (g)
Scaled Seed Motion
Matched Motion
Velocity (cm)
Displacement (cm)
Time (sec)
Normmalized Disp
Time (sec)
Normmalized Arias
Time (sec)
Spectral Acceleration (g)
Target Spectrum
Scaled Seed Motion
Matched Motion
Period (sec)
FAS Amplitude (g-sec)
Scaled Seed Motion
Matched Motion
Frequency (Hz)

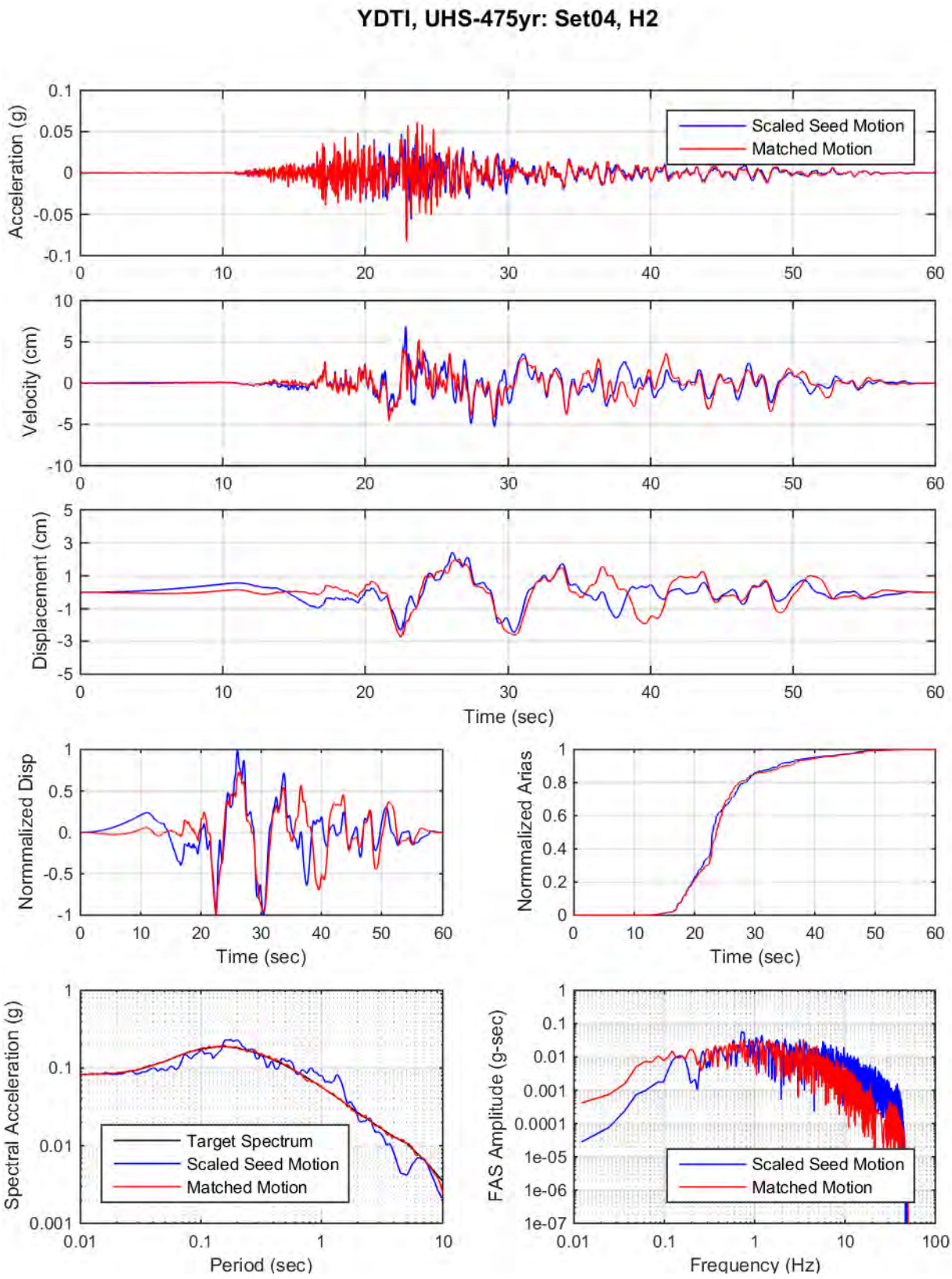
YDTI, UHS-475yr: Set04, H2
Acceleration (g)
Scaled Seed Motion
Matched Motion
Velocity (cm)
Displacement (cm)
Time (sec)
Normmalized Disp
Time (sec)
Normmalized Arias
Time (sec)
Spectral Acceleration (g)
Target Spectrum
Scaled Seed Motion
Matched Motion
Period (sec)
FAS Amplitude (g-sec)
Scaled Seed Motion
Matched Motion
Frequency (Hz)

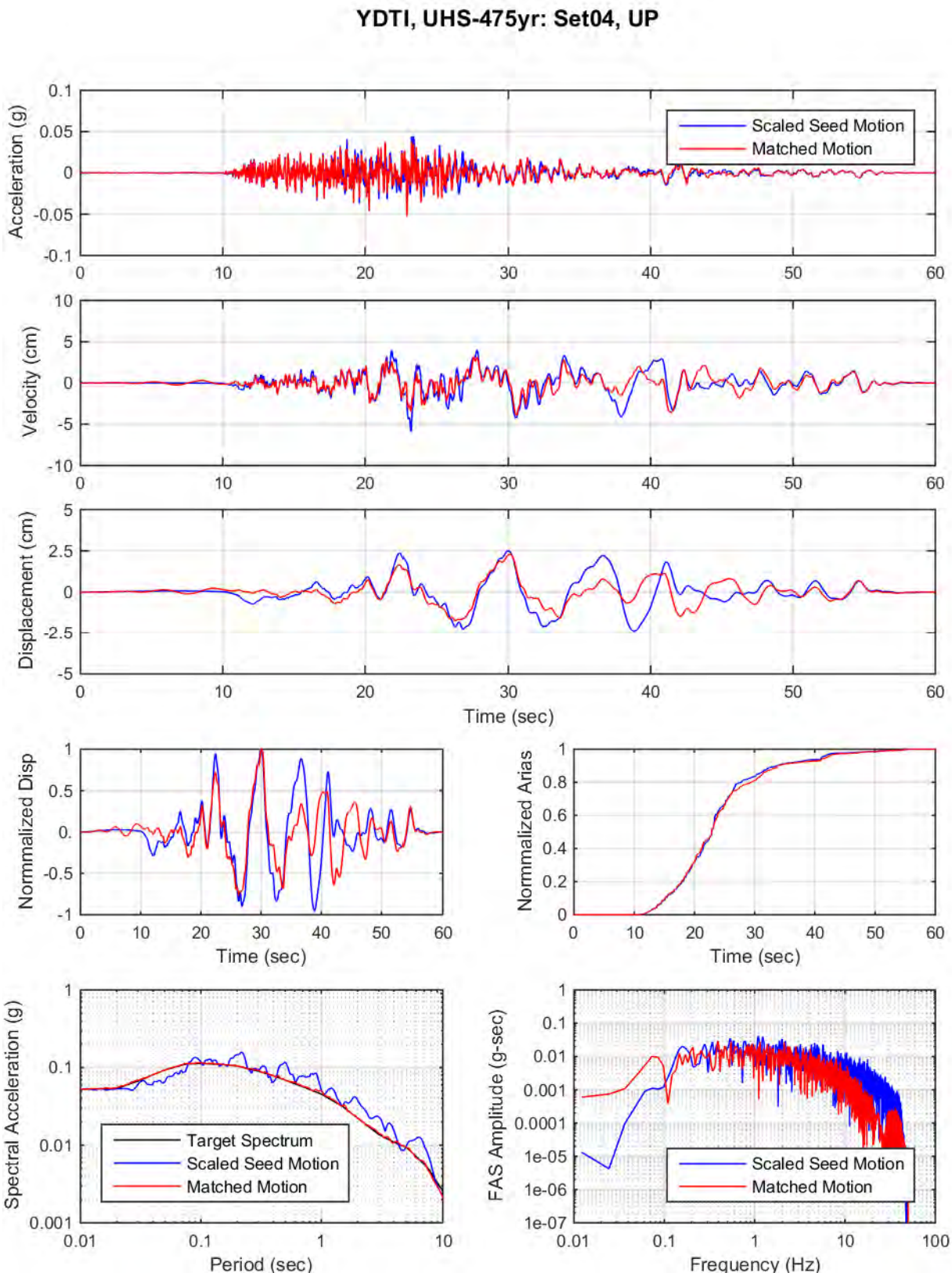
YDTI, UHS-475yr: Set04, UP
Acceleration (g)
Scaled Seed Motion
Matched Motion
Velocity (cm)
Displacement (cm)
Time (sec)
Normmalized Disp
Time (sec)
Normmalized Arias
Time (sec)
Spectral Acceleration (g)
Target Spectrum
Scaled Seed Motion
Matched Motion
Period (sec)
FAS Amplitude (g-sec)
Scaled Seed Motion
Matched Motion
Frequency (Hz)

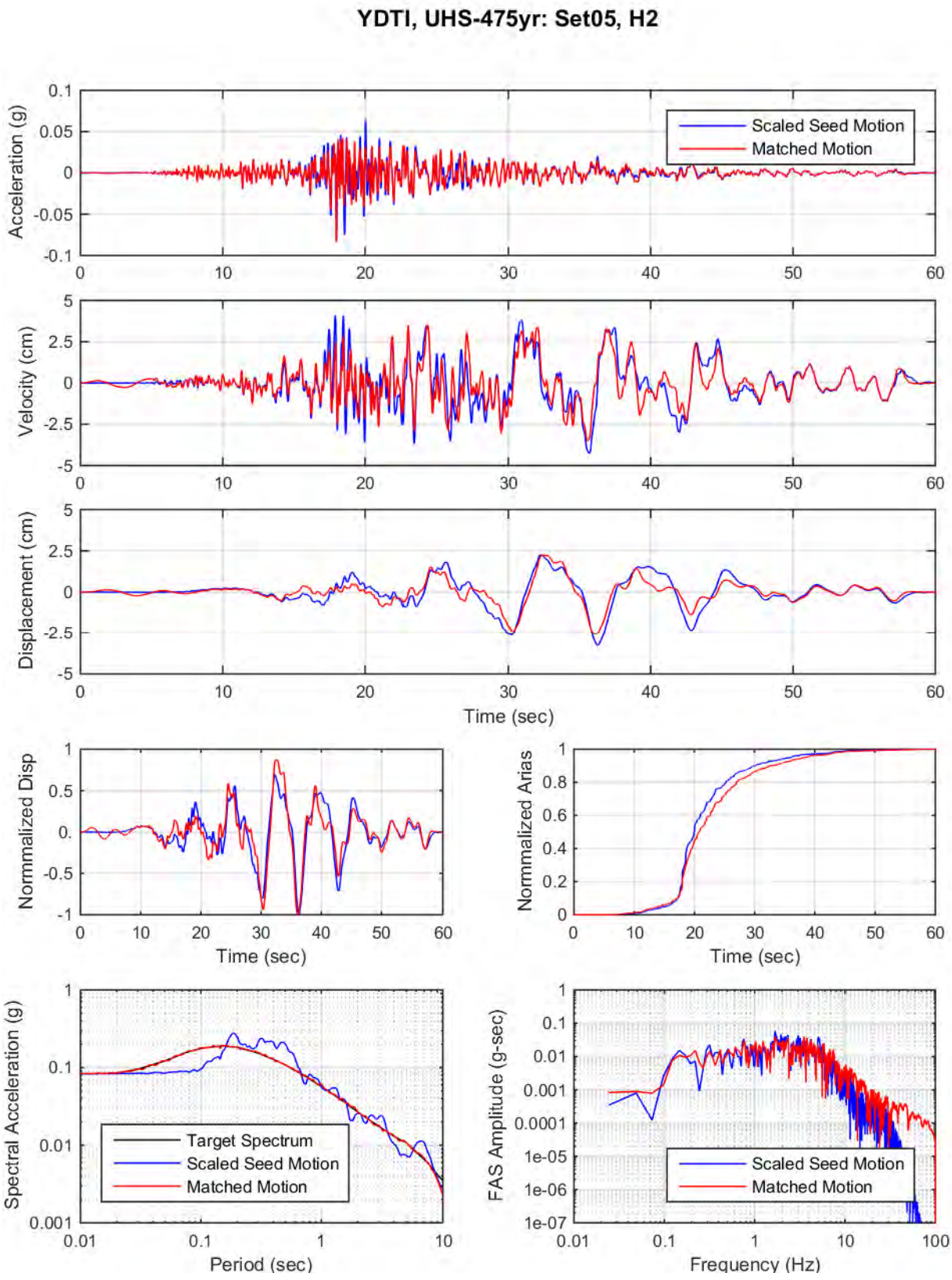
YDTI, UHS-475yr: Set05, H2
Acceleration (g)
Scaled Seed Motion
Matched Motion
Velocity (cm)
Displacement (cm)
Time (sec)
Normmalized Disp
Time (sec)
Normmalized Arias
Time (sec)
Spectral Acceleration (g)
Target Spectrum
Scaled Seed Motion
Matched Motion
Period (sec)
FAS Amplitude (g-sec)
Scaled Seed Motion
Matched Motion
Frequency (Hz)

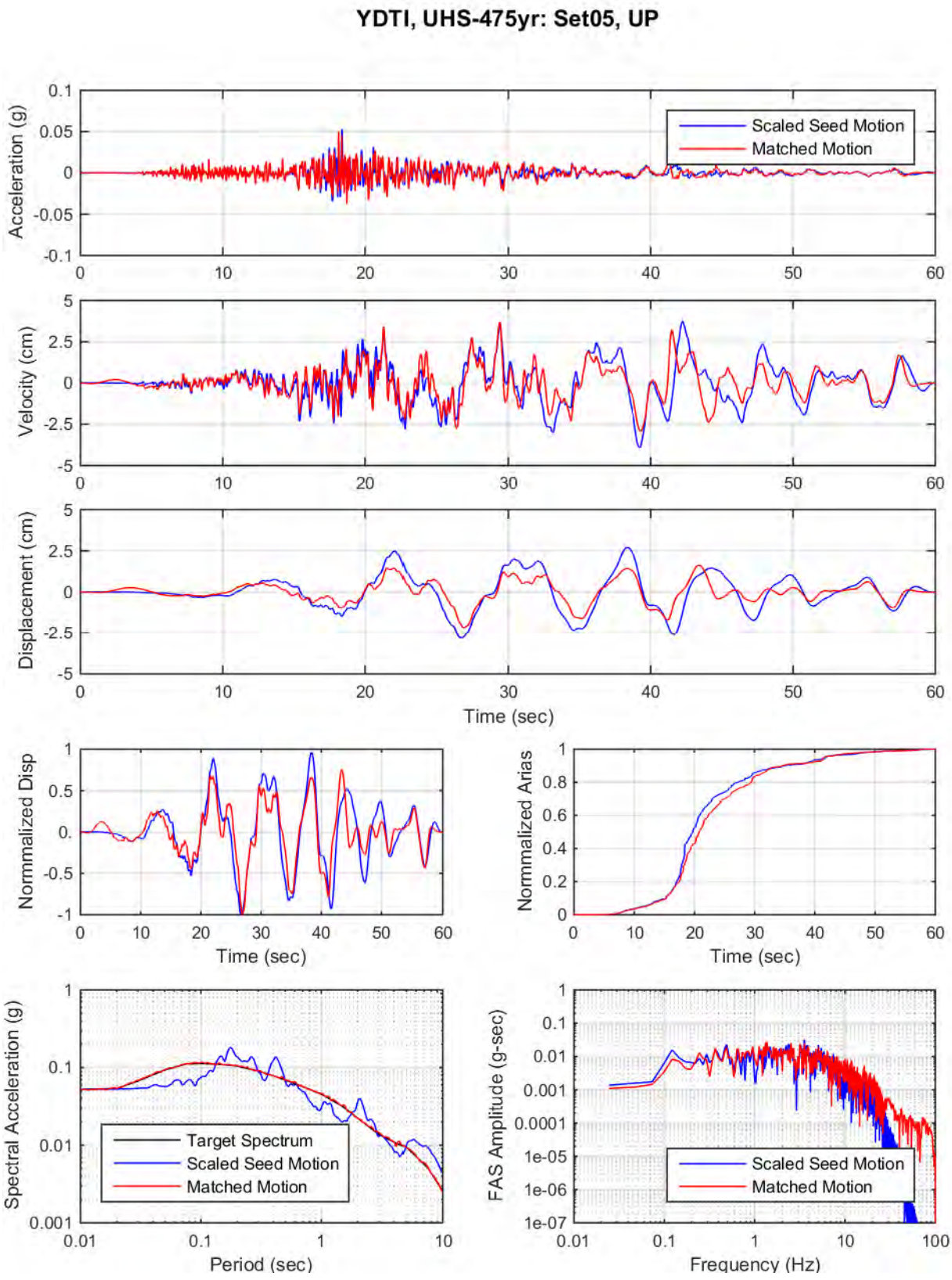
YDTI, UHS-475yr: Set05, UP
Acceleration (g)
Scaled Seed Motion
Matched Motion
Velocity (cm)
Displacement (cm)
Time (sec)
Normmalized Disp
Time (sec)
Normmalized Arias
Time (sec)
Spectral Acceleration (g)
Target Spectrum
Scaled Seed Motion
Matched Motion
Period (sec)
FAS Amplitude (g-sec)
Scaled Seed Motion
Matched Motion
Frequency (Hz)

APPENDIX III: SPECTRAL MATCHING PLOTS
1,000 YEAR DESIGN SPECTRA

YDTI, UHS-1000yr: Set01, H2

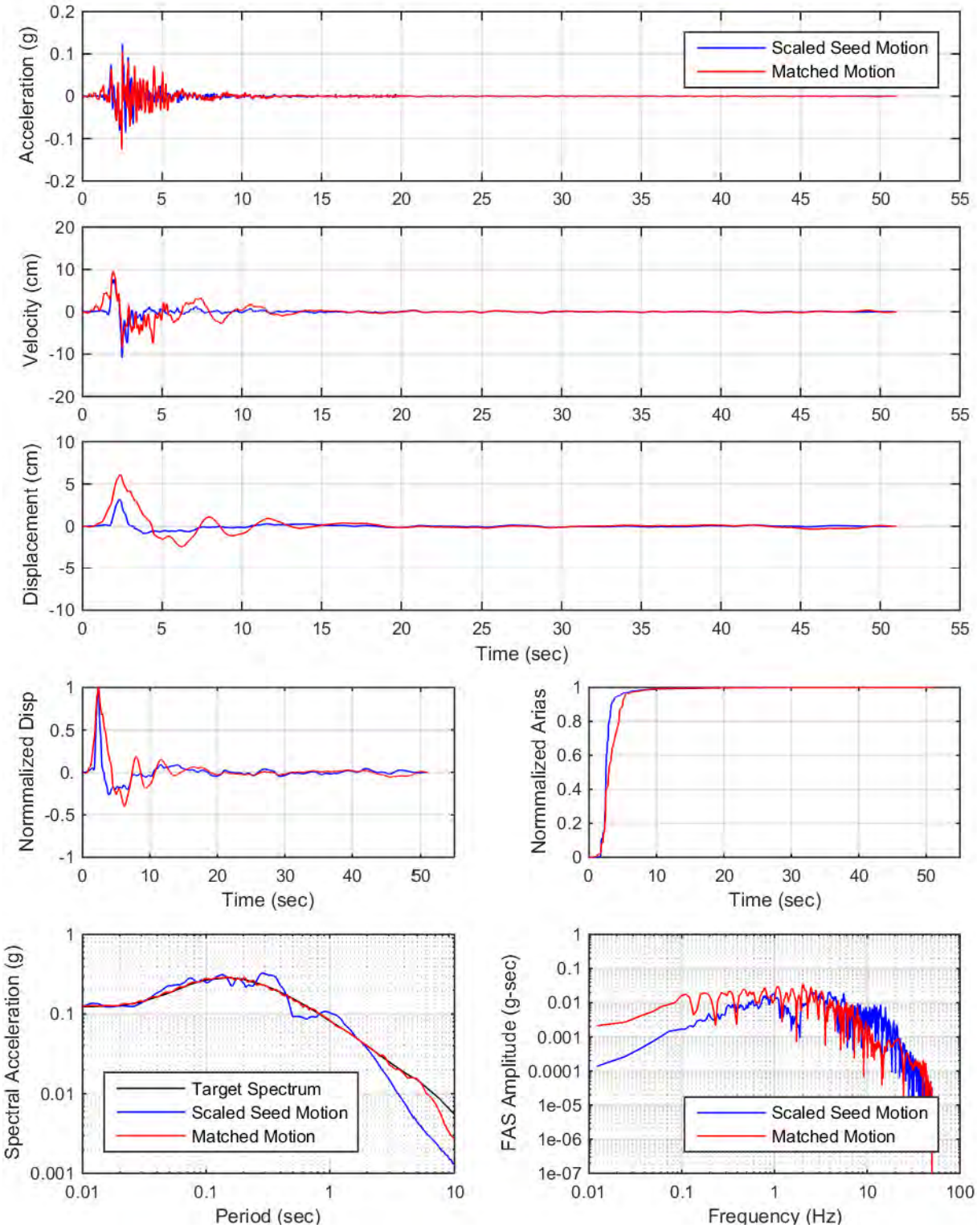

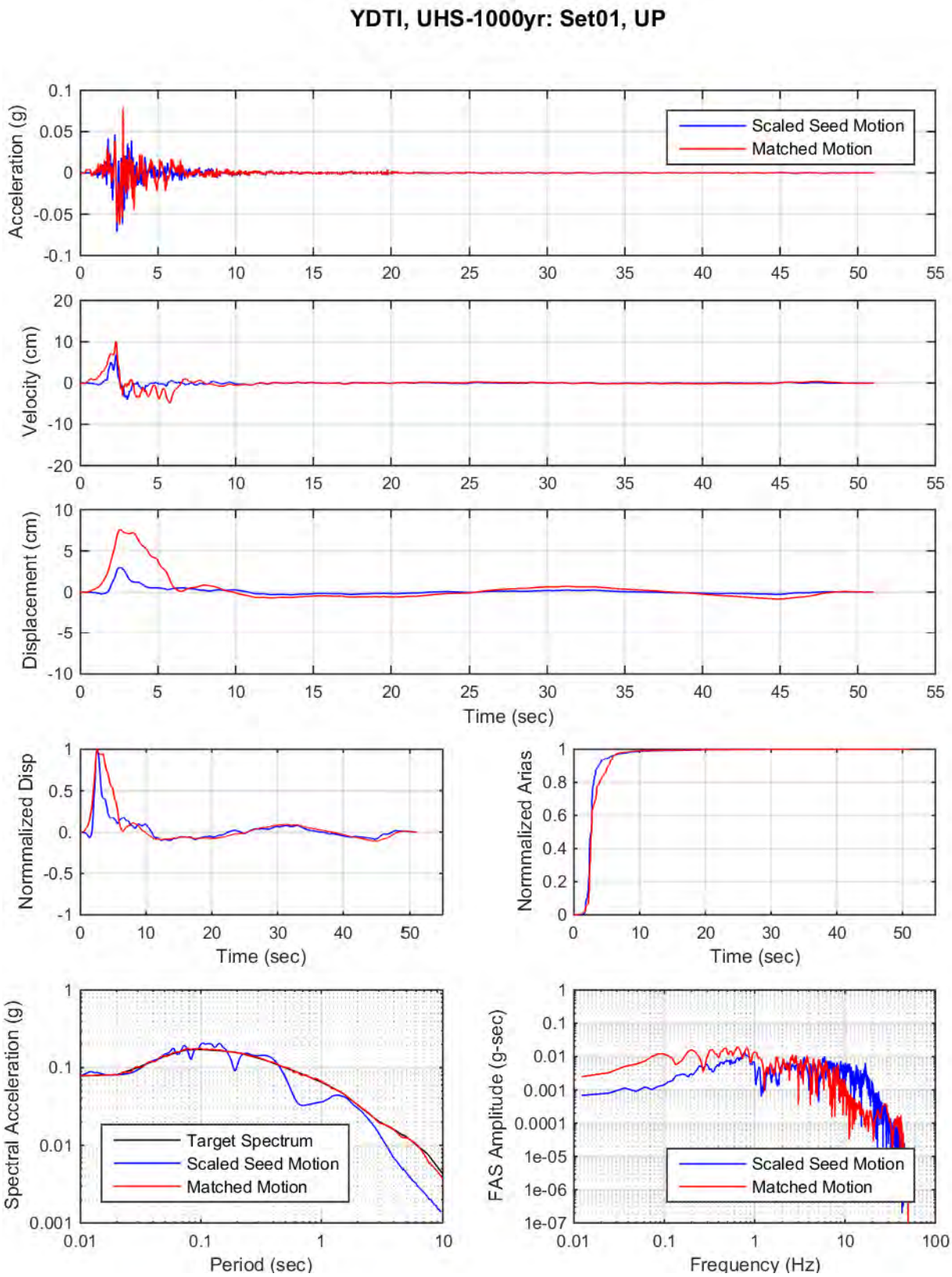
YDTI, UHS-1000yr: Set01, UP
Acceleration (g)
Scaled Seed Motion
Matched Motion
Velocity (cm)
Displacement (cm)
Time (sec)
Normmalized Disp
Time (sec)
Normmalized Arias
Time (sec)
Spectral Acceleration (g)
Target Spectrum
Scaled Seed Motion
Matched Motion
Period (sec)
FAS Amplitude (g-sec)
Scaled Seed Motion
Matched Motion
Frequency (Hz)

YDTI, UHS-1000yr: Set02, H1

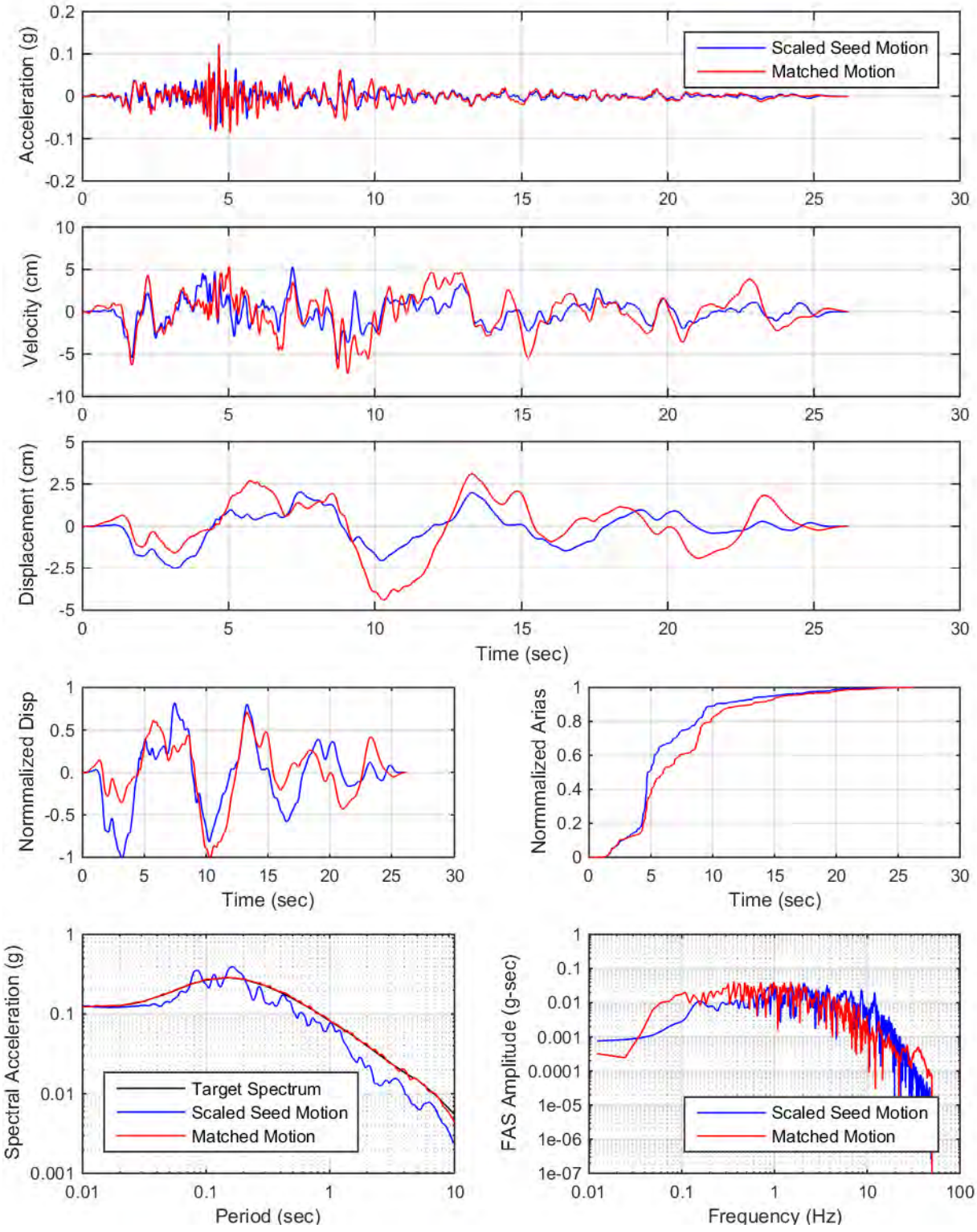

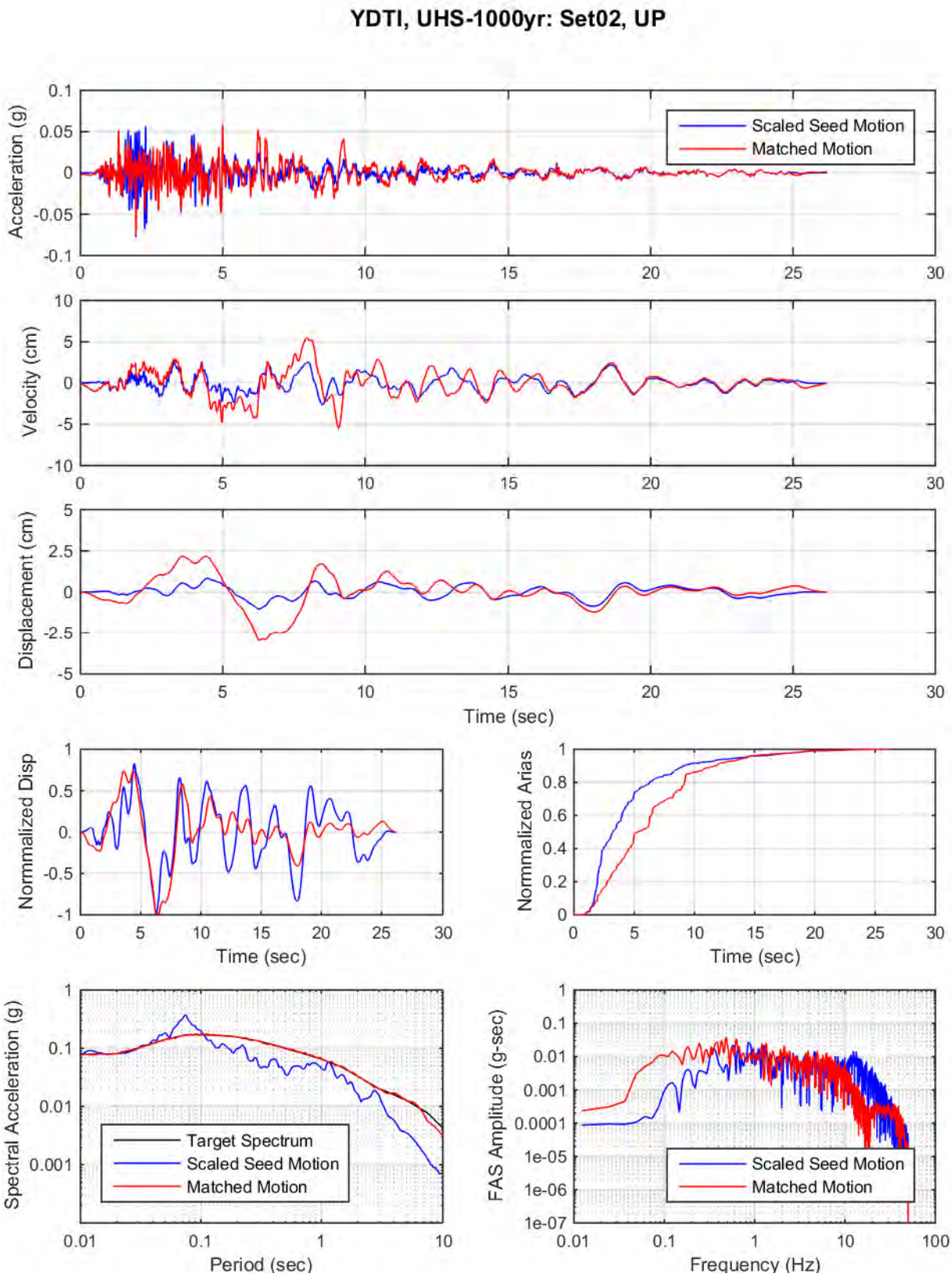
YDTI, UHS-1000yr: Set02, UP
Acceleration (g)
Scaled Seed Motion
Matched Motion
Velocity (cm)
Displacement (cm)
Time (sec)
Normmalized Disp
Time (sec)
Normmalized Arias
Time (sec)
Spectral Acceleration (g)
Target Spectrum
Scaled Seed Motion
Matched Motion
Period (sec)
FAS Amplitude (g-sec)
Scaled Seed Motion
Matched Motion
Frequency (Hz)

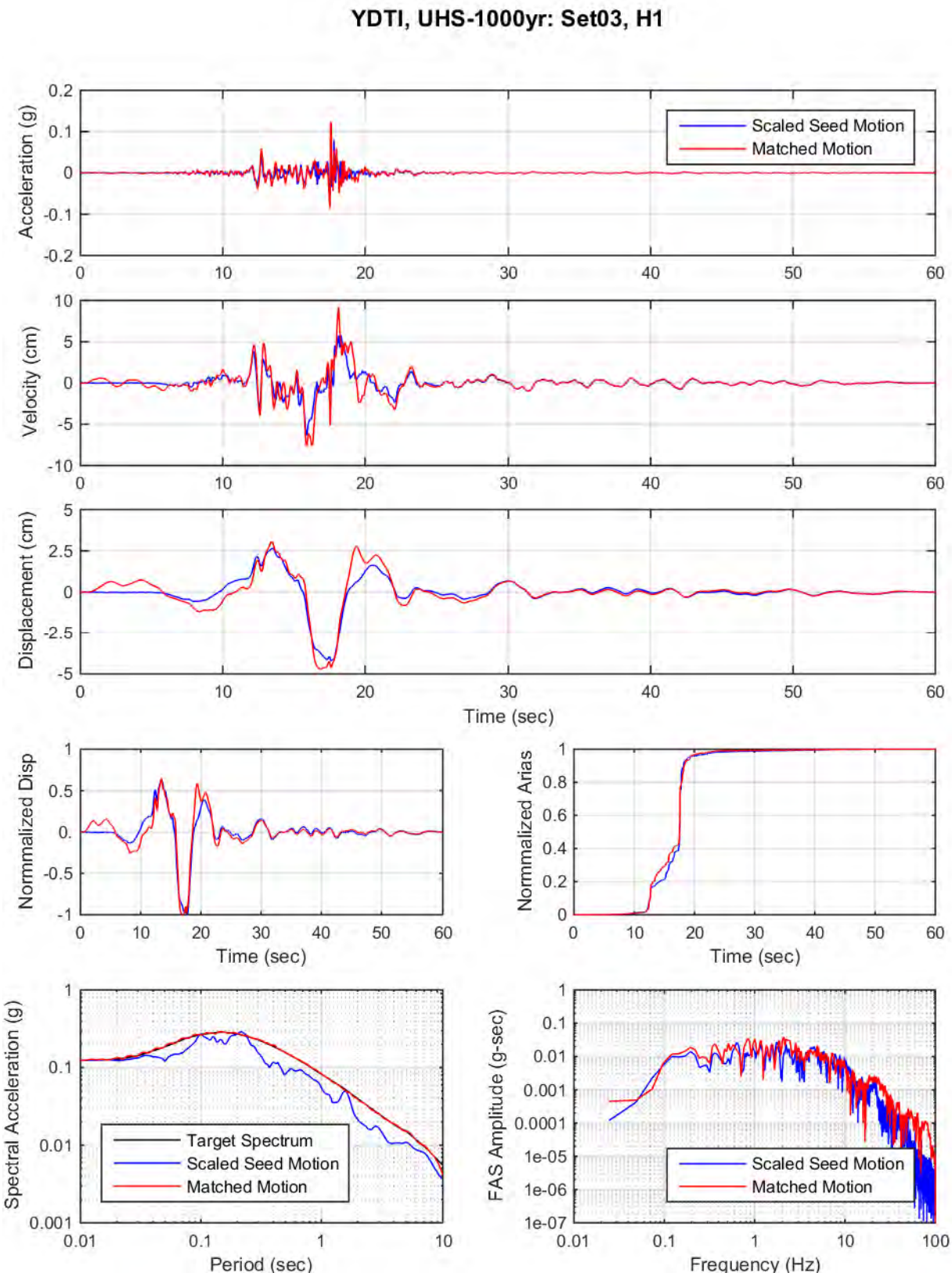
YDTI, UHS-1000yr: Set03, H1
Acceleration (g)
Scaled Seed Motion
Matched Motion
Velocity (cm)
Displacement (cm)
Time (sec)
Normmalized Disp
Time (sec)
Normmalized Arias
Time (sec)
Spectral Acceleration (g)
Target Spectrum
Scaled Seed Motion
Matched Motion
Period (sec)
FAS Amplitude (g-sec)
Scaled Seed Motion
Matched Motion
Frequency (Hz)

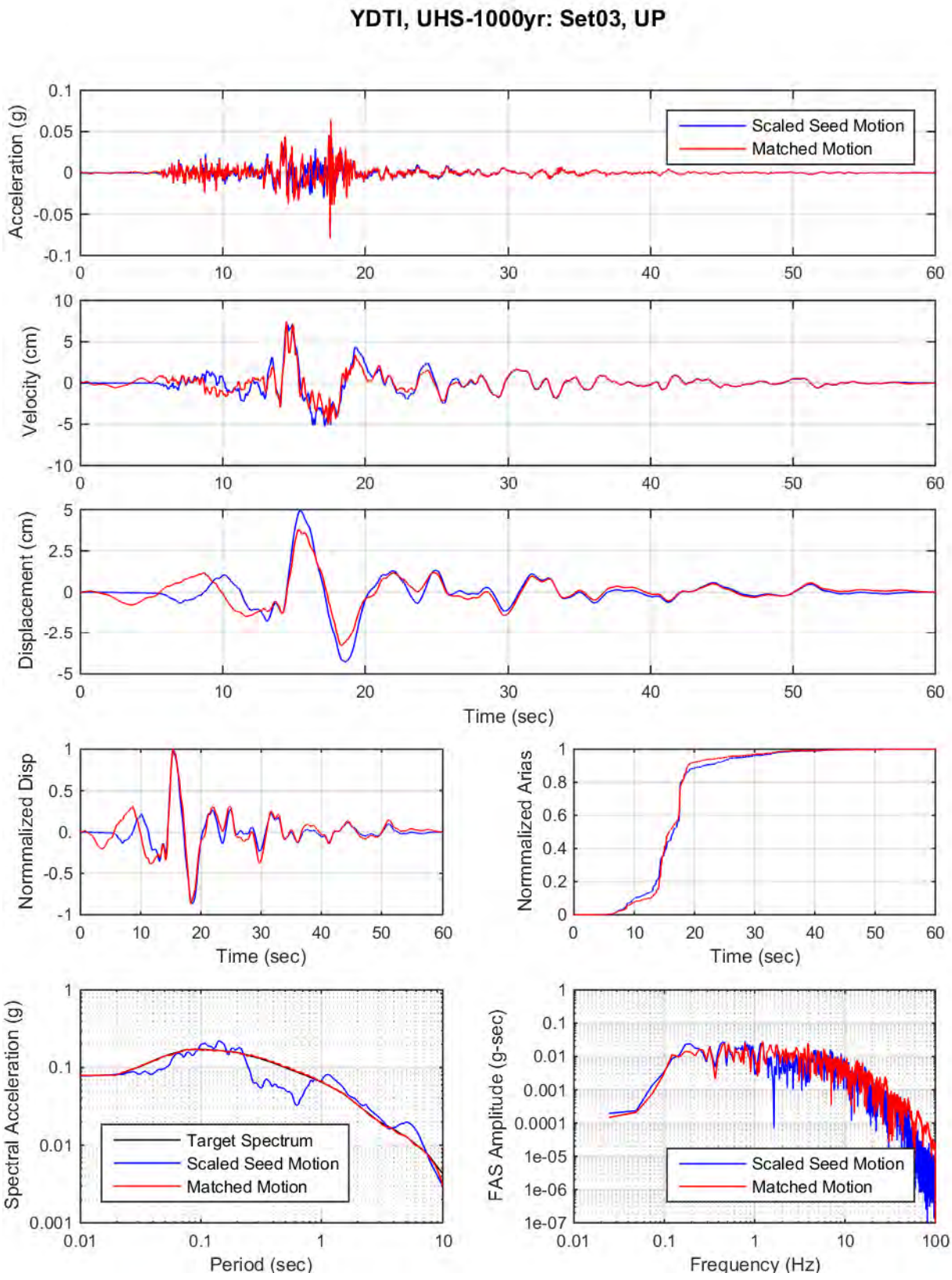
YDTI, UHS-1000yr: Set03, UP
Acceleration (g)
Scaled Seed Motion
Matched Motion
Velocity (cm)
Displacement (cm)
Time (sec)
Normmalized Disp
Time (sec)
Normmalized Arias
Time (sec)
Spectral Acceleration (g)
Target Spectrum
Scaled Seed Motion
Matched Motion
Period (sec)
FAS Amplitude (g-sec)
Scaled Seed Motion
Matched Motion
Frequency (Hz)

YDTI, UHS-1000yr: Set04, H2

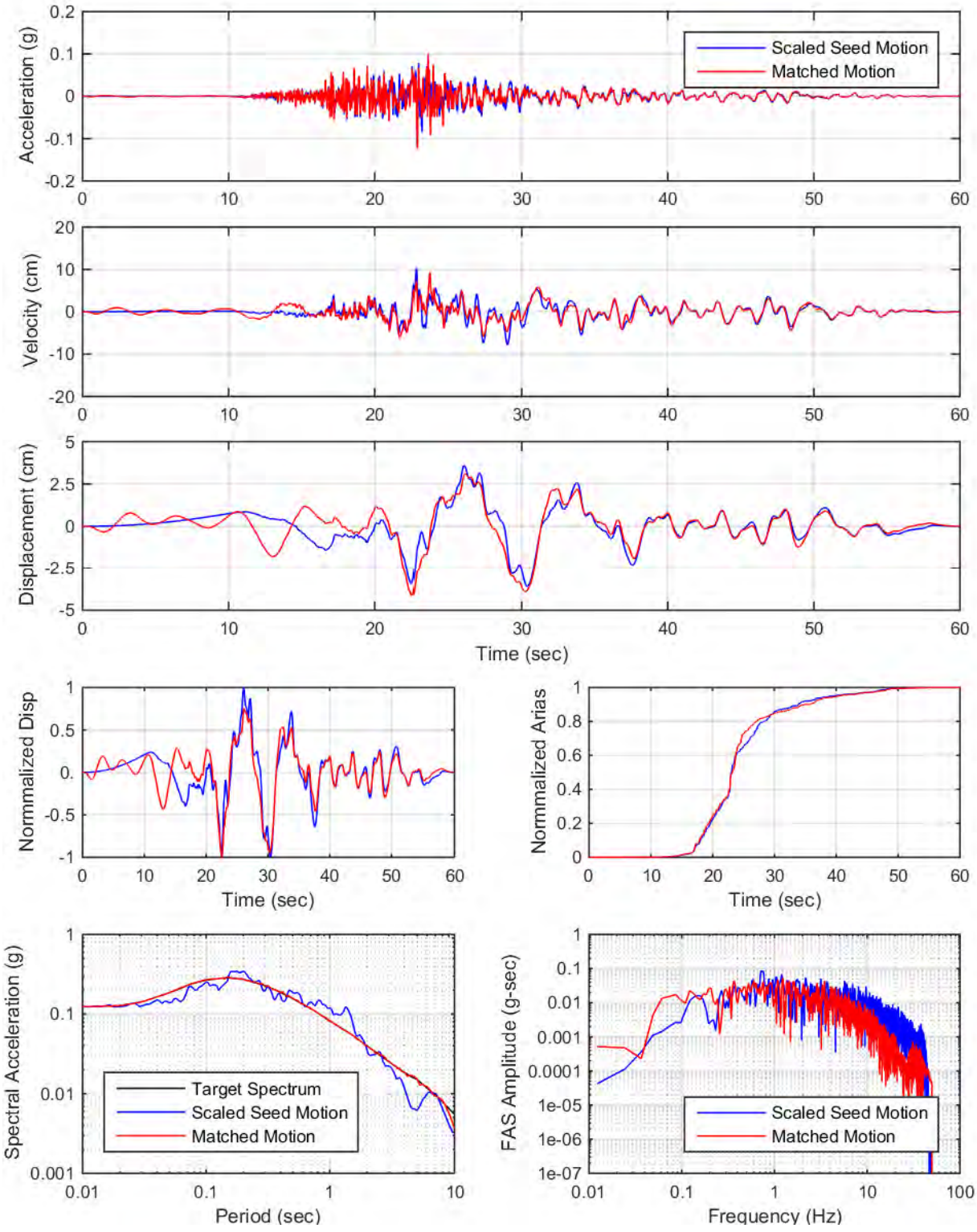

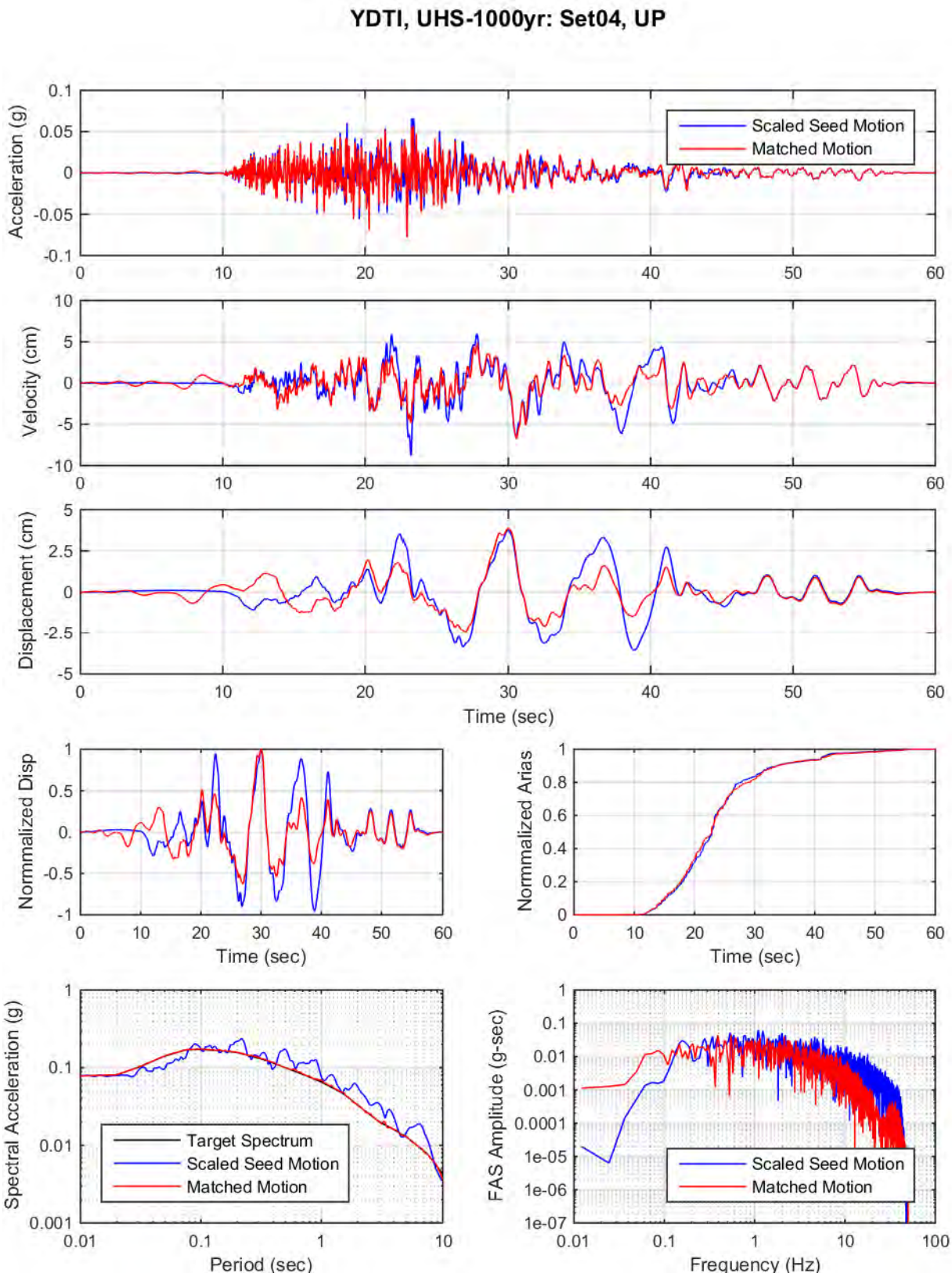
YDTI, UHS-1000yr: Set04, UP
Acceleration (g)
Scaled Seed Motion
Matched Motion
Velocity (cm)
Displacement (cm)
Time (sec)
Normmalized Disp
Time (sec)
Normmalized Arias
Time (sec)
Spectral Acceleration (g)
Target Spectrum
Scaled Seed Motion
Matched Motion
Period (sec)
FAS Amplitude (g-sec)
Scaled Seed Motion
Matched Motion
Frequency (Hz)

YDTI, UHS-1000yr: Set05, H2

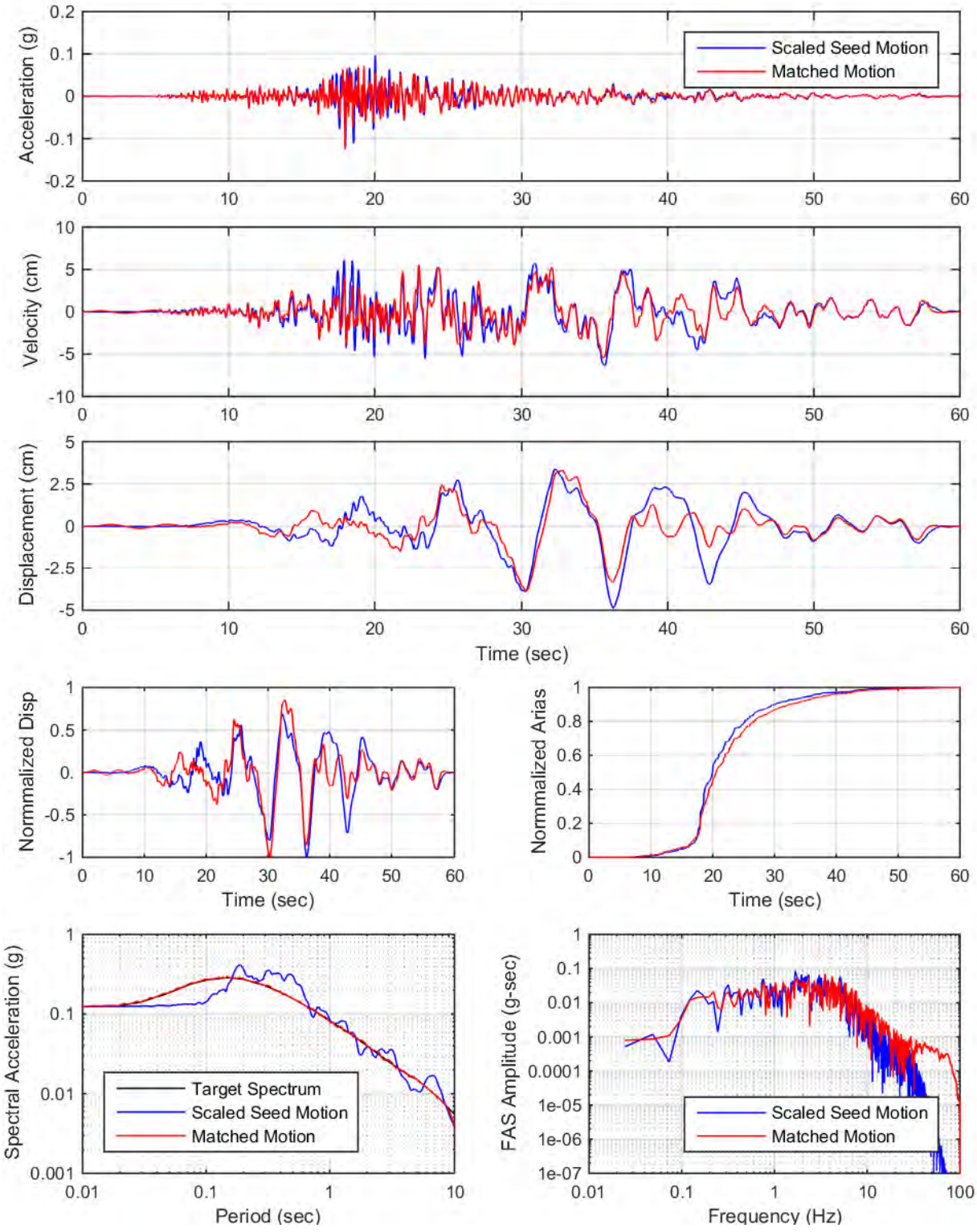

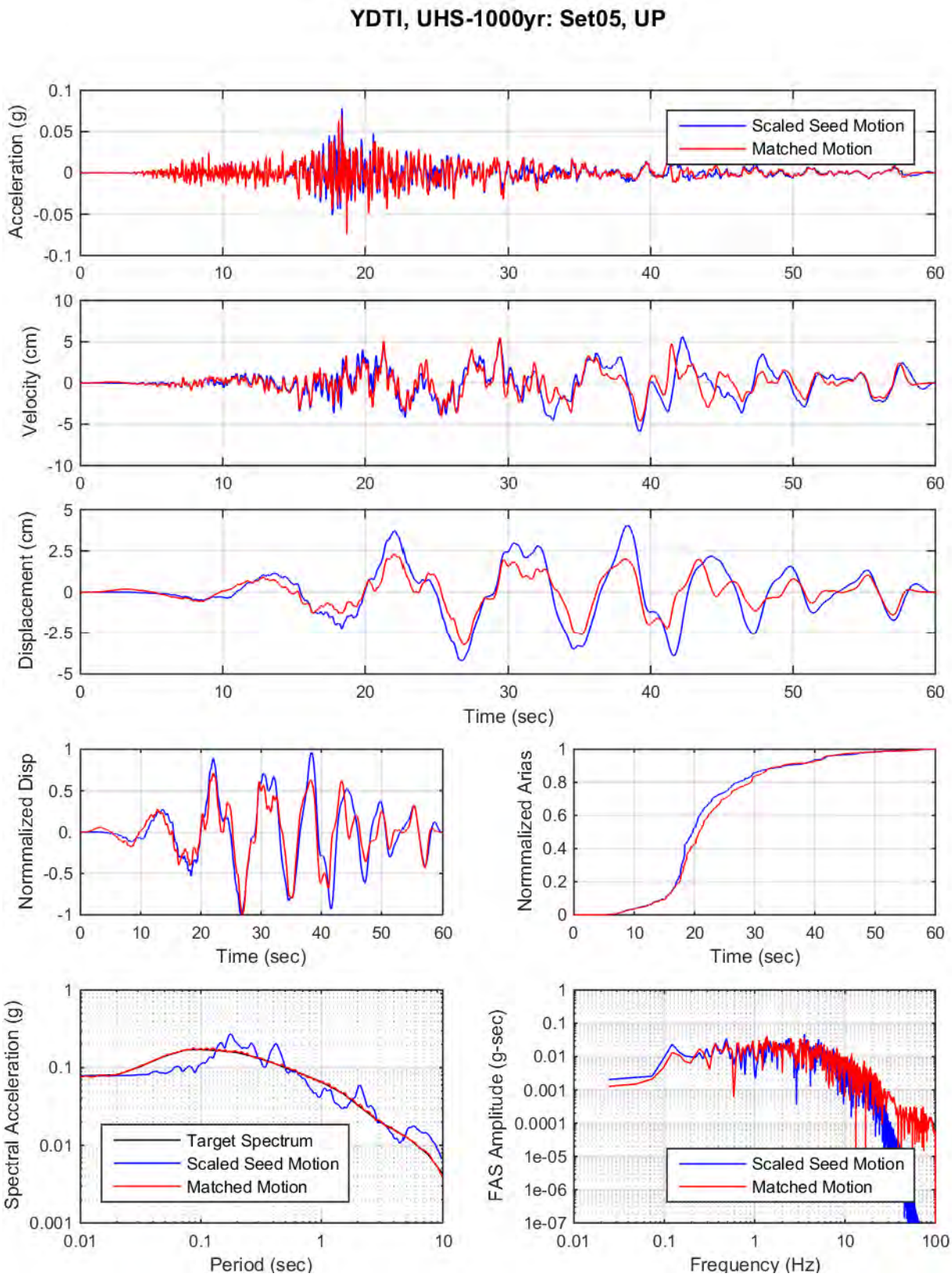
YDTI, UHS-1000yr: Set05, UP
Acceleration (g)
Scaled Seed Motion
Matched Motion
Velocity (cm)
Displacement (cm)
Time (sec)
Normmalized Disp
Time (sec)
Normmalized Arias
Time (sec)
Spectral Acceleration (g)
Target Spectrum
Scaled Seed Motion
Matched Motion
Period (sec)
FAS Amplitude (g-sec)
Scaled Seed Motion
Matched Motion
Frequency (Hz)

APPENDIX IV: SPECTRAL MATCHING PLOTS
2,475 YEAR DESIGN SPECTRA

YDTI, UHS-2475yr: Set01, H2

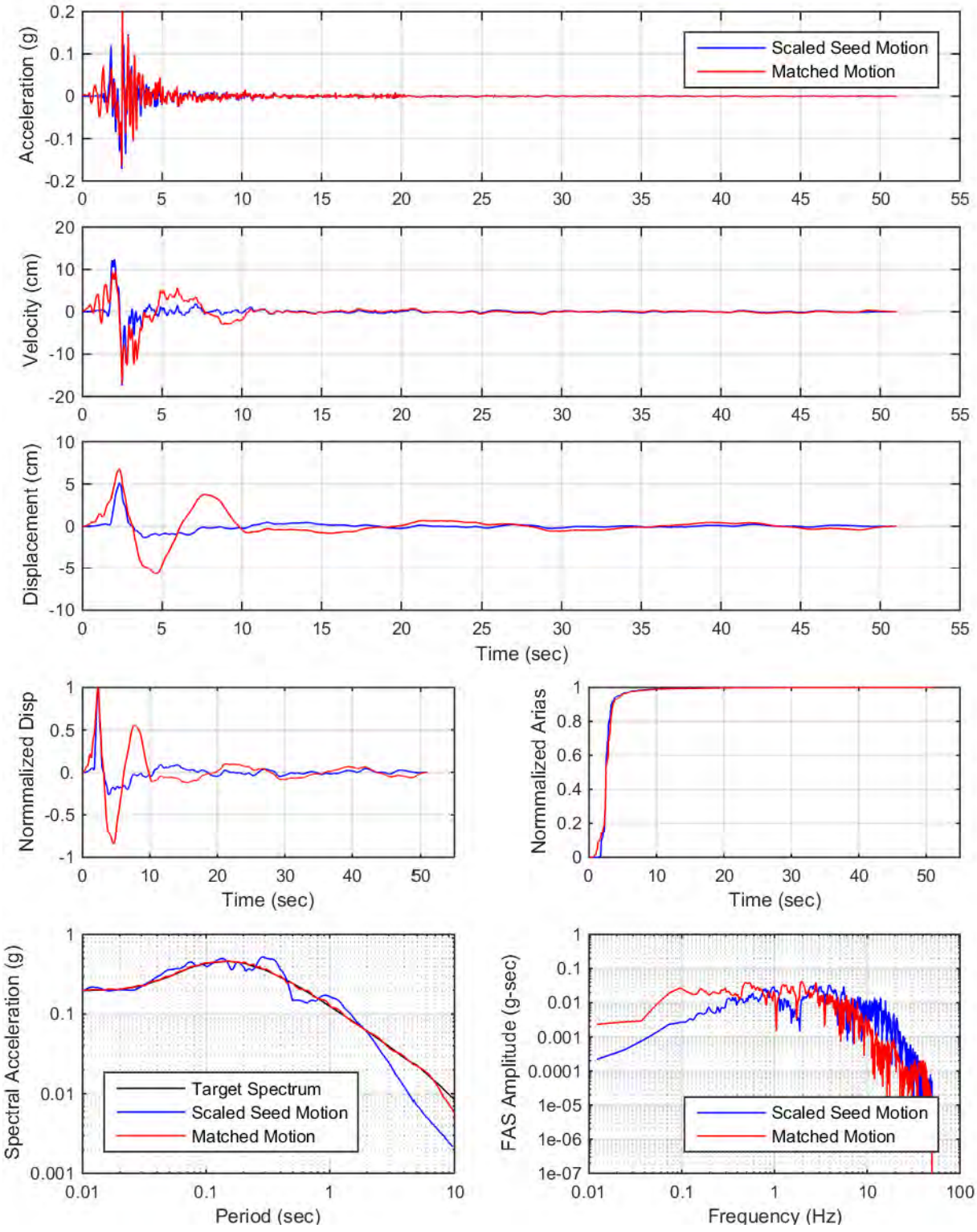

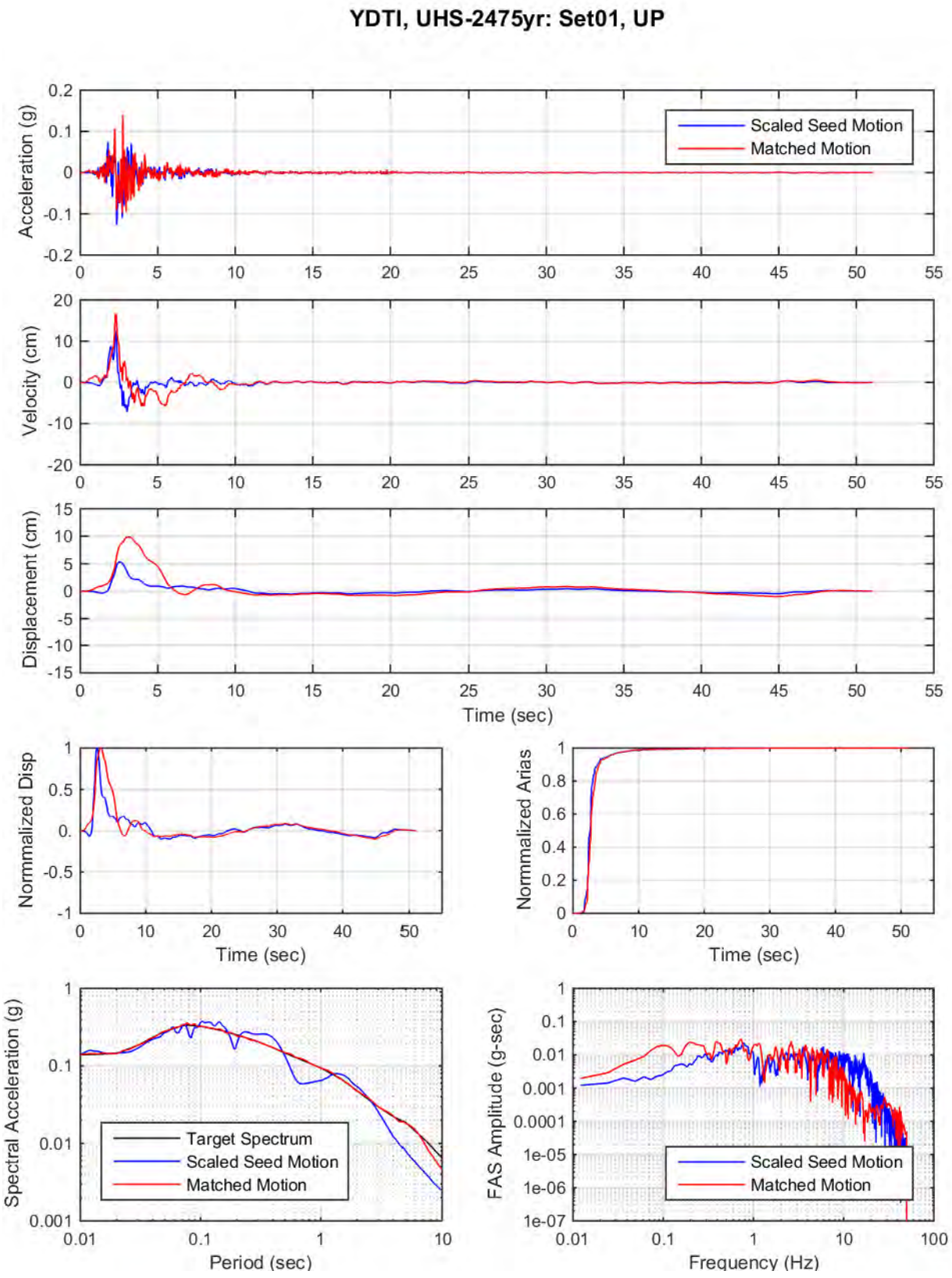
YDTI, UHS-2475yr: Set01, UP
Acceleration (g)
Scaled Seed Motion
Matched Motion
Velocity (cm)
Displacement (cm)
Time (sec)
Normmalized Disp
Time (sec)
Normmalized Arias
Time (sec)
Spectral Acceleration (g)
Target Spectrum
Scaled Seed Motion
Matched Motion
Period (sec)
FAS Amplitude (g-sec)
Scaled Seed Motion
Matched Motion
Frequency (Hz)

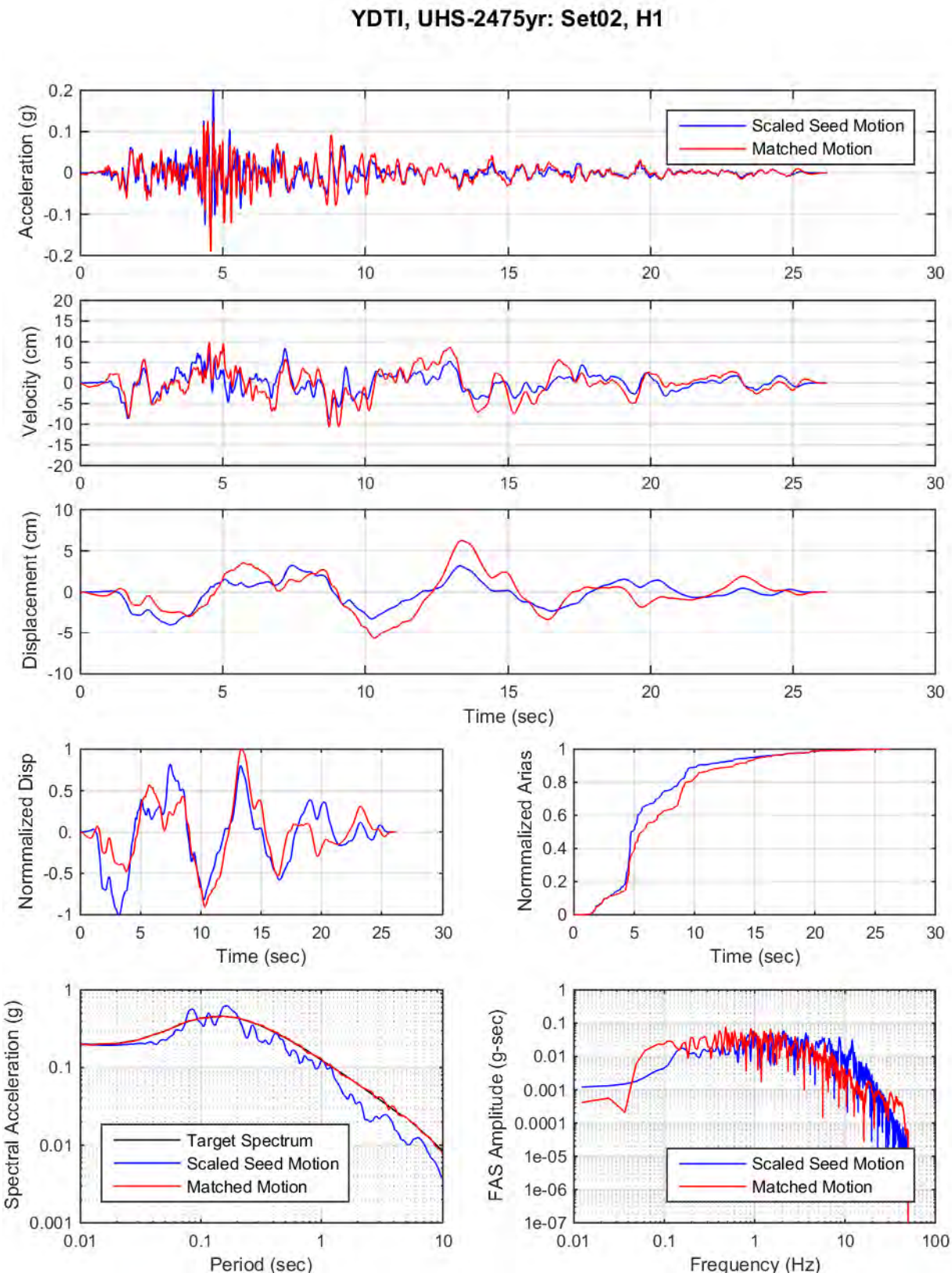
YDTI, UHS-2475yr: Set02, H1
Acceleration (g)
Scaled Seed Motion
Matched Motion
Velocity (cm)
Displacement (cm)
Time (sec)
Normmalized Disp
Time (sec)
Normmalized Arias
Time (sec)
Spectral Acceleration (g)
Target Spectrum
Scaled Seed Motion
Matched Motion
Period (sec)
FAS Amplitude (g-sec)
Scaled Seed Motion
Matched Motion
Frequency (Hz)

YDTI, UHS-2475yr: Set02, UP

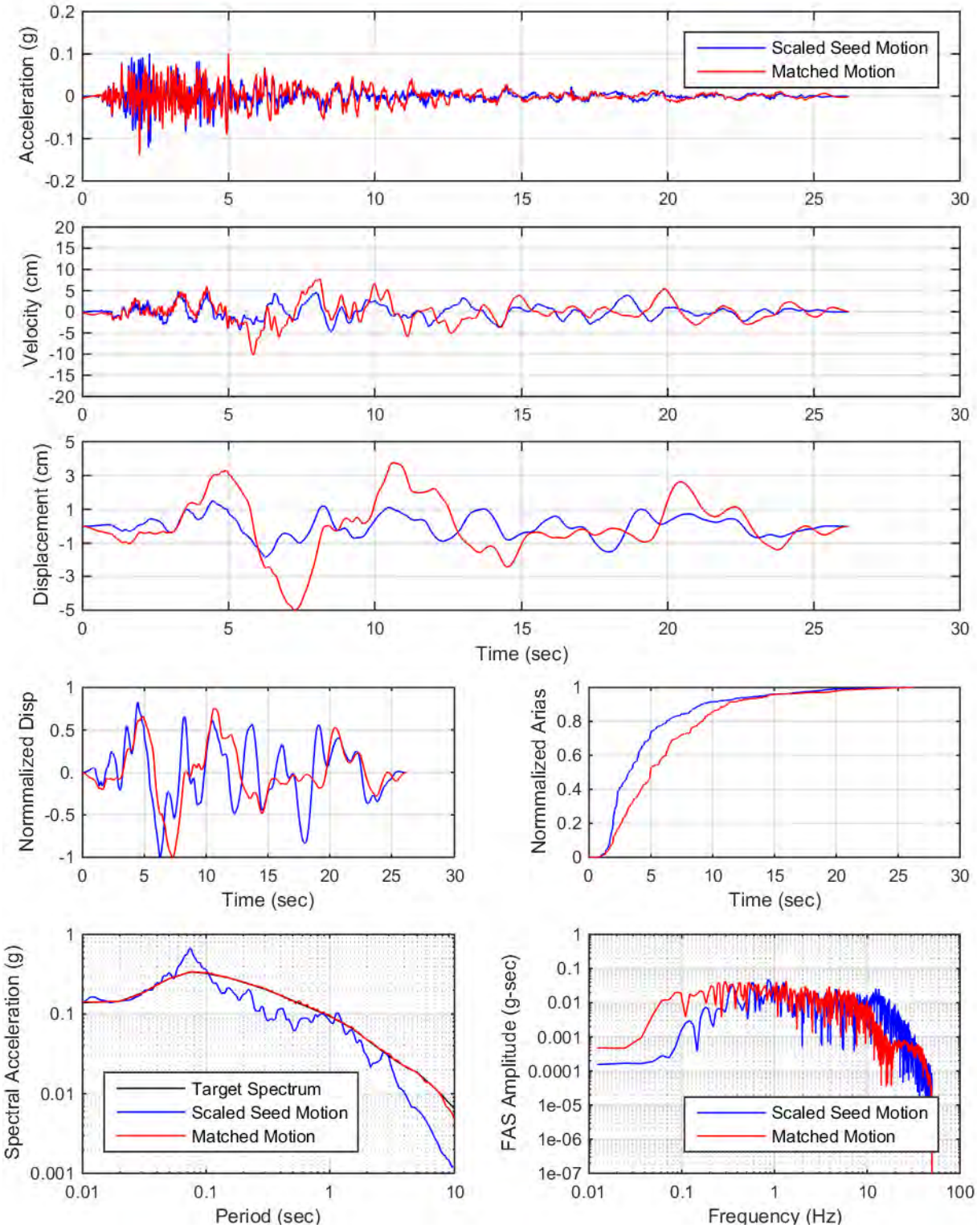

YDTI, UHS-2475yr: Set03, H1

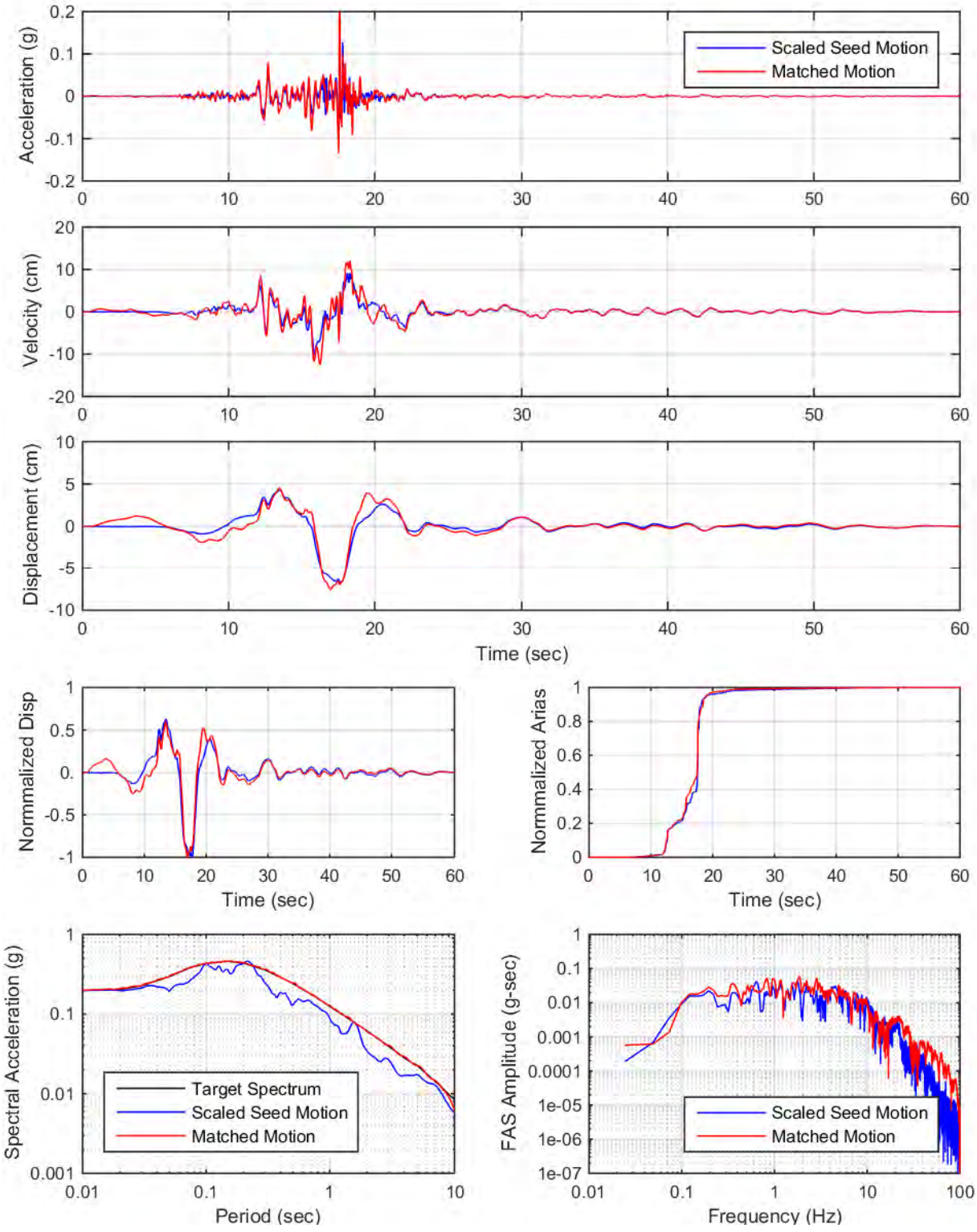

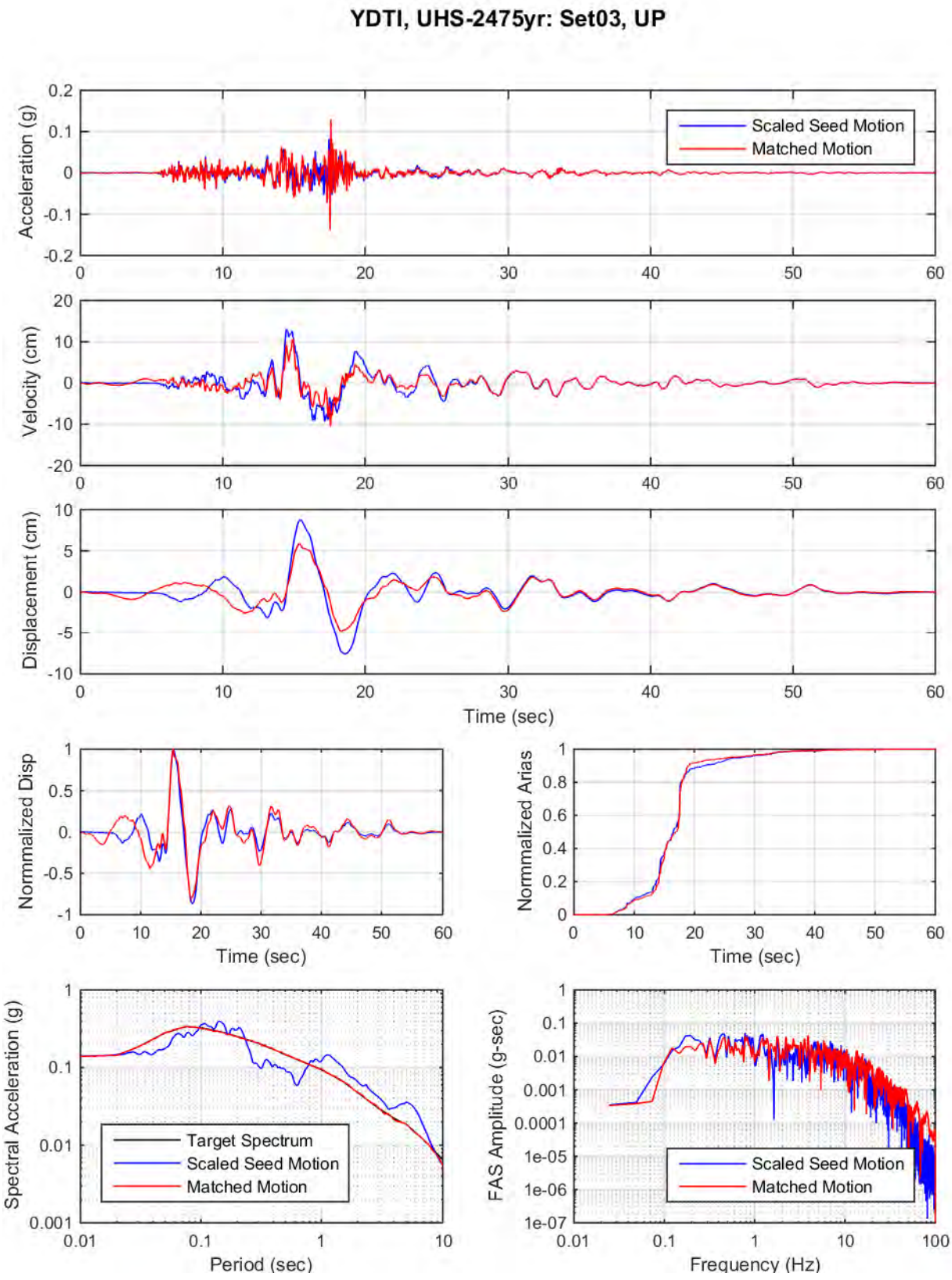
YDTI, UHS-2475yr: Set03, UP
Acceleration (g)
Scaled Seed Motion
Matched Motion
Velocity (cm)
Displacement (cm)
Time (sec)
Normmalized Disp
Time (sec)
Normmalized Arias
Time (sec)
Spectral Acceleration (g)
Target Spectrum
Scaled Seed Motion
Matched Motion
Period (sec)
FAS Amplitude (g-sec)
Scaled Seed Motion
Matched Motion
Frequency (Hz)

YDTI, UHS-2475yr: Set04, H2

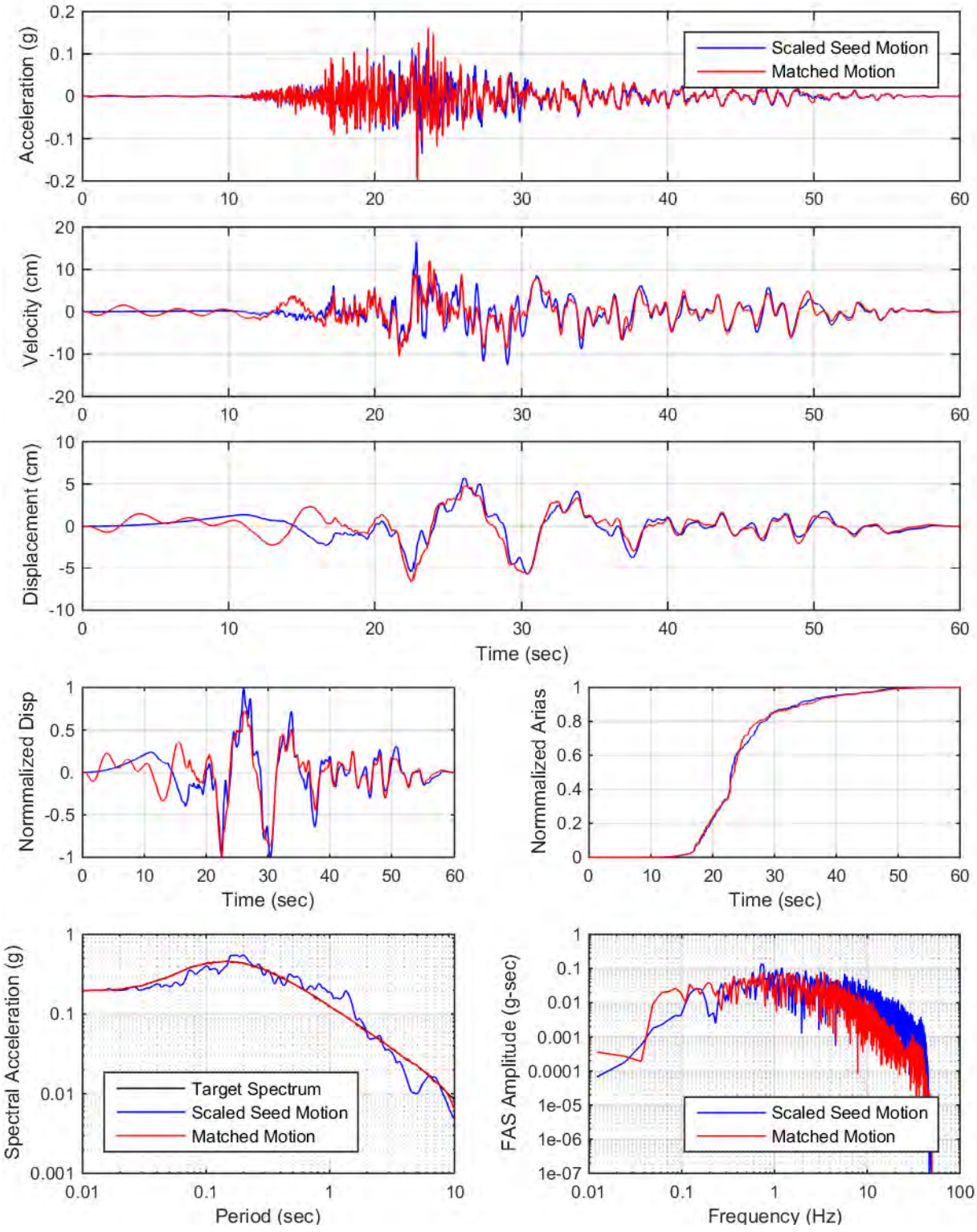

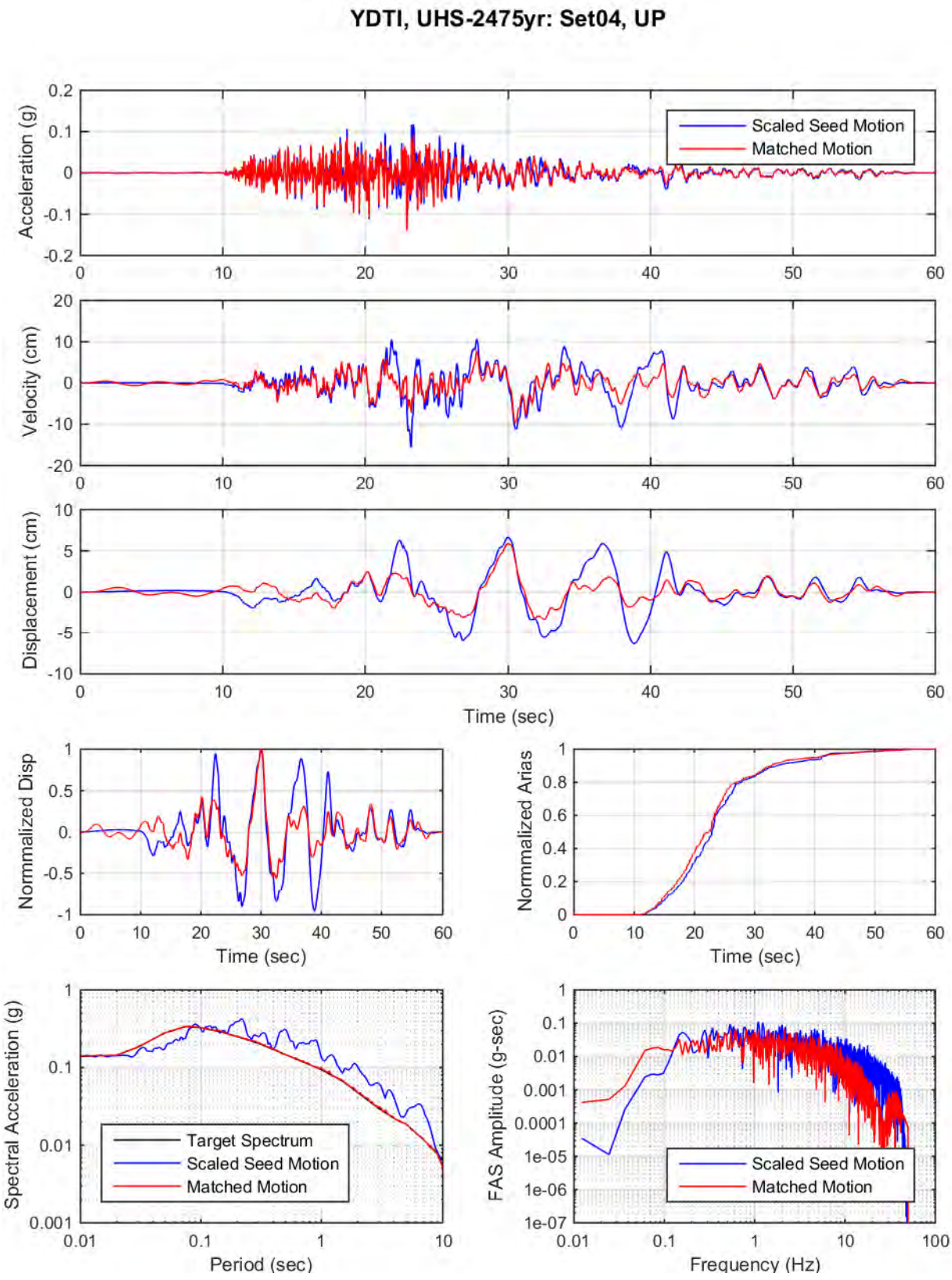
YDTI, UHS-2475yr: Set04, UP
Acceleration (g)
Scaled Seed Motion
Matched Motion
Velocity (cm)
Displacement (cm)
Time (sec)
Normmalized Disp
Time (sec)
Normmalized Arias
Time (sec)
Spectral Acceleration (g)
Target Spectrum
Scaled Seed Motion
Matched Motion
Period (sec)
FAS Amplitude (g-sec)
Scaled Seed Motion
Matched Motion
Frequency (Hz)

YDTI, UHS-2475yr: Set05, H2

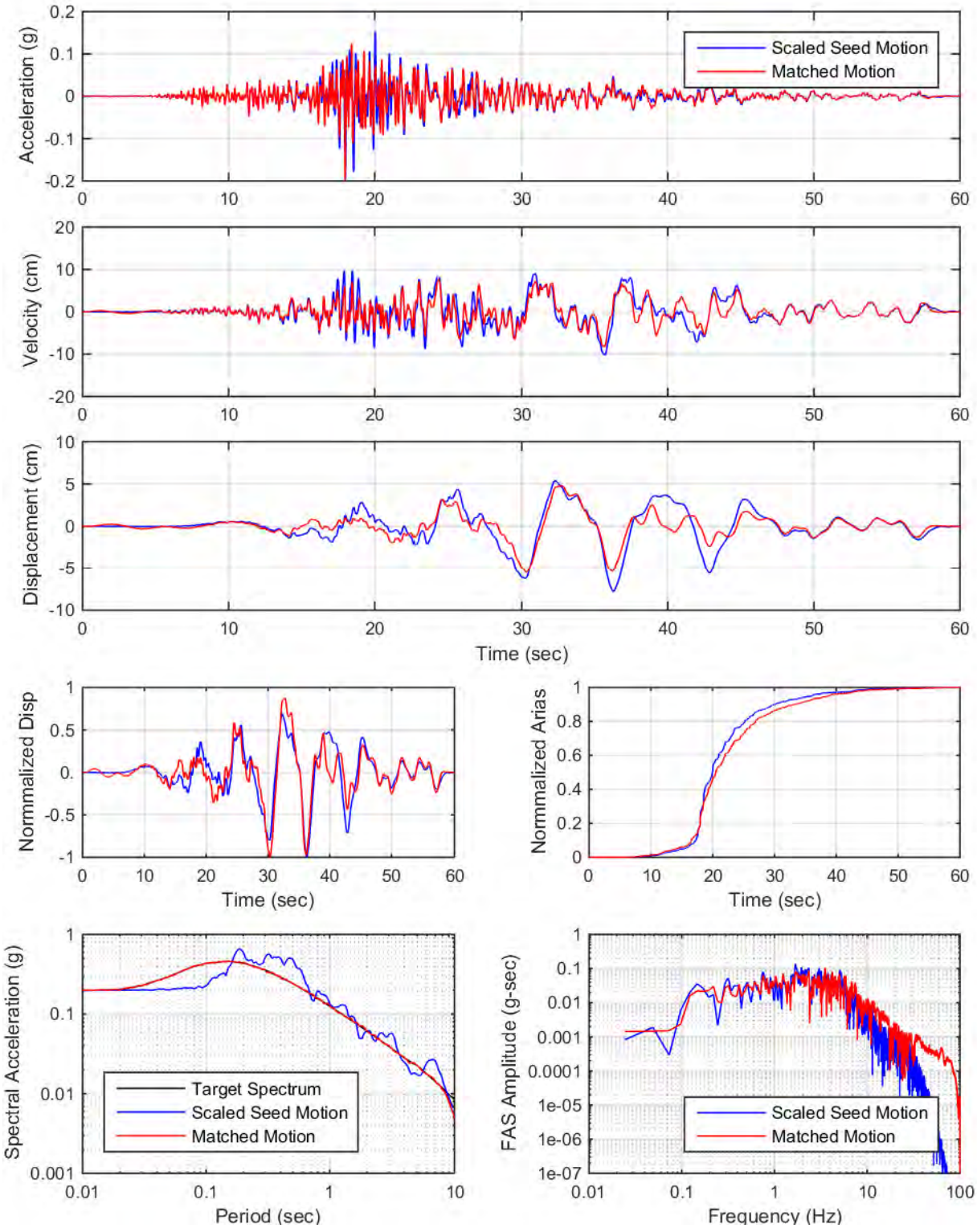

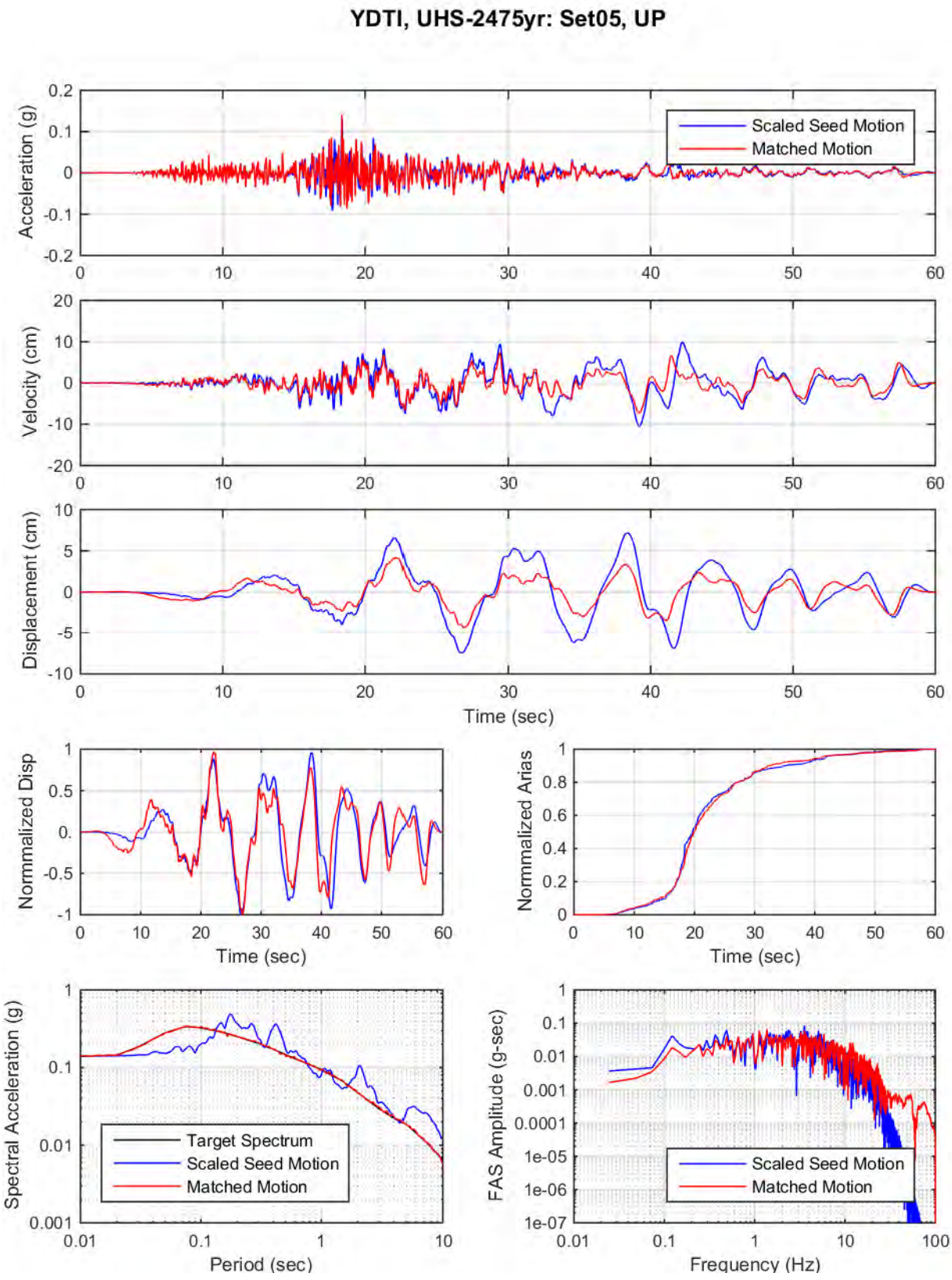
YDTI, UHS-2475yr: Set05, UP
Acceleration (g)
Scaled Seed Motion
Matched Motion
Velocity (cm)
Displacement (cm)
Time (sec)
Normmalized Disp
Time (sec)
Normmalized Arias
Time (sec)
Spectral Acceleration (g)
Target Spectrum
Scaled Seed Motion
Matched Motion
Period (sec)
FAS Amplitude (g-sec)
Scaled Seed Motion
Matched Motion
Frequency (Hz)

APPENDIX V: SPECTRAL MATCHING PLOTS
10,000 YEAR DESIGN SPECTRA

YDTI, UHS-10000yr: Set01, H2

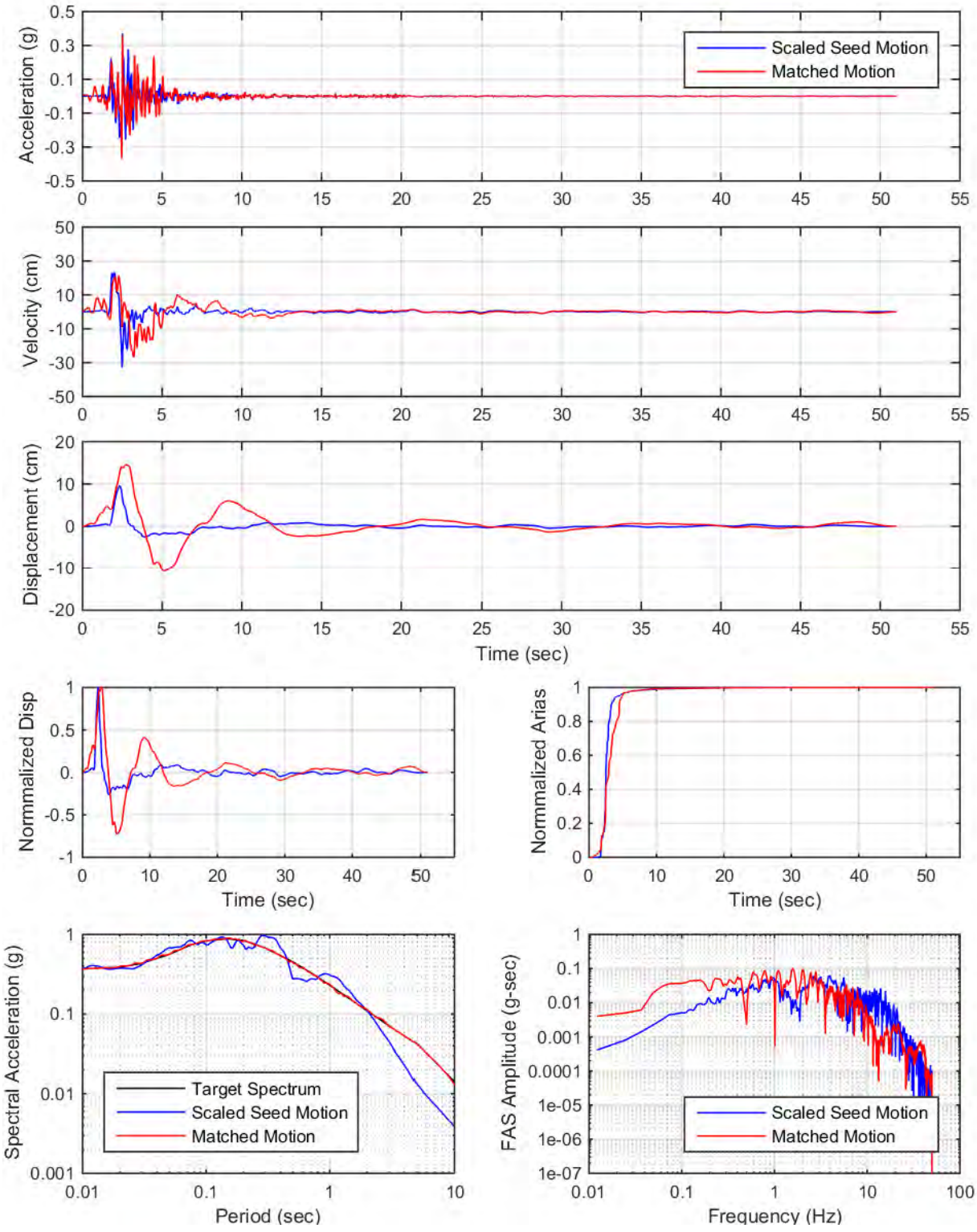

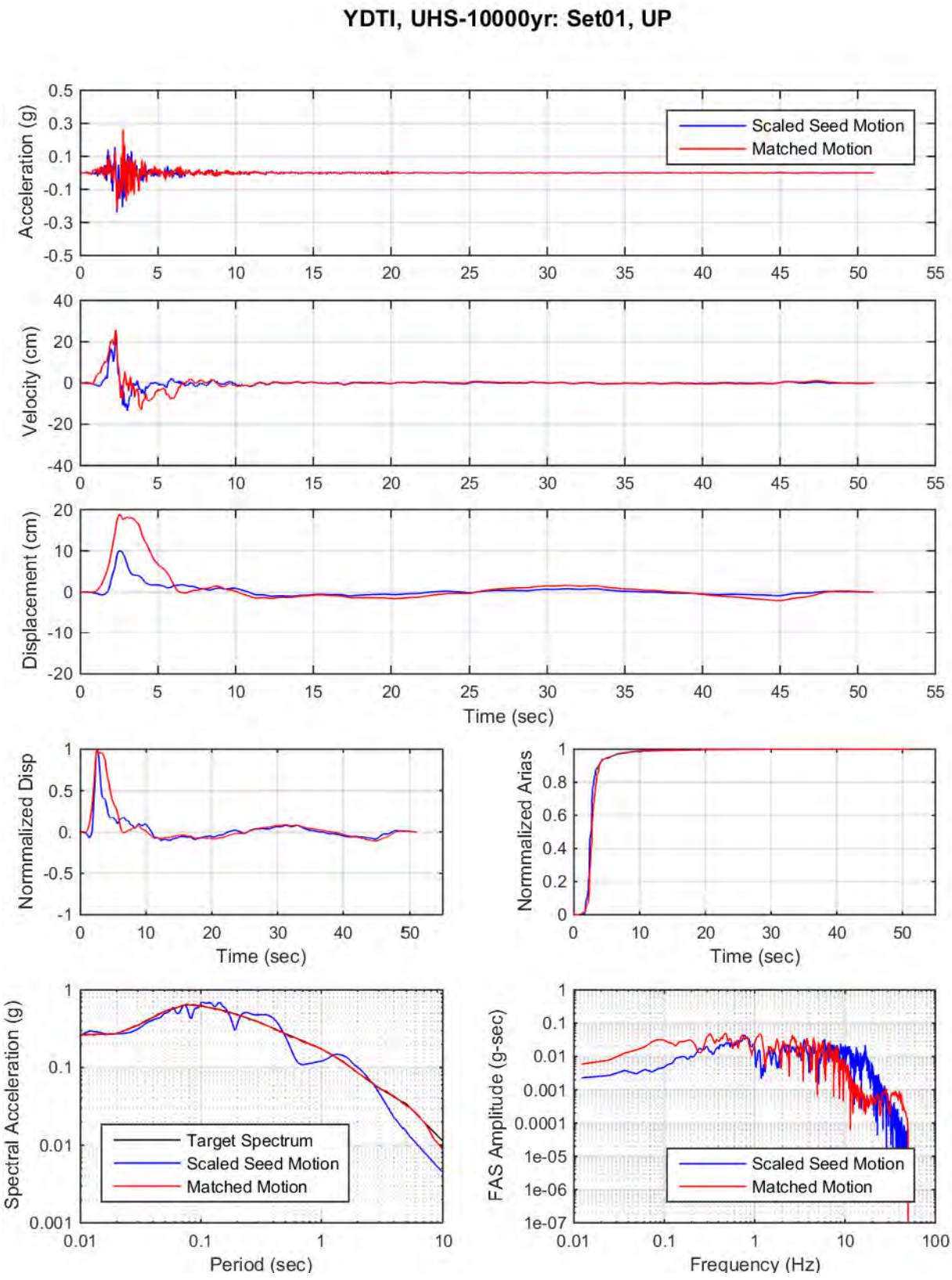
YDTI, UHS-10000yr: Set01, UP
Acceleration (g)
Scaled Seed Motion
Matched Motion
Velocity (cm)
Displacement (cm)
Time (sec)
Normmalized Disp
Time (sec)
Normmalized Arias
Time (sec)
Spectral Acceleration (g)
Target Spectrum
Scaled Seed Motion
Matched Motion
Period (sec)
FAS Amplitude (g-sec)
Scaled Seed Motion
Matched Motion
Frequency (Hz)

YDTI, UHS-10000yr: Set02, H1

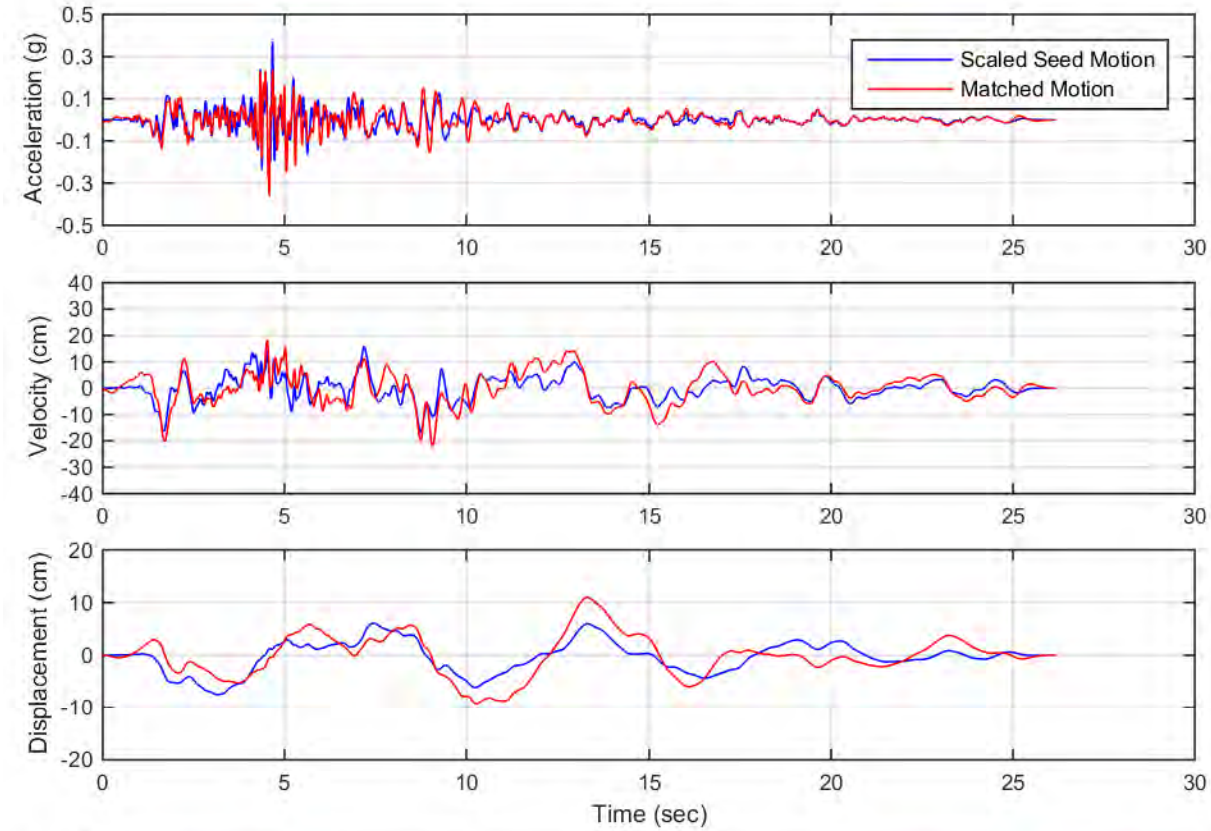

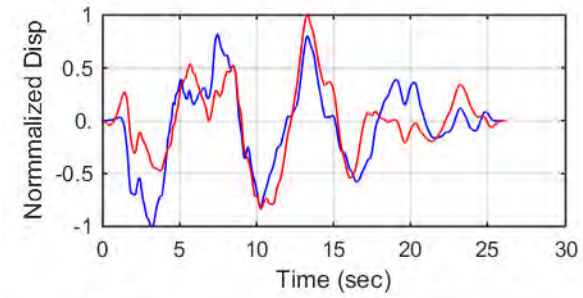

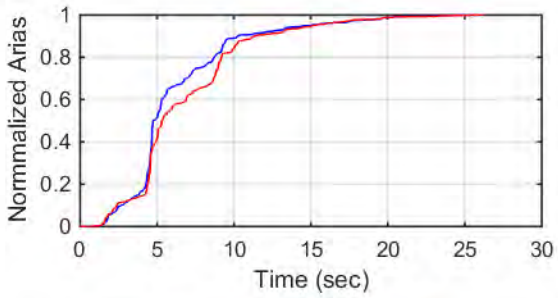

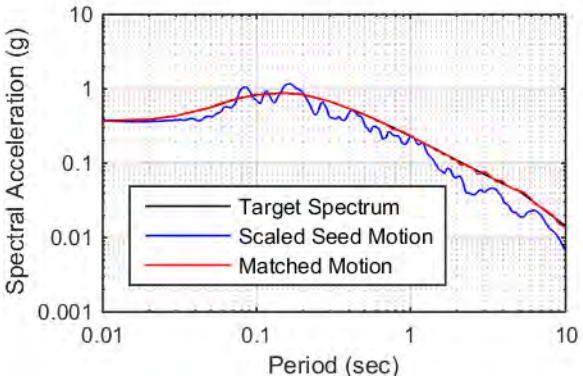

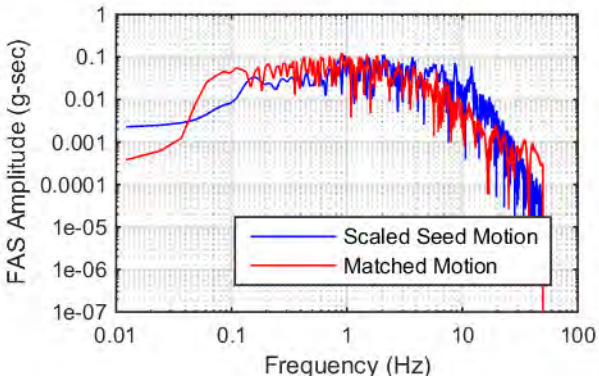

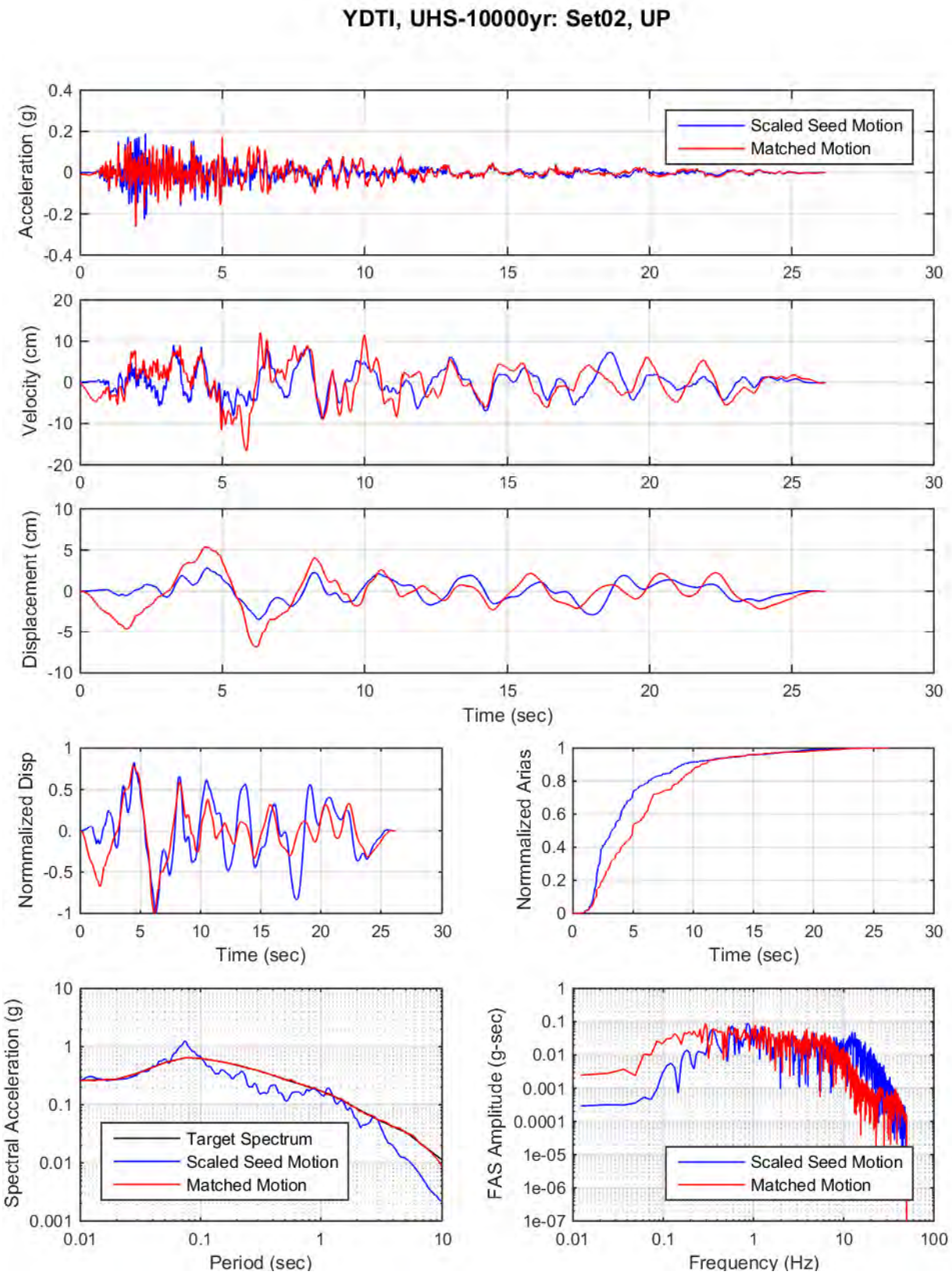
YDTI, UHS-10000yr: Set02, UP
Acceleration (g)
Scaled Seed Motion
Matched Motion
Velocity (cm)
Displacement (cm)
Time (sec)
Normmalized Disp
Time (sec)
Normmalized Arias
Time (sec)
Spectral Acceleration (g)
Target Spectrum
Scaled Seed Motion
Matched Motion
Period (sec)
FAS Amplitude (g-sec)
Scaled Seed Motion
Matched Motion
Frequency (Hz)

YDTI, UHS-10000yr: Set03, H1

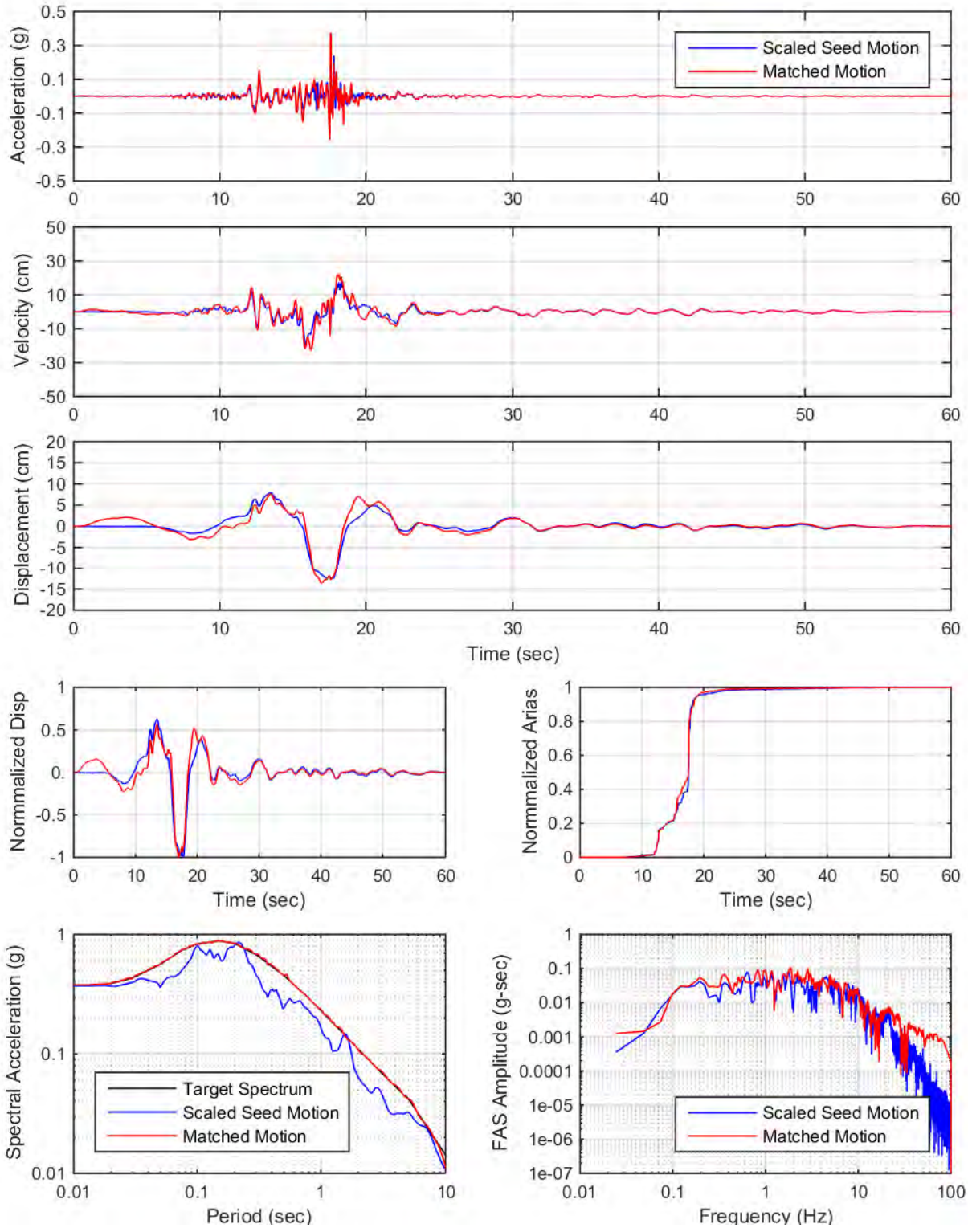

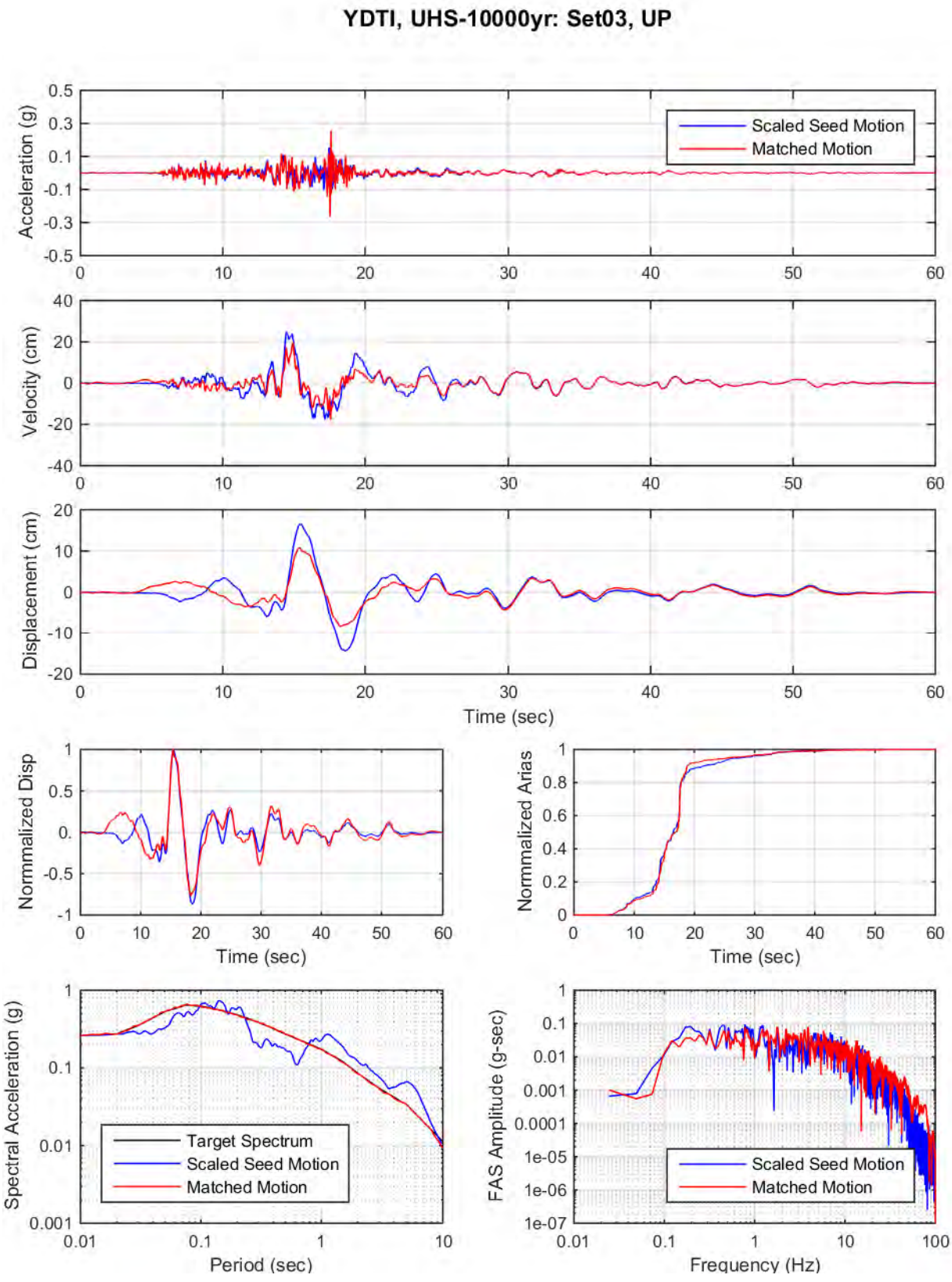
YDTI, UHS-10000yr: Set03, UP
Acceleration (g)
Scaled Seed Motion
Matched Motion
Velocity (cm)
Displacement (cm)
Time (sec)
Normmalized Disp
Time (sec)
Normmalized Arias
Time (sec)
Spectral Acceleration (g)
Target Spectrum
Scaled Seed Motion
Matched Motion
Period (sec)
FAS Amplitude (g-sec)
Scaled Seed Motion
Matched Motion
Frequency (Hz)

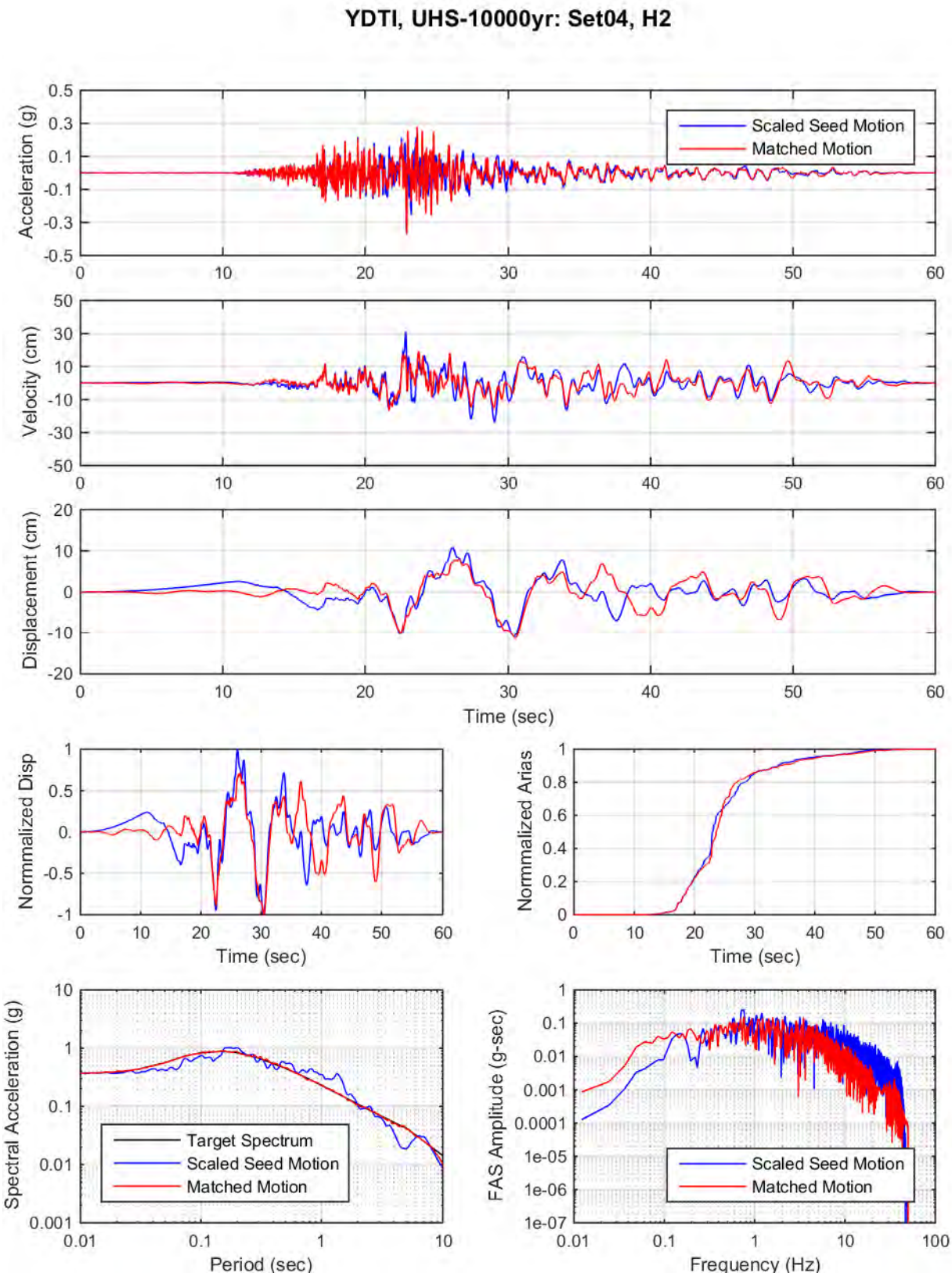
YDTI, UHS-10000yr: Set04, H2
Acceleration (g)
Scaled Seed Motion
Matched Motion
Velocity (cm)
Displacement (cm)
Time (sec)
Normmalized Disp
Time (sec)
Normmalized Arias
Time (sec)
Spectral Acceleration (g)
Target Spectrum
Scaled Seed Motion
Matched Motion
Period (sec)
FAS Amplitude (g-sec)
Scaled Seed Motion
Matched Motion
Frequency (Hz)

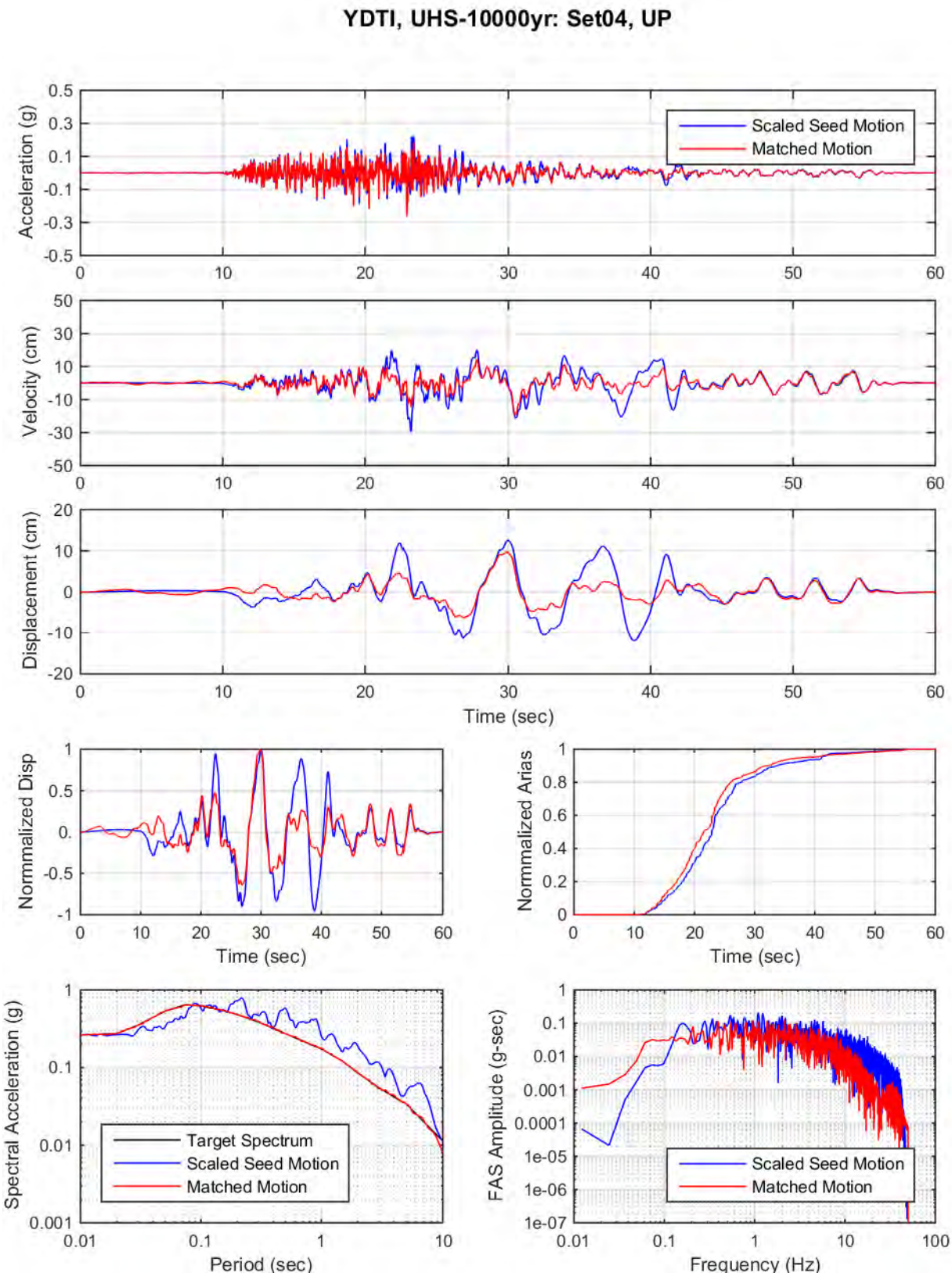
YDTI, UHS-10000yr: Set04, UP
Acceleration (g)
Scaled Seed Motion
Matched Motion
Velocity (cm)
Displacement (cm)
Time (sec)
Normmalized Disp
Time (sec)
Normmalized Arias
Time (sec)
Spectral Acceleration (g)
Target Spectrum
Scaled Seed Motion
Matched Motion
Period (sec)
FAS Amplitude (g-sec)
Scaled Seed Motion
Matched Motion
Frequency (Hz)

YDTI, UHS-10000yr: Set05, H2

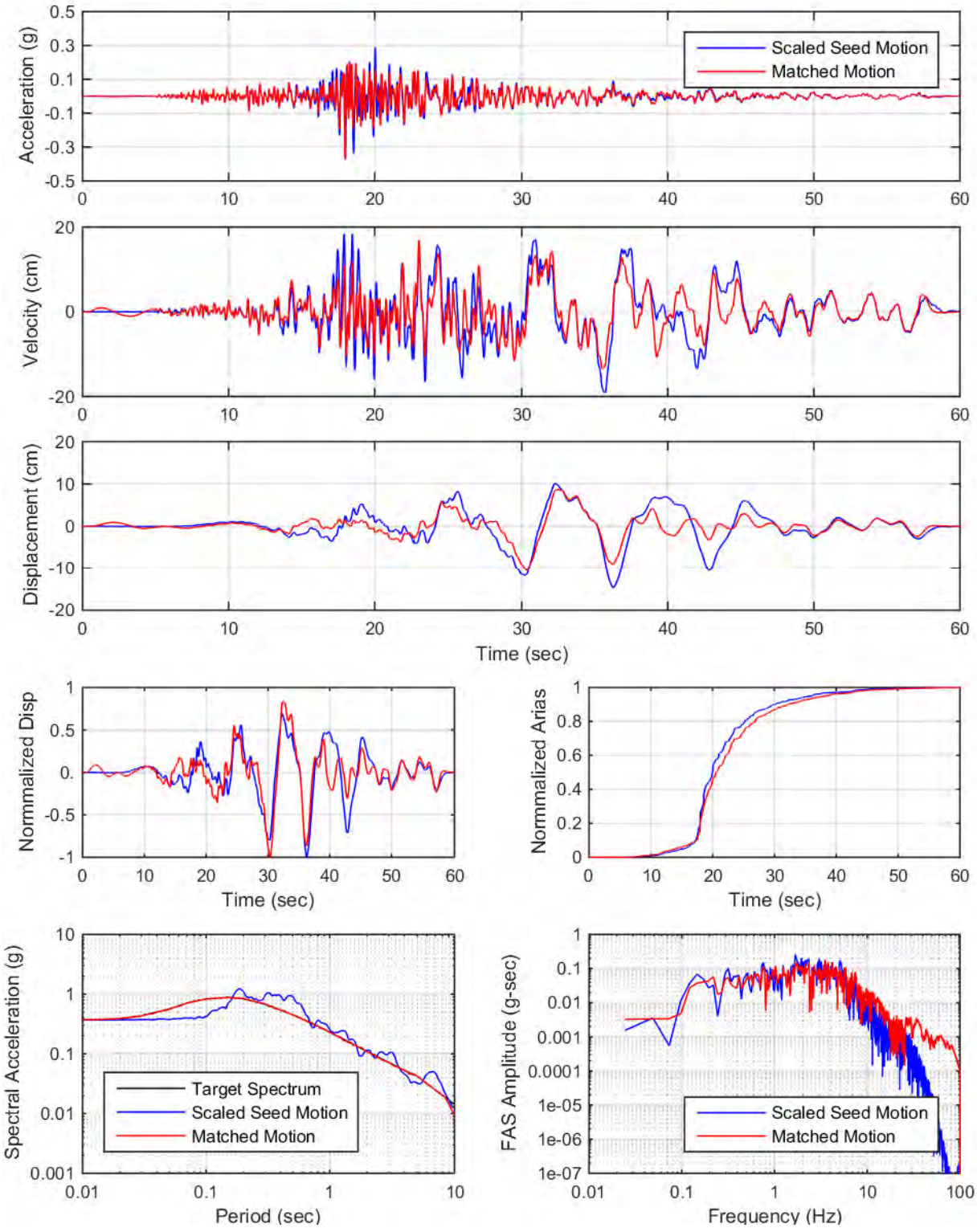

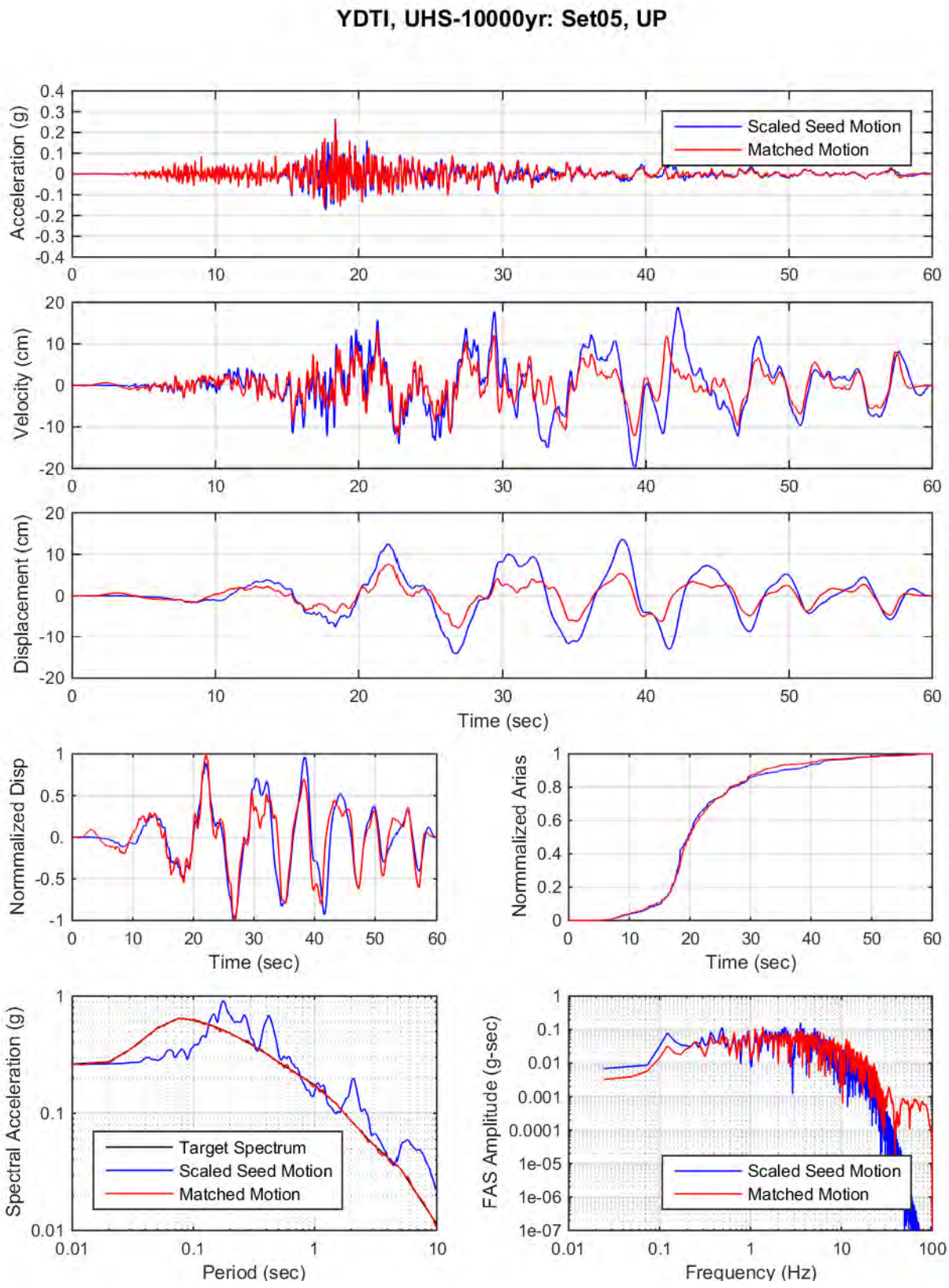
YDTI, UHS-10000yr: Set05, UP
Acceleration (g)
Scaled Seed Motion
Matched Motion
Velocity (cm)
Displacement (cm)
Time (sec)
Normmalized Disp
Time (sec)
Normmalized Arias
Time (sec)
Spectral Acceleration (g)
Target Spectrum
Scaled Seed Motion
Matched Motion
Period (sec)
FAS Amplitude (g-sec)
Scaled Seed Motion
Matched Motion
Frequency (Hz)

APPENDIX VI: SPECTRAL MATCHING PLOTS
MCE, RRUP = 1.2 KM, MEDIAN DESIGN SPECTRA

YDTI, MCE-Rrup1.2km-Med: Set01, H2

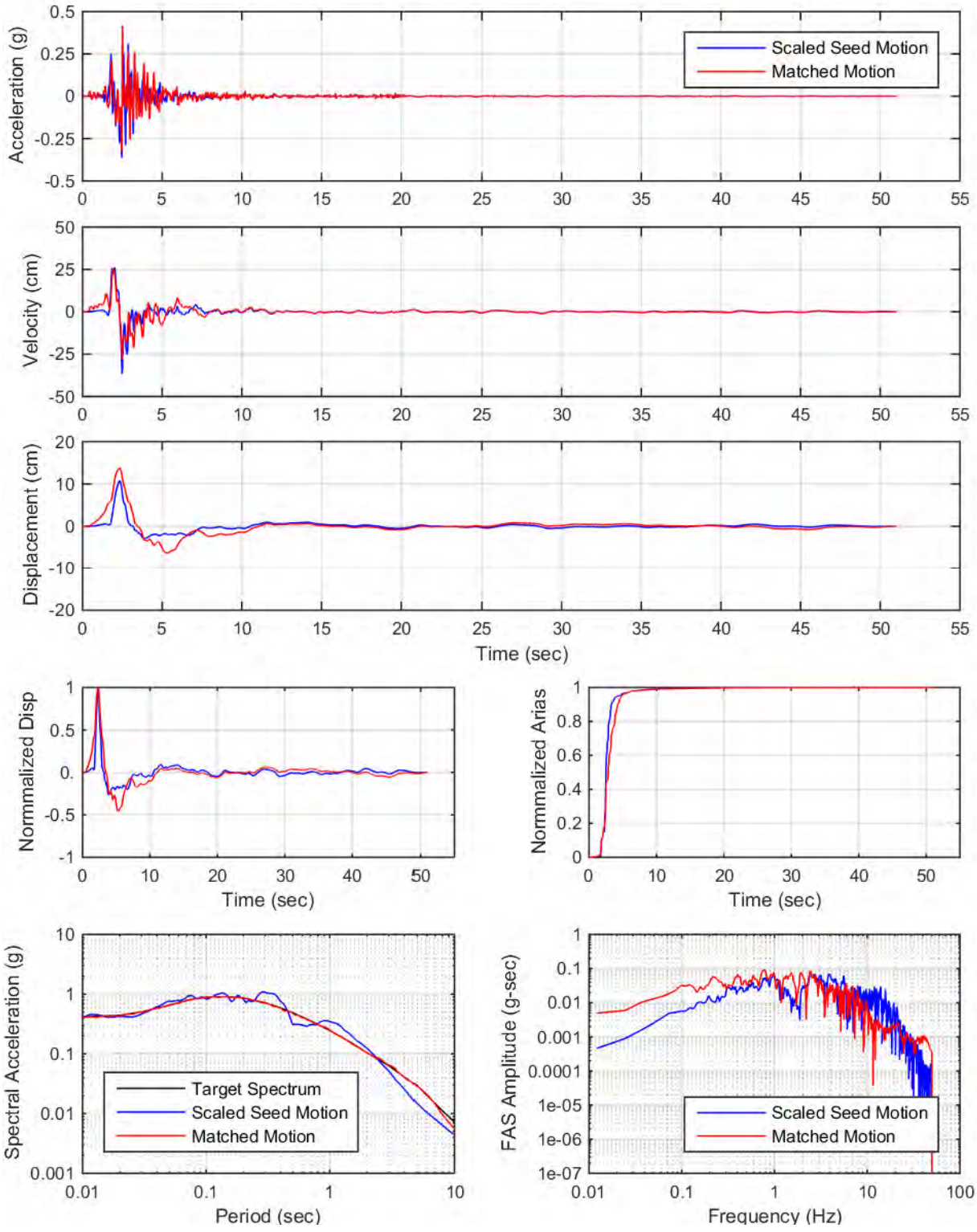

YDTI, MCE-Rrup1.2km-Med: Set01, UP

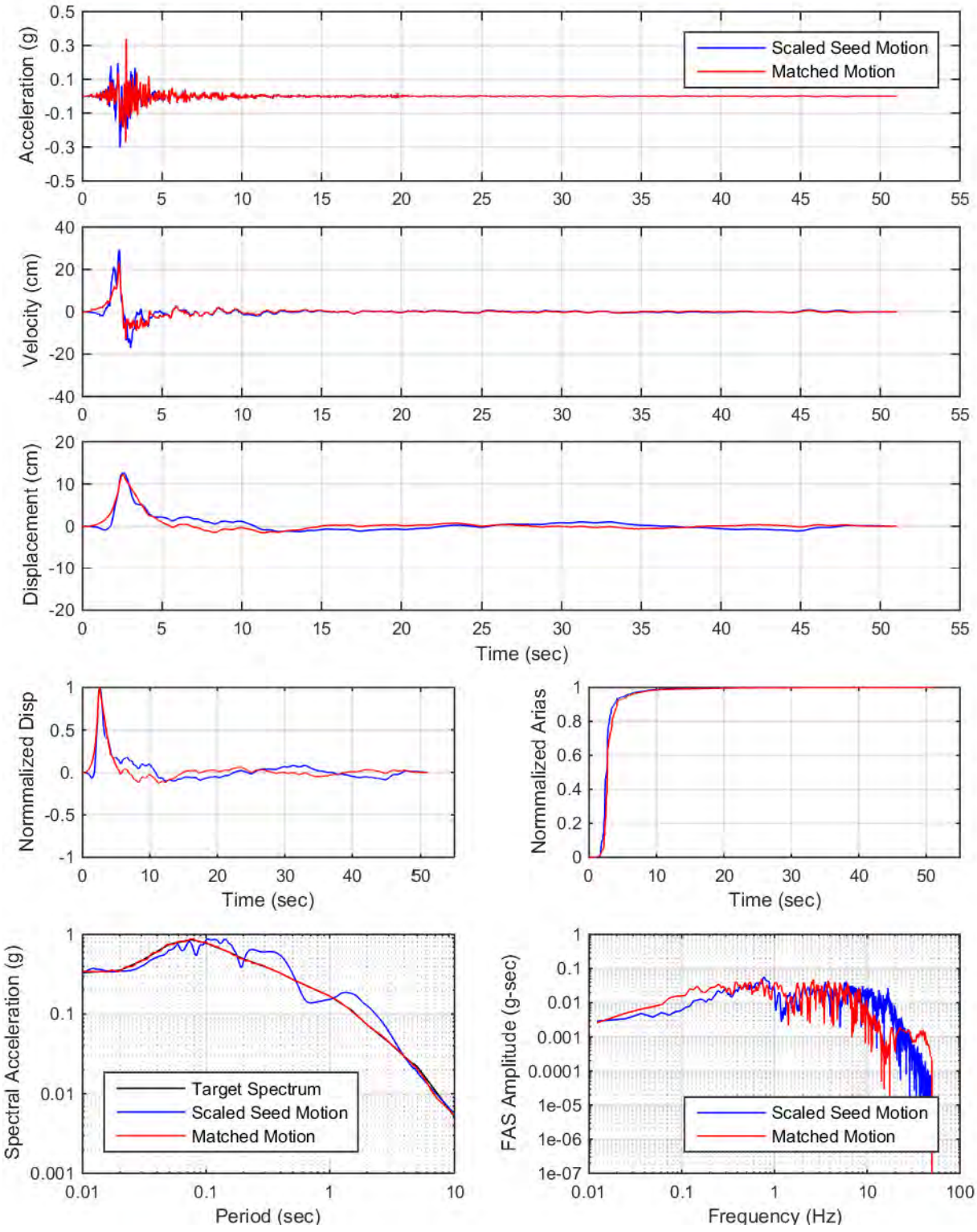

YDTI, MCE-Rrup1.2km-Med: Set02, H1

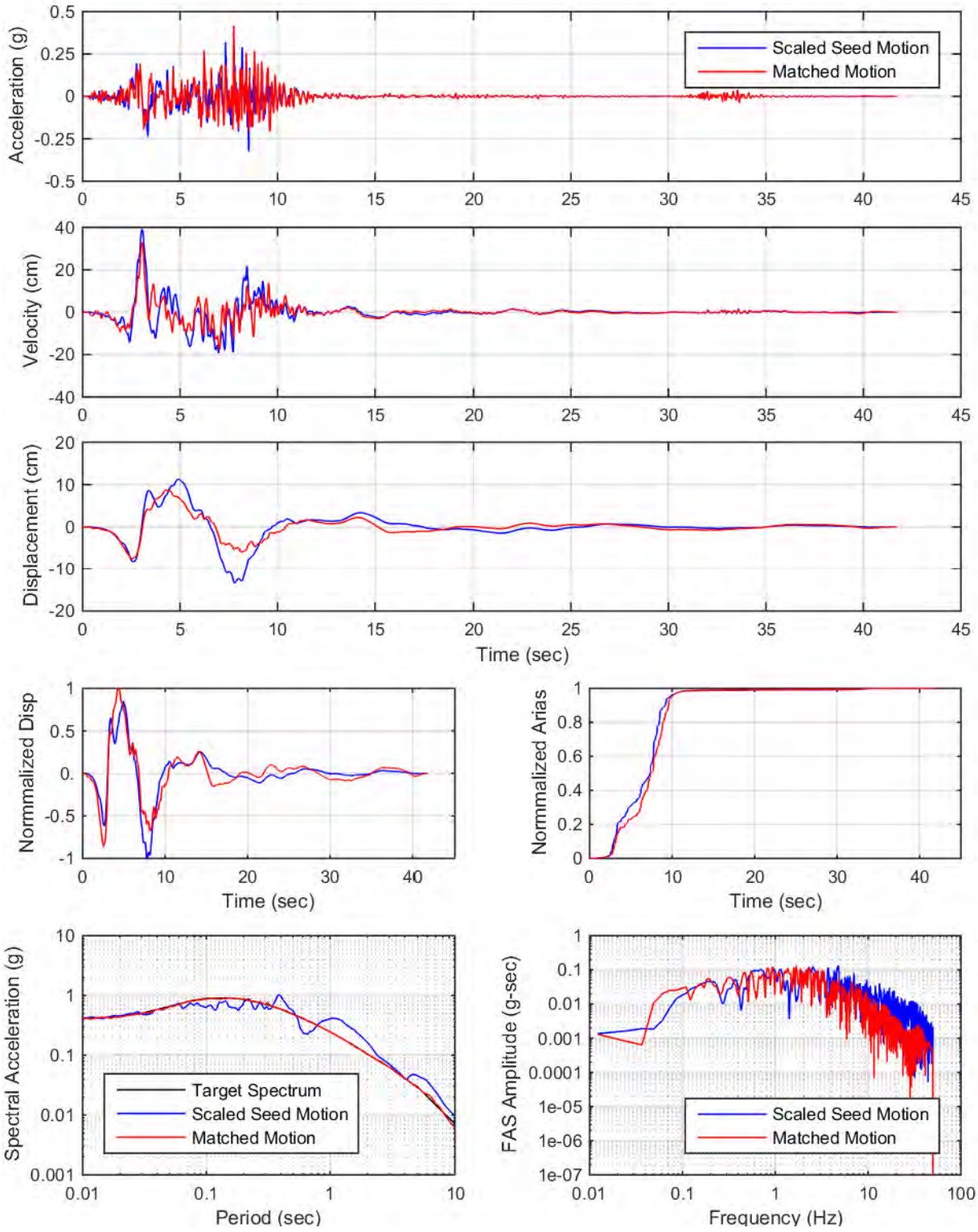

YDTI, MCE-Rrup1.2km-Med: Set02, UP

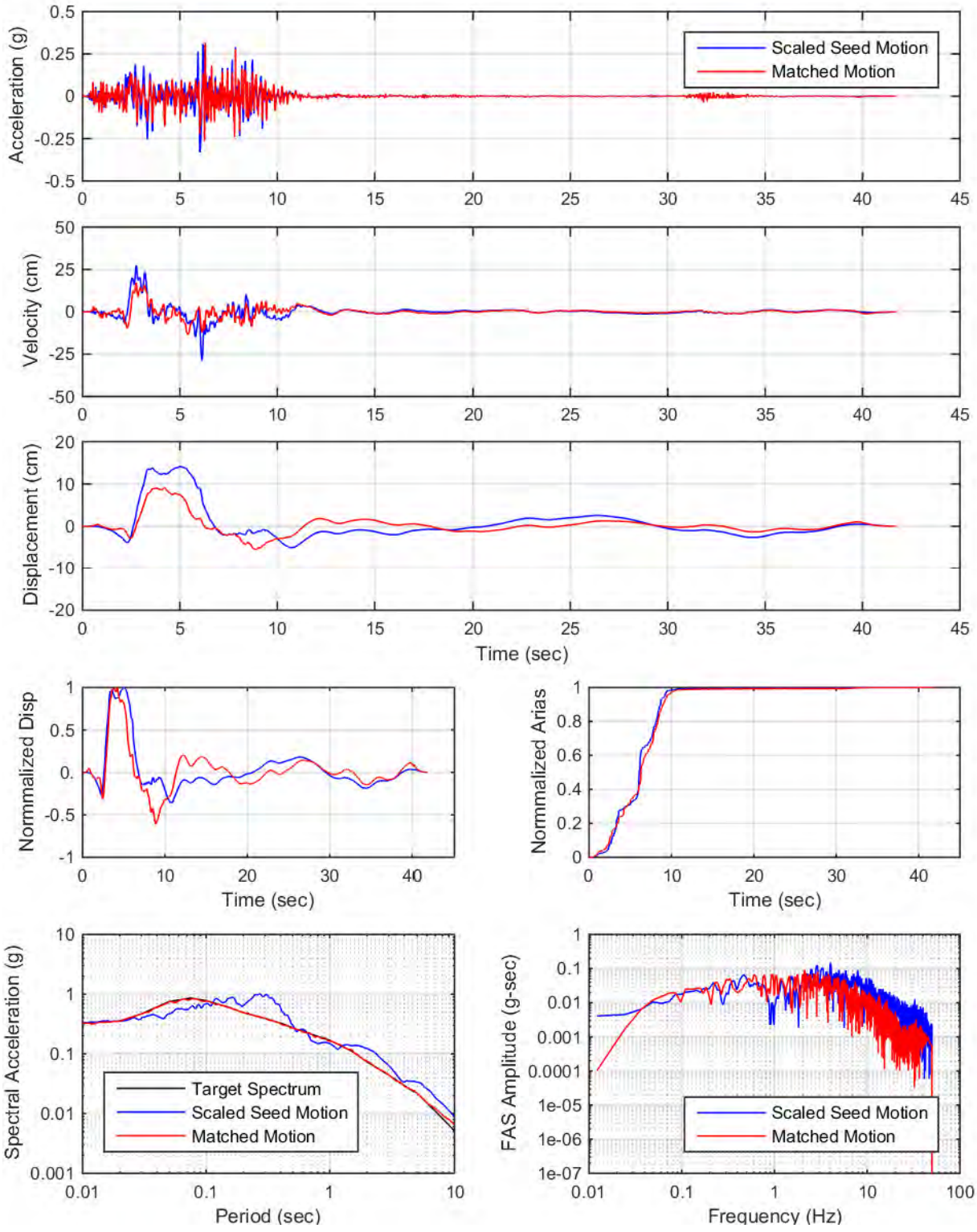

YDTI, MCE-Rrup1.2km-Med: Set03, H1

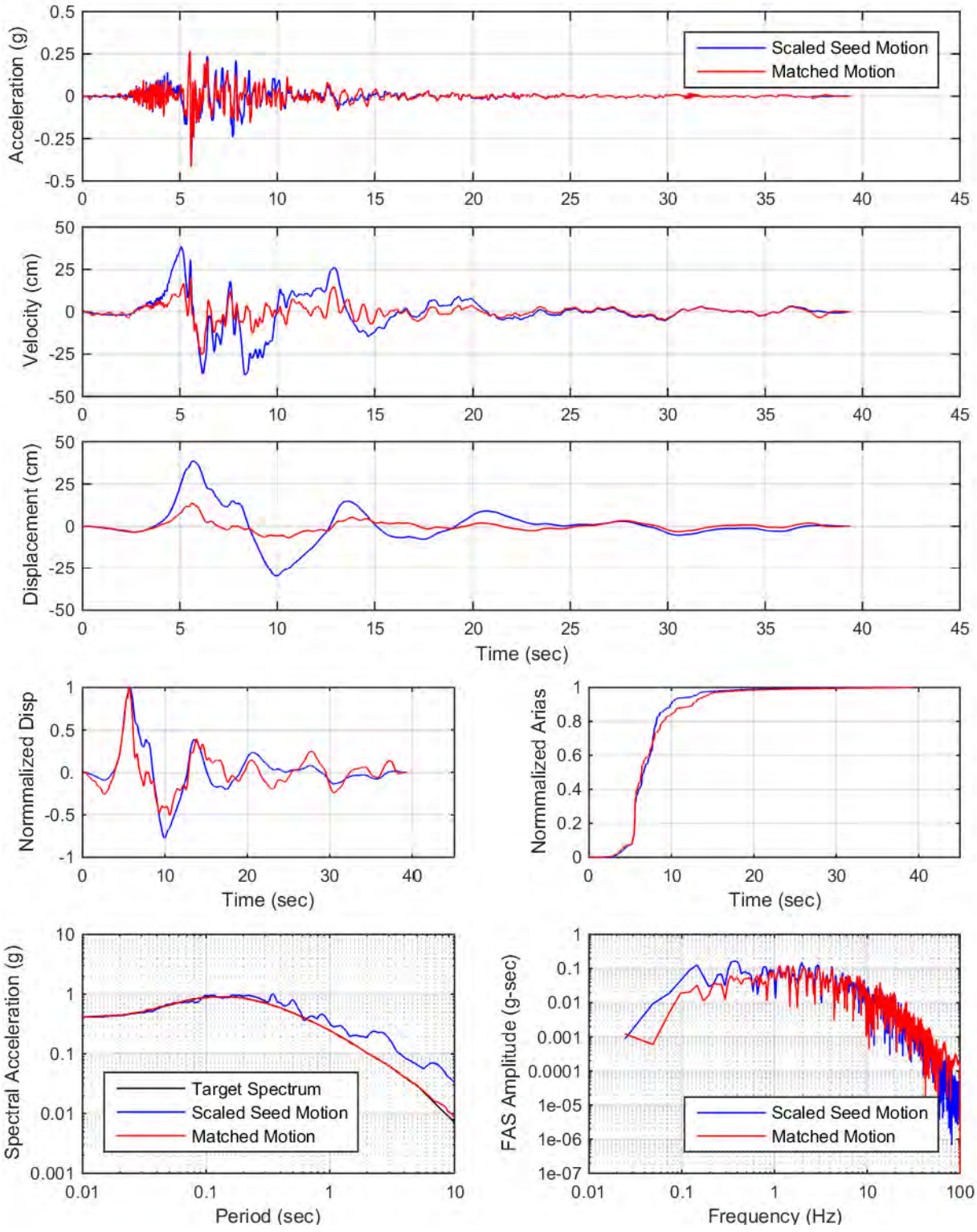

YDTI, MCE-Rrup1.2km-Med: Set03, UP

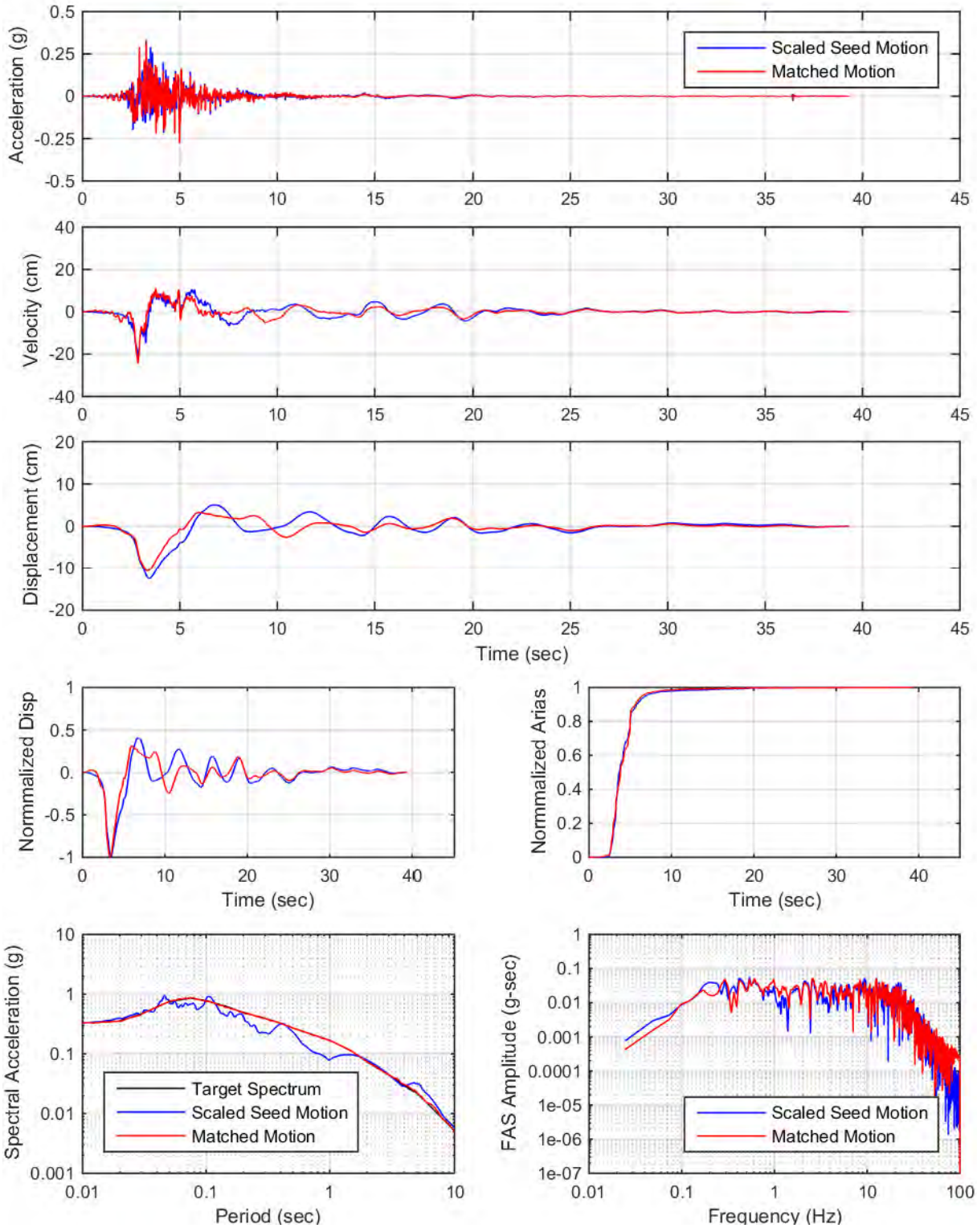

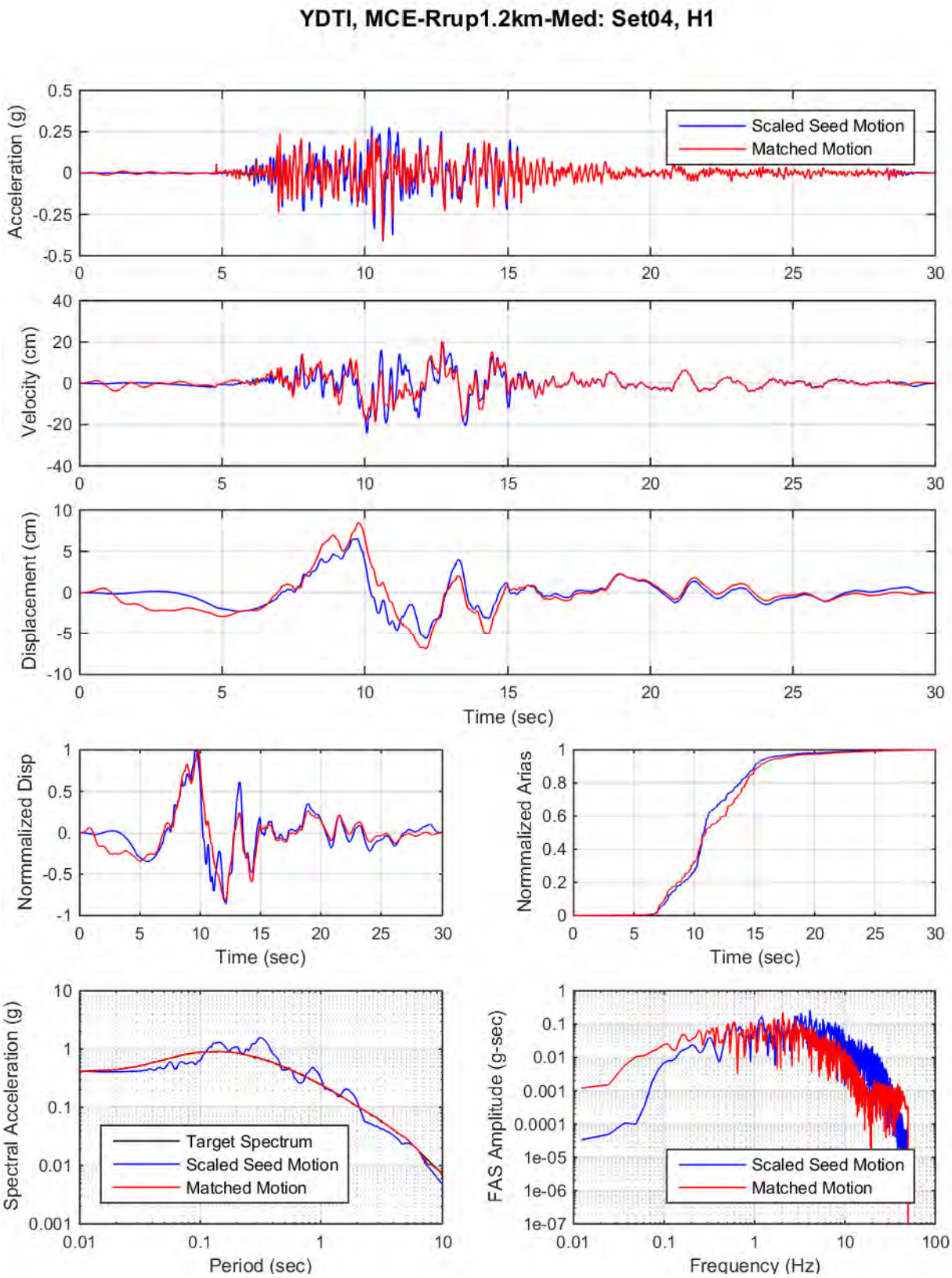
YDTI, MCE-Rrup1.2km-Med: Set04, H1
Acceleration (g)
Scaled Seed Motion
Matched Motion
Velocity (cm)
Displacement (cm)
Time (sec)
Normmalized Disp
Time (sec)
Normmalized Arias
Time (sec)
Spectral Acceleration (g)
Target Spectrum
Scaled Seed Motion
Matched Motion
Period (sec)
FAS Amplitude (g-sec)
Scaled Seed Motion
Matched Motion
Frequency (Hz)

YDTI, MCE-Rrup1.2km-Med: Set04, UP

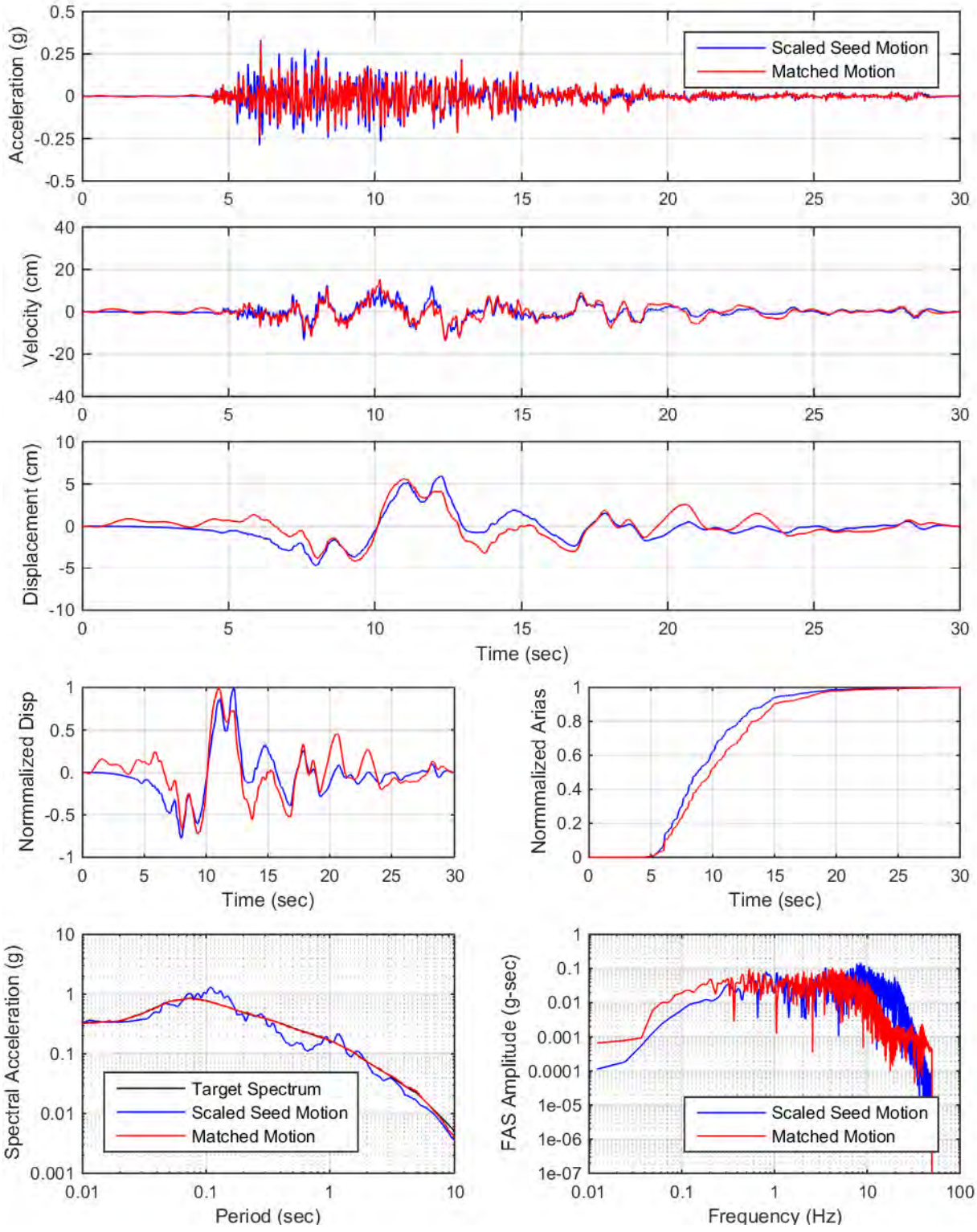

YDTI, MCE-Rrup1.2km-Med: Set05, H2

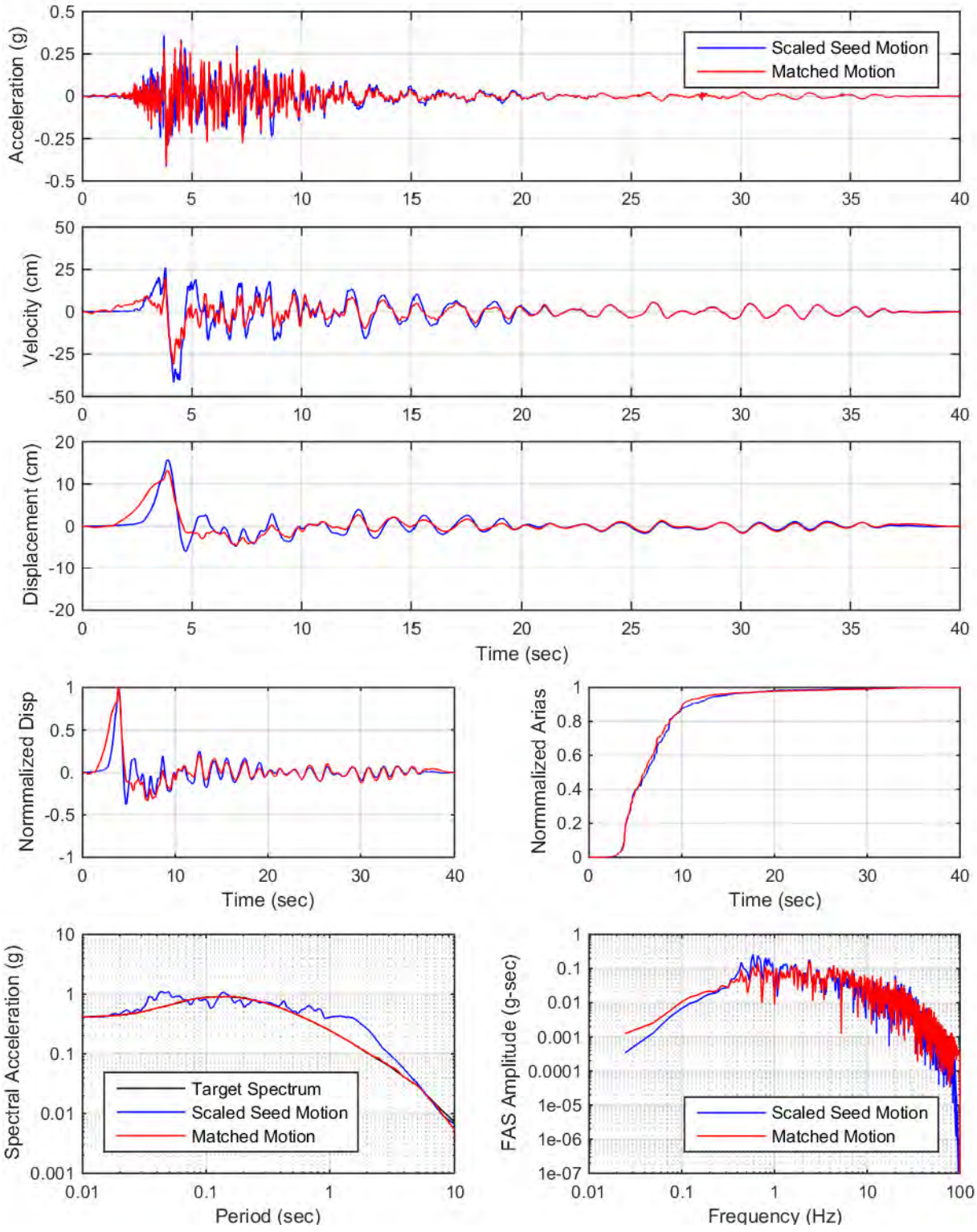

YDTI, MCE-Rrup1.2km-Med: Set05, UP

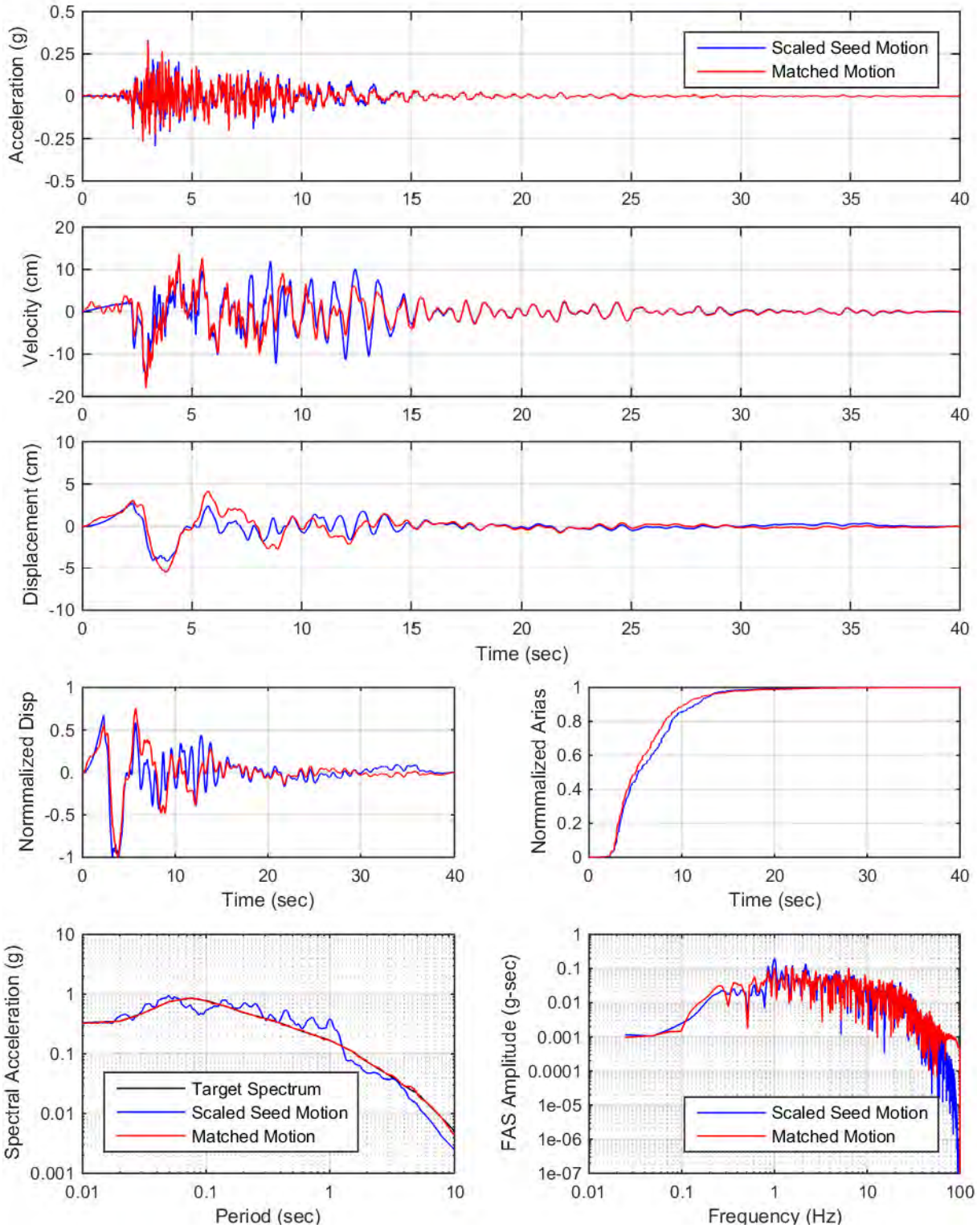

APPENDIX VII: SPECTRAL MATCHING PLOTS
MCE, RRUP = 1.2 KM, 84TH PERCENTILE DESIGN SPECTRA

YDTI, MCE-Rrup1.2km-84th: Set01, H2

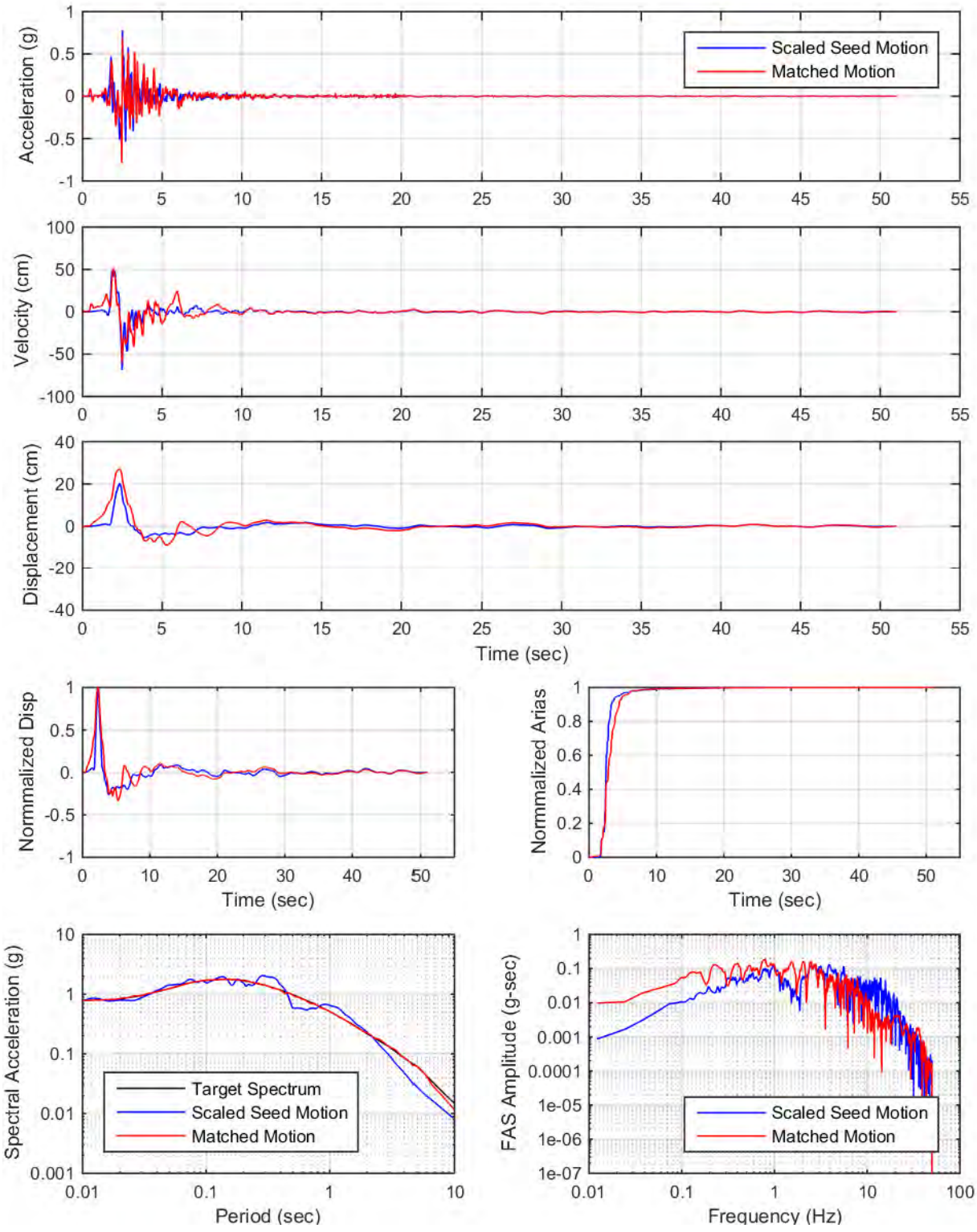

YDTI, MCE-Rrup1.2km-84th: Set01, UP

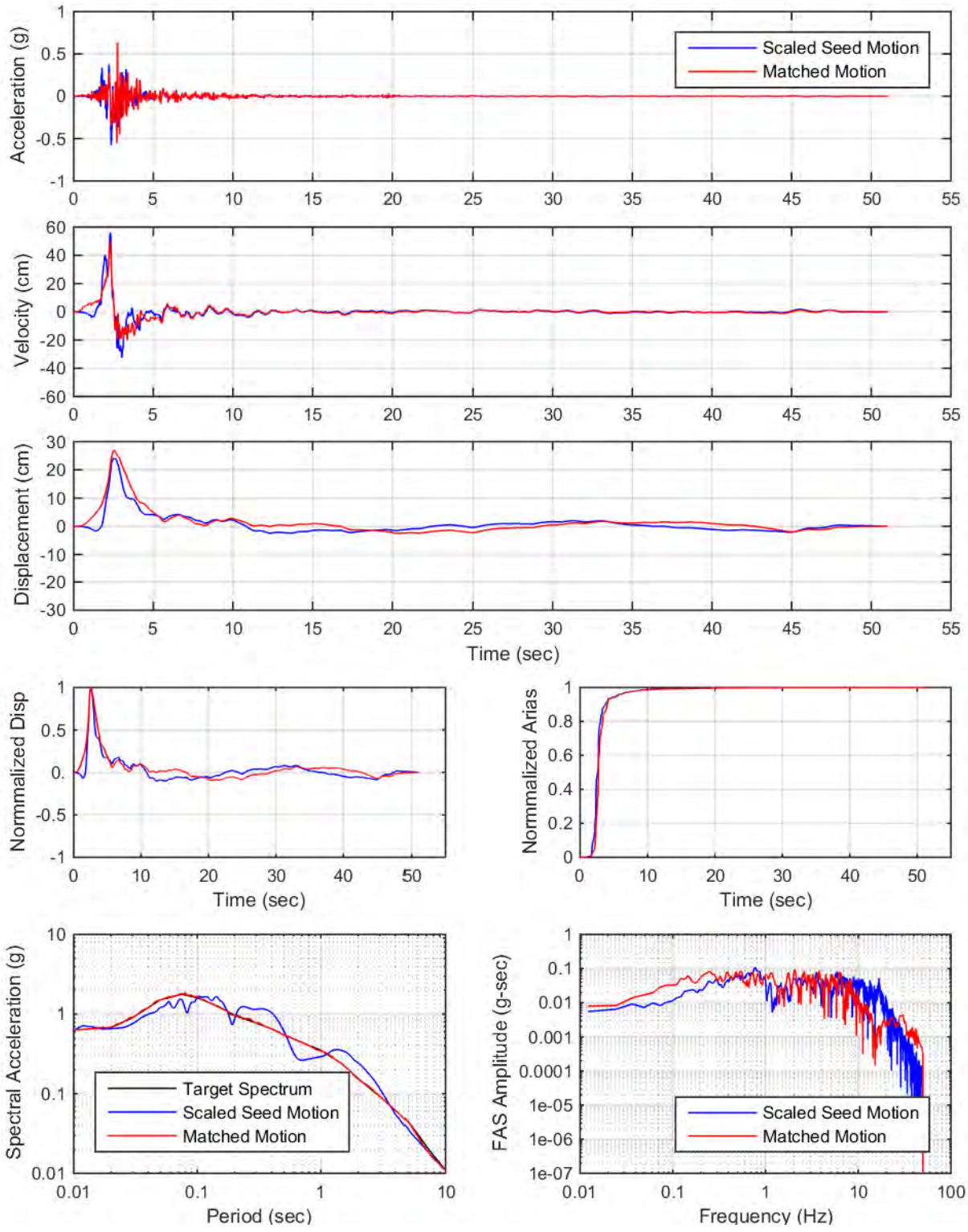

YDTI, MCE-Rrup1.2km-84th: Set02, H1

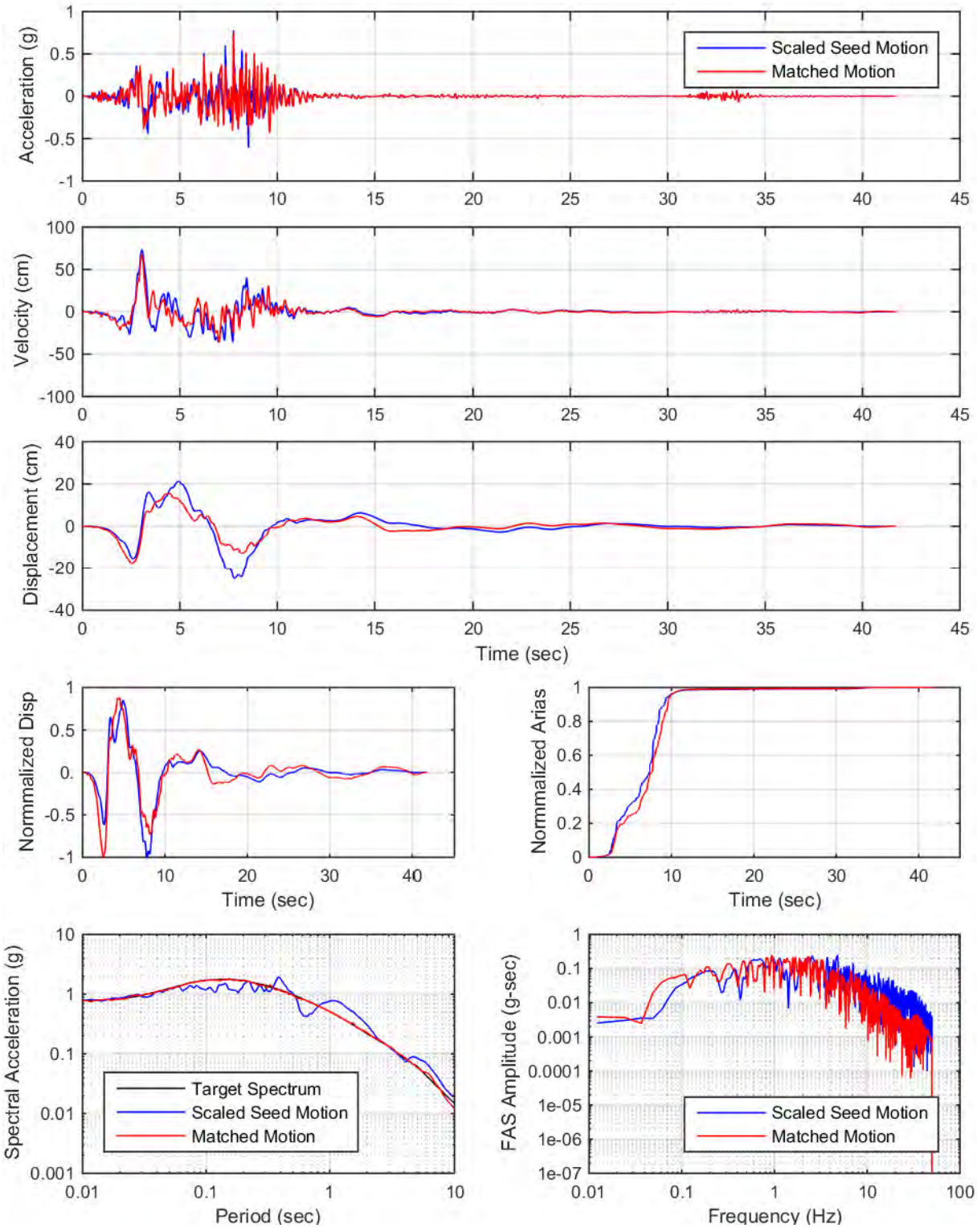

YDTI, MCE-Rrup1.2km-84th: Set02, UP

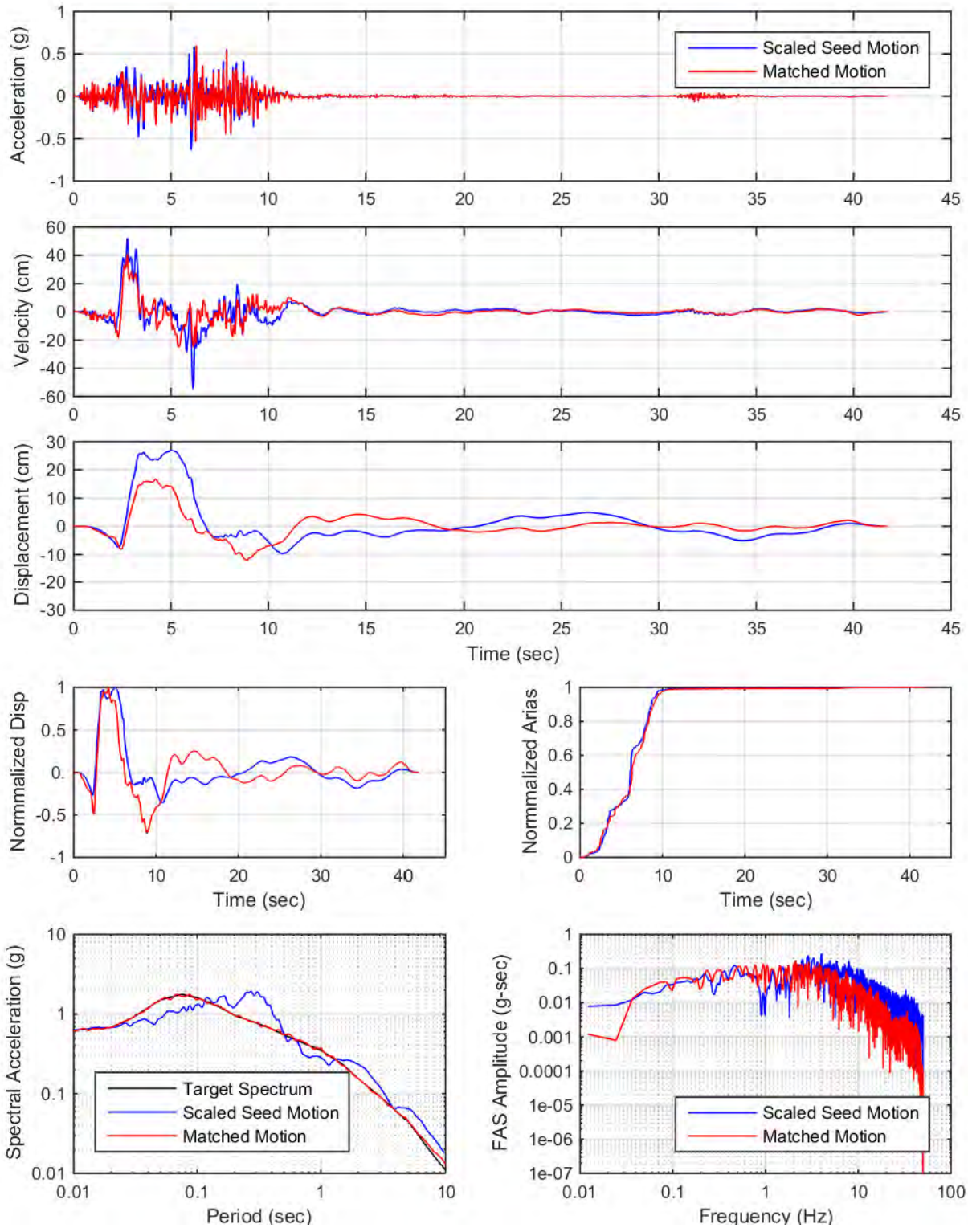

YDTI, MCE-Rrup1.2km-84th: Set03, H1

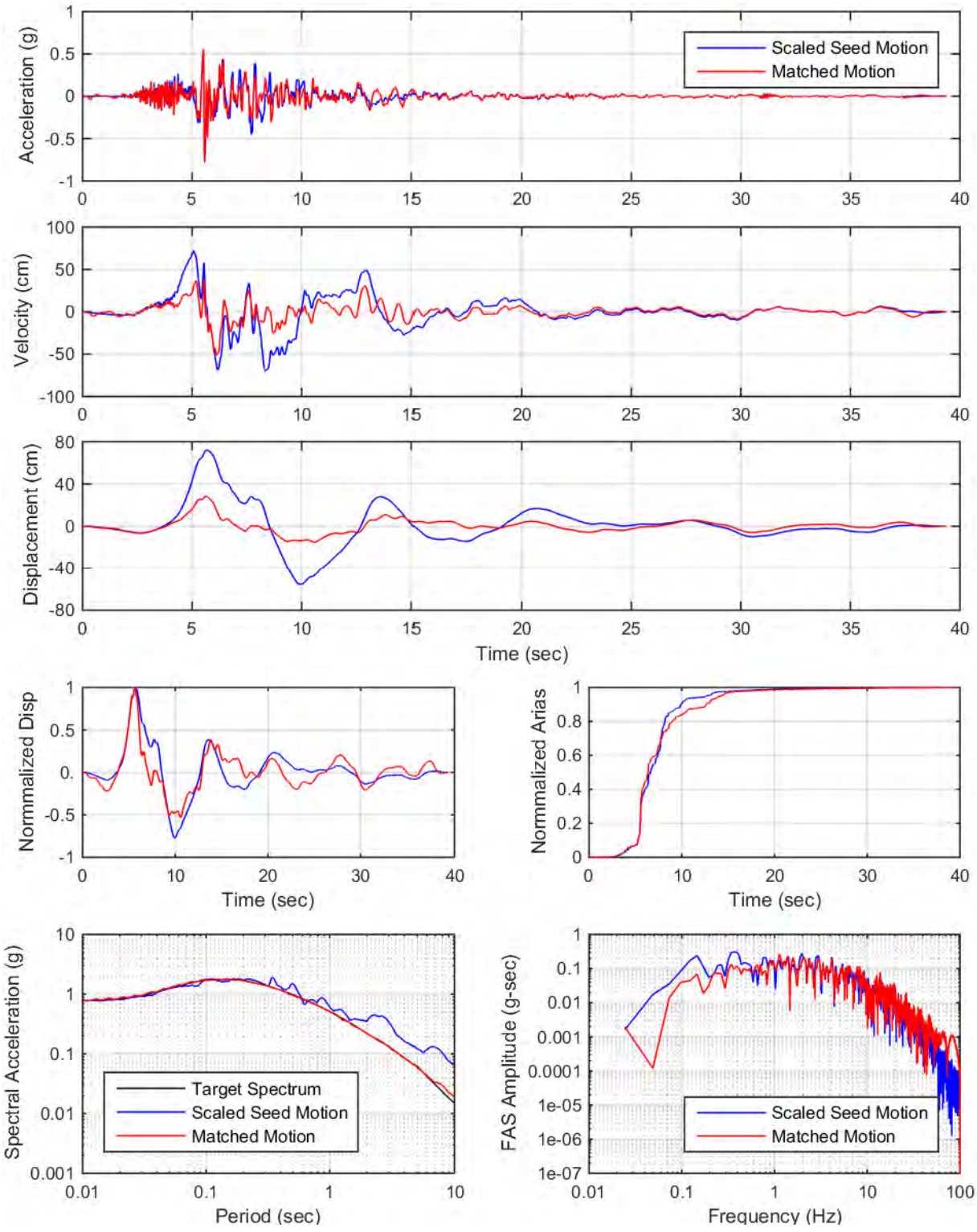

YDTI, MCE-Rrup1.2km-84th: Set03, UP

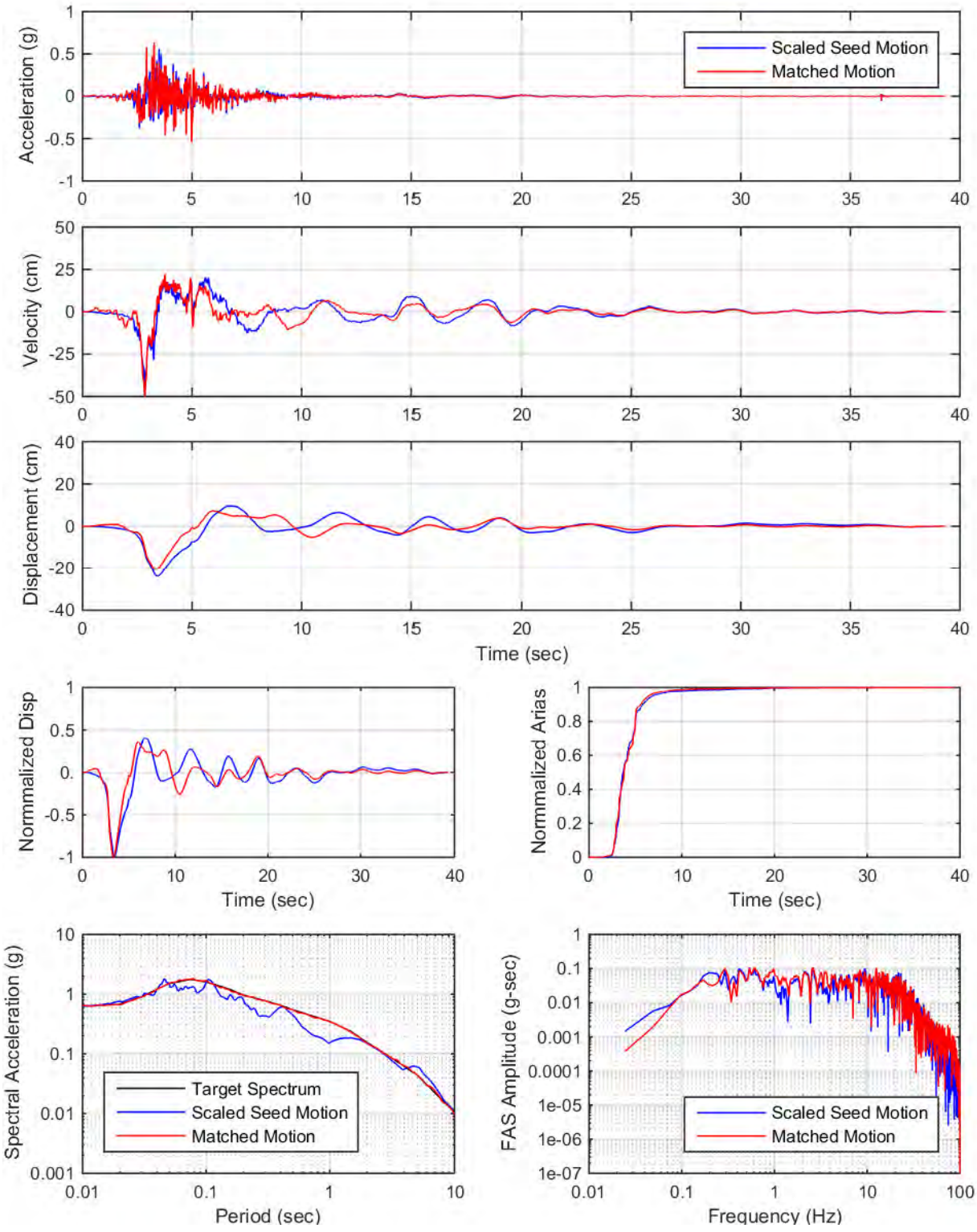

YDTI, MCE-Rrup1.2km-84th: Set04, H1

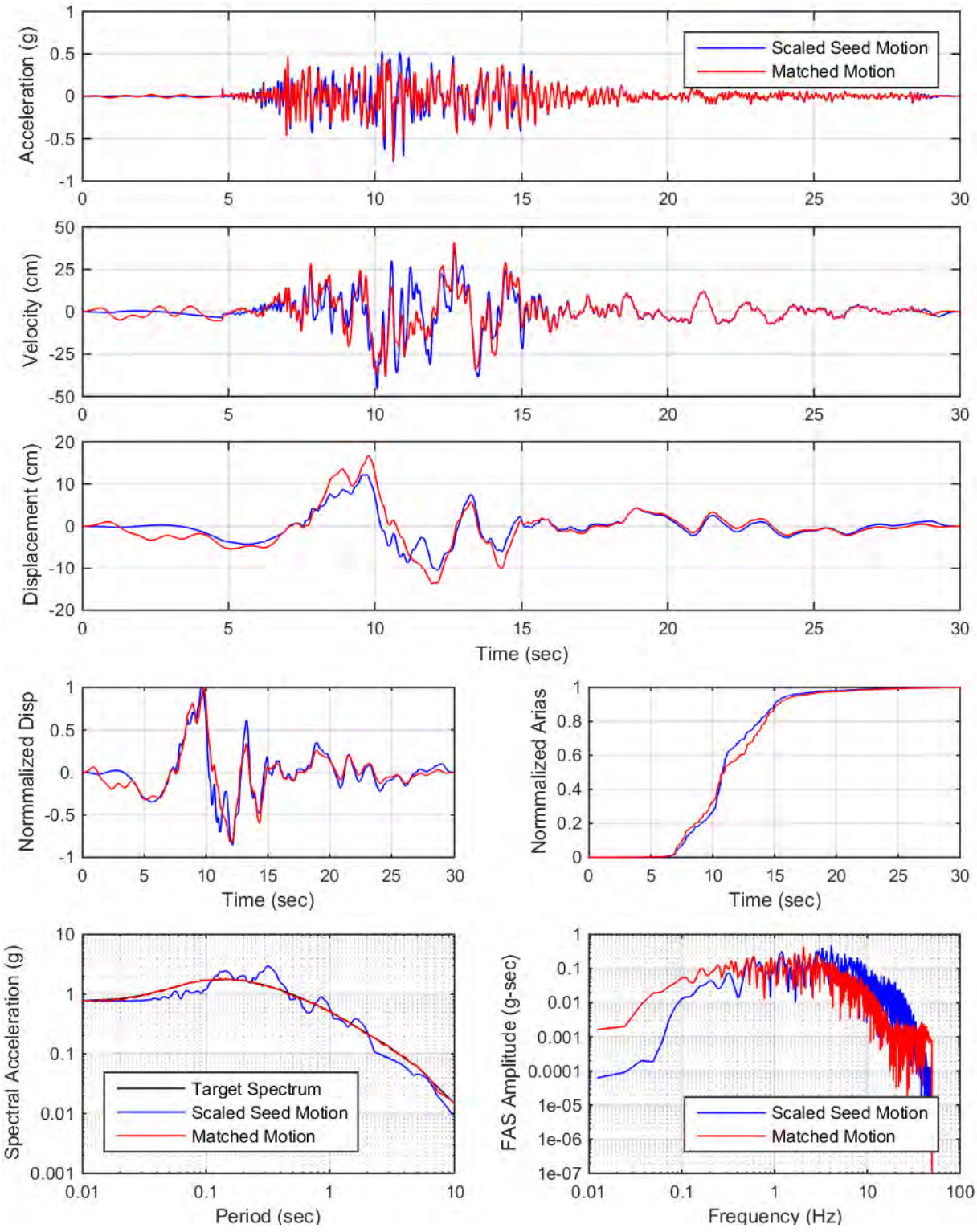

YDTI, MCE-Rrup1.2km-84th: Set04, UP

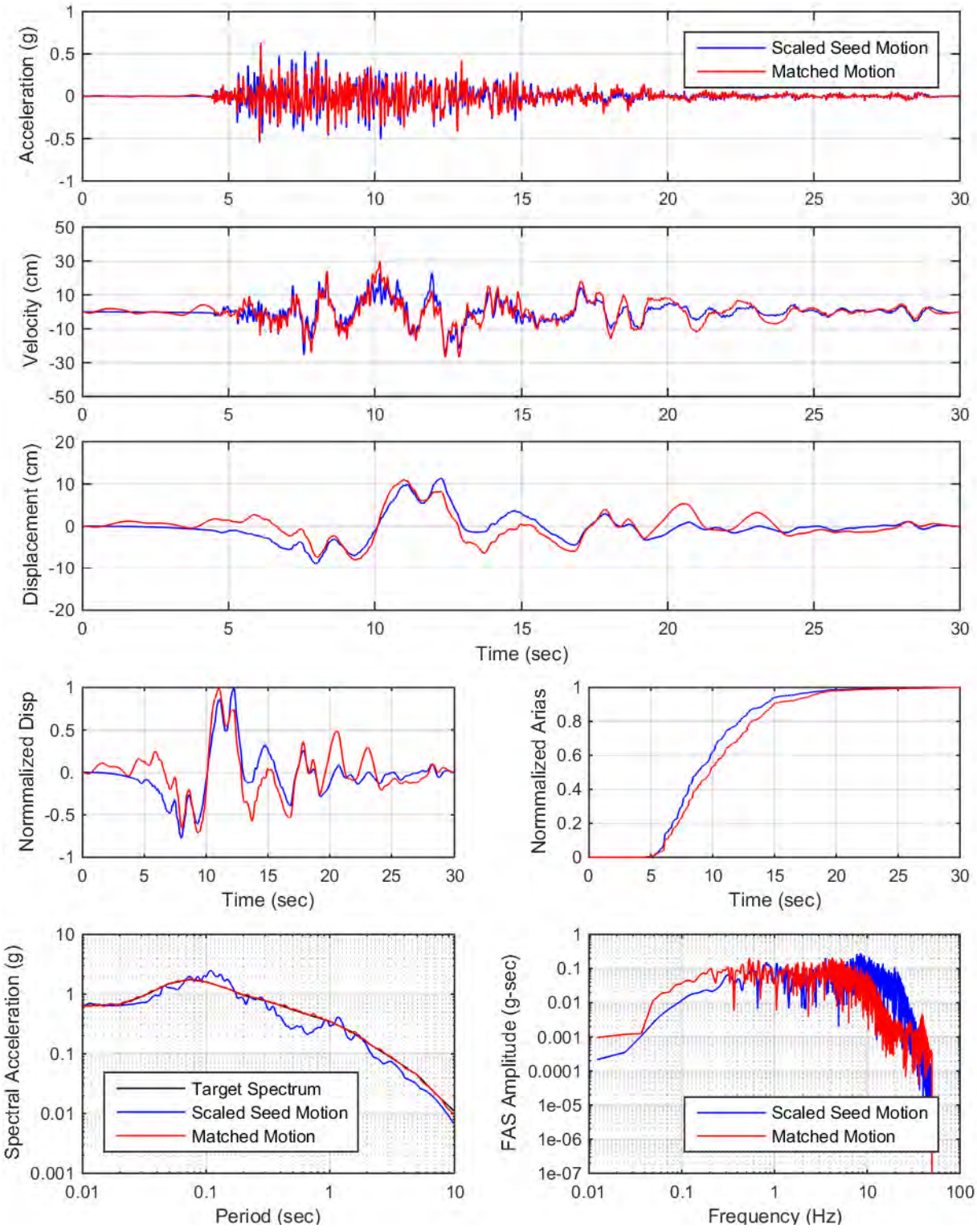

YDTI, MCE-Rrup1.2km-84th: Set05, H2

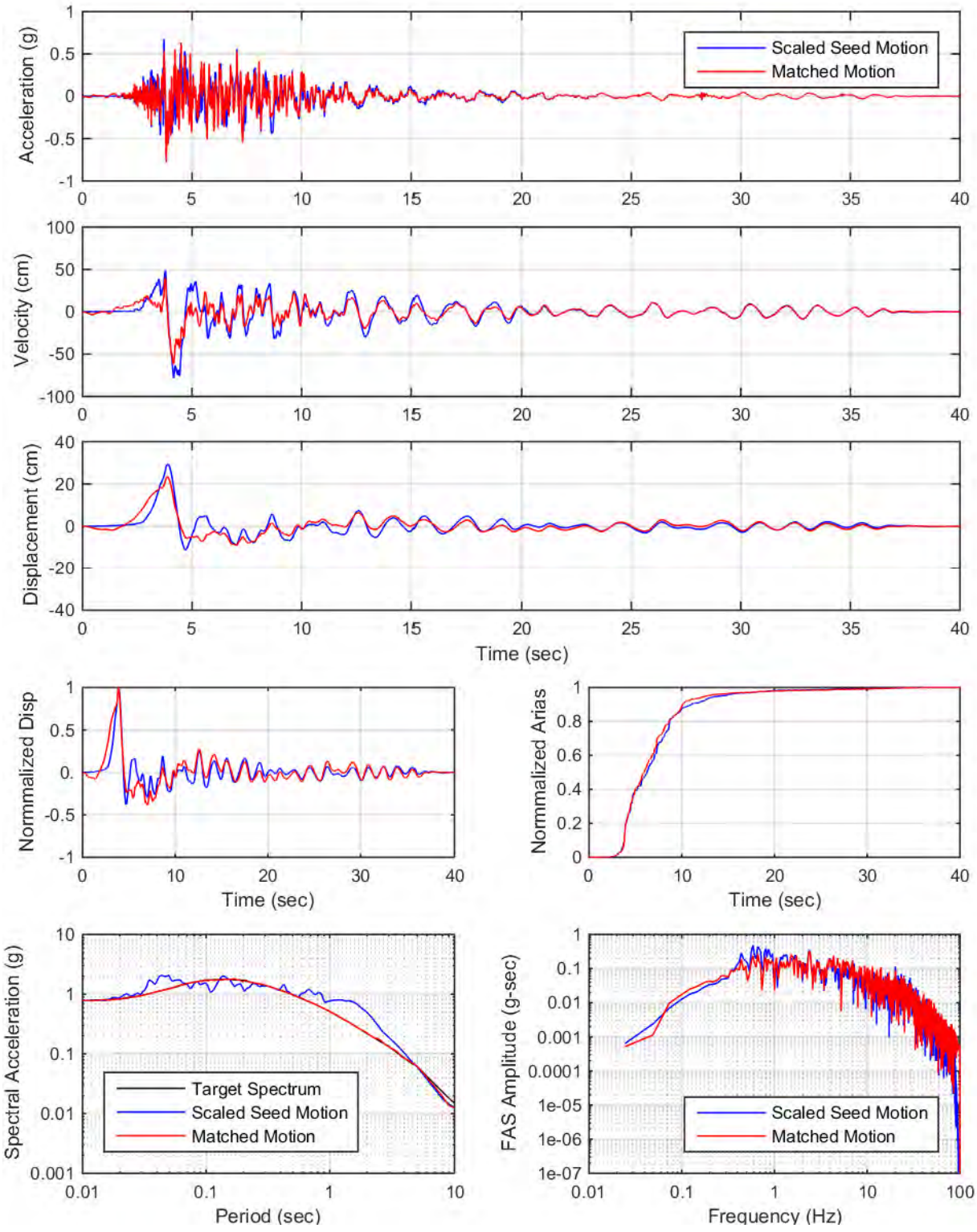

YDTI, MCE-Rrup1.2km-84th: Set05, UP

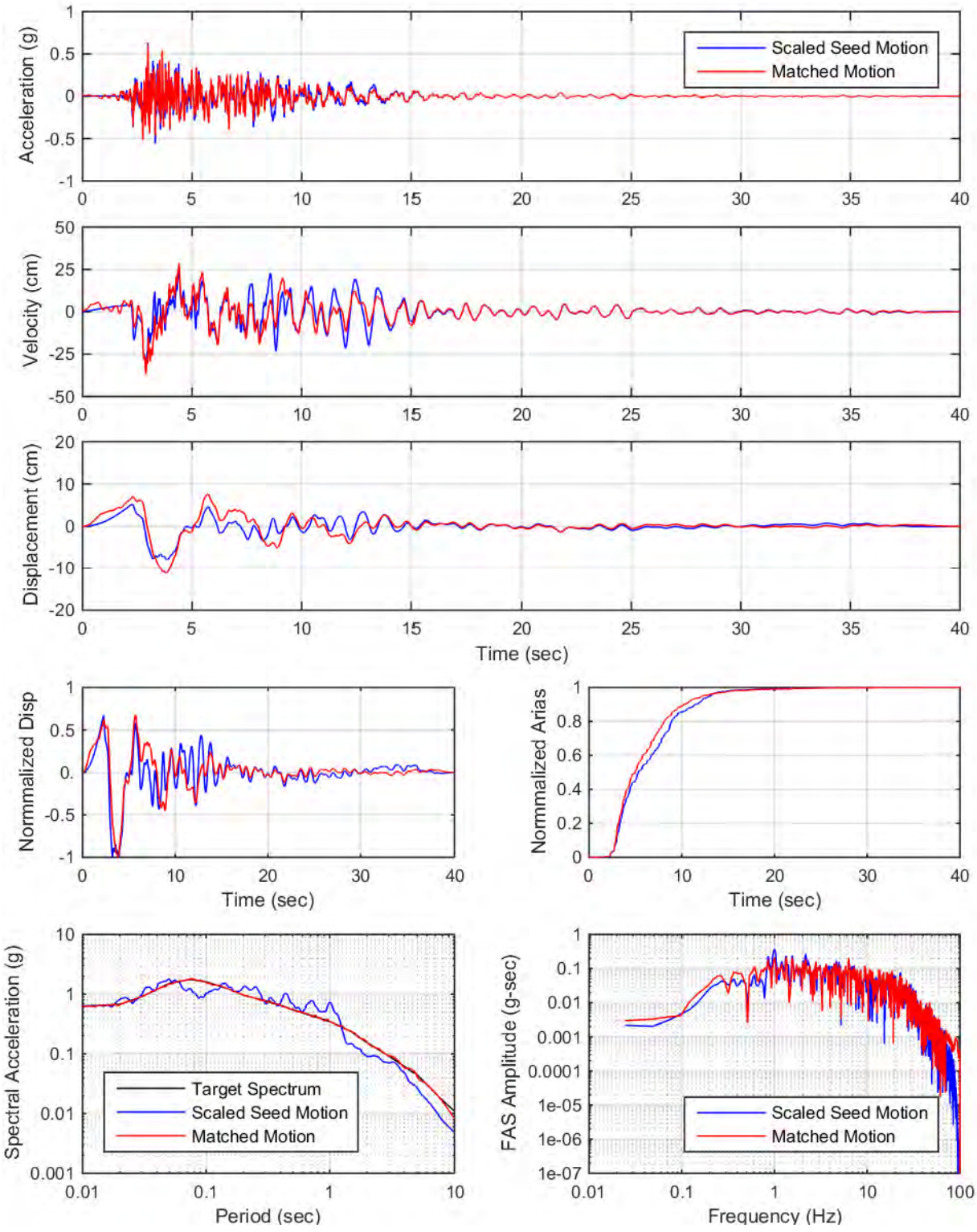

APPENDIX VIII: SPECTRAL MATCHING PLOTS
MCE, RRUP = 0.1 KM, MEDIAN DESIGN SPECTRA

YDTI, MCE-Rrup0.1km-Med: Set01, H2

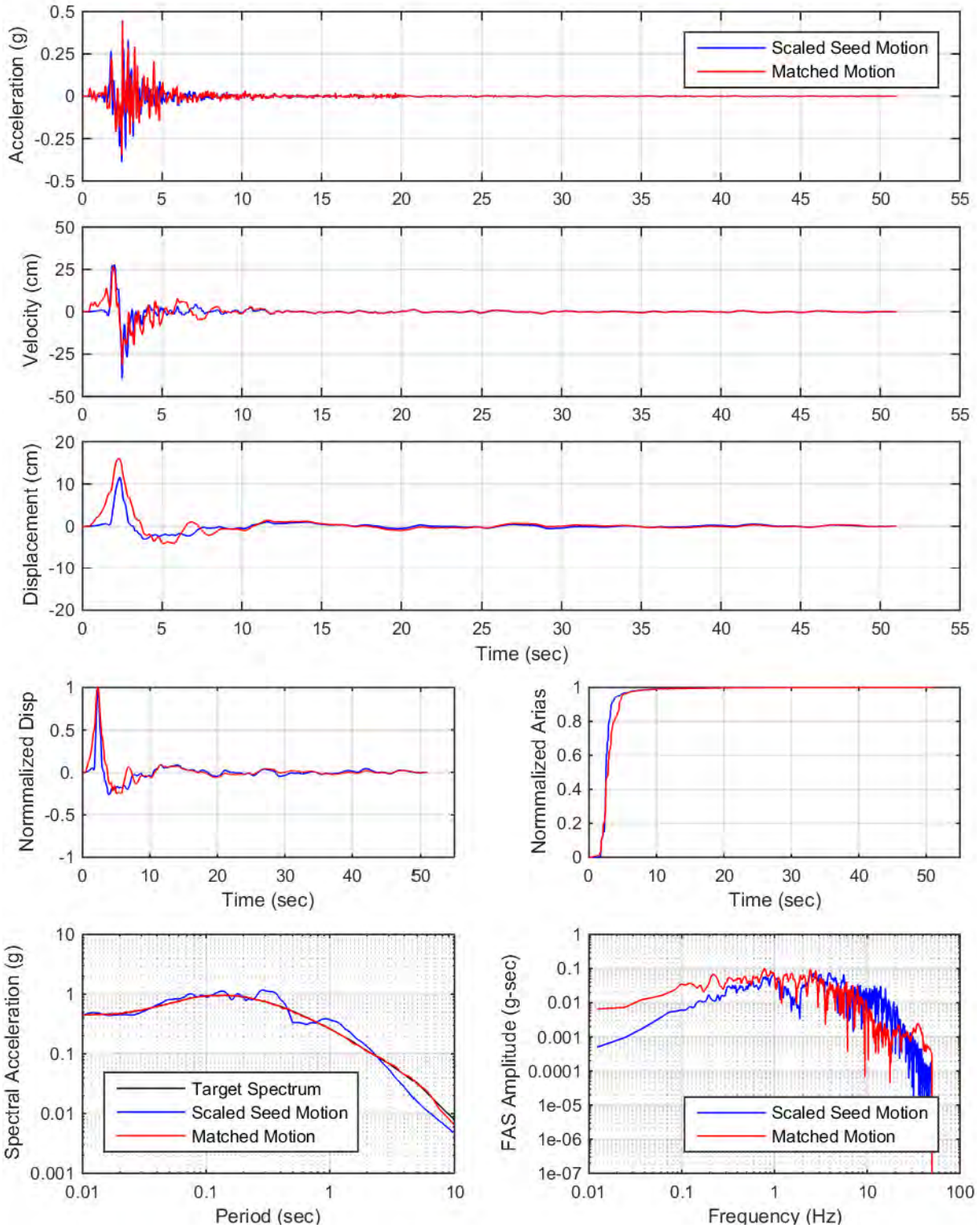

YDTI, MCE-Rrup0.1km-Med: Set01, UP

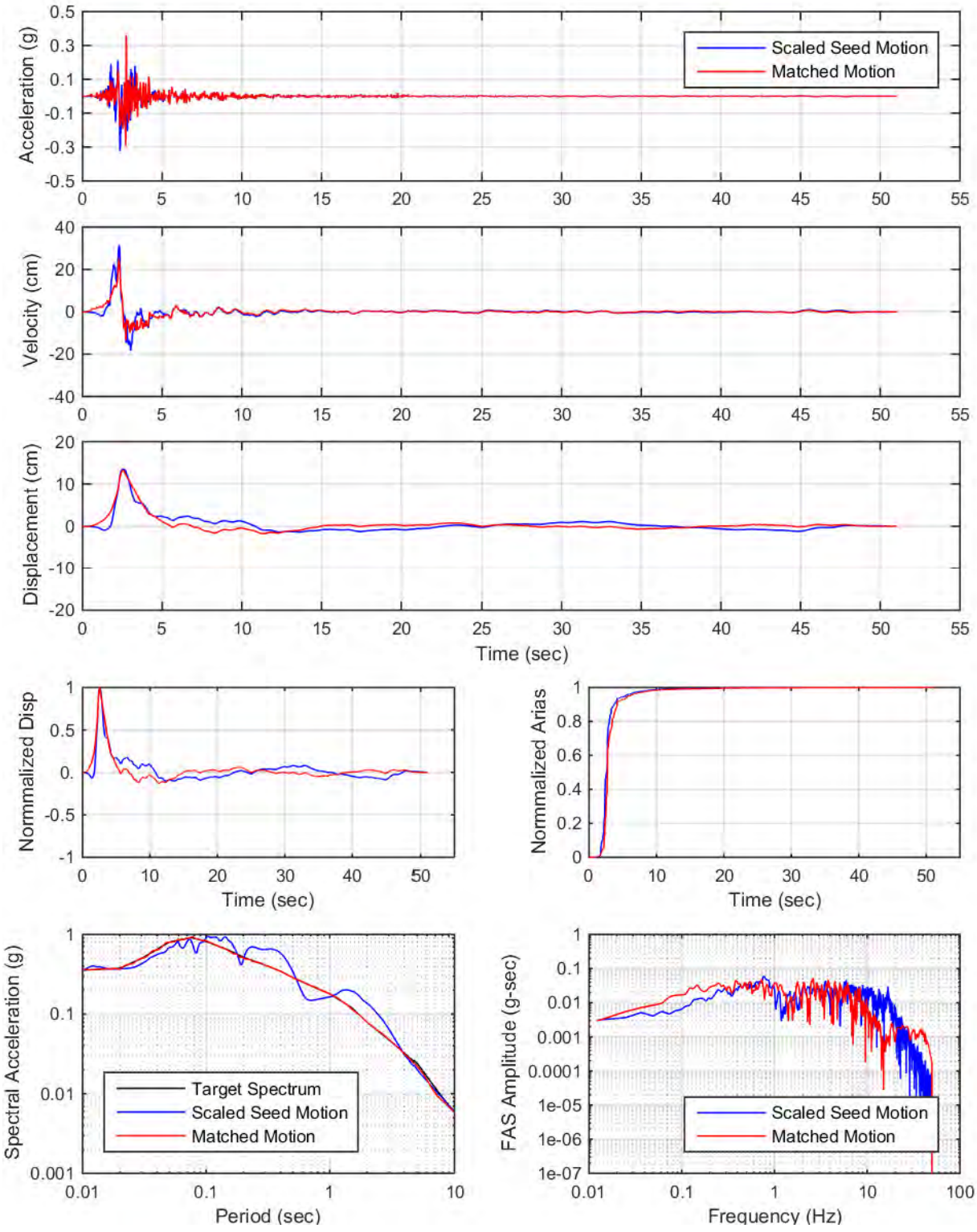

YDTI, MCE-Rrup0.1km-Med: Set02, H1

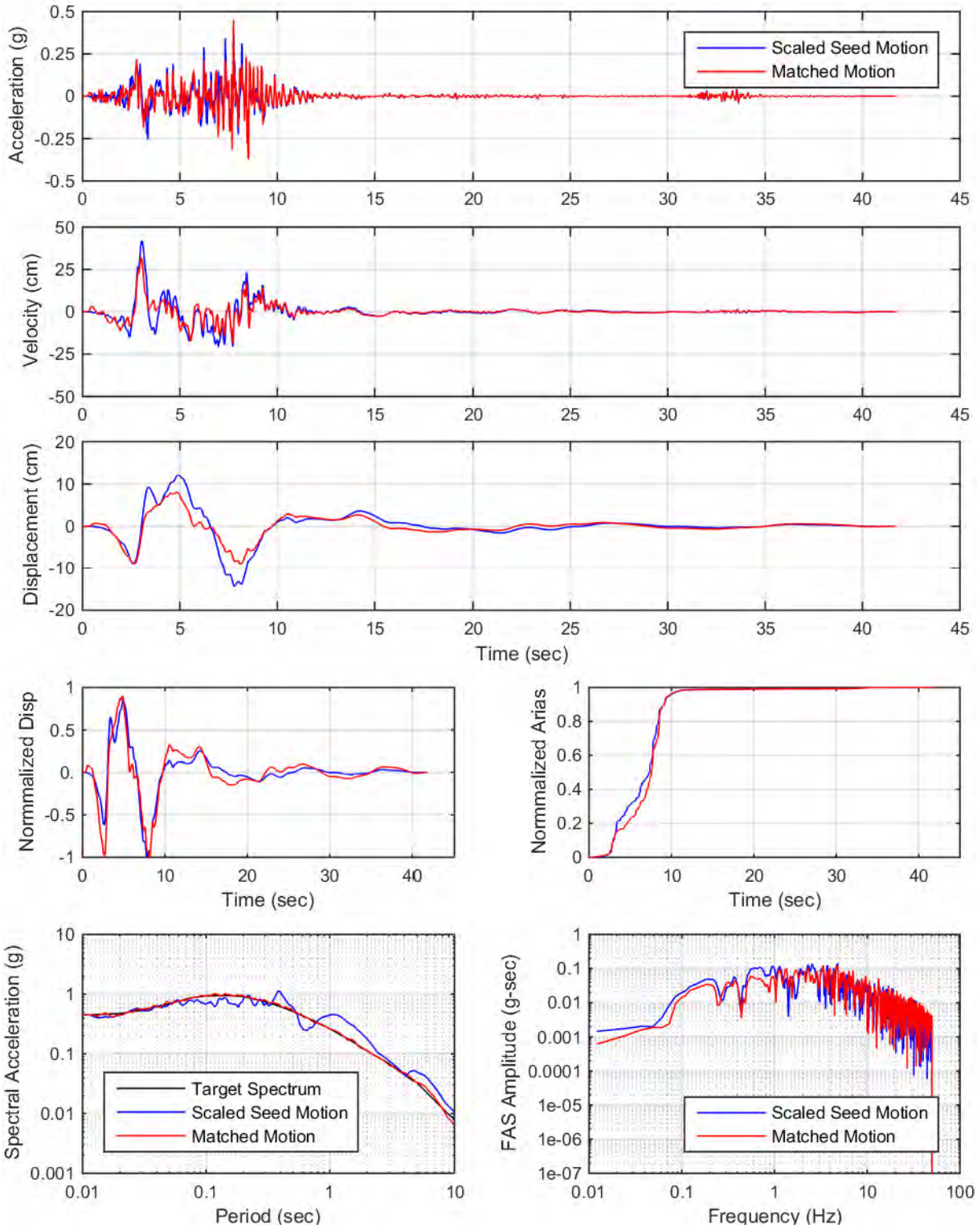

YDTI, MCE-Rrup0.1km-Med: Set02, UP

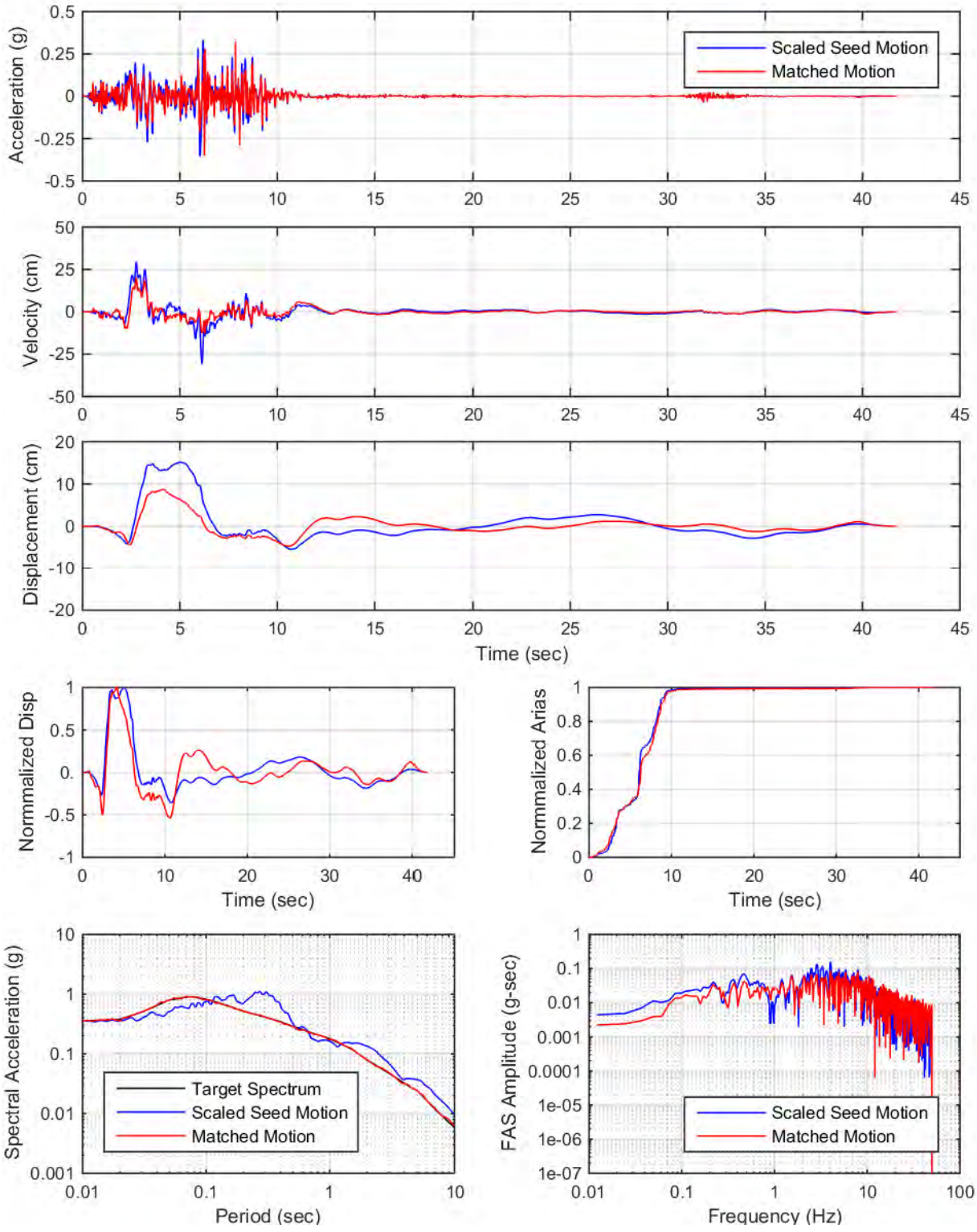

YDTI, MCE-Rrup0.1km-Med: Set03, H1

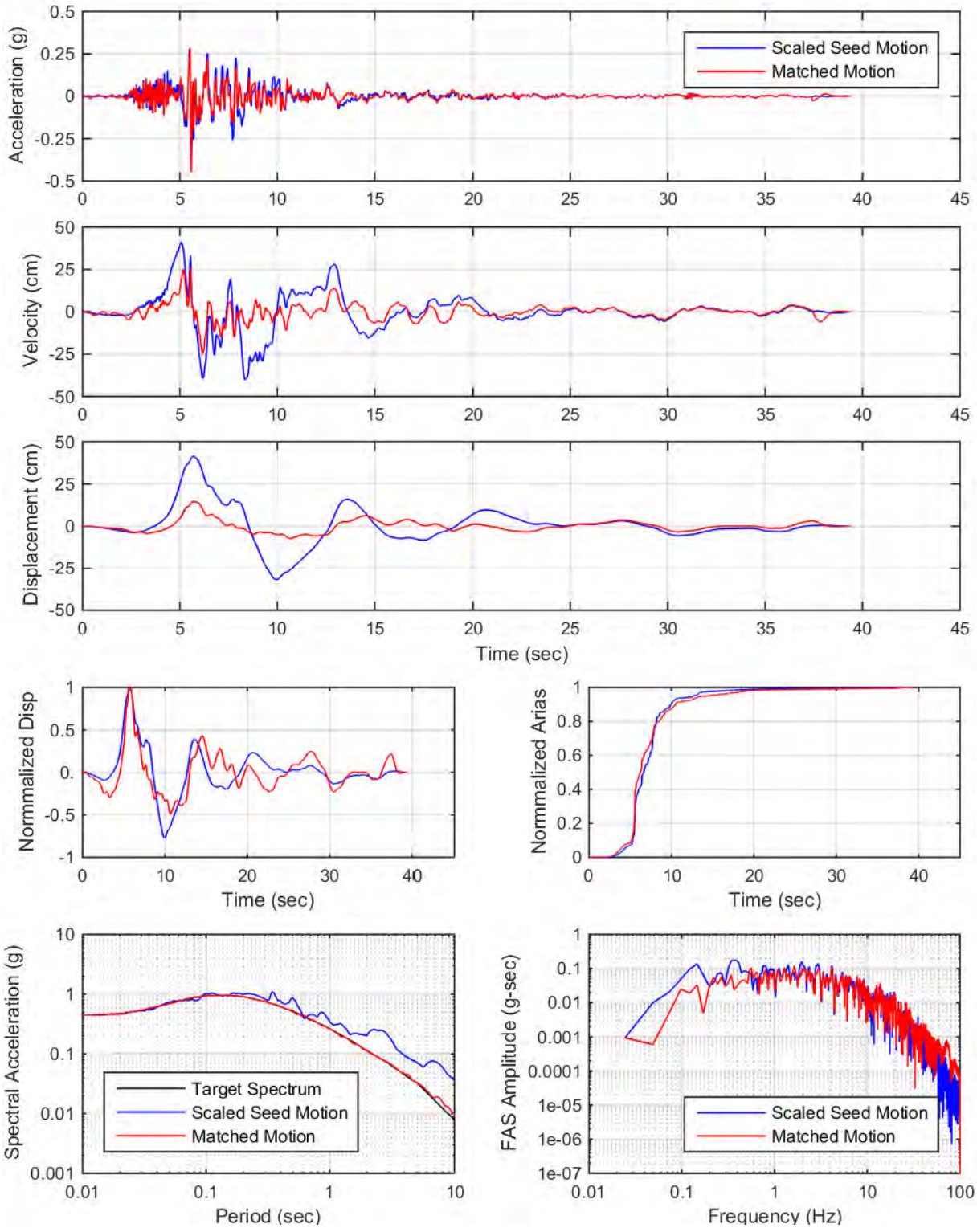

YDTI, MCE-Rrup0.1km-Med: Set03, UP

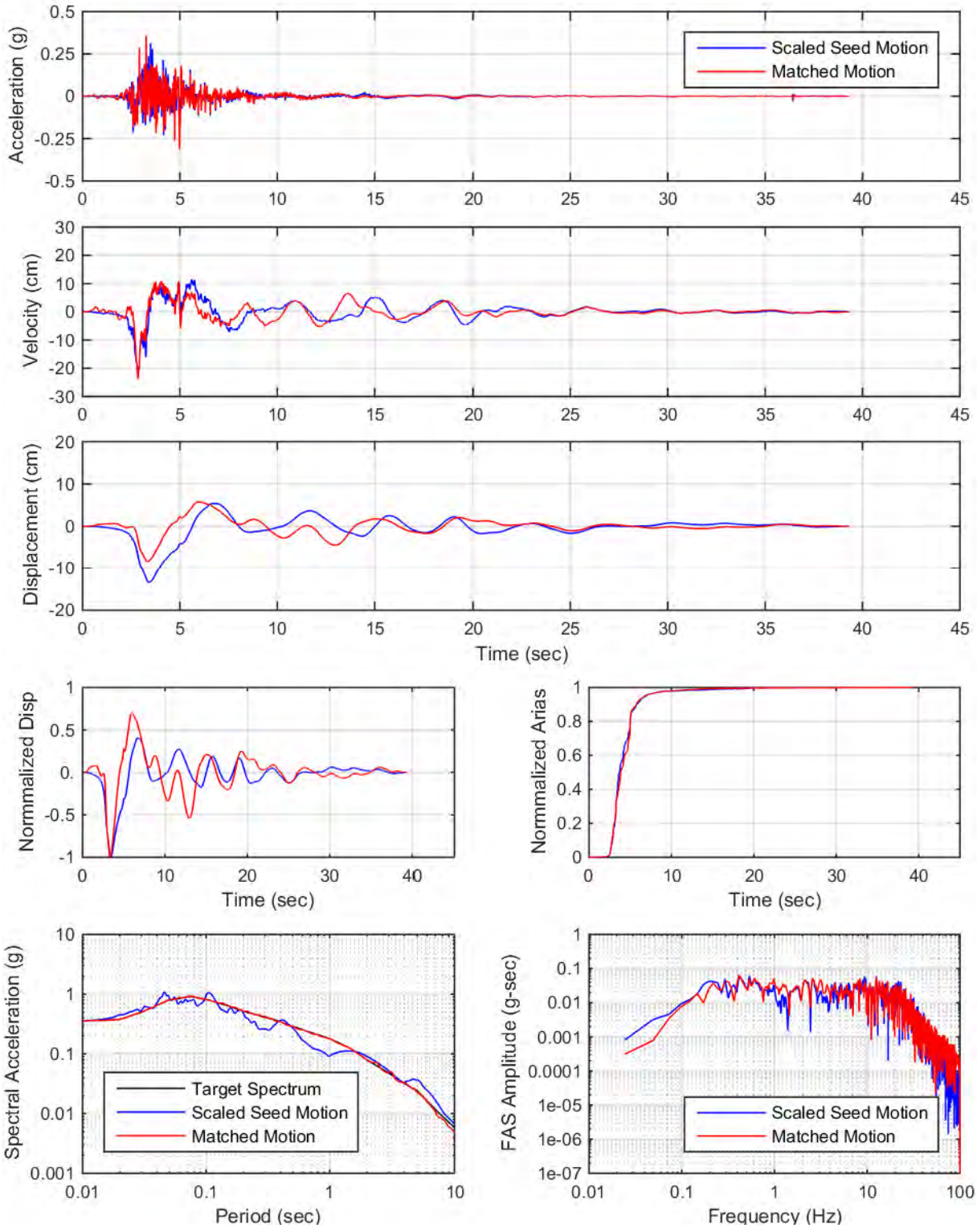

YDTI, MCE-Rrup0.1km-Med: Set04, H1

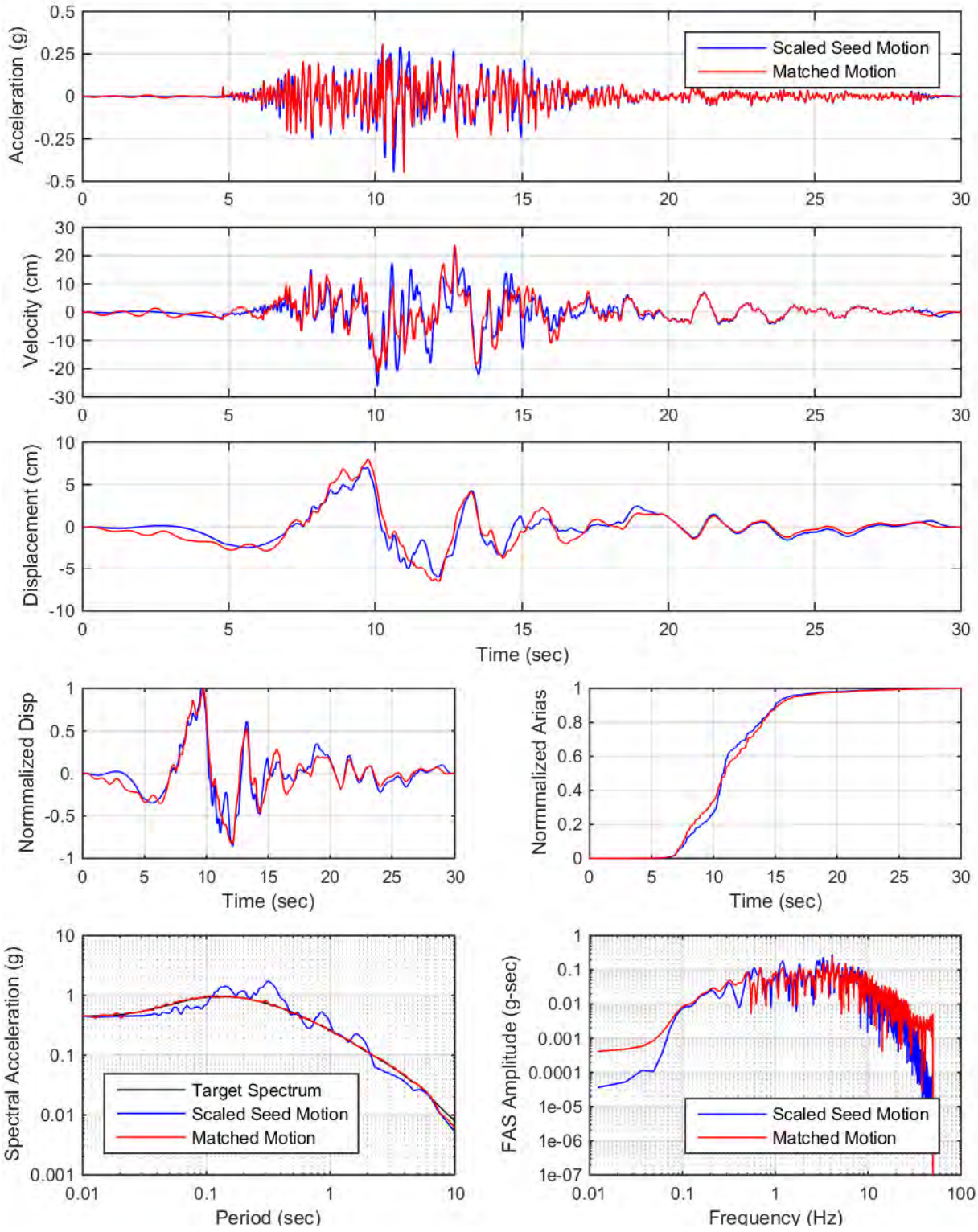

YDTI, MCE-Rrup0.1km-Med: Set04, UP

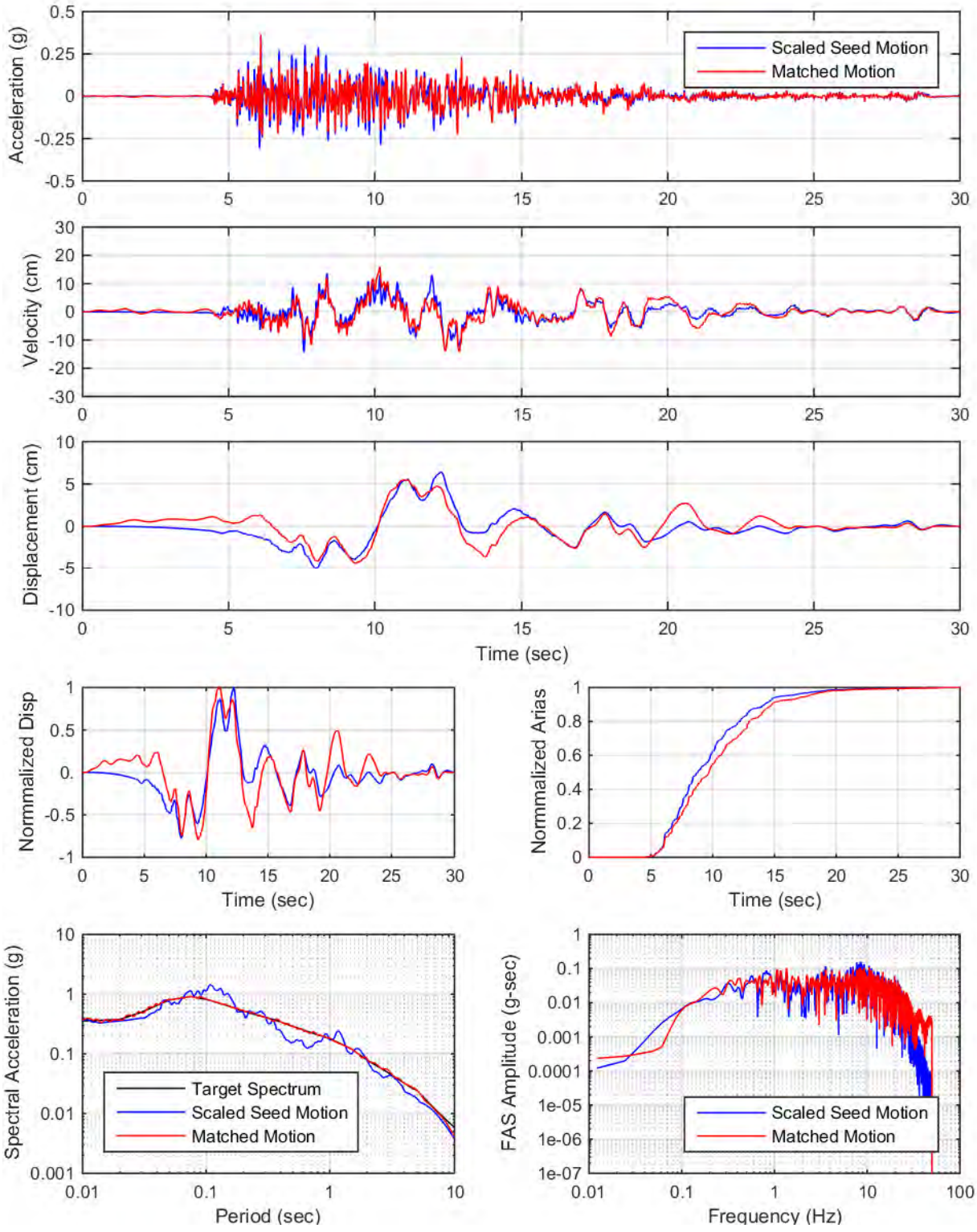

YDTI, MCE-Rrup0.1km-Med: Set05, H2

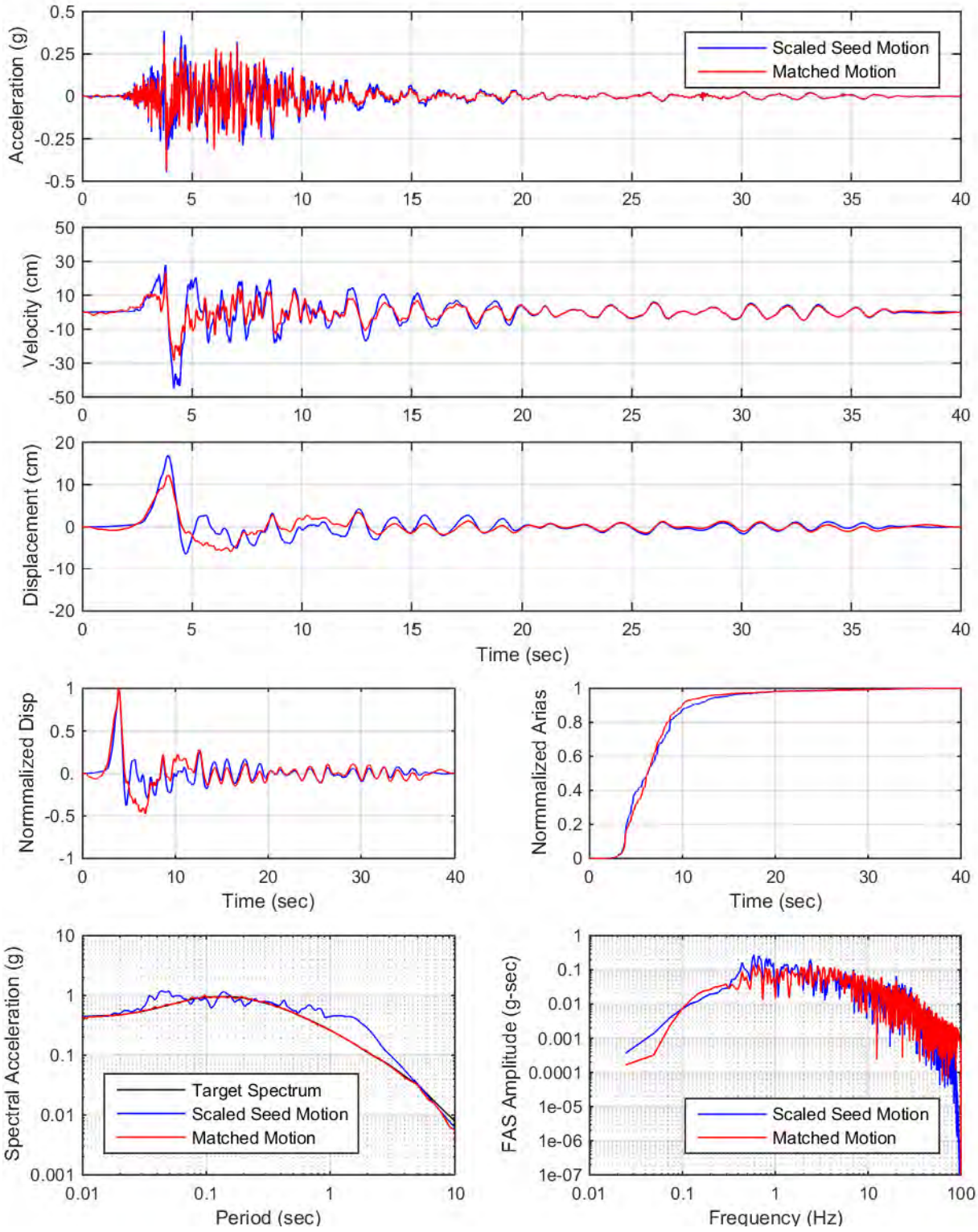

YDTI, MCE-Rrup0.1km-Med: Set05, UP

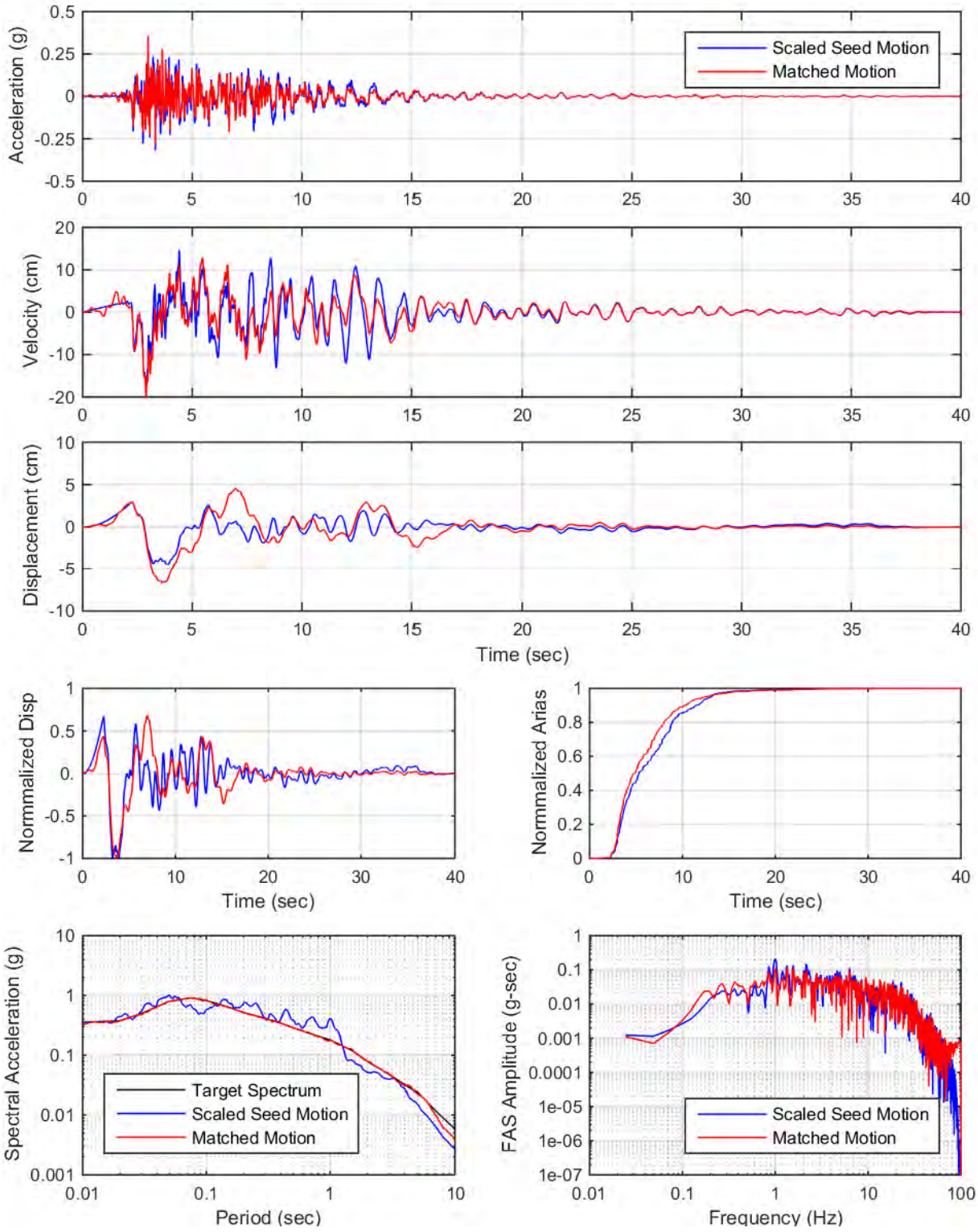

APPENDIX IX: SPECTRAL MATCHING PLOTS
MCE, RRUP = 0.1 KM, 84TH PERCENTILE DESIGN SPECTRA

YDTI, MCE-Rrup0.1km-84th: Set01, H2

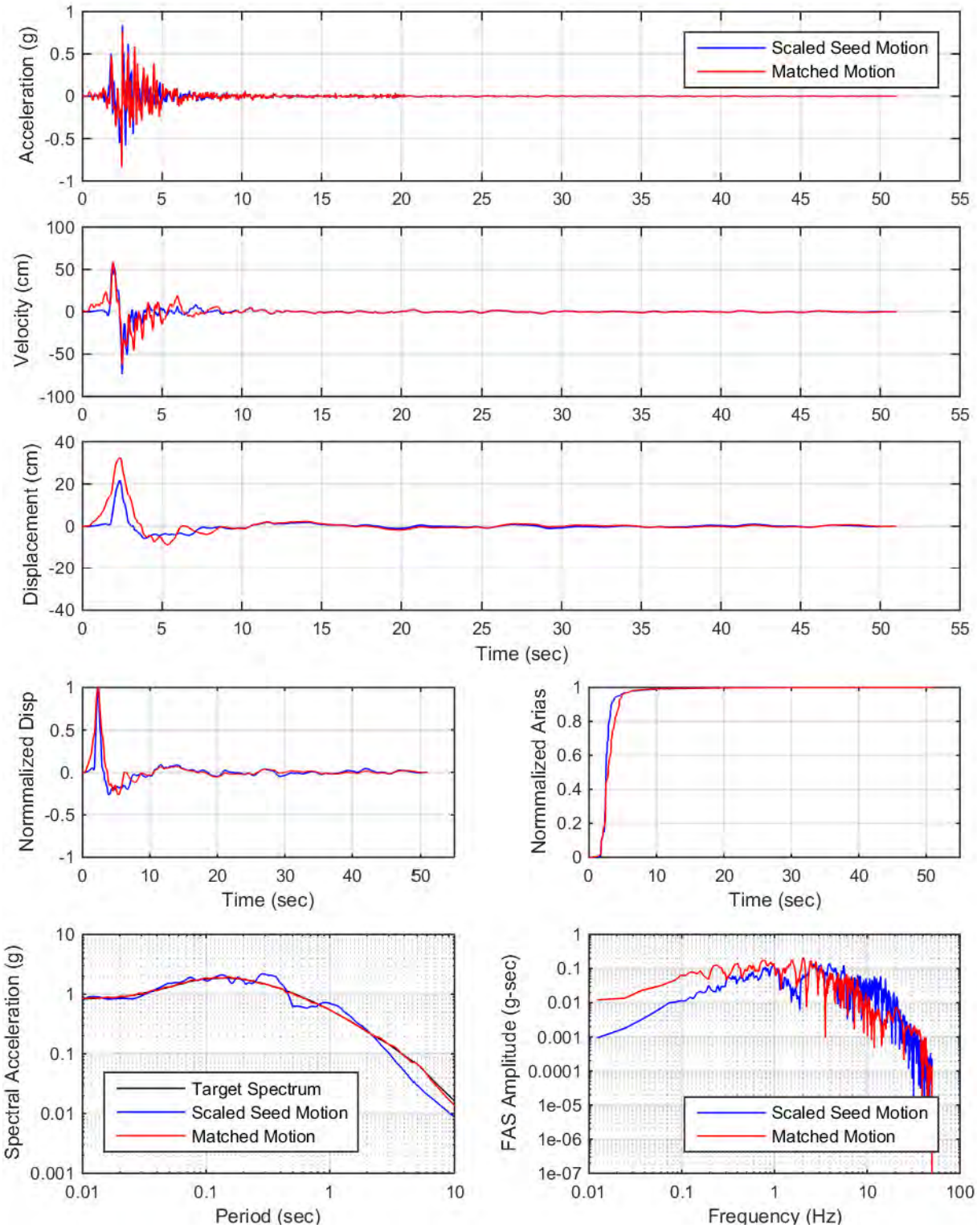

YDTI, MCE-Rrup0.1km-84th: Set01, UP

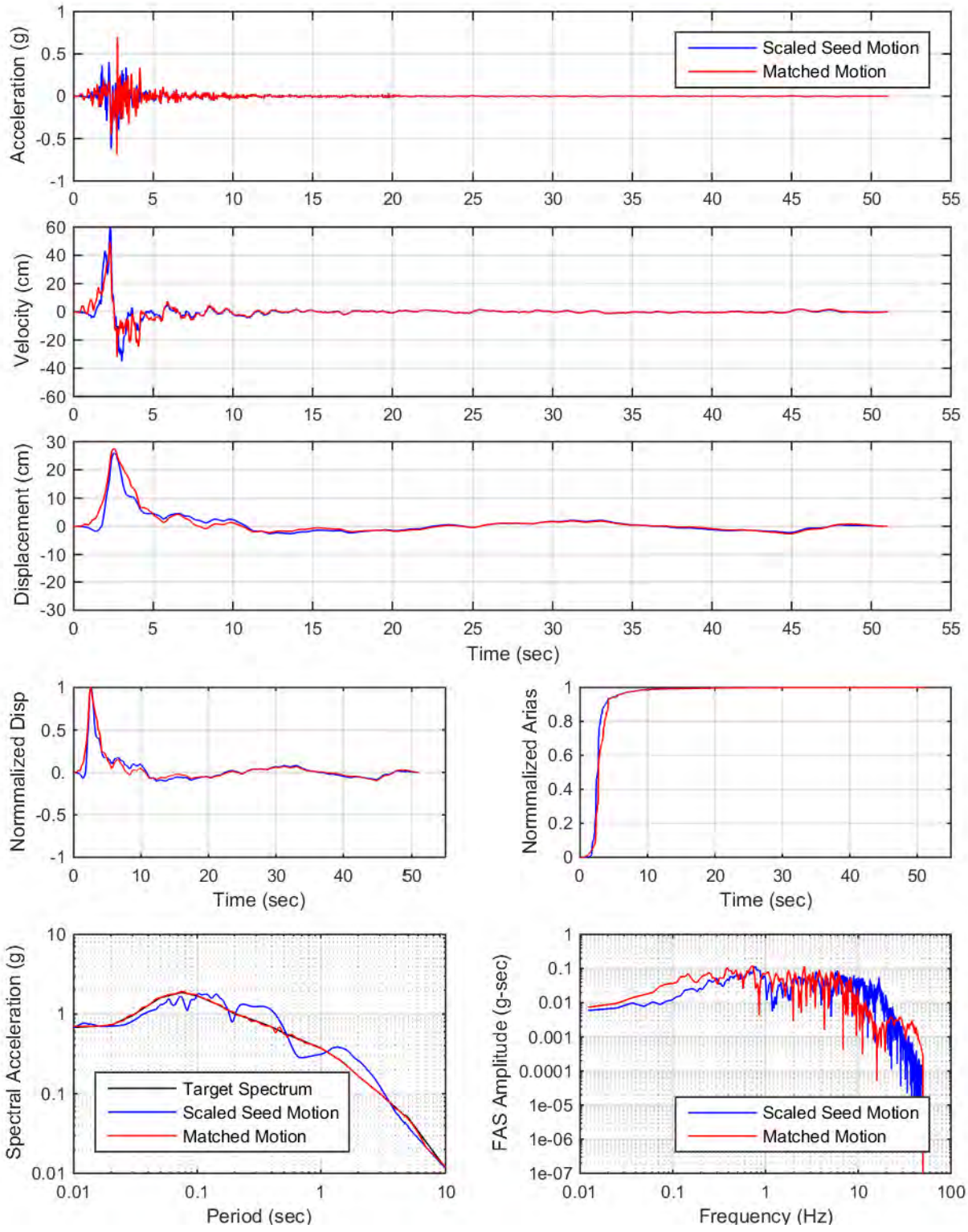

YDTI, MCE-Rrup0.1km-84th: Set02, H1

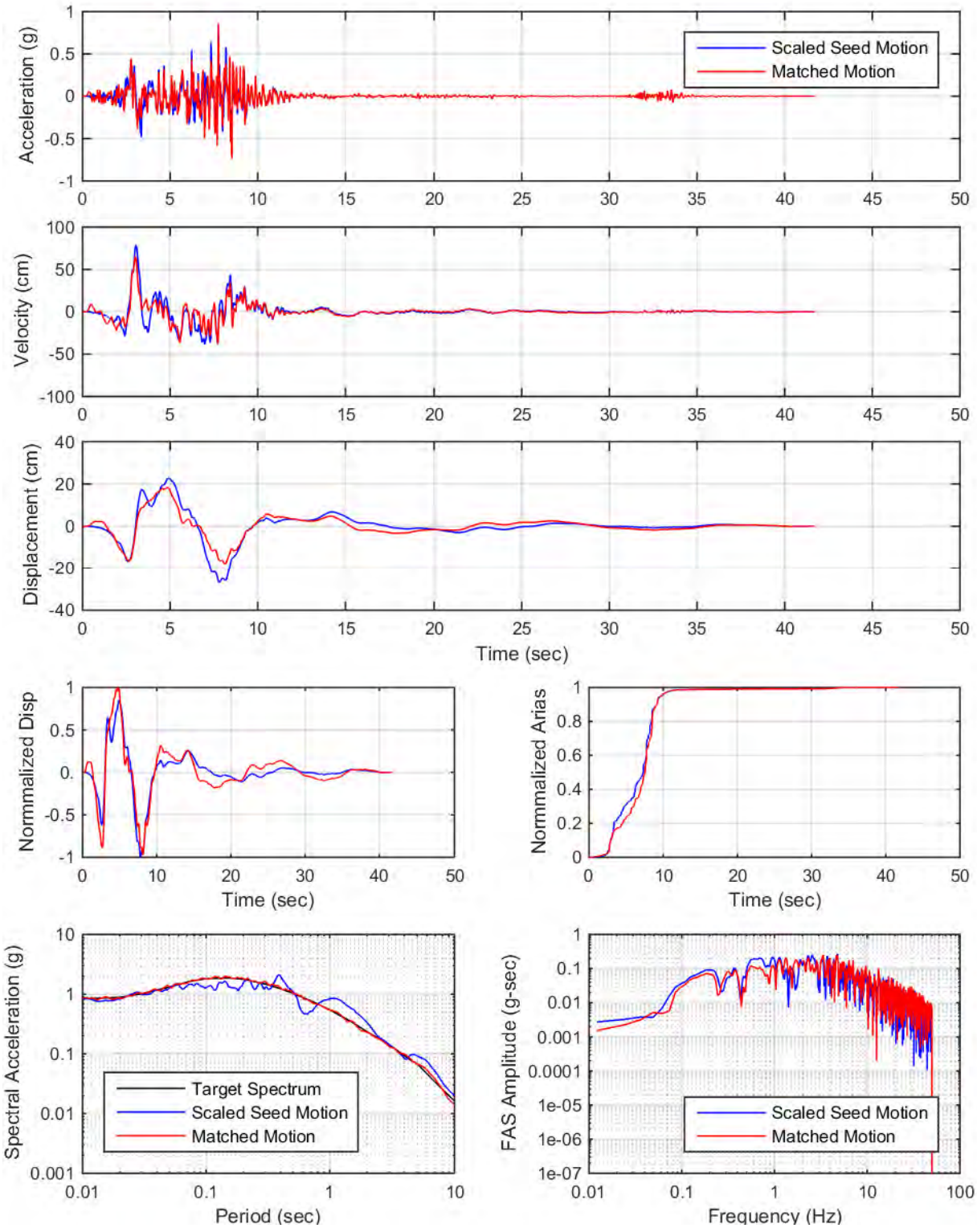

YDTI, MCE-Rrup0.1km-84th: Set02, UP

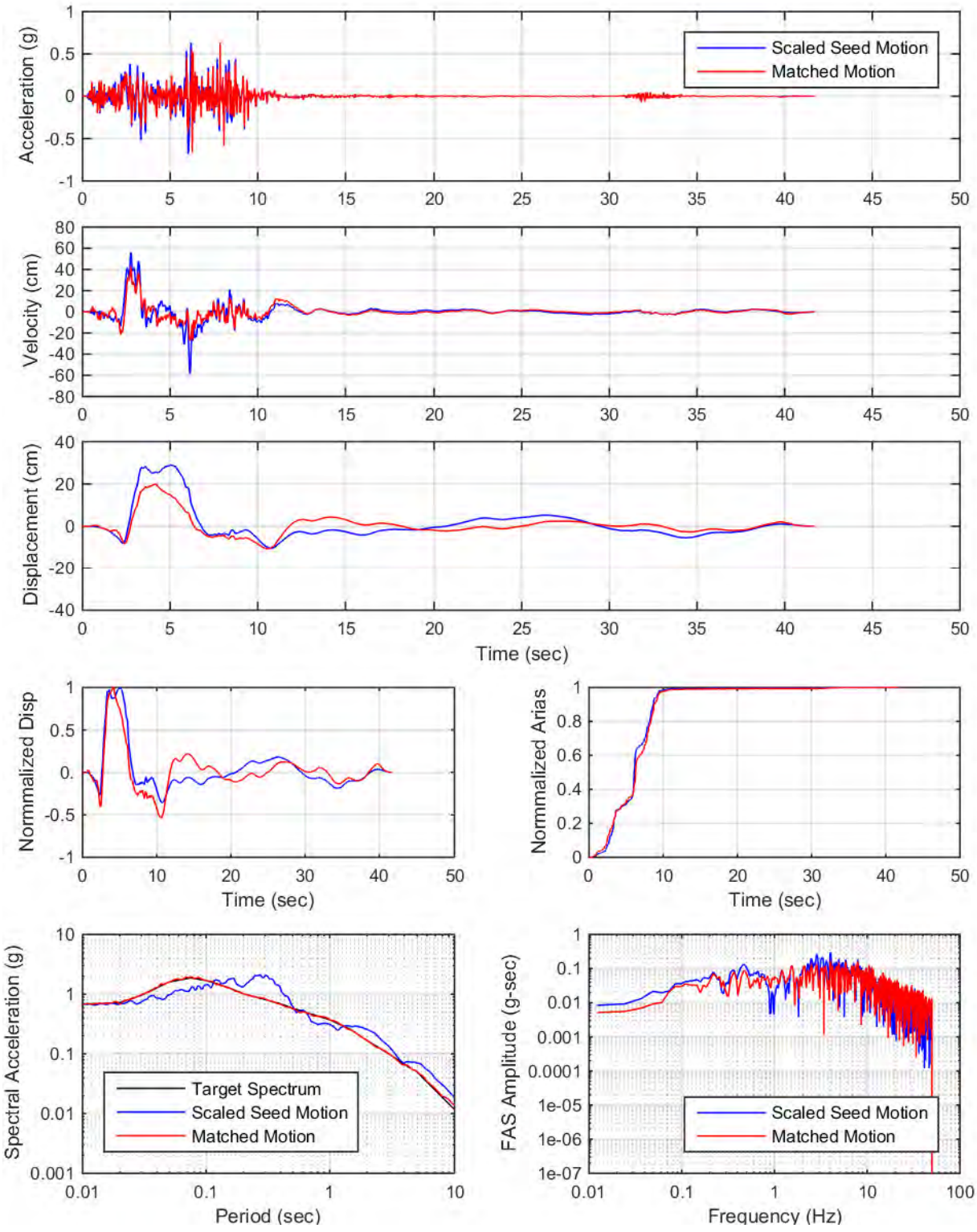

YDTI, MCE-Rrup0.1km-84th: Set03, H1

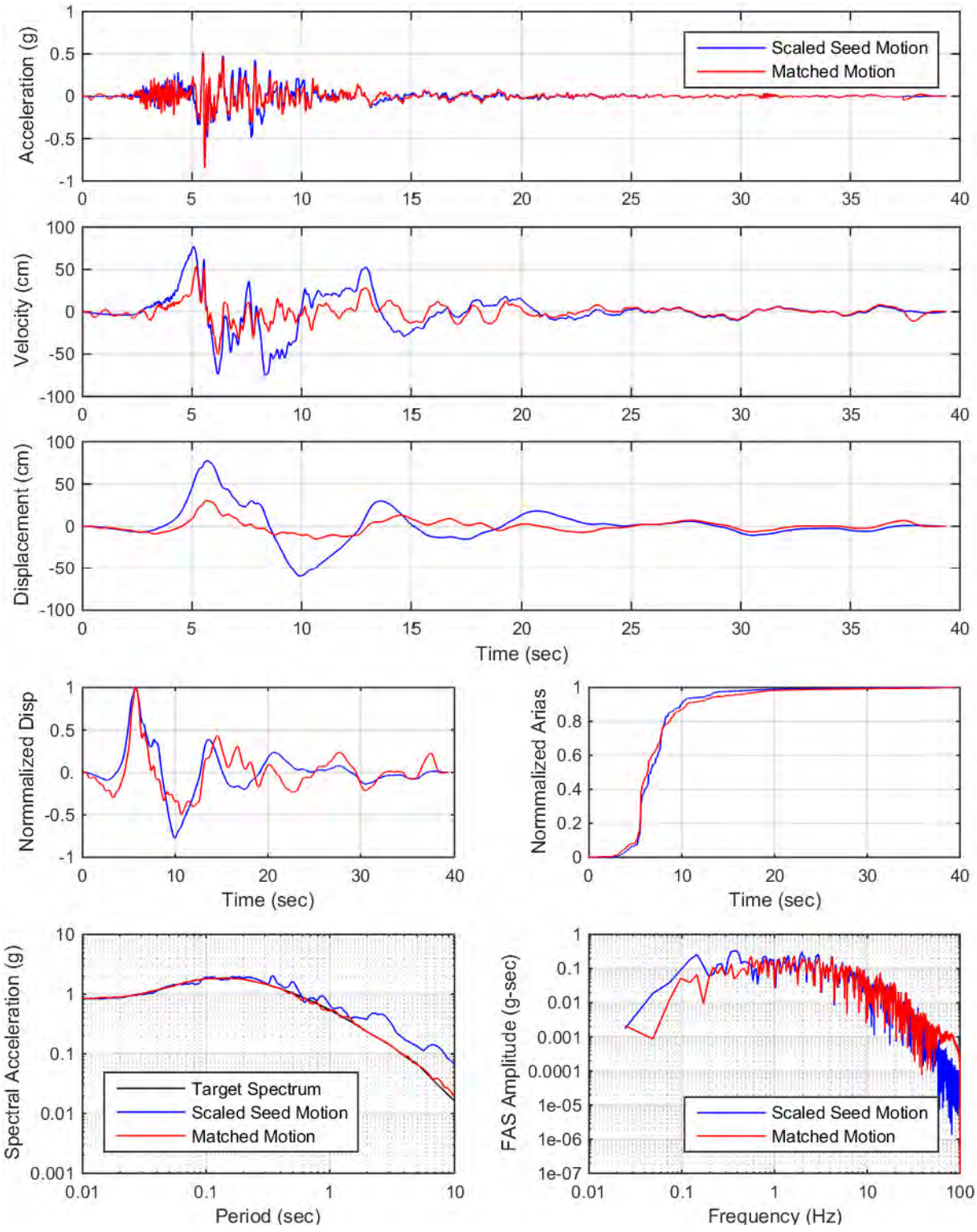

YDTI, MCE-Rrup0.1km-84th: Set03, UP

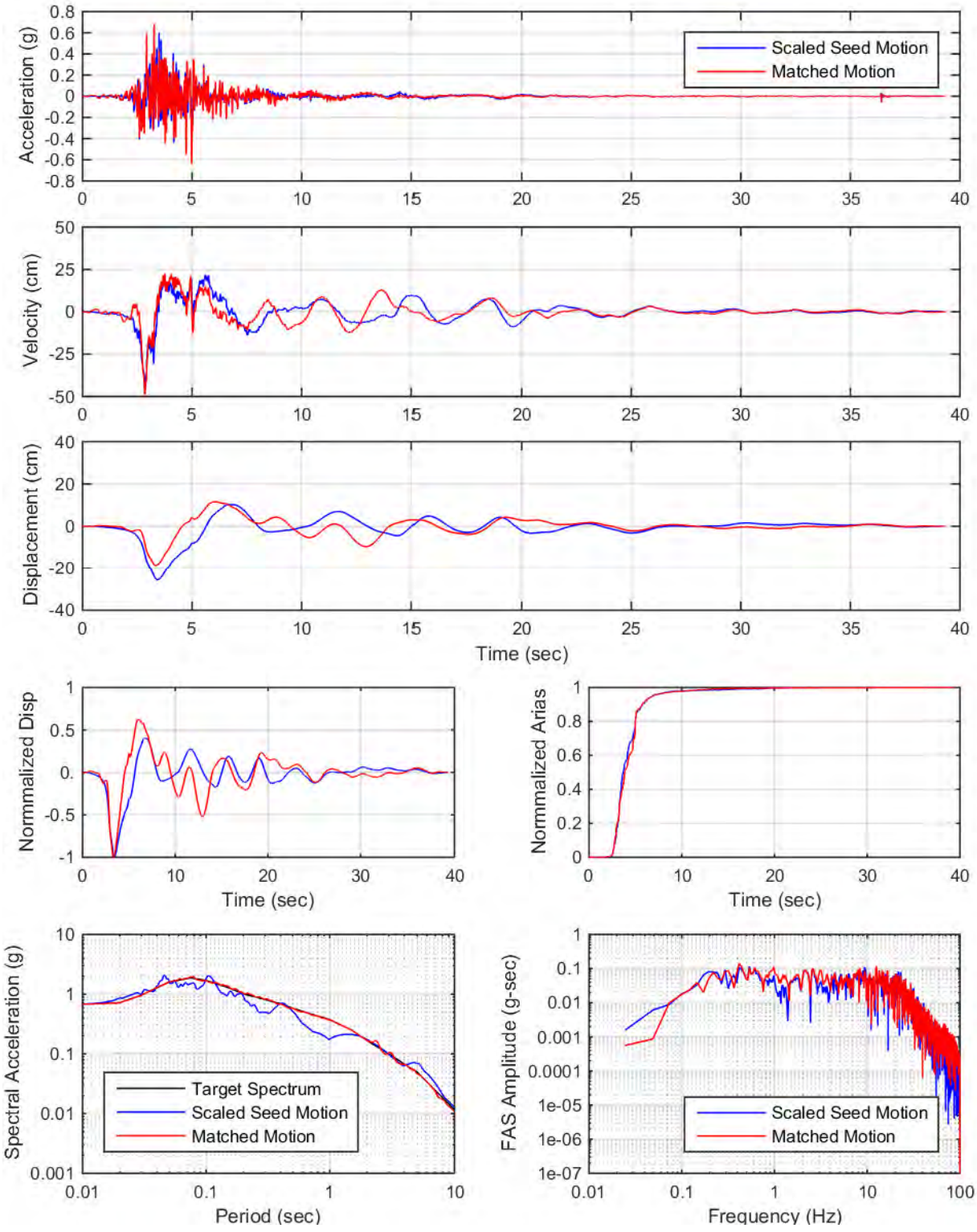

YDTI, MCE-Rrup0.1km-84th: Set04, H1

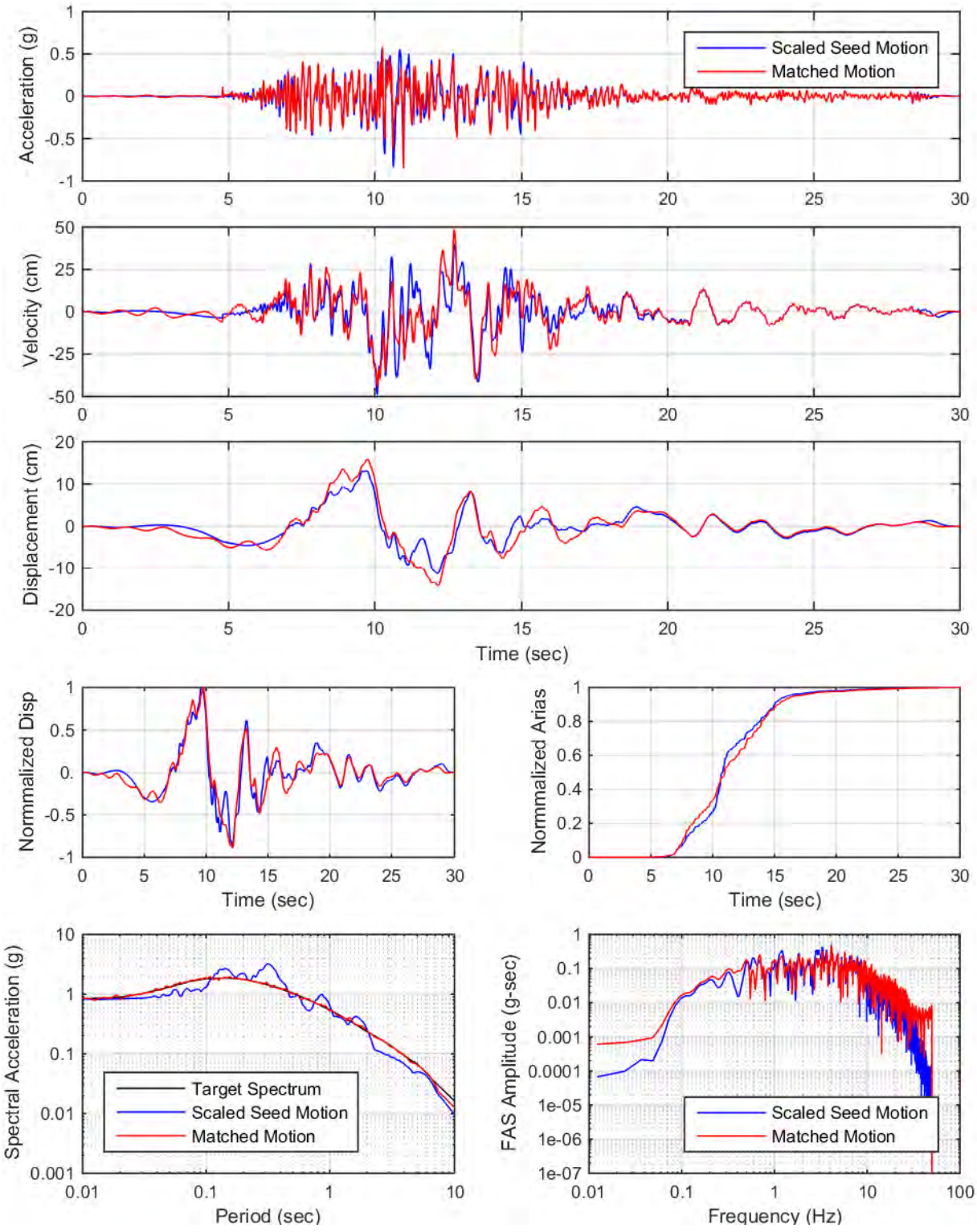

YDTI, MCE-Rrup0.1km-84th: Set04, UP

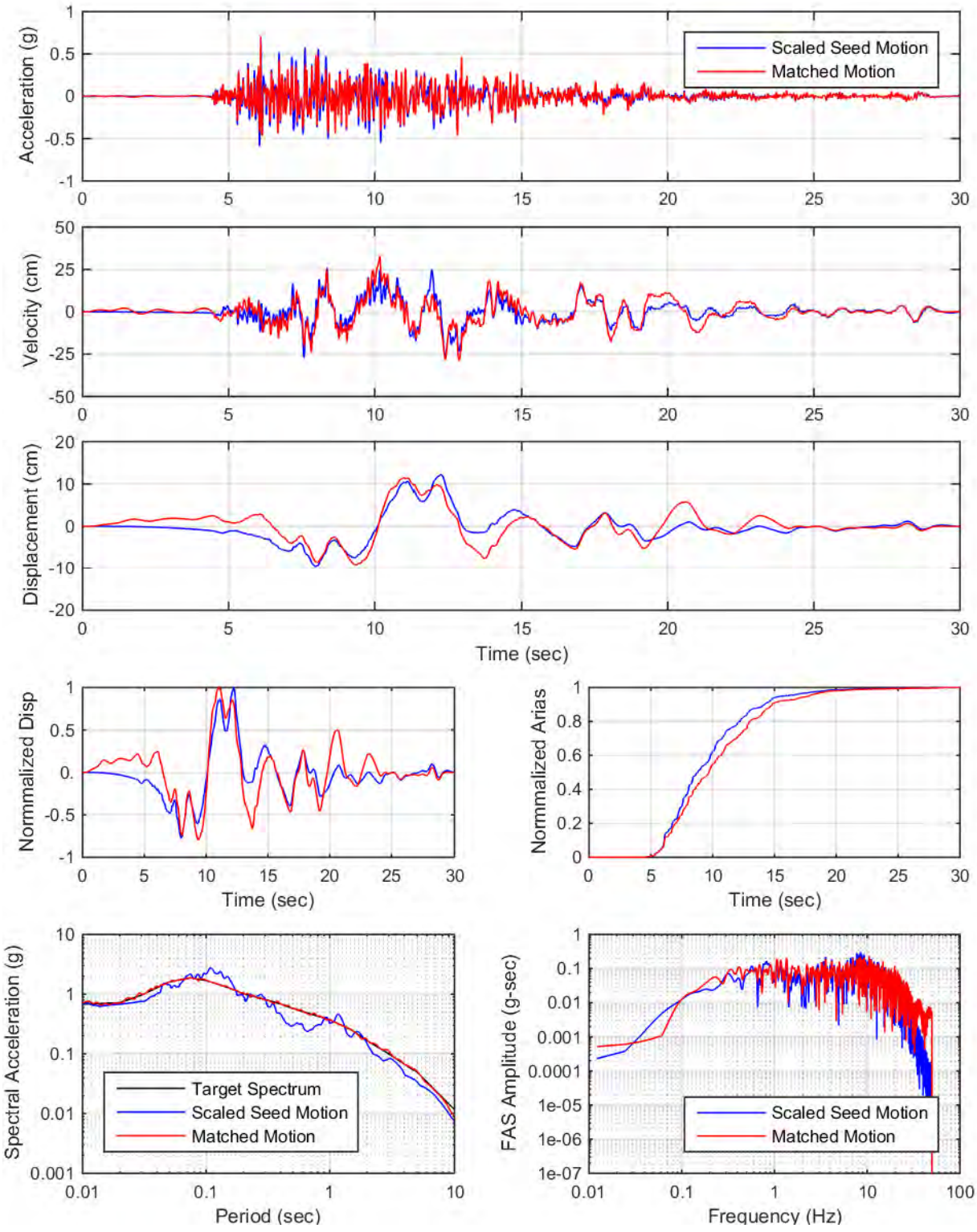

YDTI, MCE-Rrup0.1km-84th: Set05, H2

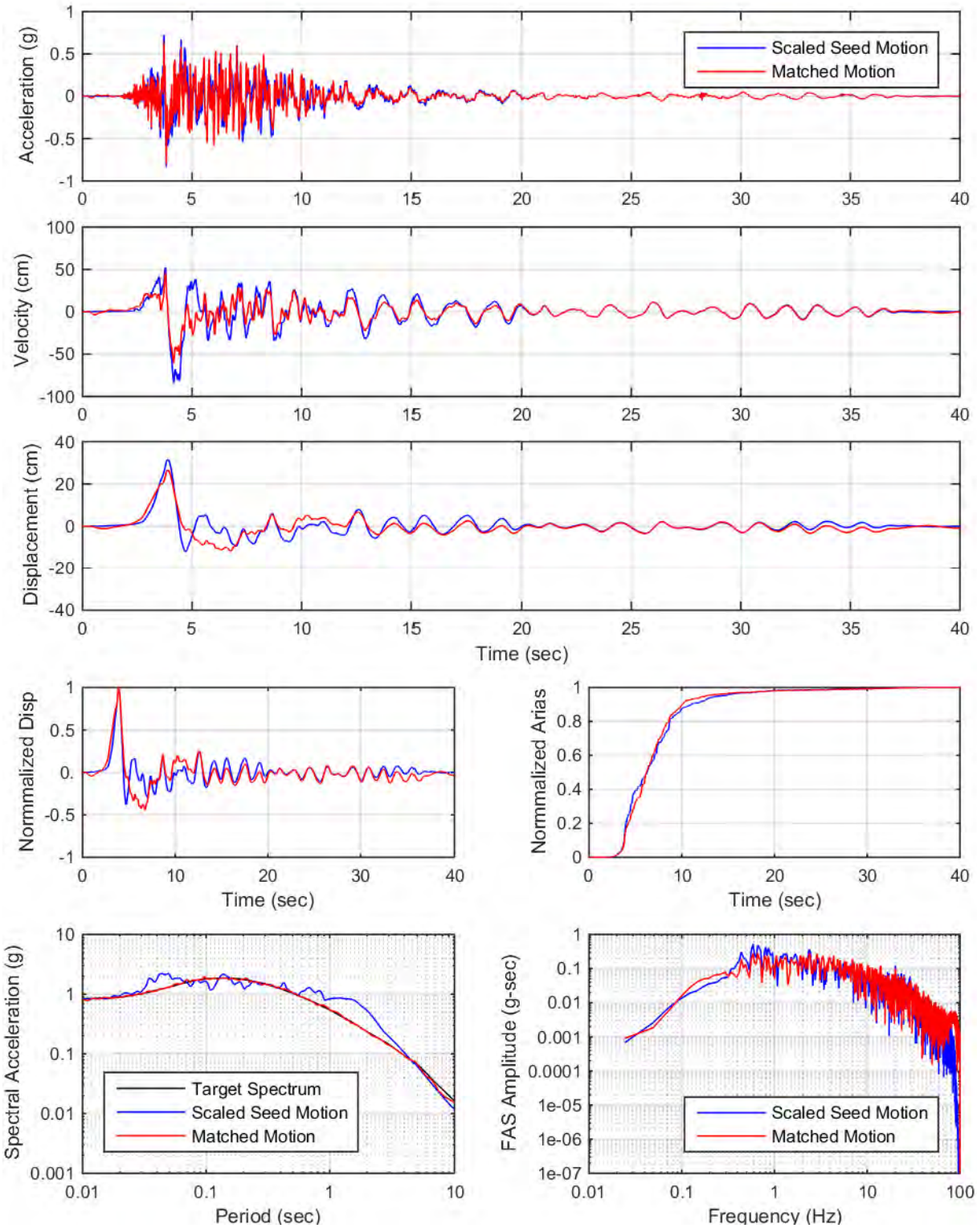

YDTI, MCE-Rrup0.1km-84th: Set05, UP

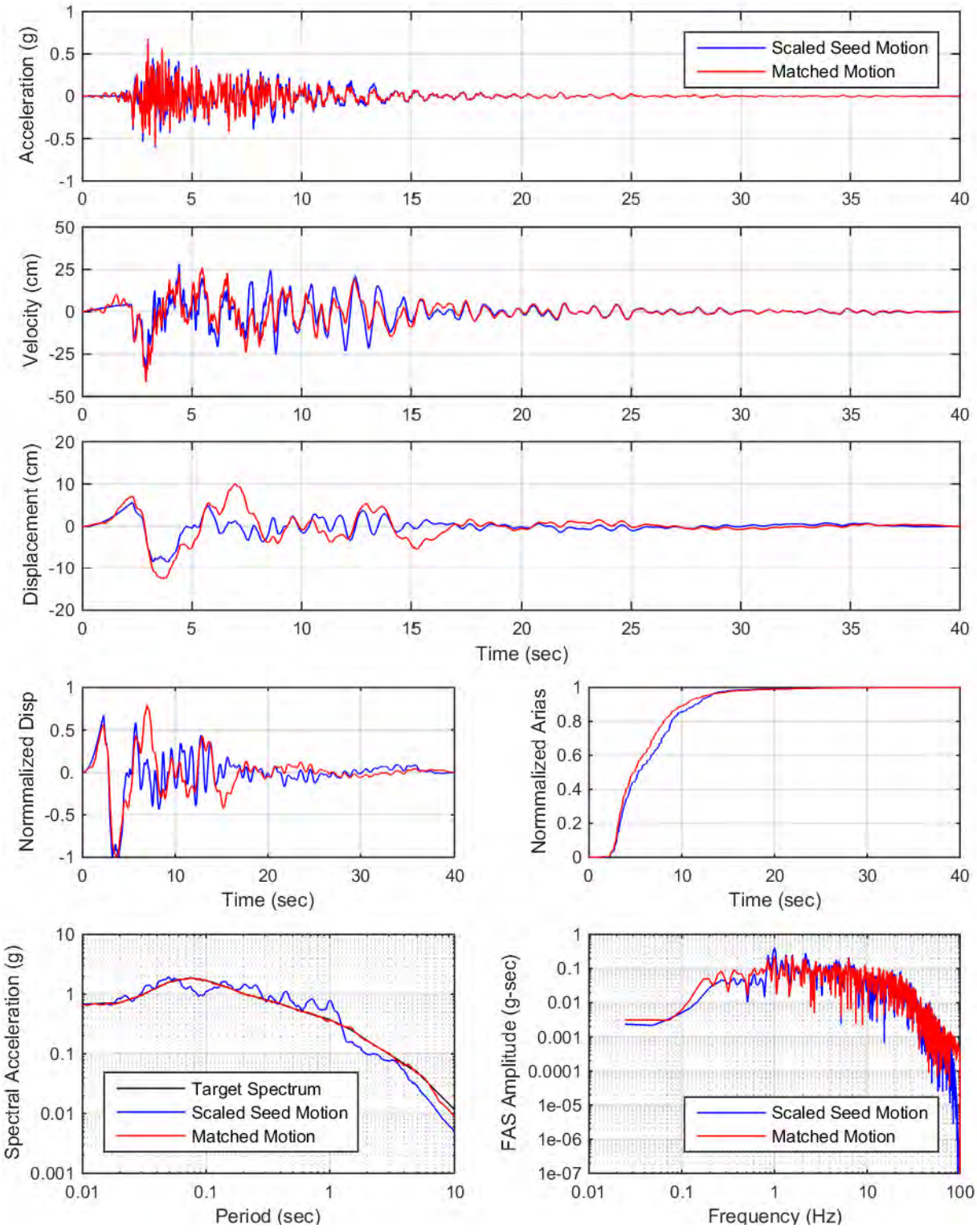

MONTANA BUREAU OF MINES AND GEOLOGY
A Department of Montana Tech of The University of Montana

Open File MBMG 627, Plate 1 of 1
Geology of the Butte mining district, MT, 2013

GEOLOGY OF THE BUTTE MINING DISTRICT, MONTANA

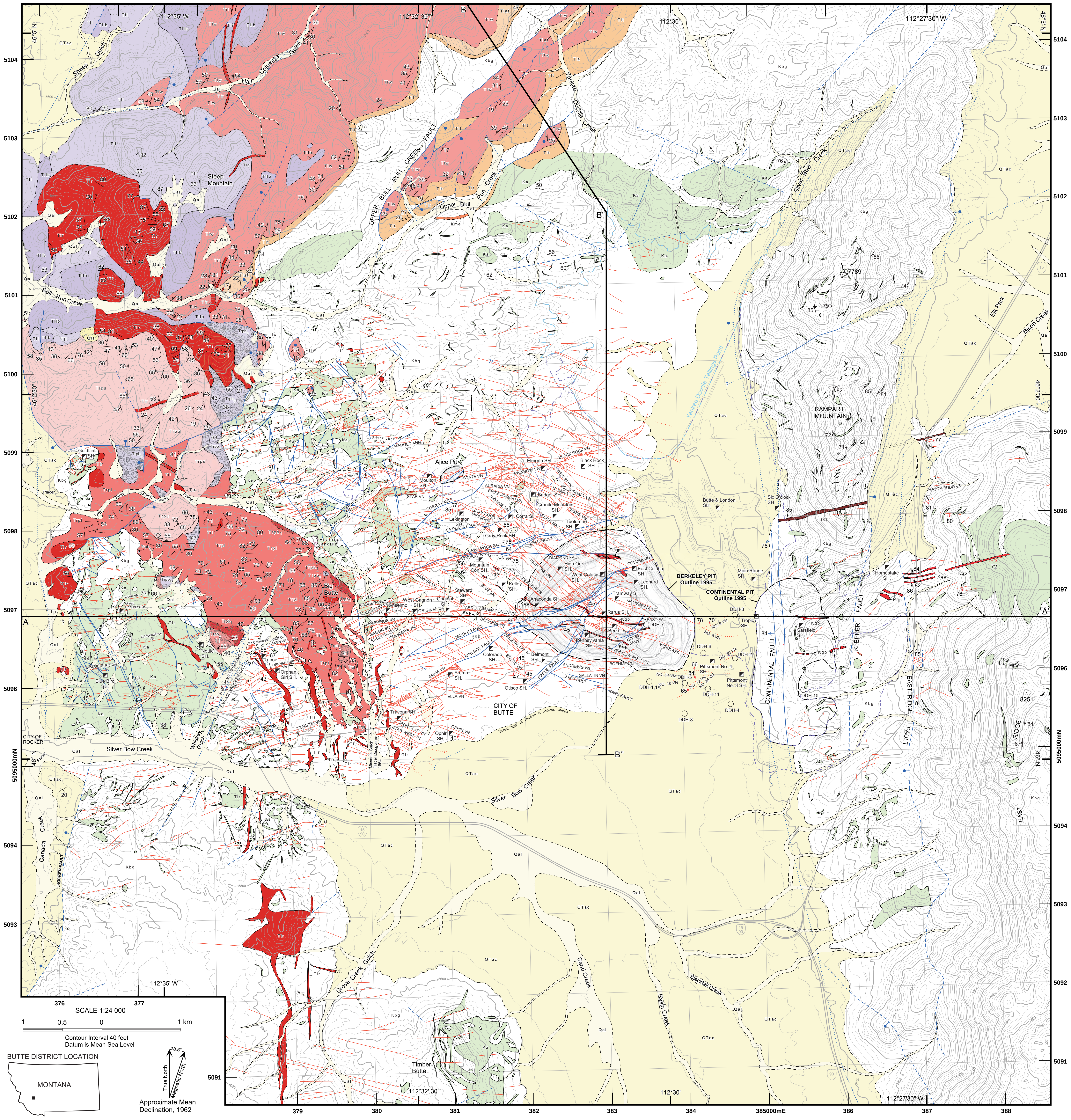

Base map modified from four U.S. Geological Survey 7.5 minute topographic quadrangles; Butte North (1989), Butte South (1989), Elk Park Pass (1985), and Homestake (1978).

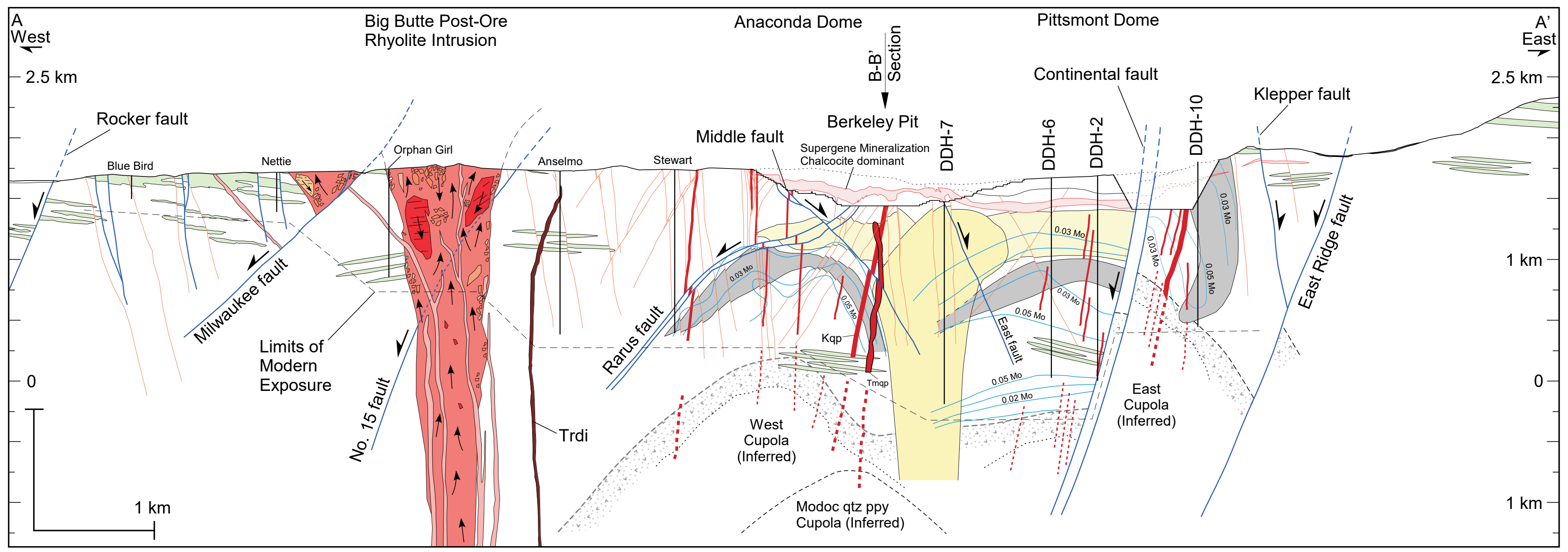

Explanation

- Fault, showing slip direction
- Main Stage vein or mineralized fault

Rock Types

- Quaternary & Tertiary sediments (Qal, QTac)

Lowland Creek Volcanics Formation Big Butte Vent Complex

- Rhyolite dikes (Tir)
- Rhyolite pyroclastics & vent breccia (Tiv, Tvcb, Tvwb)
- Trdi Middle Paleocene rhyodacite dike & breccia

Boulder Batholith

- quartz porphyry dikes (Kqp, Tmqp)
- granite cupola carapace
- aplite dikes (Ka)
- Butte Granite (Kbg)

Pre-Main Stage Mineralization

- Sparse py/Gs veins
- Sericite alteration zone
- Magnetite vein (Cu) zone

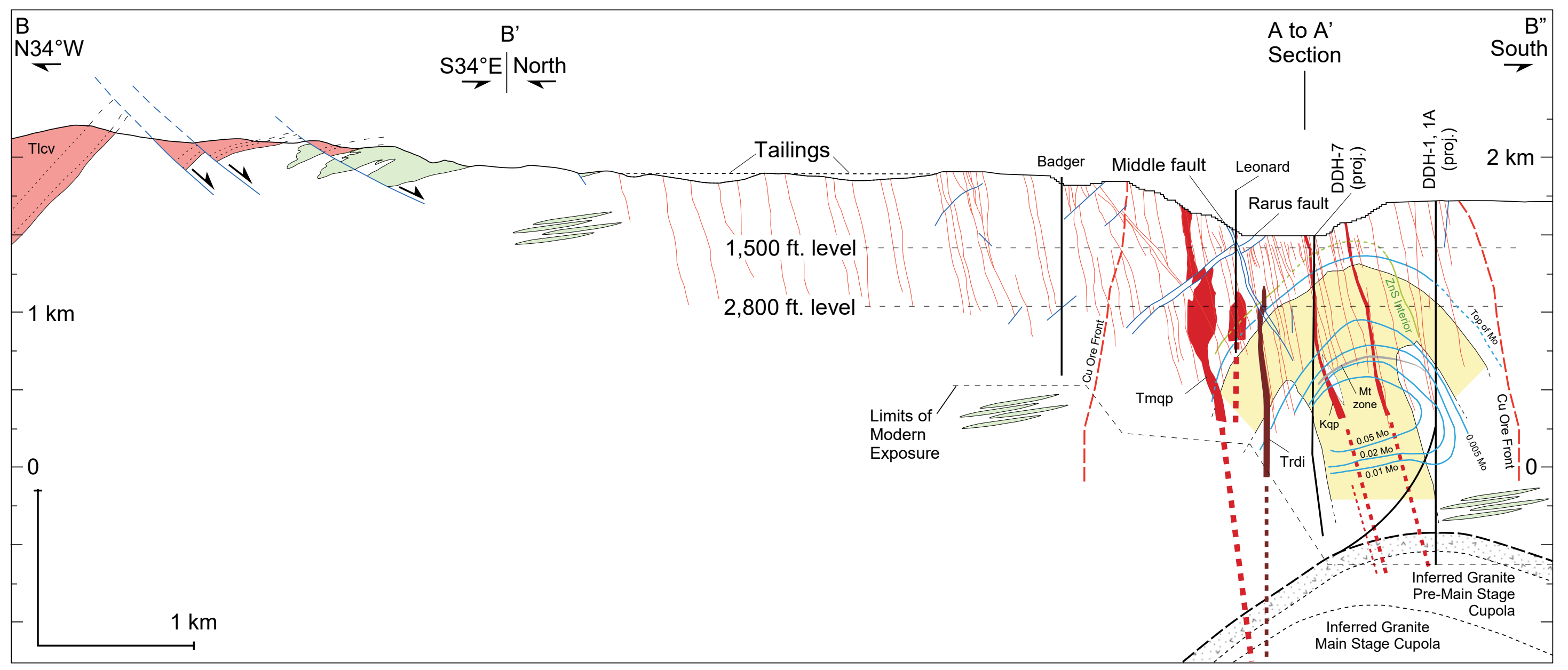

Explanation

- Fault, showing slip direction
- Main Stage vein or mineralized fault

Lowland Creek Volcanics Formation

- Tlcv Lower quartz latite pyroclastics & sediments (Tlw, Tlat, Tlt)
- Trdi Middle Paleocene rhyodacite dike & breccia

Boulder Batholith

- quartz porphyry dikes (Kqp, Tmqp)
- granite cupola carapace
- aplite dikes (Ka)
- Butte Granite (Kbg)

Pre-Main Stage Mineralization

- Sericite alteration zone
- Magnetite vein (Cu) zone

CORRELATION OF MAP AND CROSS SECTION UNITS

Units	Epoch	Period
Qal, Qls	Recent	QUATERNARY
QTac	Recent to Miocene	QUATERNARY
Tir Trpu Trpl, Trpb$_1$, Trpb$_2$, Trpb$_3$ Tll Tllb Tlw Tlat Tlt	Eocene	TERTIARY
Trdi — Main Stage Mineralization — Tmqp — Pre-Main Stage Mineralization —	Paleocene	TERTIARY
Kqp Ka Kme Kbg	Late Cretaceous	CRETACEOUS

DESCRIPTION OF MAP UNITS

QUATERNARY and TERTIARY DEPOSITS

Qal **Recent Alluvium deposits -** Clay, silt, sand, and gravel fluvial detritus from eroded local granitic and volcanic rocks. Includes colluvium, lacustrine and terrace deposits.

Qls **Landslide deposits -** Poorly sorted material derived from bedrock and surficial deposits primarily occur as slump blocks and incipient rotational slumps.

QTac **Older Alluvium and colluvium deposits** - Poorly sorted, unconsolidated to moderately indurated, well-rounded, arkosic silt, sand, pebble and cobble detritus locally derived from granitic and volcanic rocks. Basin fill sediments near the town of Rocker are approximately 180 to 300 m thick (Feiveson, 1997; Hammar-Klose, 1997). Recent to Miocene sedimentary rocks contain locally air-fall rhyolite tuffs. Rare fossil camel, rhinoceros, horse, and oreodont teeth and bones are present in deposits south of Silver Bow Creek (Smedes et al., 1973). Locally, includes talus deposits comprised of unsorted cobble to boulder angular rock fragments and debris flow deposits adjacent to the Rocker, Continental, Klepper, and East Ridge faults, and Recent valley fill and alluvial terrace deposits (Pleistocene and Pliocene age; Elliott and McDonald, 2009).

TERTIARY VOLCANIC ROCKS

Lowland Creek Volcanics Formation - Modified from Smedes, (1962)

Big Butte Vent Complex

Tir **Rhyolite dikes -** Light gray to red-brown, porphyritic rhyolite dikes and shallow irregular intrusive bodies contain plagioclase, quartz, and biotite phenocrysts surrounded in an aphanitic groundmass. Dikes south of Big Butte contain lineated flow foliation and chilled margins parallel to intrusive contacts. North of Bull Run Creek a large rhyolite intrudes dacite lavas and may be the base of an extrusive dome.

Trpu **Upper rhyolite pyroclastics -** Light gray to reddish, moderately to strongly welded rhyolite pyroclastic rocks (ignimbrite) contain 25 to 35 volume percent crystals of shattered crystals of quartz, oligoclase-andesine, biotite, and minor sanidine in a vitroclastic matrix. Abundant fiammé have an aspect ratio of approximately 6H:1V and are circular in plan view, suggesting simple compaction. The upper rhyolite pyroclastic rocks are petrographically similar to the lower rhyolite pyroclastic rocks (Trpl), but are locally overlying Trpl along a lithic-rich basal vitrophyre, up to 5 m thick. In the north west part of the district, the occurrence of several vitrophyres, up to 5 m thick, suggests multiple cooling units.

Trpb$_1$ Trpb$_2$ Trpb$_3$ **Pyroclastic breccia** - Includes three subunits consisting of angular blocks (<1 m to 30 m in diameter) of granite, aplite, quartz latite ignimbrite, dacite lava, and welded rhyolite tuff surrounded in a poorly welded matrix pyroclastic rhyolite. The matrix contains broken crystal fragments of quartz, plagioclase, sanidine, and biotite. Pyroclastic breccia (<200 m wide) locally occurs at the contact of the lower rhyolite pyroclastic (Trpl) and granite (Kbg). Three subunits are subdivided based on dominant clast lithology. Trpb$_1$, dominated by granite and aplite clasts. Trpb$_2$, dominated by quartz latite ignimbrite blocks that locally contain distinctive eutaxitic foliation. Trpb$_3$, dominated by dacite lava and breccia clasts that contain planar flow aligned plagioclase phenocrysts surrounded in an aphanitic groundmass. The pyroclastic breccia may represent the collapse of previously erupted surface rocks into the vent.

Trpl **Lower rhyolite pyroclastics** - Light gray to reddish-brown, moderately to strongly welded rhyolite pyroclastic rocks (ignimbrite) contain 25 to 35 volume percent crystals of shattered oligoclase-andesine, quartz, biotite and sanidine in a vitroclastic matrix. The ignimbrite is intercalated locally with thin (<10 m thick) breccia lenses. Abundant (up to 20 vol. %.) cognate clasts of rhyolite and lesser amounts of partially flattened fiammé (2H:1V to 1.5V aspect ratio) are orientated parallel to the near vertical fabric. This steeply dipping foliation becomes highly contorted, locally. The rhyolite pyroclastic rocks at Big Butte have a ^{40}Ar/^{39}Ar age of 52.9 ± 0.14 Ma (Dudás et al., 2010).

Extrusive

Tll **Dacite lava** - Brown to purplish red dacite lava (<120 m) consisting of abundant flow-aligned plagioclase phenocrysts (20 vol. %), biotite-rich glomerocrysts, orthopyroxene, hornblende, quartz and trace amounts of apatite and opaques are surrounded in an aphanitic groundmass (70 vol. %). There is no age determination for these dacites at Butte, but Dudás et al. (2010) suggest an age of 52.4 Ma based on a dacite sample southwest of Butte.

Tllb **Volcanic breccia -** Light-gray, brown to purplish red breccia consists of a lower matrix-supported part and an upper clast-supported part. The lower discontinuous part (up to 50 m thick) contains subangular (less than 1 m diameter) ash-flow tuff and dacite lava fragments (60 vol. %) supported by a light-brown to very pale orange devitrified ash matrix. This lower sequence may represent a volcanic debris flow or lahar. The upper part (up to 120 m thick) of the breccia unit is dominantly framework-supported angular porphyritic dacite lava boulders (90 vol. %) up to 2 m in diameter that are enclosed in a lavender-gray dacite lava matrix. The upper breccia sequence is an autobrecciated lava along the base of the overlying dacite lava (Tll).

Tlw **Quartz latite ash-flow tuff -** Light gray, reddish-brown and olive, poorly to strongly welded quartz latite ignimbrite contains shattered plagioclase, biotite, and hornblende crystals in a vitroclastic matrix. Eutaxitic textures are defined by conspicuous fiammé. Normal grading of lithic fragments occurs as repeated distinct zones upward in the section and correlates to 13 thin cooling units marked by distinct welding breaks. Locally, the ignimbrite is up to 300 m thick. In general, hornblende crystal abundance increases slightly from 1 to 5 vol. % upwards in the section. A vitrophyre up to 30 cm thick locally marks the basal contact. This ignimbrite has a ^{40}Ar/^{39}Ar age of 52.9 ± 0.14 Ma (Dudás et al., 2010)

Tlat **Rhyolitic air-fall tuff and base surge deposits -** Light gray, unwelded laminated and cross-bedded crystal-poor ash air-fall and base surge deposit (<50 m) with up to 15 vol. % lithic fragments. This upper unit is interpreted to be the base surge and airfall deposits precursor to the overlying quartz latite ignimbrite.

Tlt **Volcaniclastic sedimentary deposits -** Fluvial mudstone, siltstone, sandstone, and pebble conglomerate sedimentary sequences containing reworked volcaniclastic sedimentary rocks. Laminated micaceous mudstones and siltstones grade upward into coarse-grained and rippled arkosic and tuffaceous sandstones. Cross-bedding, ripples and petrified logs indicate a SSW-NNE bi-directional fluvial flow-direction. This sedimentary unit (<50 m) was deposited on an irregular erosional surface, locally marked by deeply weathered granite (grus) surrounding intensely weathered boulders of granite and aplite.

Intrusive

Trdi **Rhyodacite dike of Rampart Mountain** - Gray, porphyritic rock contains phenocrysts of plagioclase, quartz, and biotite and rare 2 cm orthoclase set in a fine-grained aplitic groundmass (Meyer et al., 1968). From east to west, this dike transects the district for >7 km at depth. Normal displacement along the Continental fault has exposed this dike on Rampart Mountain and further east in a I-15 roadcut. In the hanging wall of the Continental fault, at approximately the 2,000 foot level, a breccia at the apex of the dike, known as the Mountain View breccia, continues upward ~100 m, but is not exposed at surface (Meyer, et al., 1968). Available ^{40}Ar/^{39}Ar and ^{206}Pb/^{238}U monazite ages suggest emplacement at ~59 Ma (Dilles et al., 2004).

LATE CRETACEOUS PLUTONIC ROCKS

Boulder Batholith

Tmqp **Modoc quartz porphyry plug, irregular intrusions and breccia** - Light gray to grayish-green, porphyritic rock contains phenocrysts of plagioclase, rounded embayed quartz, sparse large (6 to 25 mm) K-feldspar, and biotite, in a very fine-grained groundmass of quartz and K-feldspar (64 Ma; Dilles et al., 2004). The Modoc quartz porphyry forms an irregular shaped plug that reaches a maximum width of ~300 m on the 2800 foot level of the Leonard mine (Meyer et al., 1968). Contacts are sinuous with moderate fragmentation of the granite (Meyer et al., 1968). Breccia fragments contain older quartz-molybdenite veinlets characteristic of the deep porphyry Cu-Mo zone.

Kqp **Quartz porphyry dikes** - Light colored, porphyritic rock (3 to 20 m wide) contains ca. 50 vol. % aplitic groundmass and 50 vol. % phenocrysts of euhedral plagioclase, rounded quartz eyes, orthoclase and biotite phenocrysts enclosed in a fine-grained groundmass of quartz and orthoclase (66 Ma; Lund et al., 2002).

Ka **Aplite, granoaplite, and pegmatite dikes and irregular intrusions -** Light colored to pink dikes consisting of orthoclase, quartz, oligoclase-andesine and trace amounts of biotite, contain local occurrences of pyrite, chalcopyrite, magnetite, albitic plagioclase and very rare pyrrhotite in quartz in the core zones (Meyer et al., 1968; Smedes et al., 1962). Black tourmaline and molybdenite also occur in miarolitic cavities and are most abundant in the deepest plutonic exposures along East Ridge. Granoaplite dikes (described as a granite-aplite hybrid rock; Roberts, 1975) contain phenocrysts of plagioclase, biotite, hornblende and rounded quartz eyes entrained in fine-grained aplitic quartz and alkali feldspar groundmass (76 Ma; Lund et al., 2002). Most dikes are gently-dipping and make up parallel sheeted sets. Aplite dikes are cm- to m-thick and typically have sharp contacts with the granite. Aplite dikes locally exceed 20 m thickness and commonly zone inward to pegmatitic cores (Meyer et al., 1968). Most granoaplite dikes occur as massive gently dipping planar sheets that exceed 20 m in thickness. Contacts are gradational with the granite. Sheeted aplite dikes are abundant in the western and eastern parts of the Butte district and intrude parallel to subhorizontal joint sets observed throughout the Butte district.

Kme **Mafic enclaves** - Dark-green to black ellipsoidal nodules (15 to 50 cm dia.) containing crystals of plagioclase, hornblende, biotite, quartz, magnetite and minor apatite. South and adjacent to Bull Run Creek, abundant nodules occur in a linear collection (~15 by 400 meters). At this location nodules are surrounded by fine-grained granite (Kbg). Elsewhere, isolated nodules occur throughout the district. Enclaves cut by aplite dikes.

Kbg **Butte Granite** - Gray, medium- to coarse-grained equigranular rock consists of plagioclase (35-40 vol. %), orthoclase (20-25 vol. %), quartz (15-25 vol. %), and about 20 vol. % biotite, hornblende, magnetite, titanite, ilmenite, and apatite (76.5 Ma; Meyer et al., 1968; Martin et al., 1999; Martin and Dilles, 2000, Lund et al., 2002). The granite has distinctive euhedral poikilitic K-feldspar megacrysts up to 3 cm in length (Smedes et al., 1962; Meyer et al., 1968). Occasional mafic enclaves and aplite dikes are present throughout the granite (Houston, 2001).

85	**Contact** - showing dip; dashed where approximately located; and dotted where concealed
78 D U	**Fault** - showing dip; dashed where approximately located; dotted where concealed; Names shown on principal faults
64 D U	**Vein or mineralized fault** - showing dip; dotted where concealed; Names shown on principal veins
25	**Strike and dip of beds** - shown in all bedded units including sedimentary rocks and sedimentary interbeds within lava flows
15	**Strike and dip of compaction foliation structure**
10	**Strike and dip of rheomorphic foliation**
75	**Strike and dip of joint**
	Bidirectional paleoflow indicator
○ DDH-8	**Anaconda/ARCO Deep Drill Hole Locality**
◪	**Productive Mine Shaft**
	Open-pit outline: Berkeley Pit and Continental Pit
	Waste rock
	Tailings pond
	Historic landfill

References

1. Dilles, J., 1998, 2002, 2012, 1:24,000, this study.
2. Dilles, J., Stein, H., and Martin, M., and Rusk B., 2004, Re-Os and U-Pb ages for the Butte Copper District, Montana: IAVCEI Meeting, Púcon, Chile.
3. Dresser, H., 2000, Stereo Picture Guidebook to Big Butte Volcanics: Tobacco Root Geological Society, Annual Meeting, Butte, MT, August 3-6, 73 p.
4. Duaime, T., Kennelly, P., and Thale, P., 2004, Butte, Montana: Richest Hill on Earth, 100 years of underground mining, Montana Bureau of Mines and Geology: Miscellaneous Contribution 19, 1 sheet, 1:9,000.
5. Dudás, F., Ispolatov, V., Harlan, S., and Snee, L., 2010, ^{40}Ar/^{39}Ar Geochronology and Geochemical Reconnaissance of the Eocene Lowland Creek Volcanic Field, west-central Montana: The Journal of Geology, v. 118, No. 3, p. 295-304.
6. Elliott, C. and McDonald, C., 2009, Geologic map and geohazard assessment of Silver Bow County, Montana: Open-File Report 585, Montana Bureau of Mines and Geology, 81 p., 3 plates.
7. Feiveson, D., 1997, Seismic reflection investigation to support the existence of a normal fault in Rocker, Montana: Unpublished Senior thesis, Northfield, Minnesota, Department of Geology, Carleton College, 4 p.
8. Hammar-Klose, E., 1997, A high-resolution seismic reflection at Rocker Timber Treatment and Framing Plant site, Rocker, Montana: The College of Wooster, Keck Research Symposium in Geology, 10th, Wooster, Ohio, April 1997, p. 302–305.
9. Houston, R., 1998, 1999, mapped at 1:12,000 and 1:24,000, compiled at 1:24,000; this study.
10. Houston, R., 2001, Geology and structural history of the Butte district, Montana: Unpublished M.Sc. thesis, Corvallis, Oregon, Oregon State University, 45 p., 10 plates.
11. Lewis, R., 1998, Geologic map of the Butte 1° x 2° quadrangle, Southwestern Montana: Montana Bureau of Mines and Geology, Open File report 363, scale 1:100,000, 1 sheet, 17 p.
12. Lund, K. Aleinikoff, J., Kunk, M., Unruh, D., Zeihen, G., Hodges, W., Du Bray, E., and O'Neill, J., 2002, SHRIMP U-Pb and 40Ar/39Ar age contrasts for relating plutonism and mineralization in the Boulder Batholith region, Montana: Economic Geology, v. 97, p. 241-267.
13. Martin, M. and Dilles, J., 2000, Timing and duration of the Butte porphyry system: Tobacco Root Geological Society, Annual Meeting, Butte, Montana, August 3-6, 2000, p. 1.
14. Martin, M., Dilles, J., and Proffett, J.M, 1999, U-Pb geochronologic constraints for the Butte porphyry system [abs.]: Geological Society of America Abstracts with Programs, v. 31, no. 7, p. A380.
15. Meyer, C., Shea, E., Goddard, C., Jr., and Staff, 1968, Ore deposits at Butte, Montana, in Ridge, J., ed., Ore deposits of the United States, 1933-67, v. 2: New York, American Institute of Mining, Metallurgical, and Petroleum Engineers, p. 1373-1416.
16. Proffett, J.M., Jr., 1973, Structure of the Butte district, Montana: in Miller, R., ed., Guidebook for the Butte field meeting of the Society of Economic Geologists, The Anaconda Company, Butte, Montana, p. G-1 to G-12, plus figures.
17. Proffett, J.M., Burns, G., and Anaconda staff, 1982, Geologic map of the Butte district, Montana: Anaconda Archives, American Heritage Museum, Laramie, Wyoming, scale 1:12,000.
18. Reed, M., 1979 a and b, written communication.
19. Roberts, S., 1975, Early hydrothermal alteration and mineralization in the Butte district, Montana: Ph.D. thesis, Cambridge, Mass., Harvard University, 173 p.
20. Sales, R., 1914, Ore deposits at Butte, Montana: American Institute of Mining and Metallurgical Engineers Transactions, v. 46, p. 4-106.
21. Smedes, H., 1962, Lowland Creek Volcanics, an Upper Oligocene formation near Butte, Montana: Journal of Geology, v. 70, p. 255-266.
22. Smedes, H., 1967, Preliminary geologic map of the northeast quarter of Butte South Quadrangle, Montana: U.S. Geological Survey, Open File Map, 1:24,000.
23. Smedes, H., 1968, Preliminary geologic map of part of the Butte North Quadrangle, Silver Bow, Deer Lodge and Jefferson Counties, Montana: U.S. Geological Survey Open-File Report, Scale 1:48,000.
24. Smedes, H., Klepper, M., Pinckney, D., Becraft, G., and Ruppel, E., 1962, Preliminary geologic map of the Elk Park Quadrangle, Jefferson and Silver Bow Counties, Montana: U.S. Geological Survey map MF-246, Scale 1:24,000.
25. Smedes, H., Klepper, M., and Tilling, R., 1973, The Boulder Batholith, Montana: in Miller, R., ed., Guidebook for the Butte field meeting of the Society of Economic Geologists, The Anaconda Company, Butte, Montana, p. E-1 to E-16.
26. Smedes, H., Klepper, M., and Tilling, R., 1988, Preliminary map of plutonic units of the Boulder Batholith, southwestern Montana: Montana Bureau of Mines and Geology, Open-File Report 88-283, Scale 1:200,000 (& digital reprinted USGS Data Series 454, 2009).
27. Weed, W.H., 1912, Geology and ore deposits of the Butte district, Montana: U.S. Geological Survey Professional Paper 74, 262 p.

Acknowledgments

This research was supported by grants from the Tobacco Root Geological Society to Houston, and by NSF grants EAR-9614683 and EAR-0001230 to Dilles and Cyrus Field of Oregon State University. We greatly thank the many geologists who contributed scientific research to advance the knowledge of the geology of the Butte deposit over the last 140 years, and we acknowledge the research sponsorship until 1986 by the Anaconda Company and its successor the Atlantic Richfield Company. Steve Czehura of Montana Resources Inc. kindly provided many informative discussions as well as unpublished data of the Butte district, including geologic maps made by George Burns and John Proffett. Review of an earlier version by Professors Cyrus Field, Edward Taylor and Robert Yeats, when it was part of a M.Sc. thesis by Houston, is greatly appreciated. We gratefully acknowledge two Economic Geology reviewers John Proffett and David Cooke, who reviewed the map as part of the formal review process of the manuscript (Houston and Dilles, 2013). Finally, the senior author is indebted to the residents of the study area who freely gave their permission to traverse their properties.

Maps may be obtained from:
Publications Office
Montana Bureau of Mines and Geology
1300 West Park Street
Butte, Montana 59701-8997
Phone: (406) 496-4167 Fax: (406) 496-4451
http://www.mbmg.mtech.edu

Index Map showing credit for geologic mapping noted by reference number

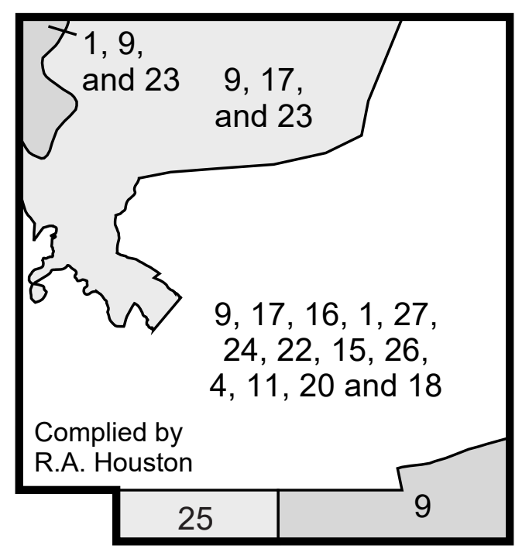

Montana Bureau of Mines and Geology
Open File MBMG 627

GEOLOGY OF THE BUTTE MINING DISTRICT, MONTANA

Robert A. Houston[1] and John H. Dilles[2]

2013

[1]Oregon Department of Geology and Mineral Industries, Albany, Oregon
[2]Oregon State University, Corvallis, Oregon

This map supplements Houston and Dilles, 2013, Structural Geologic Evolution of the Butte District, Montana: Economic Geology, v. 108, no. 6, p. 1397-1424.